Middle Rio Grande Bosque del Apache Reach Report:

Morpho-dynamic Processes and Silvery Minnow Habitat from US-380 Bridge to the Southern Boundary of Bosque Del Apache National Wildlife Refuge

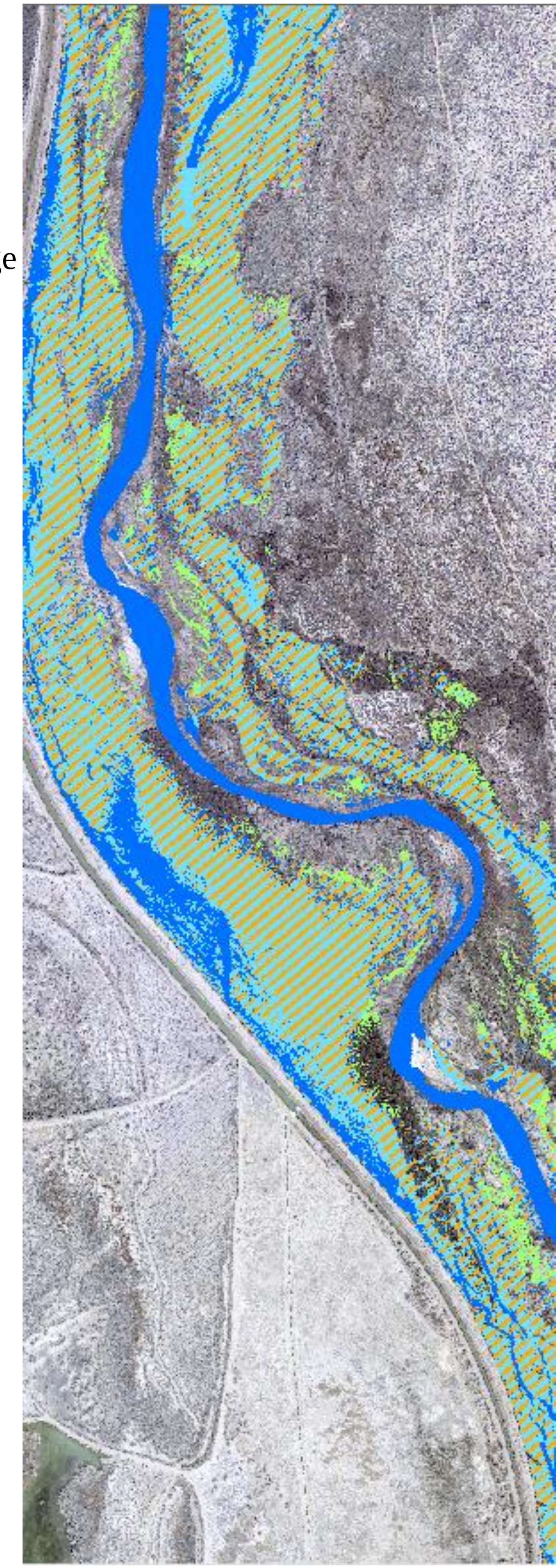

Andrew Schied
Josh Sperry
Dr. Pierre Julien

May 2022
Final report prepared for the
United States Bureau of Reclamation

Colorado State University
Engineering Research Center
Department of Civil and Environmental Engineering
Fort Collins, Colorado 80523

Abstract

The Bosque del Apache reach spans approximately 16 miles of the Middle Rio Grande (MRG), from the US Highway 380 Bridge near San Antonio, New Mexico to the southern boundary of the Bosque del Apache National Wildlife Refuge (BNWR). This reach report, prepared for the United States Bureau of Reclamation (Reclamation), presents a summary of results to aid in a better understanding of the morpho-dynamic processes within the Bosque del Apache reach. The reach is divided into five subreaches (B1, B2, B3, B4, and B5) to illustrate the spatial and temporal trends of the channel geometry and morphology of the dynamic river, still changing in response to anthropogenic impacts over the last century (Posner, 2017).

Discharge and sediment data from the United States Geological Survey (USGS) were used to identify the seasons of peak discharge and sediment load in the reach. Peak flows are generated by snowmelt with their associated larger flow volume as well as by summer thunderstorms. Monsoonal thunderstorms often transport the greatest amount of sediment. Since 2011, the average discharge has been about 0.47 million acre-ft/yr with an average suspended sediment load of about 7,000 tons per day during the period of available data at the San Antonio gage.

Maps and aerial photographs dating back to 1918 were analyzed through geographic information system (GIS) to evaluate the changes in width and sinuosity. Anthropogenic changes and droughts led to significant narrowing throughout the early to mid-1900s. This narrowing trend continued at a slower rate into the 2000s, but ultimately the widths have stabilized as of 2012 between 100 and 250 feet, depending on the subreach. The sinuosity of the reach has stabilized at a low sinuosity for most subreaches (at or below 1.05). Two subreaches are moderate to high in sinuosity with one subreach appearing trending towards increasing sinuosity. Changes to bed elevation were observed using cross-section geometry files provided by the reclamation Technical Service Center. The majority of the Bosque del Apache reach has experienced net aggradation throughout the period of available data. The aggradation is most pronounced in the middle of the reach (up to six feet), while the end of the reach exhibits less aggradation and even recent trends of erosion.

The geomorphic conceptual model of Massong et al. (2010) was applied to the Middle Rio Grande. The Bosque del Apache subreaches are classified as either aggrading or migrating stages. After analyzing changes to the cross-section geometry and aerial imagery, all subreaches appeared to be within Stage A4 or actively transitioning between A4 and A5. Stage A4 indicates high levels of sediment deposition and perching of the channel above its floodplain, while stage A5 is the initiation of a sediment plug within the main channel, which has been observed during the study period. These high levels of aggradation are the result of a sediment supply that exceeds the river’s transport capacity.

Additional work was performed with HEC-RAS to understand habitat availability for the endangered Rio Grande Silvery Minnow (RGSM) throughout the Bosque del Apache Reach. A width-slice method in HEC-RAS was developed to calculate the hydraulically suitable RGSM habitat based on flow velocity and depth criteria for the larval, juvenile, and adult stages at various discharges. Calculations for a wide range of discharges up to 10,000 cfs were conducted for four geometric river conditions over a span of 50 years. Subreaches B1 and B2 provide the least amount of hydraulically suitable habitat, while subreaches B3 and B5 show the greatest potential for RGSM habitat. Detailed mapping for year 2012 was performed based on detailed LiDAR data at a 10-foot resolution to illustrate the RGSM habitat areas within the study

reach. Because of the significant perching within the Bosque del Apache reach, flooded areas on these maps identified as suitable habitat may not actually be well connected to the main channel and therefore accessible to the RGSM. These areas include large portions of subreaches B1 and B2, the middle portion of subreach B3, and the end portion of subreach B5.

Acknowledgement

This final report has been prepared for the United States Bureau of Reclamation under Award Number R17AC00064. The authors gratefully acknowledge the numerous constructive comments and thoughtful suggestions to improve a draft version of this report. We are particularly thankful to Ari Posner, Drew Baird, Nathan Holste and Nate Bradley at Reclamation. The detailed discussions contributed to key improvements including the addition of a synthesis section, a review of HEC-RAS files, and fine-tuning of multiple graphics and calculation procedures.

These reports have been prepared in collaboration with the University of New Mexico (UNM) and the American Southwest Ichthyological Researchers (ASIR). We specifically treasure our collaboration with Tom Turner, Steven Platania, Robert Dudley and Jake Mortensen whose aquatic habitat expertise on the Rio Grande Silvery Minnow (RGSM) provided an underlying framework for this reach report.

Table of Contents

List of Tables

List of Figures

Appendix A List of Figures

Appendix B List of Figures

Appendix C List of Figures

Appendix D List of Figures

Appendix E List of Figures

Appendix F List of Figures

1. Introduction

The purpose of this reach report is to evaluate the morpho-dynamic conditions of the Middle Rio Grande (MRG) which extends from the Cochiti Dam to the Narrows in Elephant Butte Reservoir. The report focuses on the Bosque del Apache reach, which begins at the US 380 Bridge near San Antonio, New Mexico and ends at the southern boundary of the Bosque Del Apache National Wildlife Refuge (BDNWR) (Figure 1).

Figure 1: Map with the Middle Rio Grande outlined in blue. It begins at the Cochiti Dam (top) and continues downstream to the Narrows in Elephant Butte Reservoir (bottom). The lime green highlights the Bosque del Apache reach.

It is part of a series of reports commissioned by Reclamation, which includes morpho-dynamic reach reports, reports on the biological-habitat conditions for the Rio Grande Silvery Minnow, and process linkage reports. The process linkage reports will ultimately connect morpho-dynamic conditions with the required biological-habitat conditions. This report focuses on understanding trends of the physical conditions of the Bosque del Apache reach. Specific objectives include:

- Delineate the reach into subreaches based on shared geomorphic characteristics;
- Summarize the flow and sediment discharge conditions and trends for the period of record available from United States Geological Survey (USGS) gages;
- Analyze geomorphic characteristics at a subreach level (sinuosity, width, bed elevation, bed material, bed slope, and other hydraulic parameters).
- Link changes in the river geomorphology with shifts in sediment and flow trends; and
- Classify subreaches using a geomorphic conceptual model.

Finally, in preparation for a future process linkage report, attempts were made to characterize fish habitat throughout the Bosque del Apache reach. These methods were based on HEC-RAS one-dimensional hydraulic models, which were used to understand and predict the conditions on the Middle Rio Grande. This series of reports will support Reclamation's mission for the Middle Rio Grande to improve habitat for species listed by the Endangered Species Act and to support channel sustainability while continuing to provide effective water delivery (U.S. Bureau of Reclamation, 2012).

1.1 Site Description

The Rio Grande begins in the San Juan mountain range of Colorado and continues into New Mexico. It follows along the Texas-Mexico border before reaching the Gulf of Mexico. The Middle Rio Grande is the stretch from the Cochiti Dam to Elephant Butte Reservoir. The MRG has historically been affected by periods of drought and large spring flooding events due to snowmelt. These floods often caused large scale shifts in the course of the river and rapid aggradation (Massong et al., 2010). Floods helped maintain aquatic ecosystems by enabling connection of water between the main channel and the floodplains (Scurlock, 1998), but consequently threatened human establishments that were built near the Rio Grande.

Beginning in the 1930's, levees were installed to prevent flooding by the Middle Rio Grande Conservancy District (MRGCD). Beginning in the 1950s, Reclamation undertook a significant channelization effort involving jetty jacks, river straightening and other techniques. Upstream dams built in the 1950s were used to store and regulate flow in the river. Agricultural drains were also installed to lower the water table adjacent to the channel. In the end of the 1960s a Low Flow Conveyance Channel was constructed to divert water from the main channel from the 1960s to the 1980s (Makar, 2006). While these efforts enabled agriculture and large-scale human developments to thrive along the MRG, they also fundamentally changed the river, which led to reduced peak flows and sediment supply while altering the channel geometry and vegetation (Makar, 2006). In parts of the MRG, narrowing of the river continues, with channel degradation due to limited sediment supply and the formation of bank attached vegetated bars that encroach upon the channel (Varyu, 2013; Massong et al., 2010). Farther downstream, closer to Elephant Butte Reservoir, aggradation and sediment plugs have been observed. These factors have created an ecologically stressed environment, as seen in the decline of species such as the Rio Grande Silvery Minnow (Mortensen et al., 2019). The Bosque del Apache reach is a part of the Middle Rio Grande located in central New Mexico. This reach begins at the US HWY 380 Bridge near San Antonio, New Mexico and continues 15.8 miles downstream to the southern boundary of BWNR. A diagram detailing the major historical events and alterations to the Rio Grande is provided by Makar, 2006 in Figure 2.

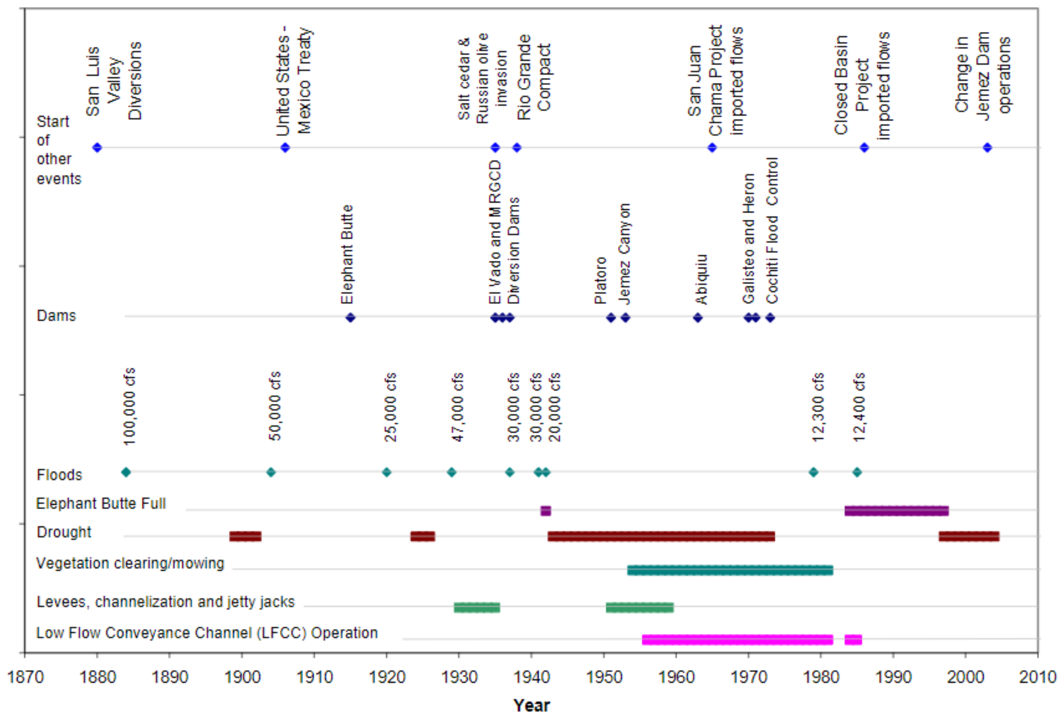

Figure 2: Timeline of significant events (Makar, 2006).

1.2 Aggradation/Degradation Lines and Rangelines

Aggradation/degradation lines (agg/deg lines) are “spaced approximately 500-feet apart and are used to estimate sedimentation and morphological changes in the river channel and floodplain for the entire MRG” (Posner, 2017). Each agg/deg line is reapproximated through prismatic cross sectional methods roughly every 10 years, when Reclamation performs monitoring, and is established as a cross-section in the Rio Grande HEC-RAS models. The most recent entire MRG survey available was performed in 2012. Cross-sectional geometry at each agg/deg line is available from models developed by the Technical Service Center (Varyu, 2013). Models are available for 1962, 1972, 1992, 2002 and 2012. The 2012 model was developed from LiDAR data, but models prior to 2012 used photogrammetry techniques. All models use the NAVD88 vertical datum. In addition to agg/deg lines, rangelines are used as location identifiers in this analysis. The rangelines, and agg/deg lines were determined in association with geomorphic factors, such as migrating bends, incision, or river maintenance issues. Repeat surveys are implemented along these cross-section lines, as well as bed material samples.

1.3 Subreach Delineation

To analyze the hydraulic trends, the Bosque del Apache reach was divided into five subreaches. Within the Bosque del Apache reach there are no major river tributaries, bridges, or other large distinguishing factors that would impact the hydraulic characteristics, though the Highway 380 bridge did mark the beginning of the overall reach. To delineate the reach, sections where geomorphic trends distinguished by changes in width and depth were identified. The resulting boundaries for the subreaches and their corresponding agg/deg lines were then compared to a previous delineation conducted by Paris et al. (2011). The width and depth analysis matched closely to boundaries identified in Paris et al. (2011)

at agg/deg lines 1496 and 1603. All plots showing cumulative channel width and depth used in the delineation can be round in Appendix A

These cumulative width and depth plots were developed using a HEC-RAS model with the 2002 and 2012 geometry provided by Reclamation. A flow of 3,000 cfs was selected for cumulative plots of hydraulic variables to be consistent with previous reach reports (LaForge et al., 2019; Yang et al., 2019; Beckwith et al. 2020). This is the nominal discharge that fills the main channel without overbanking. The daily percent exceedance for 3,000 cfs is approximately 3.7% at the Highway 380 bridge near San Antonio, NM, at the upstream end of the reach (Gage 08355490). A downstream boundary condition with a slope of 0.0007 was selected based on an average slope for the entire reach. An overall delineation map is provided in Figure 3 whereas delineation maps of subreaches B1, B2, B3, B4, and B5 are provided in Figures 4, 5, 6, 7, and 8 respectively.

Subreach Bosque 1 (B1) extends from the San Antonio Highway 380 Bridge (agg/deg line 1475) downstream to where the channel begins to decrease in depth (agg/deg line 1496). Subreach B2 begins at this point and continues to agg/deg line 1516, where the cumulative width of the channel begins to increase at an inflection point. Subreach B3 is the longest subreach in the delineation and continues to a bend at which the channel begins to narrow again (agg/deg line 1582). Subreach B4 is characterized by further narrowing as well as by a previous subreach delineation by Paris et al. (2009) (Agg/deg line 1603). Subreach B5 is characterized by a very straight and narrow channel, ending at the BNWR southern boundary (agg/deg line 1637). A summary of the results of the delineation are presented in Table 1. Aerial images with every agg/deg line labeled are included in Appendix A.

Table 1: Bosque del Apache Subreach Delineation

Bosque del Apache Reach		
Subreach	**Agg/deg lines**	**Justification**
B1	Start: 1475 End: 1496	Start: HWY 380 Bridge End: Depth decrease, Agg/Deg by Paris et al. (2009)
B2	Start: 1496 End: 1516	Start: Depth decrease, Agg/Deg by Paris et al. (2009) End: Width increase
B3	Start: 1516 End: 1582	Start: Width increase End: Width decrease
B4	Start: 1582 End: 1603	Start: Width decrease End: Width decrease, Agg/Deg by Paris et al. (2009)
B5	Start: 1603 End: 1637	Start: Width decrease, Agg/Deg by Paris et al. (2009) End: Boundary of BAWR

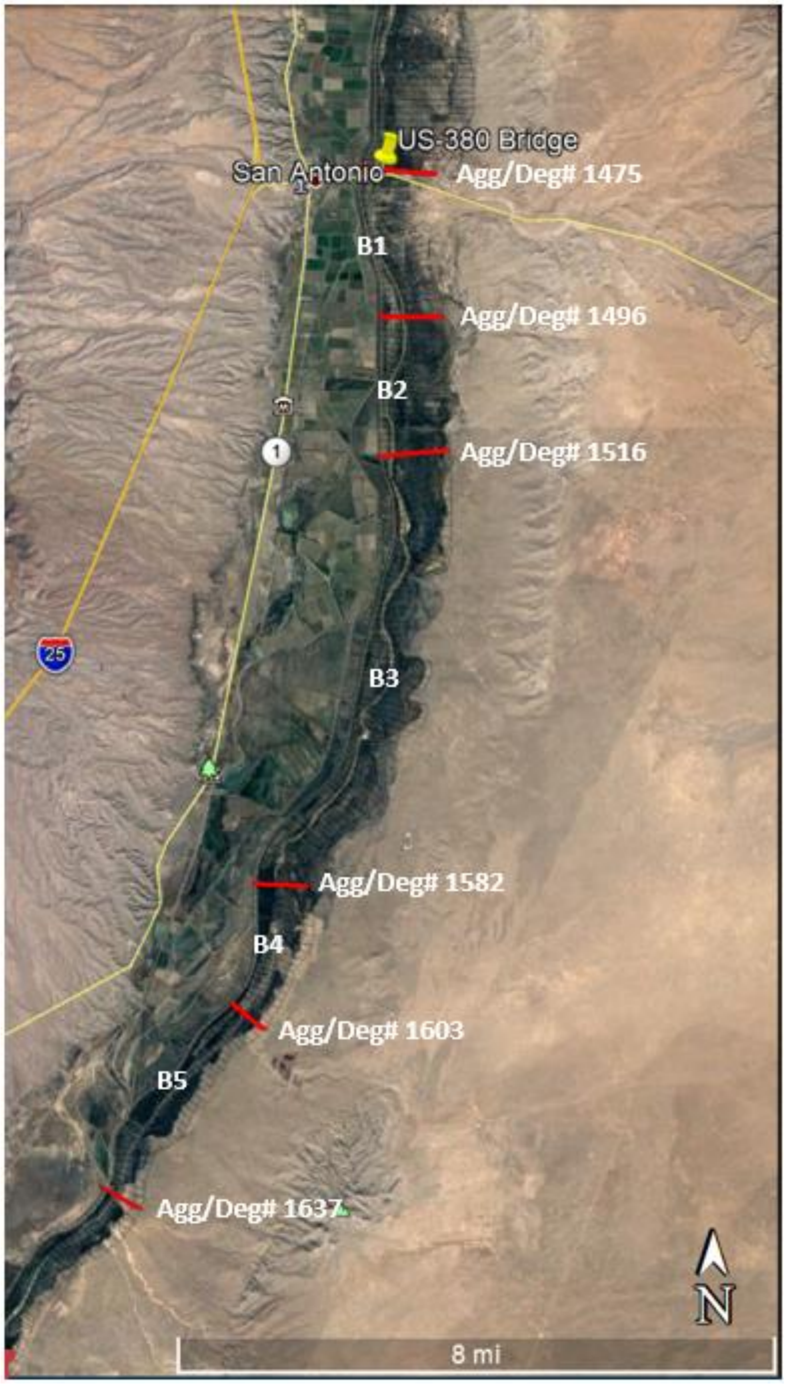

Figure 3: Aerial Imagery of Bosque del Apache (Google Earth 2020)

Figure 4: Aerial imagery of Bosque subreach B1 (Google Earth 2020)

Figure 5: Aerial Imagery of Subreach B2 (Google Earth 2020)

Figure 6: Aerial Imagery of Subreach B3 (Google Earth 2020)

Figure 7: Aerial Imagery of Subreach B4 (Google Earth 2020)

Figure 8: Aerial Imagery of Subreach B5 (Google Earth 2020)

2. Precipitation, Flow and Sediment Discharge Analysis

2.1 Precipitation

Precipitation data are collected along the MRG by the Bosque del Apache Ecosystem Monitoring Program from University of New Mexico (BEMP Data, 2017). The locations of the data collection are shown in Figure 9. The Sevilleta site is near the San Acacia Diversion Dam, the Lemitar site is North of Escondida, just outside of Lemitar, New Mexico, and the Mesilla site is located in Las Cruces, New Mexico. All sites were used in the precipitation analysis.

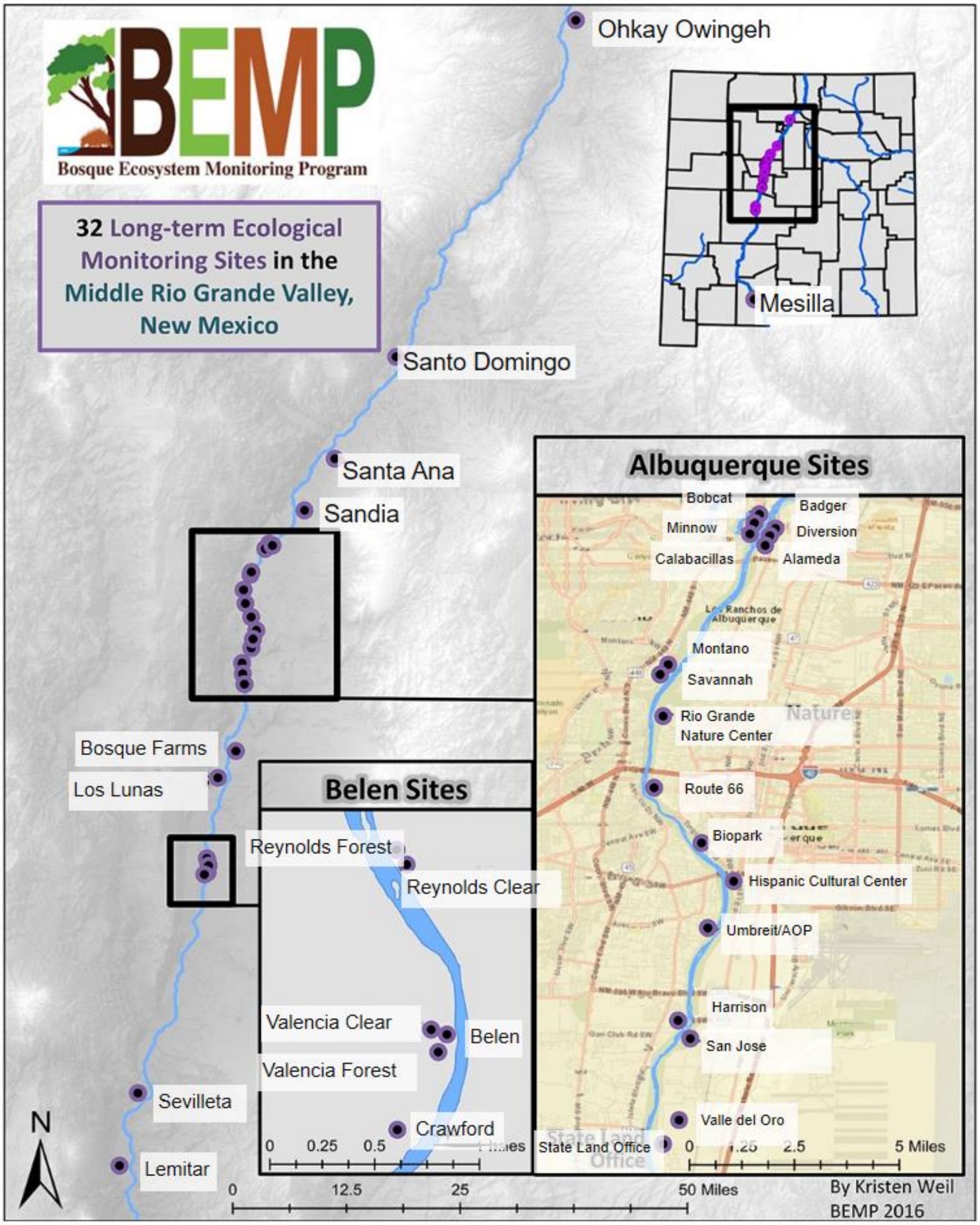

Figure 9: BEMP data collection sites (figures source: http://bemp.org)

The precipitation data are shown in Figure 10. The highest precipitation peak occurred in August of 2006 at the Lemitar gage, with 5.5 inches of rainfall. A general trend was observed with highest precipitation values occurring during monsoon season (late July through early September). A cumulative plot of rainfall (Figure 11) shows that individual rain events can greatly affect the overall trend of the data. It further highlights the impacts of monsoonal rains, which create a “stepping” pattern with higher rainfall in August and September, and lower levels throughout the rest of the year. The comparison of the cumulative precipitation at the two sites also shows that the Lemitar gage recieves more precipitation than the Sevilleta gage throughout the time observed. Though data for the Mesilla gage only extends back to July 2011, its magnitude and timing of precipitation follow the same trends observed at the Lemitar and Sevilleta gages.

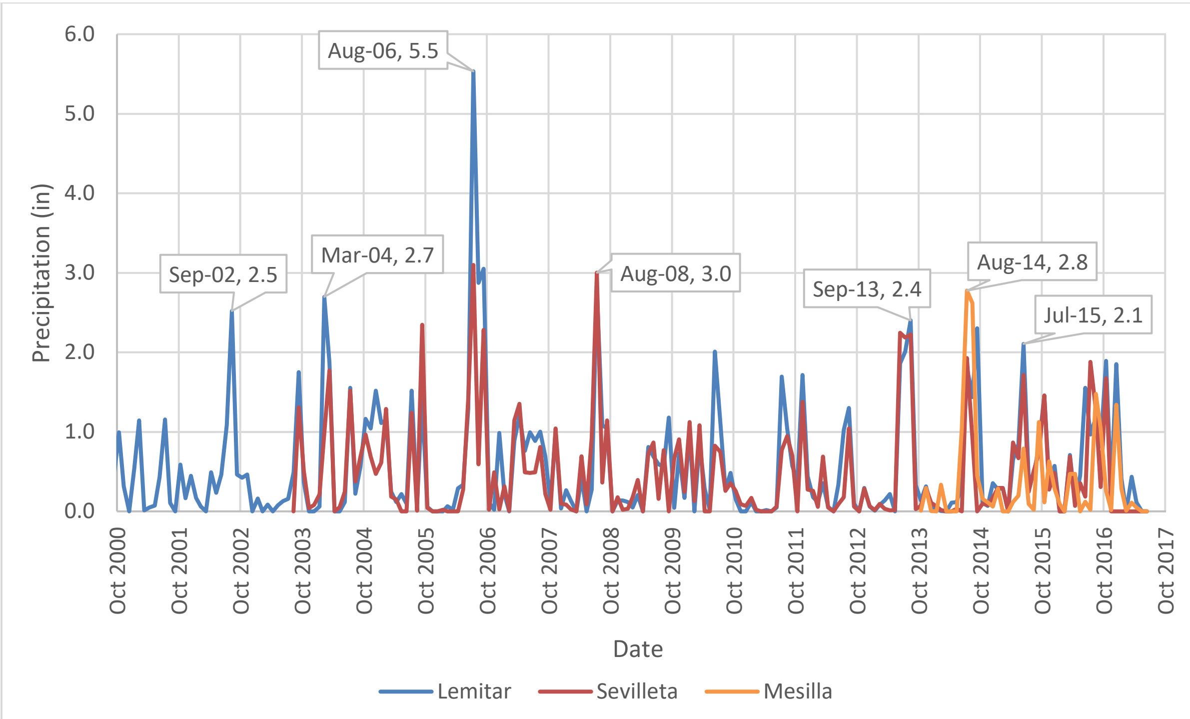

Figure 10: Monthly precipitation near Bosque del Apache reach

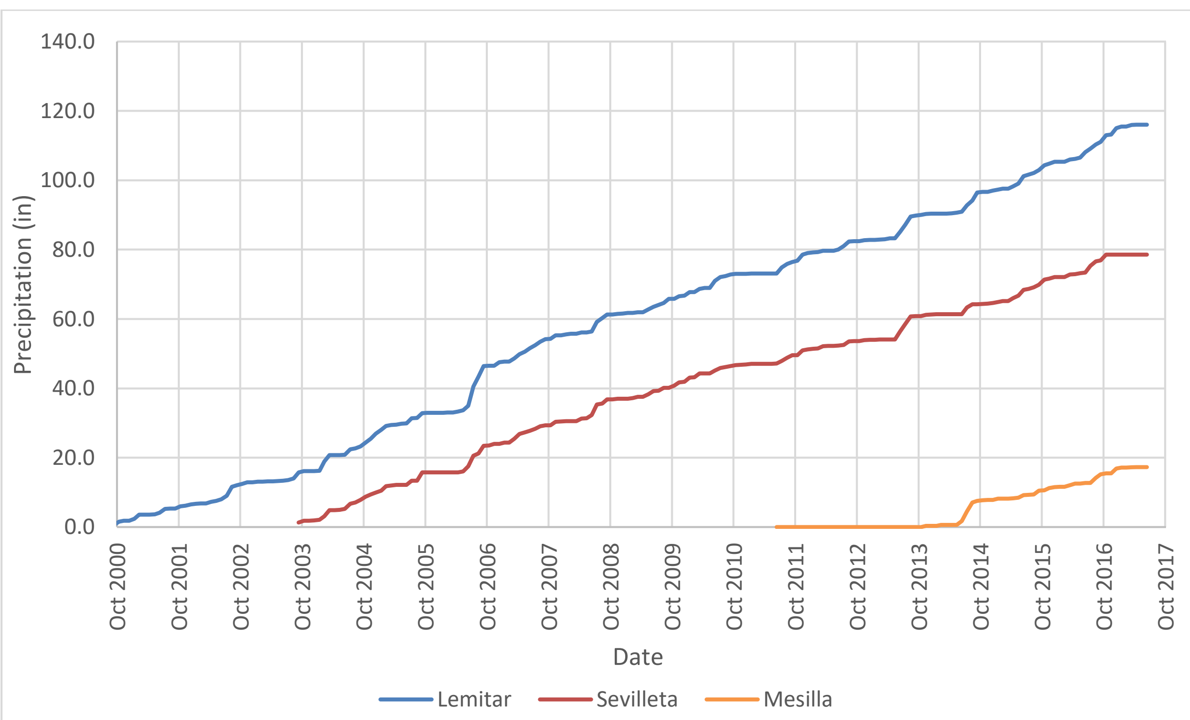

Figure 11: Cumulative precipitation near the Bosque del Apache reach

2.2 River Flow

Information regarding river flow was gathered from the USGS National Water Information System. The gages in the area relevant to the study are included in Table 2.

Table 2 List of gages used in this study

Station	Station Number	Mean Daily Discharge	Daily Suspended Sediment
Rio Grande at Bridge Near Escondida, NM	08355050	October 1, 2005 to present	No data
Rio Grande above US HWY 380 near San Antonio, NM Rio Grande at San Antonio, NM (Inactive)	08355490 08355500	September 30, 2005 to present April 1, 1951 to June 30, 1957	October 1, 2011 to September 30, 2019 No data
Rio Grande Floodway at San Marcial Rio Grande at San Marcial, NM (Inactive)	08358400 08358500	October 1, 1949 to present January 1, 1899 to September 29, 1964	October 1, 1956 to September 30, 2019 No data

The gage at San Marcial (08358400) is located south of the BNWR, just downstream of the railway crossing near San Marcial and was included in this reach report due to its long data record for both sediment and water discharge. The raster hydrograph for this gage and its no longer active but historic predecessor (08358500) are shown in Figures 12 and 13 respectively and represent the same location. The raster hydrographs of the daily discharge at the bridge near Escondida (08355050) and US HWY 380 near San Antonio (08355490) gages are shown in Figures 14 and 15, respectively. The raster hydrograph from the inactive site at San Antonio (08355500), which only recorded data between 1951 and 1957, is shown in Figure 16.

The figures show seasonal flow patterns, with peak flow often occurring from snowmelt runoff from April through June, low flow throughout the rest of the summer (except for strong summer thunderstorms), and medium flow from November onwards representing the end of the irrigation season.

The raster hydrograph at San Marcial shows much lower flows between 1960 and 1975. While there were periods of drought in the 1960s and 1970s, the severe lack of water at the San Marcial gage in this time period was primarily due to the usage of a Low Flow Conveyance Channel diverting the water away from the main channel.

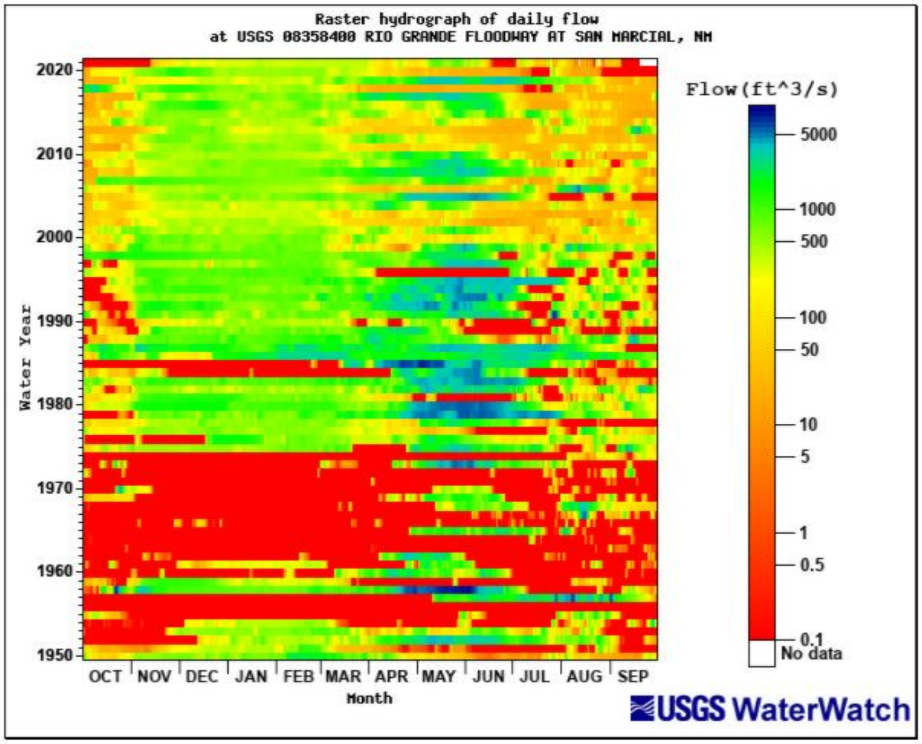

Figure 12: Raster hydrograph of daily discharge at USGS Station 08358400 near San Marcial, NM

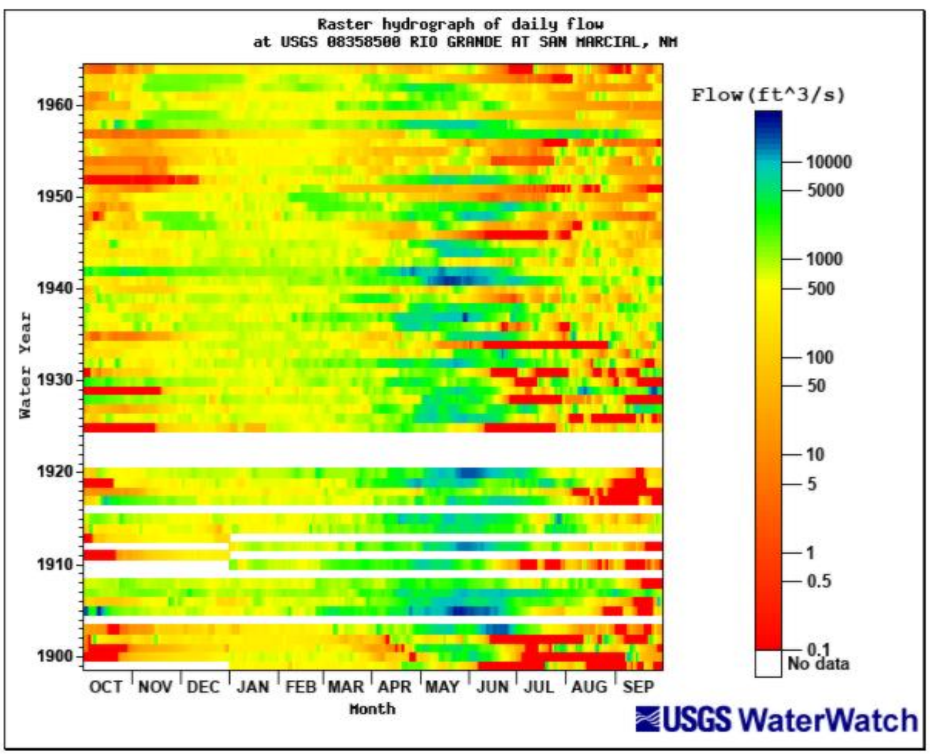

Figure 13: Raster hydrograph of daily discharge at USGS Station 08358500 near San Marcial, NM

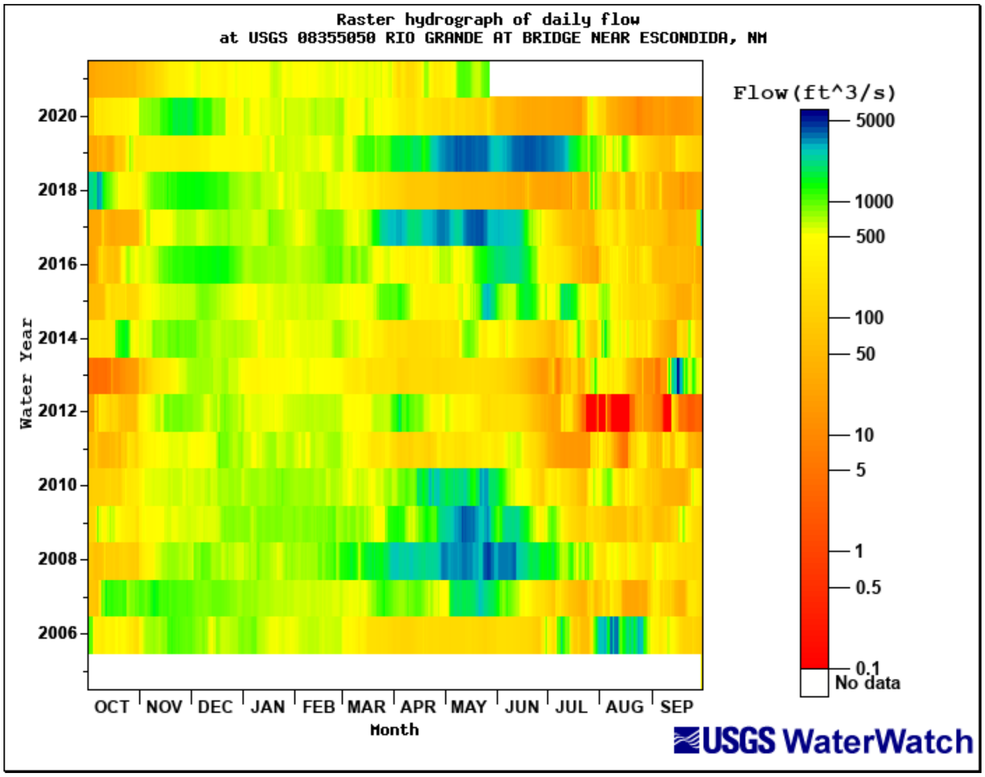

Figure 14: Raster hydrograph of daily discharge at USGS Station 08355050 near Escondida, NM

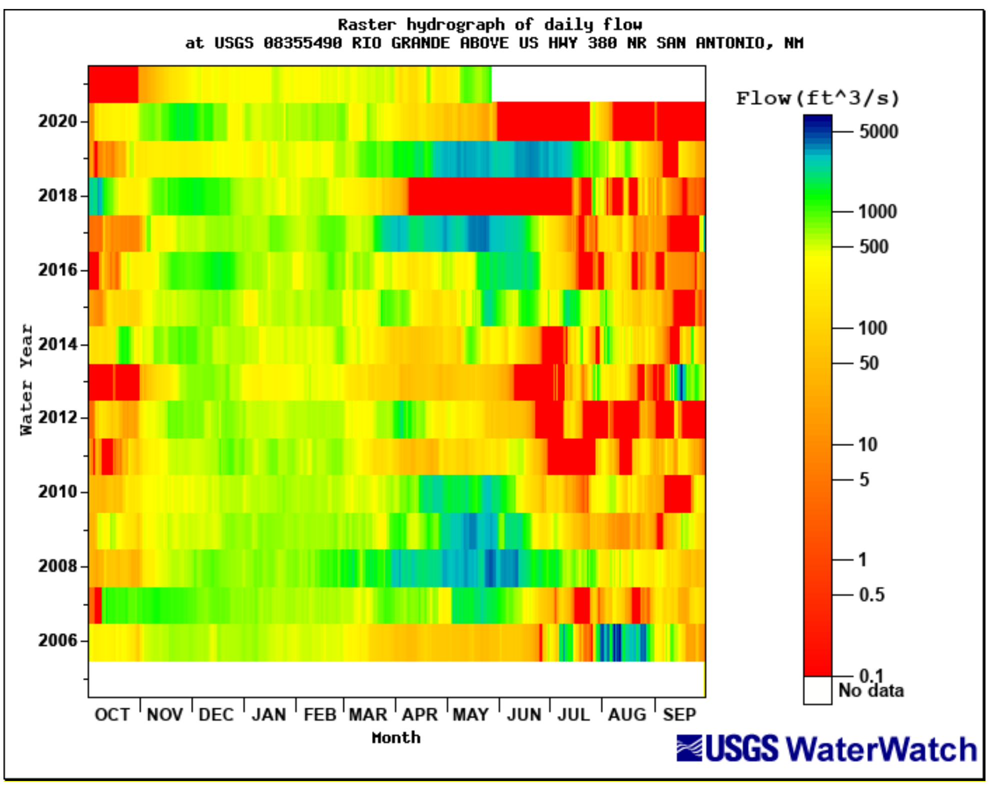

Figure 15: Raster hydrograph of daily discharge at USGS Station 08355490 near US HWY 380 Bridge San Antonio, NM

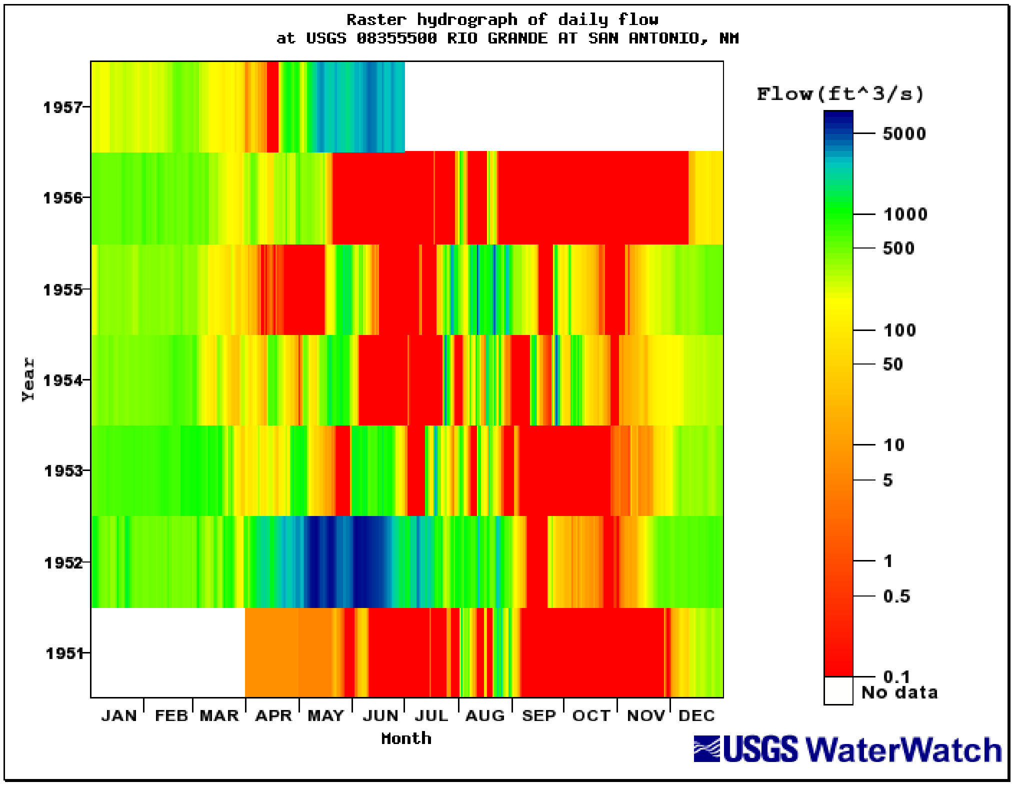

Figure 16: Raster hydrograph of daily discharge at USGS Station 08355500 near US HWY 380 Bridge San Antonio, NM

Cumulative discharge curves show changes in annual flow volume over a given time period. The slope of the line of the mass curve gives the mean annual discharge, while breaks in the slope show changes in flow volume. Figure 17 shows the mass curves of the gages near Escondida and San Antonio as well as the low flow conveyance channel which may be partially responsible for the reduction in flow between the two gages. The mass curves were divided into time periods of similar slopes to analyze long term patterns in discharge. Typically, cumulative discharge plots are useful for analyzing long-term trends in flows. Occasionally, large, flow altering events can be identified. To help identify these individual events, a one-week moving average was used to determine significant inflection points in the slope. The data callout points represent these inflection points at which changes in slope were greater than the 97.5th percentile of moving-average slope values. This helps to depict the times in which the most rapid increases in cumulative discharge occurred. These large increases typically occur between April and June (likely from snowmelt), although noticeable increases can also occur in late August or September from summertime, monsoonal thunderstorms.

Figure 18 shows a mass curve created from data at the Rio Grande Floodway gage near San Marcial, NM. This gage has data for a much longer period of record which can help in identifying long term trends. The period of data ranges from 1949 to the present for single mass curve. Based on the San Marcial single mass curve, there are periods where the discharge volume in the river was lower, such as from 1949 to the late 1970s and again from the early 2000s to present, represented by flatter slopes (0.246 million acre-ft/yr and 0.343 million acre-ft/year respectively. During the early 1980s to the late 1990s this slope increases to 0.897 million acre-ft/year, representing an overall increase in discharge. Given the longer time period analyzed, the detail for many specific events gets washed out. Similar to the cumulative discharge plots at the gages in the Bosque del Apache reach, the steeper slopes at the San Marcial gage often occur in the spring months, indicating that snowmelt may have the greatest impact on increasing the flow in the Middle Rio Grande.

Figure 19, which relates the cumulative precipitation and cumulative monthly discharges, can further demonstrate the time periods that experience higher discharges due to snowmelt. A steeper slope indicates that the discharges are increasing with relatively little precipitation. This increase in discharge could occur from snowmelt or possibly controlled release of water from a dam. As seen in Figure 19, increases in discharge with little precipitation can occur between February and May. However, there are several noticeable increases in November or October, which could be due to regulated water being released from a dam upstream.

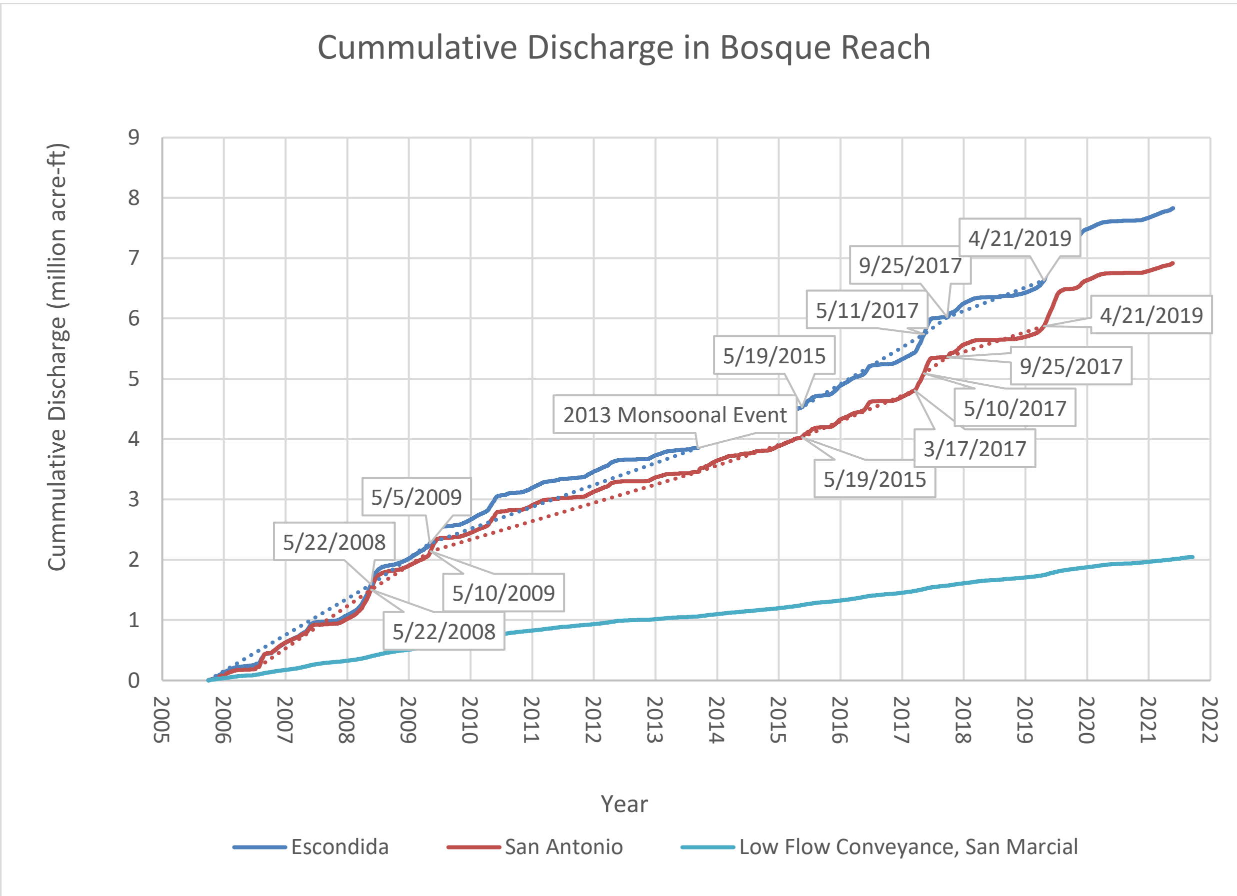

Figure 17: Discharge single mass curve at the Escondida and San Antonio gages (top) and San Acacia gage (middle), and low flow conveyance channel (bottom).

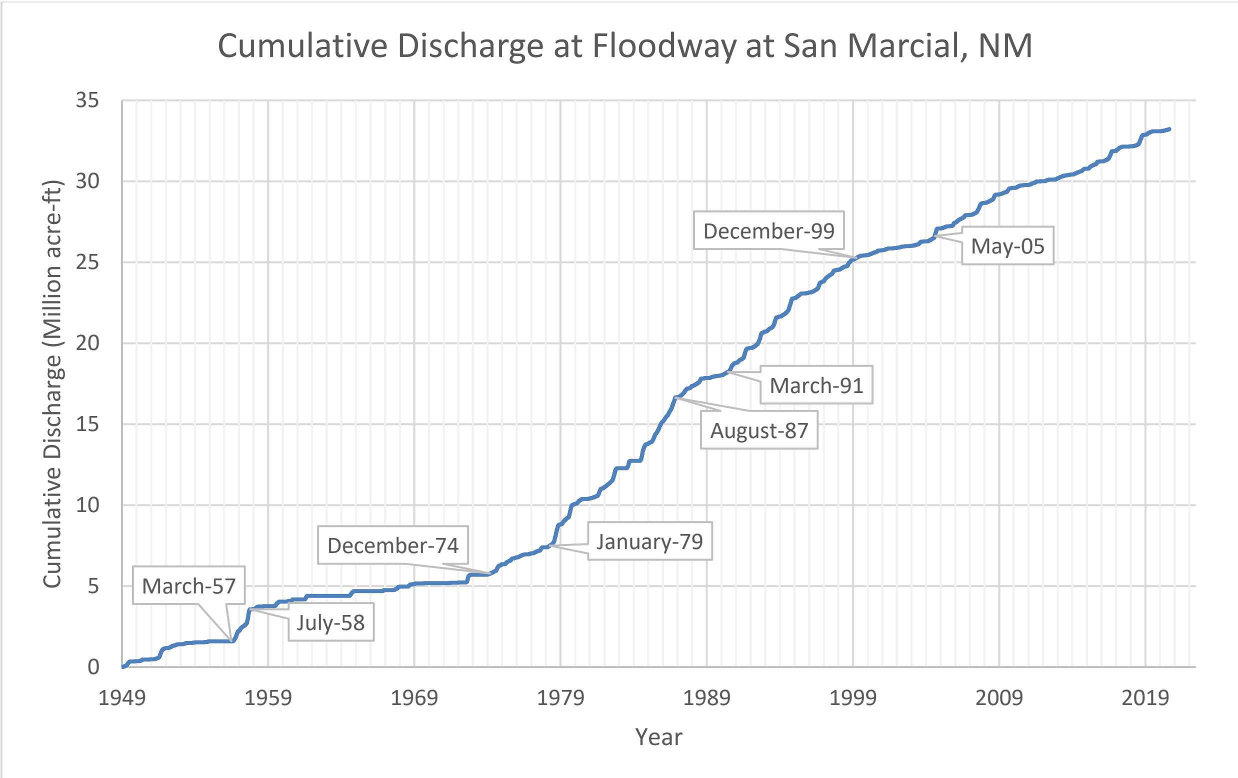

Figure 18: Cumulative discharge for the Floodway at San Marcial Gage, NM

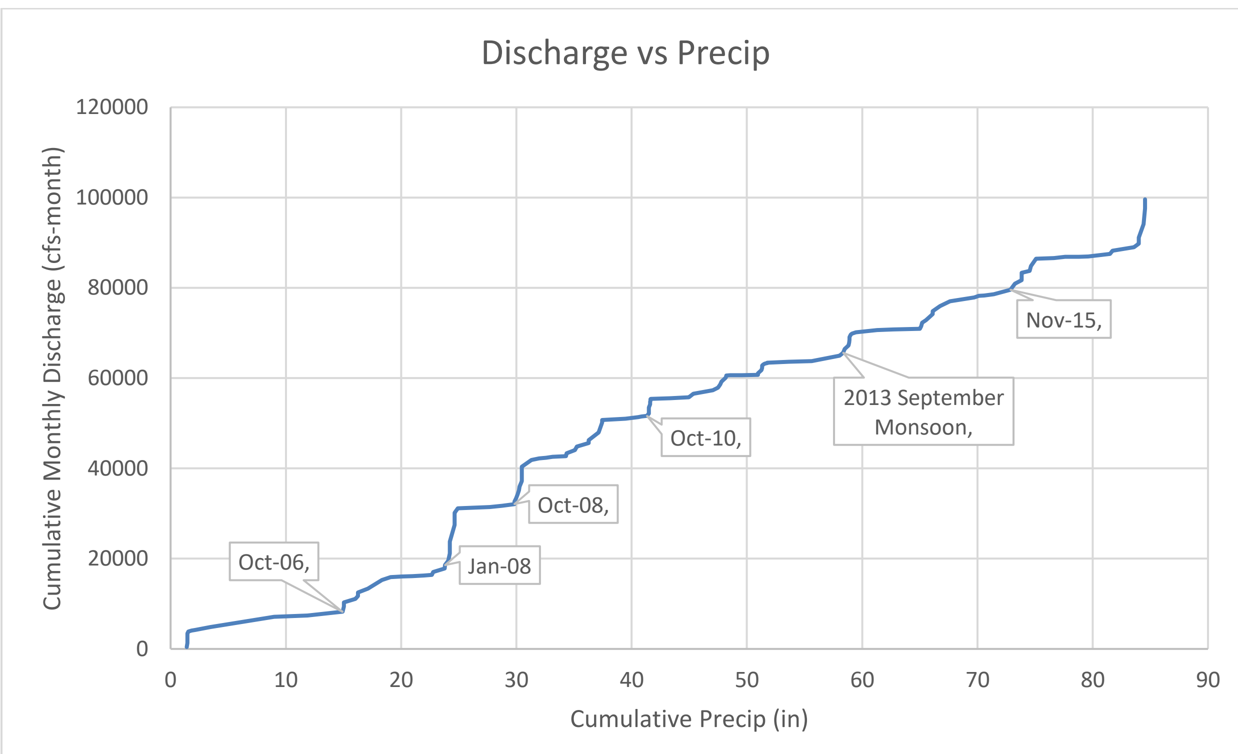

Figure 19: Cumulative discharge plotted against cumulative precipitation at the US 380 gage near San Antonio, NM

2.2.1 Flow Duration

Flow duration curves were developed using the mean daily flow discharge values for the Escondida and San Antonio gages for the complete record (years 2005 to 2021) and for the San Marcial gage from 1949. The curves are shown in Figures 20 and 21. Table 3 shows exceedance values calculated from the flow duration curves. The values for the San Antonio gage are slightly lower at every exceedance percentage. The values of the San Marcial gage are considerably higher at lower exceedance probabilities due to its longer gage record and measurements prior to several flow alterations in the following decades.

Table 3 Probabilities of exceedance

	Discharge (cfs)			
Probability of Exceedance	08355050 Rio Grande At Bridge Near Escondida, NM (September 30, 2005 - present)	08355490 Rio Grande At HWY 380 Bridge Near San Antonio, NM (September 30, 2005 - present)	08358500 & 08358400 Rio Grande Bridge at San Marcial, NM (Jan 1, 1899-present)	08358400 Rio Grande Bridge at San Marcial, NM (September 30, 2005 - present)
1%	3900	3730	10800	3480
10%	1640	1600	3260	1340
25%	831	724	1150	638
50%	570	465	580	358
75%	170	83	170	53
90%	55	5	15	22

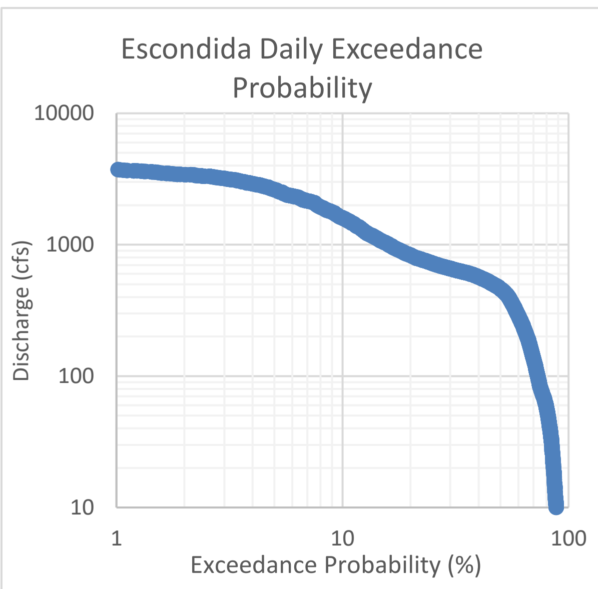

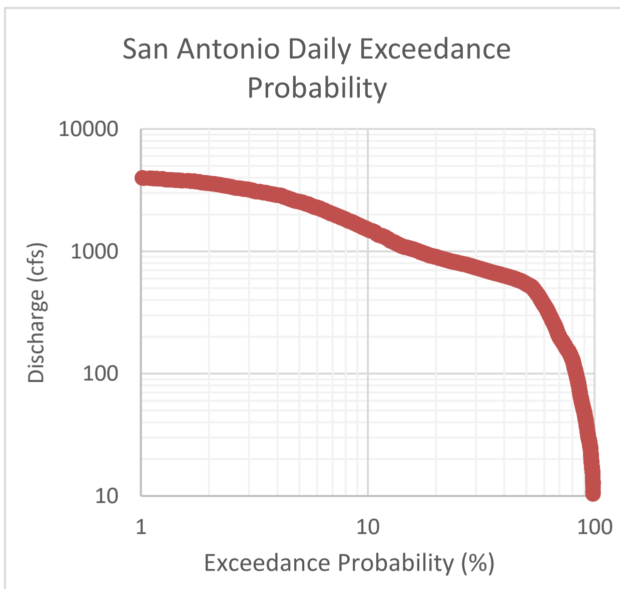

Figure 20: Flow duration curves for Escondida gage and the San Antonio gage

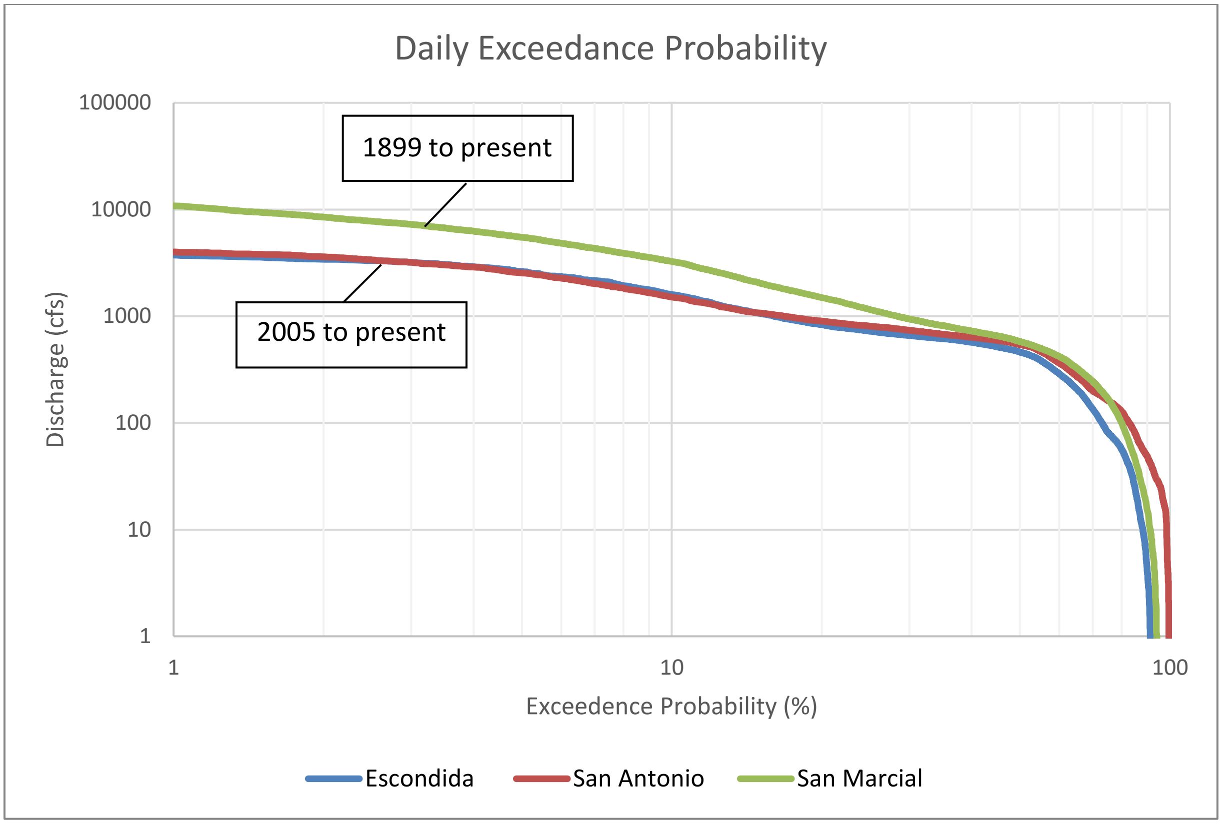

Figure 21: Comparison of flow duration curves. The Escondida and San Antonio Gage include data since the year 2005 and the San Marcial Gage includes data since 1899

In addition to flow duration curves, the number of days in the water year exceeding identified flow values at each gage was analyzed. This is purely a count of days and does not consider consecutive days. The analysis was performed for the entire record for both the Escondida and San Antonio gages. The data are displayed in Figure 22 and Figure 23, where a period of lower flow can clearly be seen from 2011 to 2013. The year 2013 seemed to exhibit the most varied flow regime with the highest number of low flow days below 500 cfs of any year, while also having the highest number of days with extreme high flows above 5000 and 6000 cfs. These high outlier values are associated with a monsoonal storm event that occurred in September of 2013. Remnants of two hurricanes pushed warm humid air north, which clashed with a cold front, resulting in heavy rainstorms throughout Colorado and New Mexico (Pinson et al., 2014). Figures 22 and 23 also show that the Escondida gage has at least a small amount of water in the channel year-round, whereas the gage at San Antonio has years that will go several months without any water.

Figure 24 shows the current US 380 gage data near San Antonio along with the data recorded at the inactive site in the 1950s. Although the record was relatively short, it appears that prior to the Cochiti dam and operation of the Low Flow Conveyance Channel, there were more days that exceeded 6000 cfs or higher discharge values in general.

Figure 25 shows the data for the San Marcial gage dating back to 1949. The figure highlights how severely low the discharge levels were at this location. From the 1960s to mid 1970s the channel was often dry for most of the year. After this period, more flow had returned to the channel in part due to flows provided by the San Juan-Chama project (Glasser, 1998) with still intermittent channel drying events such as in the early 1980s. Beginning in the late 2000s, larger discharges had become less frequent, however channel drying events had also become less frequent.

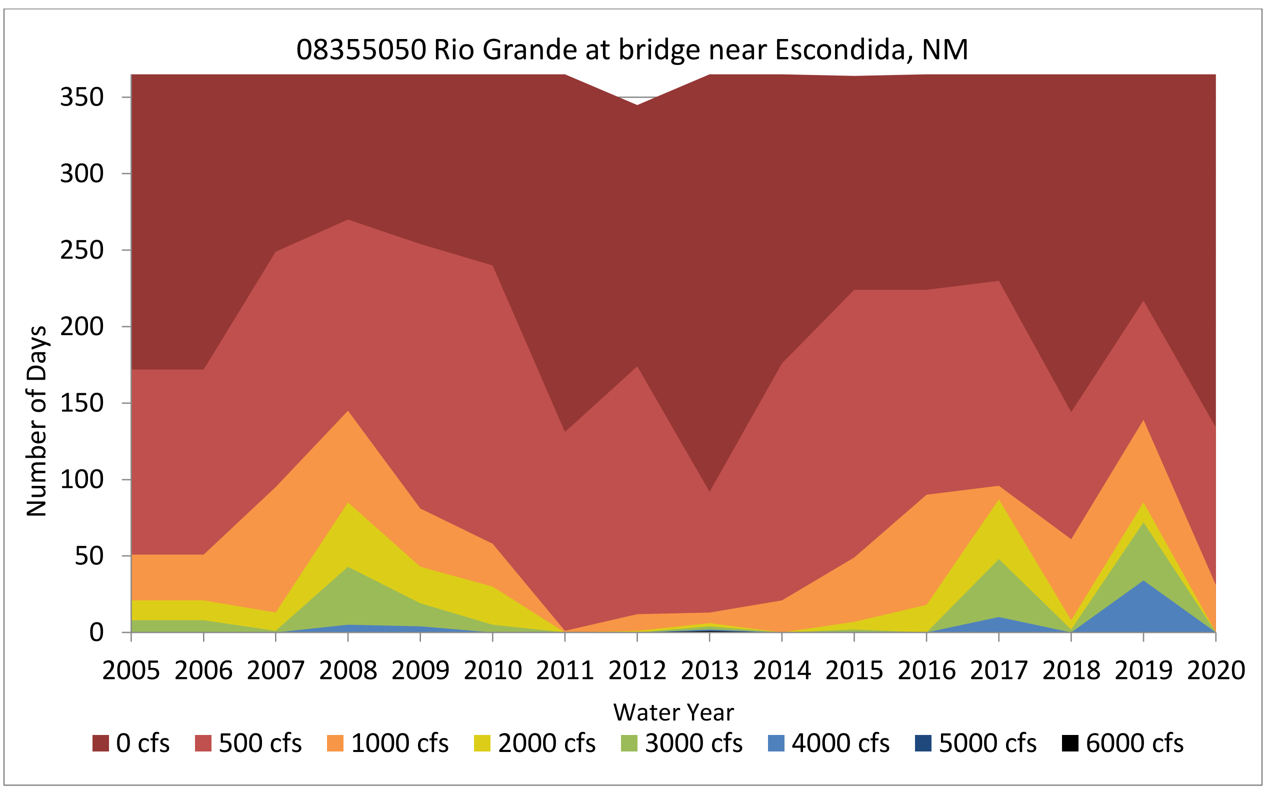

Figure 22: Number of days over an identified discharge at the Escondida gage

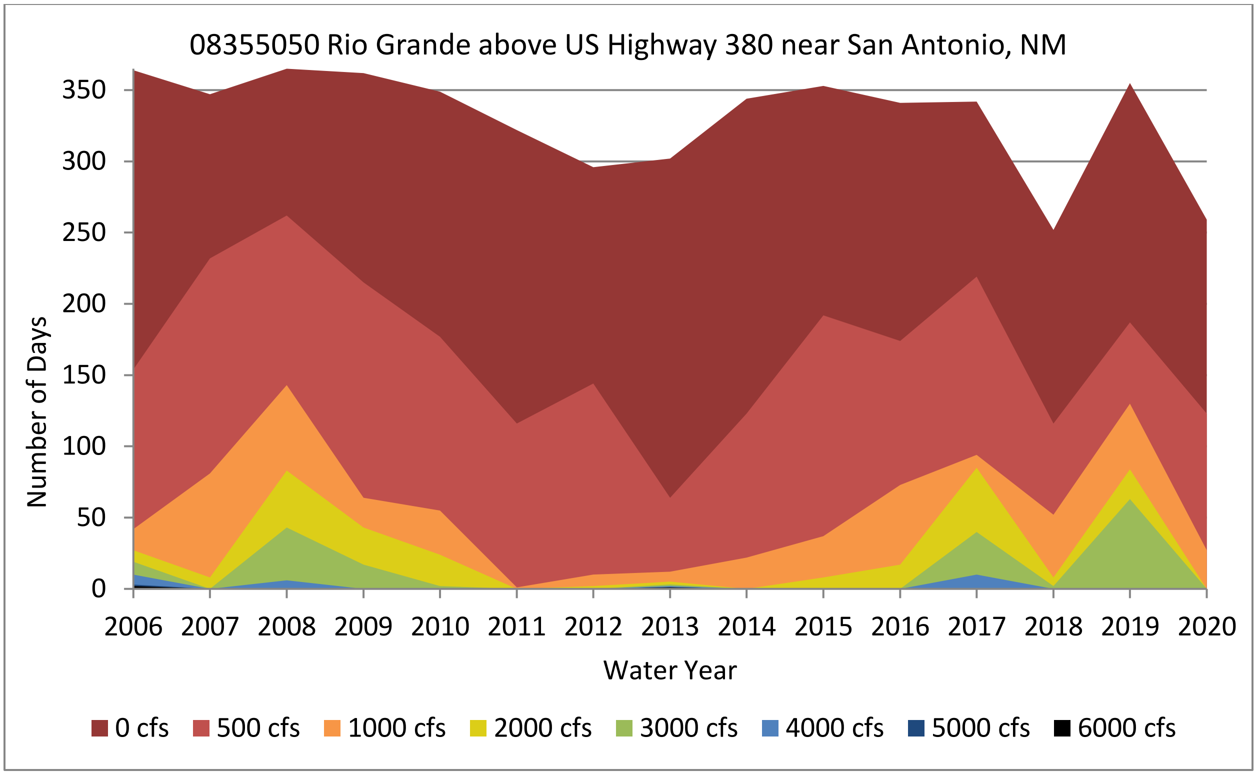

Figure 23: Number of days over an identified discharge at the HWY 380 gage

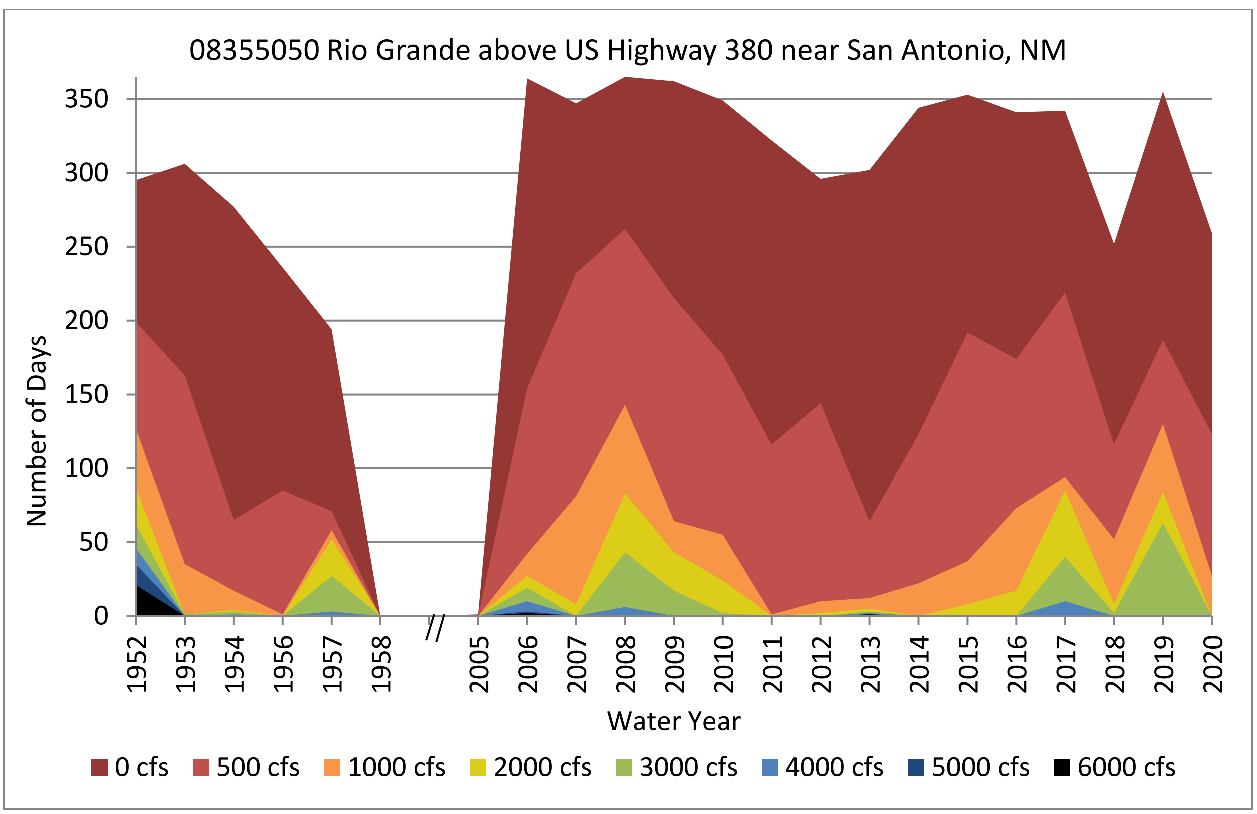

Figure 24: Number of days over an identified discharge at the HWY 380 gage including historical gage data

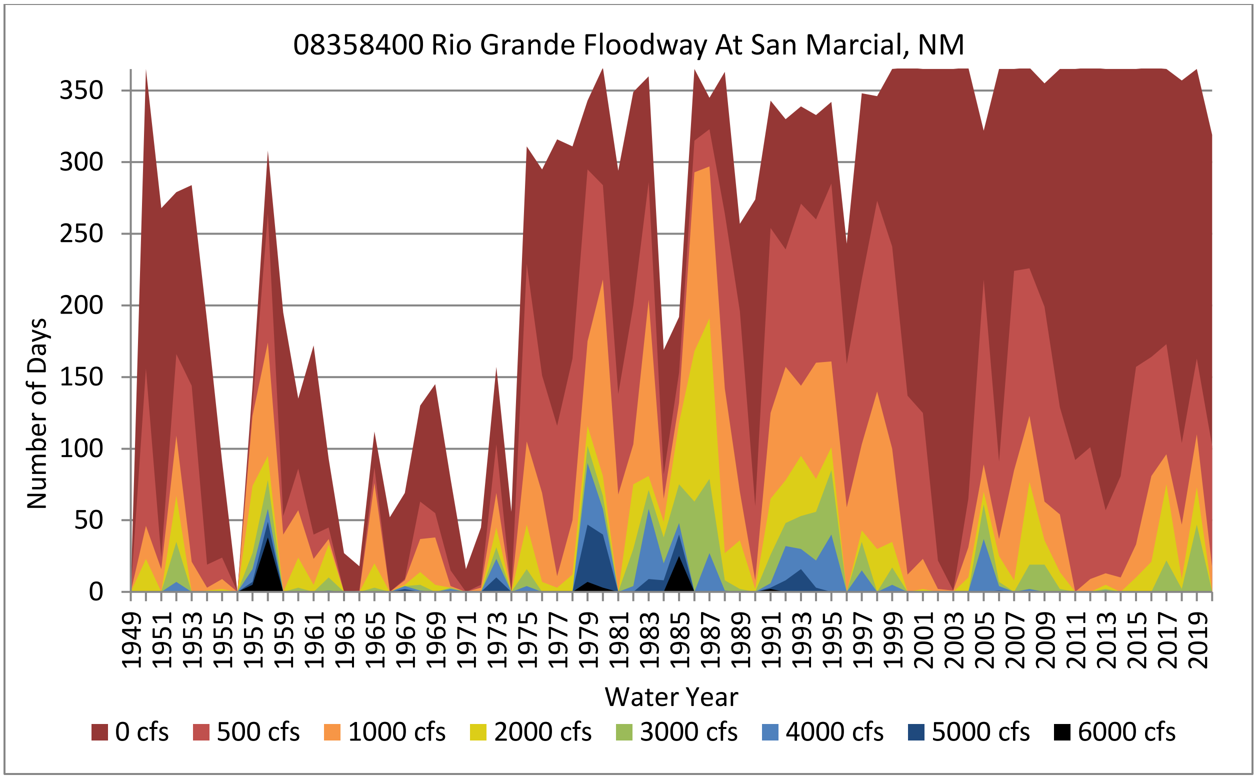

Figure 25: Number of days over an identified discharge at the San Marcial gage

2.3 Suspended Sediment Load

2.3.1 Mass Curves

Single mass curves of cumulative suspended sediment (in millions of tons) at the San Antonio gage and the San Macrial gage are shown in Figure 26 and 27 respectively. Data comes from the USGS gage near US HWY 380 in San Antonio, NM (08355490) and the USGS gage at the Rio Grande Floodway at San Marcial, NM (08358400). There is no sediment monitoring at the USGS gage at Escondida. For the San Antonio single mass curve, the analysis was performed in water years beginning in 2011, when the collection of suspended sediment data began. The dashed line was created using the same technique as the previous cumulative discharge plot. A one-week moving average was used to determine the 97.5th percentile of slope changes. If a slope change is greater than this value, a point is created along the line indicating a time with one of the greatest increases in sediment transport.

The breaks in slope along the single mass curve show the changes in sediment flux. As previously determined from the cumulative discharge plot in Section 2.2.1, the large increases in flow in the Bosque del Apache reach occurred in the spring from snowmelt, with some increases in the summer from seasonal thunderstorms. However, the cumulative sediment discharge curve shows that the greatest increases in sediment occur during the monsoonal storms that occur in the summer. The monsoonal event mentioned earlier is seen by the large increase in suspended sediment in September of 2013. The second largest increase in sediment flux occurred as a result of a series of heavy thunderstorms in the summer of 2014.

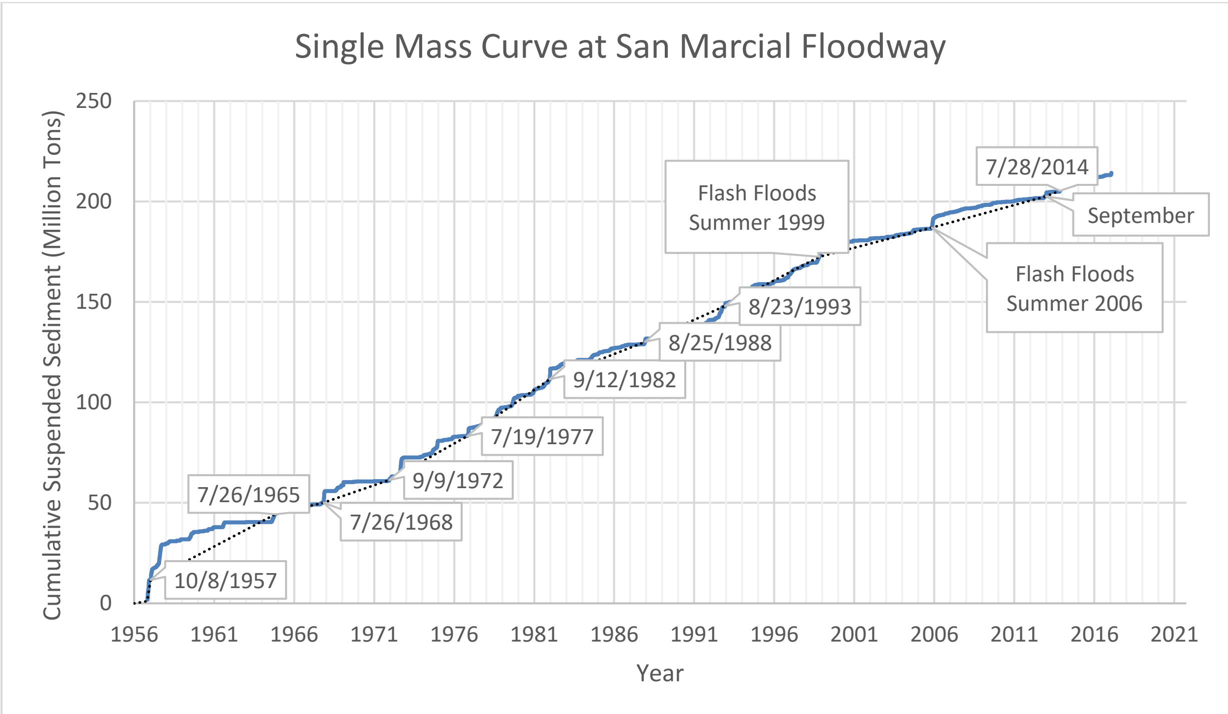

Figure 26: Suspended sediment discharge single mass curve for US 380 Bridge USGS gage Near San Antonio, NM

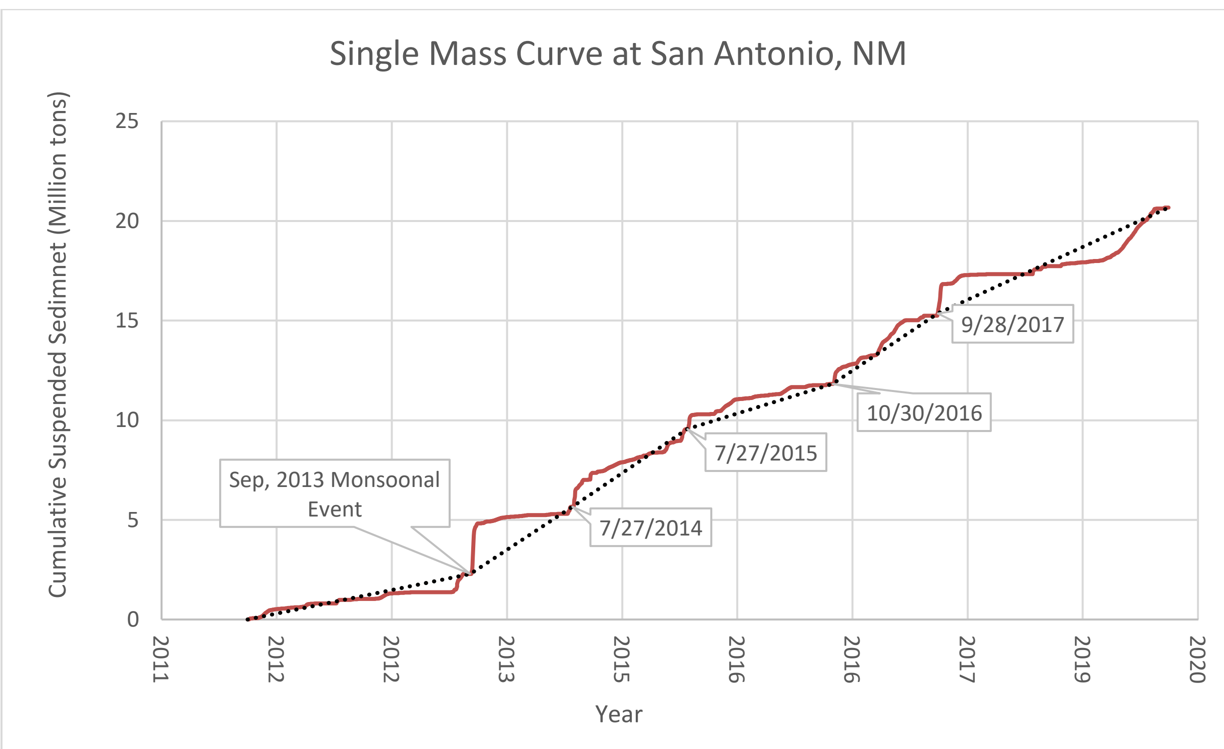

Figure 27: Suspended sediment discharge single mass curve for Rio Grande Floodway at San Marcial, NM

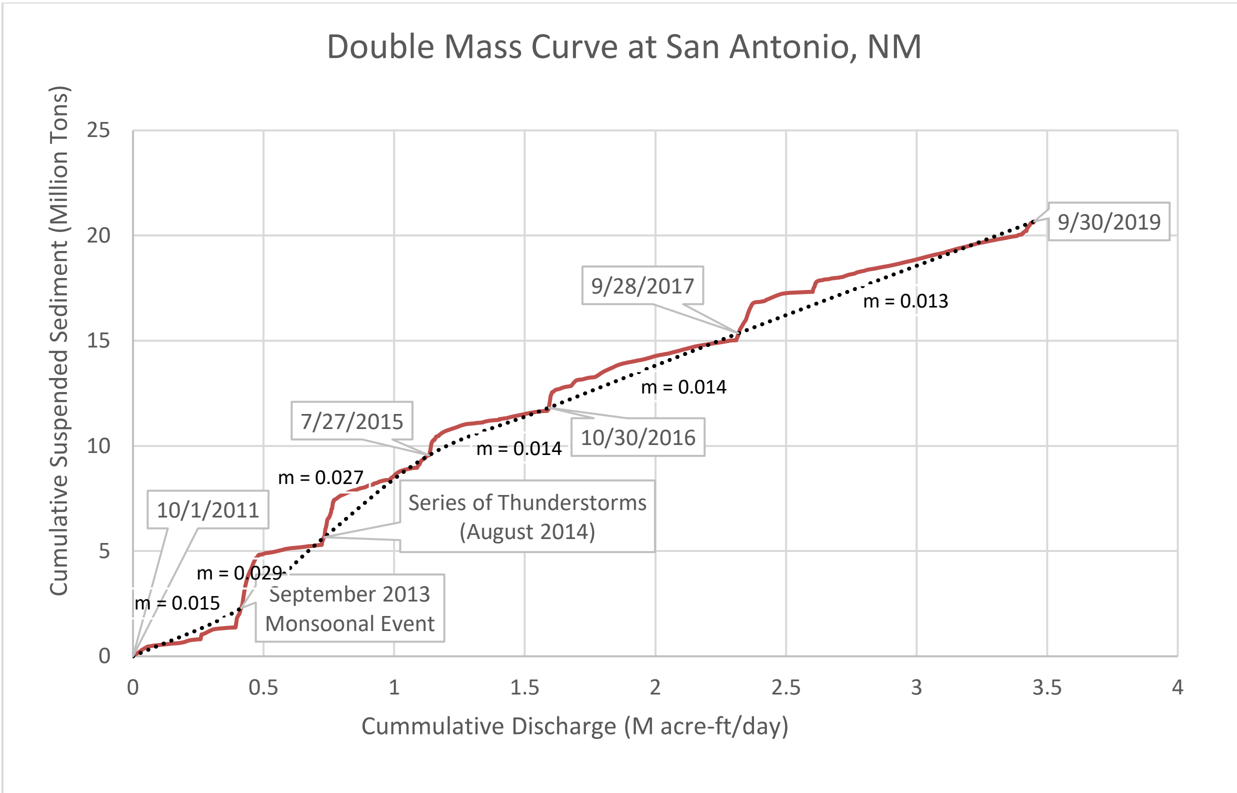

Figure 28: Double mass curves show how suspended sediment volume relates to the daily discharge volume. The slope of the double mass curve represents the mean sediment concentration. Slopes 'm' of dotted lines are in units of (tons of sediment) / (Acre-ft of water/year)

The double mass curve in Figure 28 is for USGS gage at San Antonio (08355490). The greatest changes in cumulative sediment load with respect to cumulative discharge typically occur during the summer months between June and September when thunderstorms are more prevalent, indicating that the thunderstorms have a greater impact on sediment load than the spring snowmelt. Figure 29 relates the cumulative average monthly suspended sediment at the San Antonio gage to the cumulative precipitation at the Lemitar gage to further demonstrate the effects of monsoon-related sediment transport. A steeper slope indicates that there was an increase in suspended sediment with very little change in the cumulative discharge. Specific monsoon events can clearly be seen in the figure, such as the monsoonal event from August 2013 to September 2013 and a series of thunderstorms from July 2014 to August 2014. These events impact the suspended sediment in the Bosque del Apache reach.

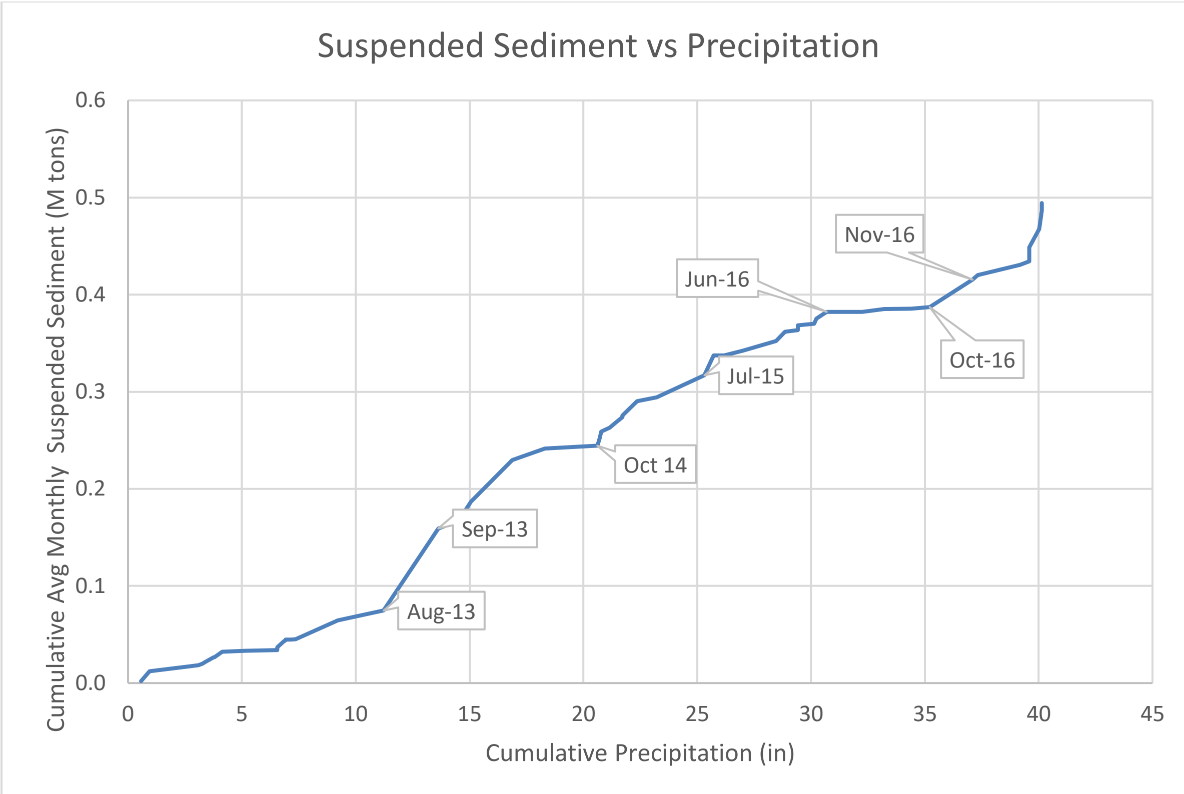

Figure 29: Cumulative suspended sediment (data from the US 380 gage at San Antonio, NM) versus cumulative precipitation at the Lemitar gage.

2.3.2 Monthly Sediment Variation

A plot of monthly average discharge and suspended sediment was created for the San Antonio gage to help reveal any important seasonal trends. Figure 30 and Figure 31 show the seasonal trends of suspended sediment load and concentration, respectively, along with the discharges that correspond with the years. As seen previously, although the spring snowmelt brings some of the larger discharge volumes, the increased flows from the intense thunderstorms or monsoon seasons are what transport the most sediment. Figure 32 is the cumulative suspended sediment plotted on an annual basis. When represented in this way, the annual patterns of sediment discharge become more obvious. From this plot, it appears that large quantities of suspended sediment are transported in the summer months between June and September. A SEMEP analysis of total sediment load in the MRG can be found in Appendix B.

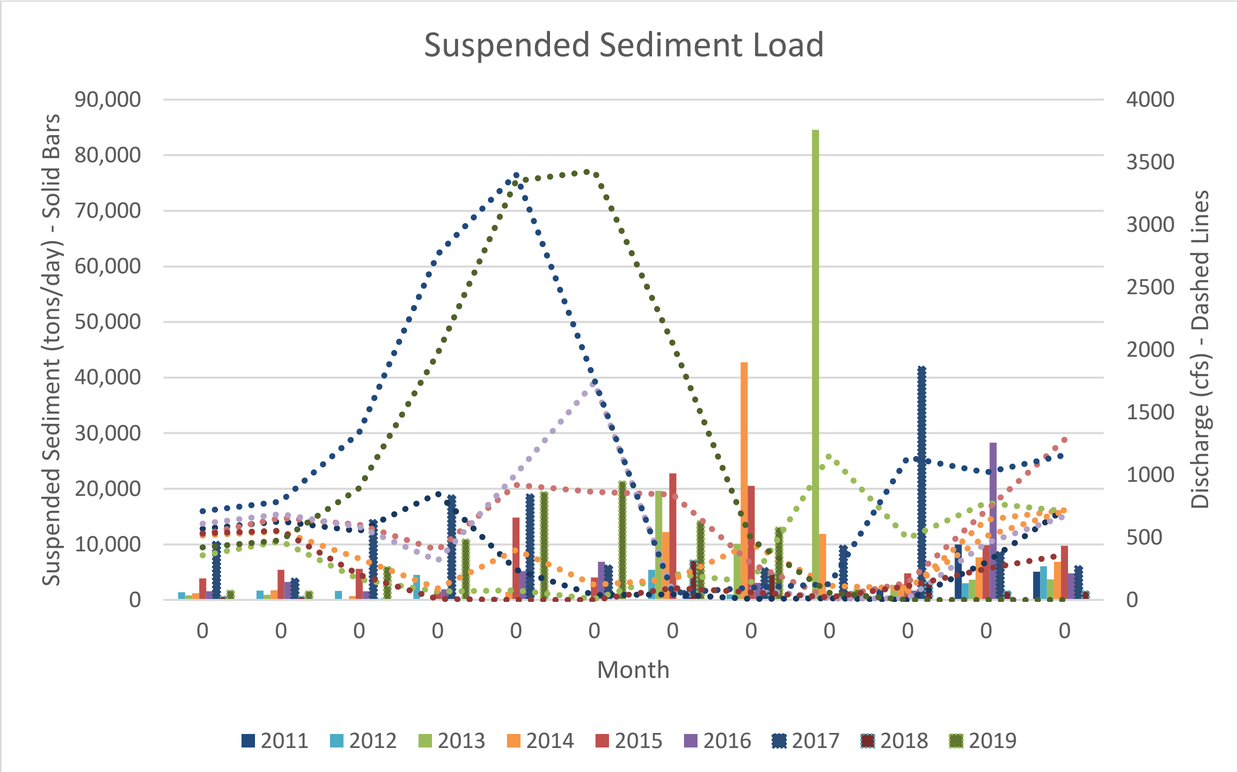

Figure 30 Monthly average suspended sediment and water discharge. Discharge and Sediment data from the HWY 380 gage.

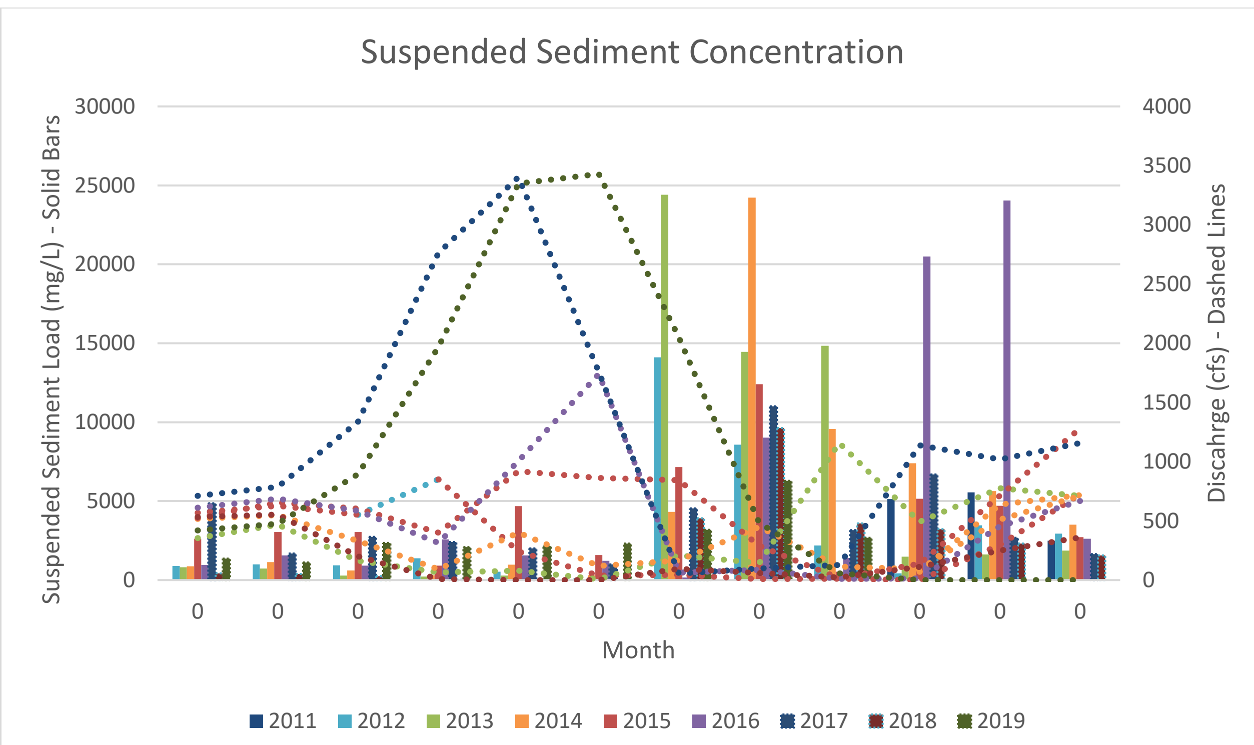

Figure 31 Monthly average suspended sediment concentration and water discharge. Discharge and Sediment data from the HWY 380 gage.

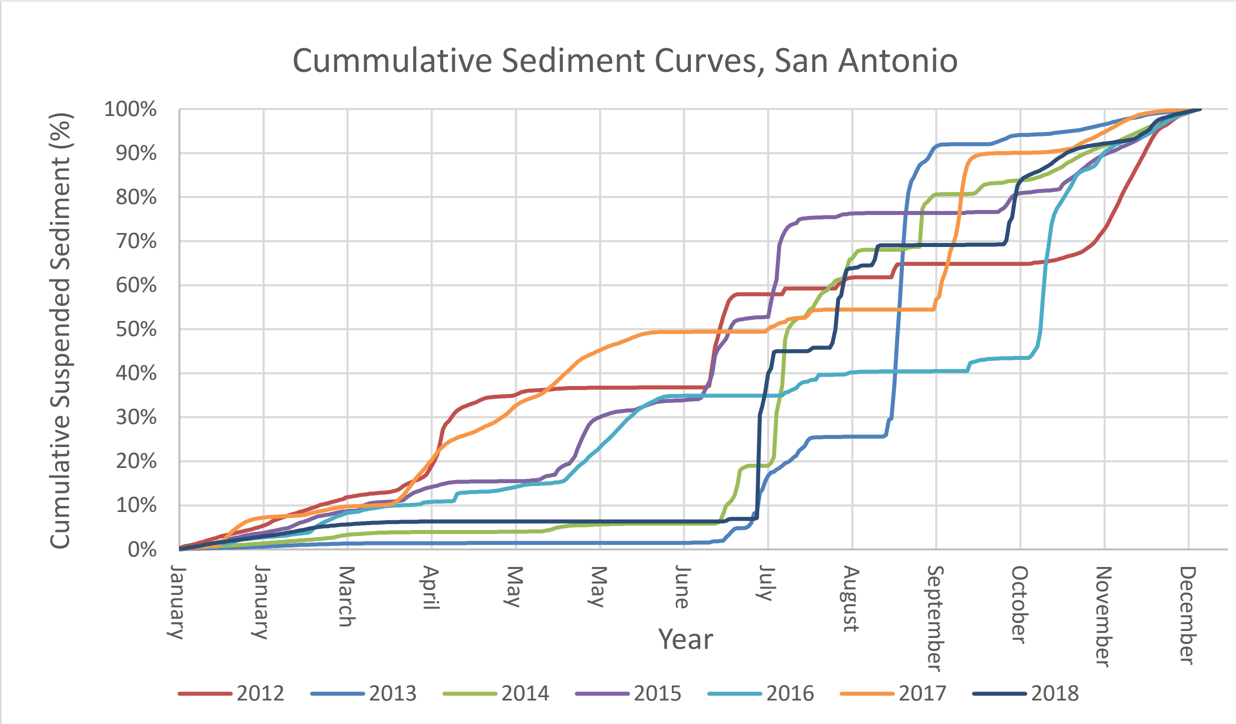

Figure 32 Cumulative annual suspended sediment at the San Antonio gage.

3. River Geomorphology

3.1 Wetted Top Width

Wetted top width can provide significant insight into at-a-station hydraulic geometry. Typically, wetted top width in a compound channel would slowly increase as discharge values increase until there is a connection with the floodplain. At this point, the top wetted width would quickly increase as the water spills onto the floodplains. Then, a gradual increase in width would continue. Analysis of the wetted top width can be used to help understand bankfull conditions and how they vary spatially and temporally in the Bosque del Apache reach. A HEC-RAS model was created to analyze a variety of top width metrics. Starting at 500 cfs and increasing incrementally until 10,000 cfs, the top width analysis was conducted for the years with available cross-sectional data: 1962, 1972, 1992, 2002 and 2012.

Figure 33 and Figure 35 show the moving cross sectional averaged top wetted width at 1,000 cfs and 3,000 cfs from the HEC-RAS model results. The top width shown at each agg/deg line comes from the moving average from five consecutive cross sections: the identified agg/deg line, two upstream agg/deg lines, and two downstream agg/deg lines. Figures 33 and 34 show the cumulative widths through the reach at discharges of 1,000 cfs and 3,000 cfs respectively.

From Figure 33 all subreaches appear to have lost variation in wetted top width from 1962 to 2012 and have instead become more uniform, measuring approximately between 300 and 500 feet wide at 1,000 cfs.

This flow generally represents the width of just the main channel, as the floodplain did not become activated in a majority of the reach. Historically, subreach B3 had the highest variation in its mean width at a range of approximately 780 ft (870 ft to 80 ft) in 1962, but in 2012 this range had decreased to 190 ft (525 ft to 335 ft). A potential explanation for this dramatic difference between 1962 and 2012 is channelization efforts that occurred after 1962. The most dramatic recent shift has been seen in subreach B5, which saw an increase of approximately 200 feet in average width between 2002 and 2012. Additional figures from this analysis can be found in Appendix C, including plots with the corresponding top width for each agg/deg line rather than the moving average.

In Figure 34, the trends explained in Figure 33 are also demonstrated cumulative width plot. In this figure, a steeper slope represents a wider channel, a flatter slope represents a narrower channel, and a constant slope represents an unchanged width. 1962 still varies the most frequently and at a largely magnitude than other years. By 2012 the slope of the line is almost constant, representing an almost uniformly wide channel.

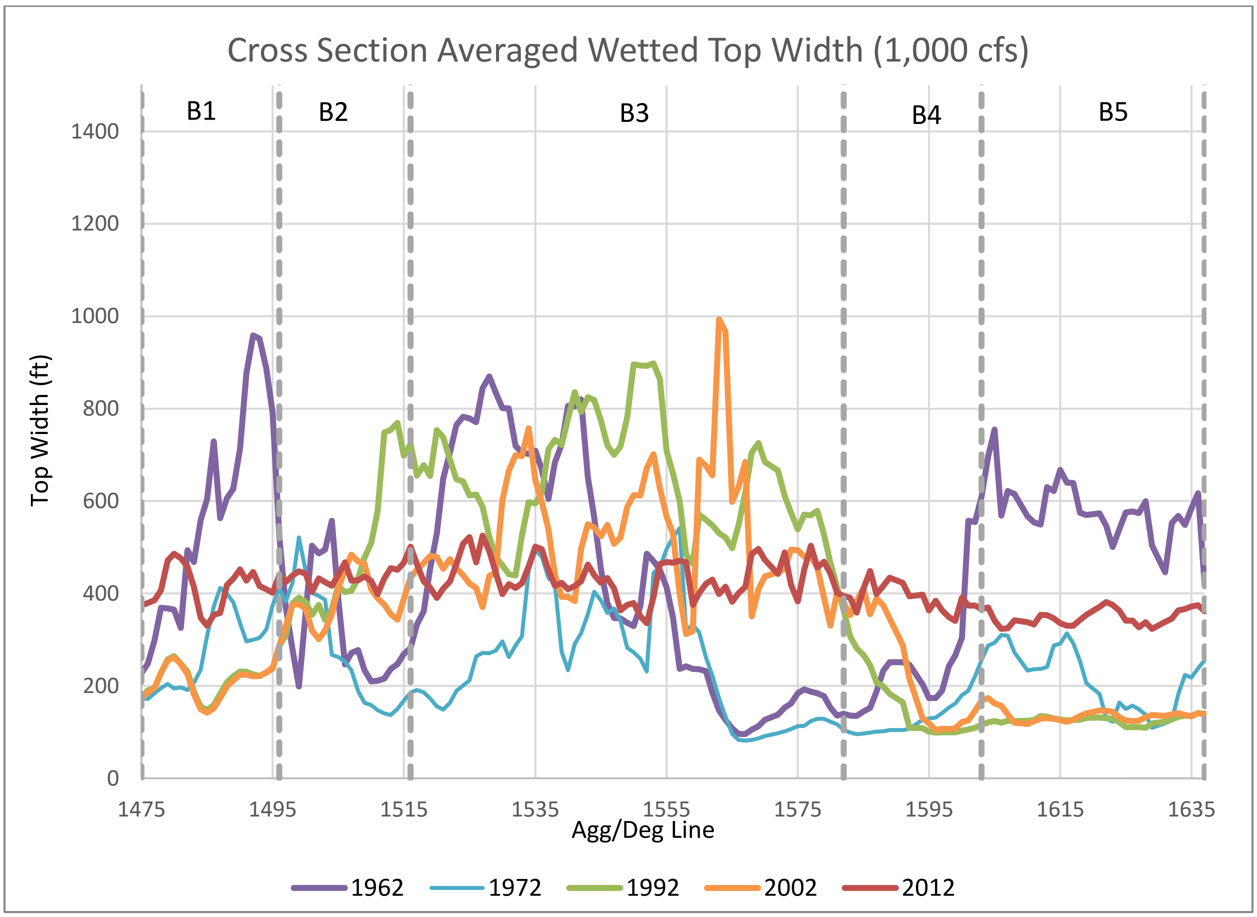

Figure 33 Moving cross sectional average of the wetted top width at a discharge of 1,000 cfs

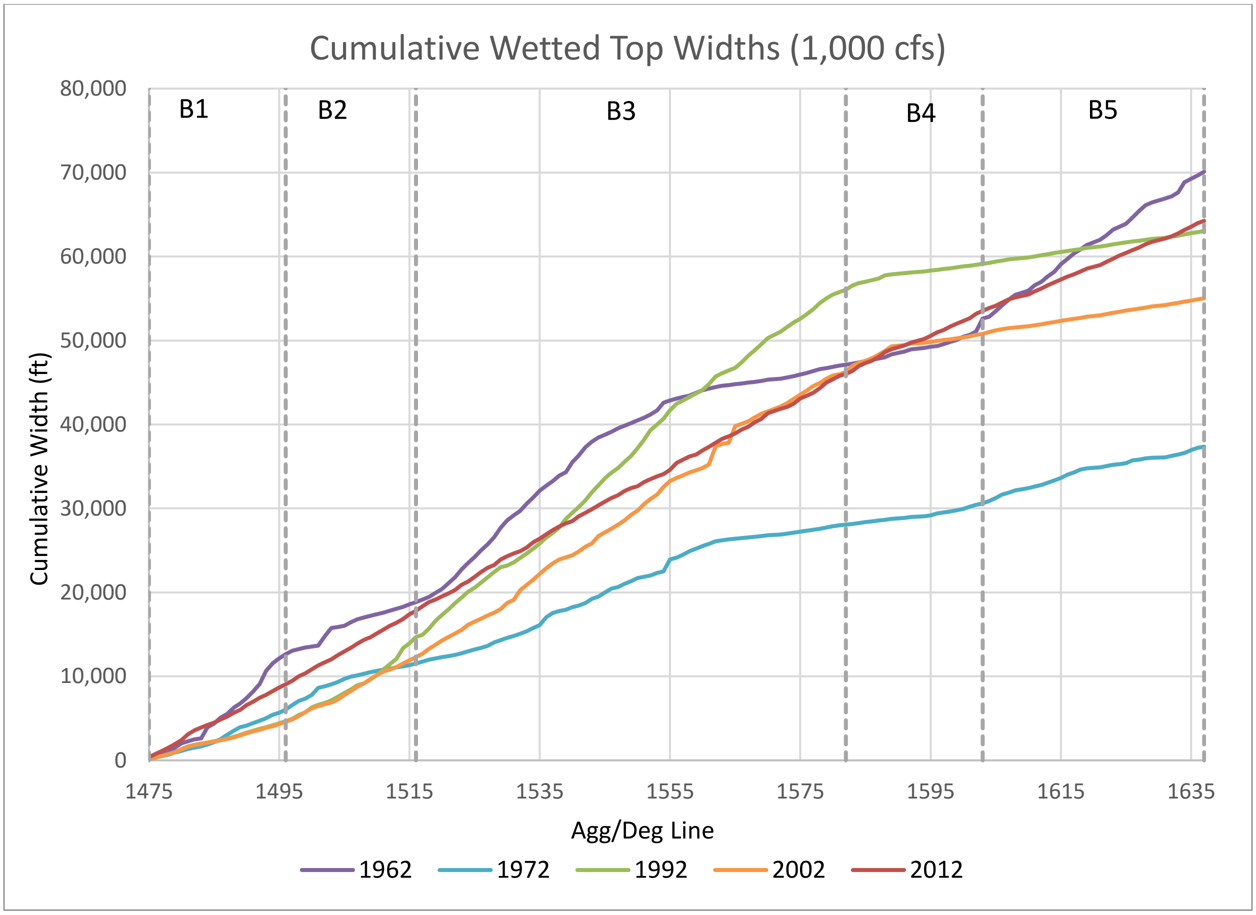

Figure 34 Cumulative wetted top widths at a discharge of 1,000 cfs

In Figure 35, 3000 cfs generally represents the flow within the Bosque del Apache reach at which bankfull is exceeded and the floodplain is activated. In all subreaches, especially subreaches B1, B2, and B4 there appears to have been a net increase in wetted top width between 1962 and 2012. Most notably, the width of the wetted area at 3,000 cfs fluctuates widely for each subreach (>1000 ft variation). This effect could be the result of large amounts of channel perching found in each subreach combined with the limitations of the 1D modeling. In reality, the transition between varying widths of the channel would be smoother.

In Figure 35, the trends explained in Figure 36 are now demonstrated cumulative width plot. In this figure, a steeper slope represents a wider channel, a flatter slope represents a narrower channel, and a constant slope represents an unchanged width. Compared to Figure 34, all the cumulative width plots for 3,000 cfs are more uniform in slope. As described above, 3,000 cfs likely represents a discharge in which overtopping of the banks occurs and the floodplains are inundated. What this means is that relative variation between main channel widths is higher than the variation in the overall width of the floodplain corridor.

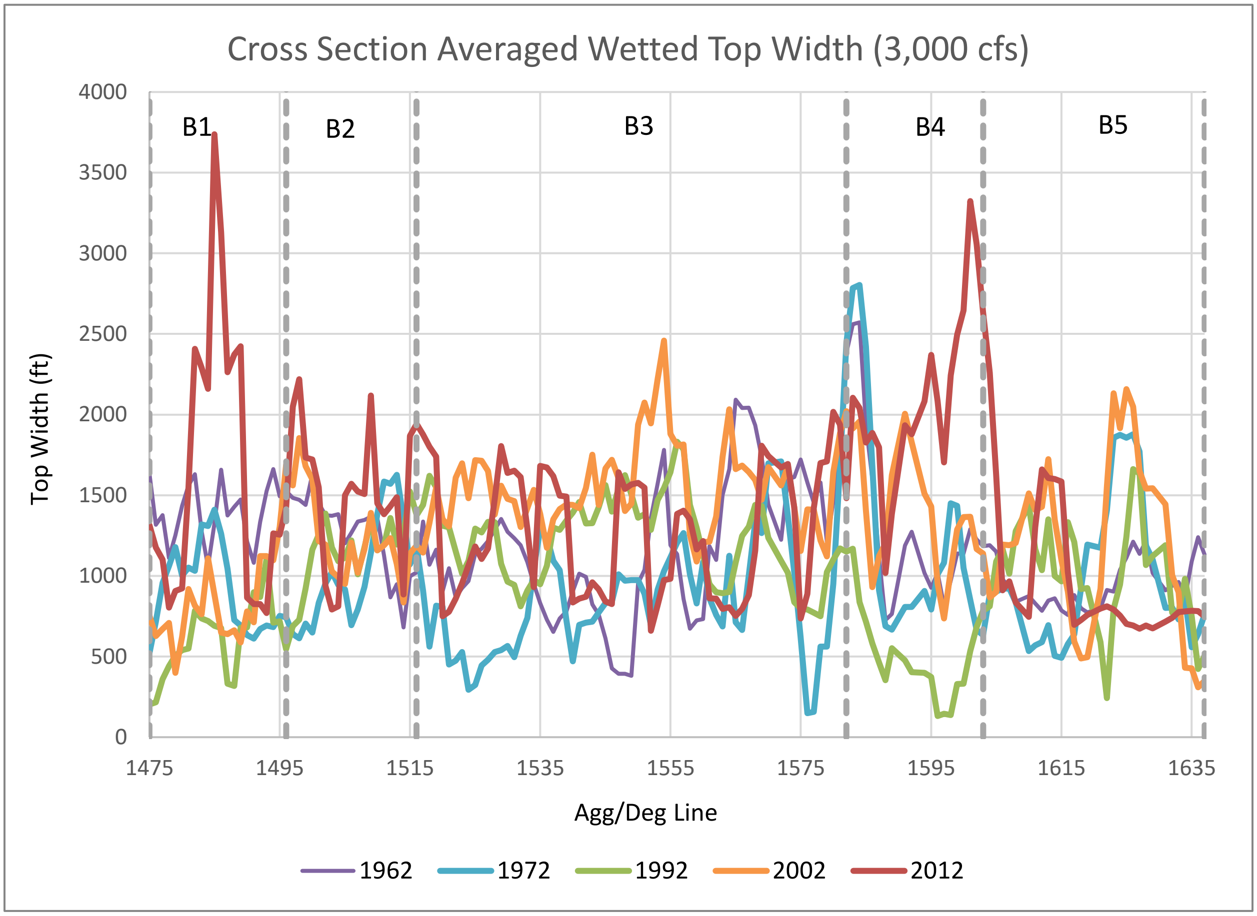

Figure 35 Moving cross sectional average of the wetted top width at a discharge of 3,000 cfs

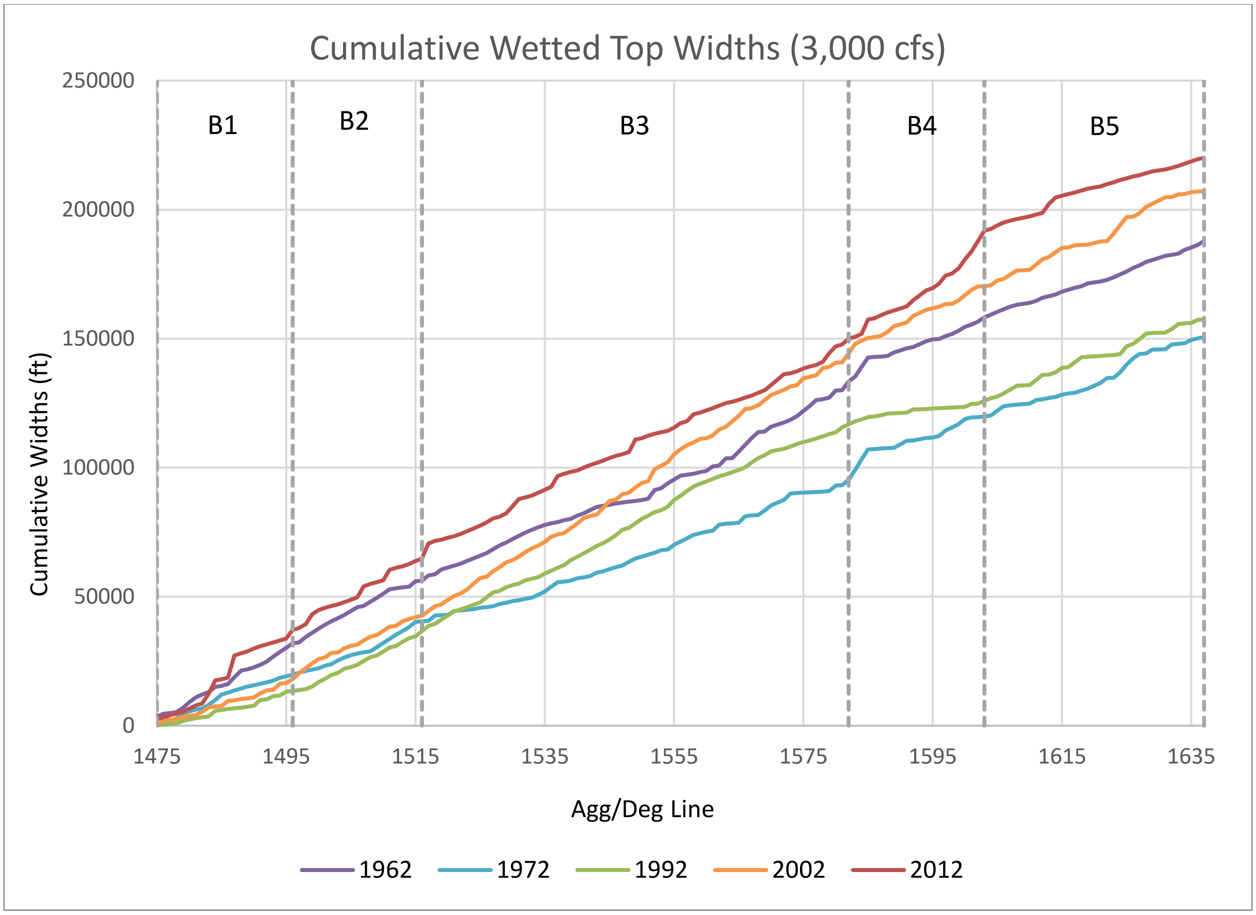

Figure 36 Cumulative wetted top widths at a discharge of 3,000 cfs

The average top width for each subreach was also plotted for the years analyzed in Figure 37 for discharges up to 5,000 cfs. The average top width decreased the most in subreach B1 between 1962 and 1992. Generally, the top widths decreased in all subreaches with the exception of subreach B4, which saw a decrease in width in 1992 and then an increase in width. In most subreaches, 2012 represented the lowest or the second lowest channel widths on record.

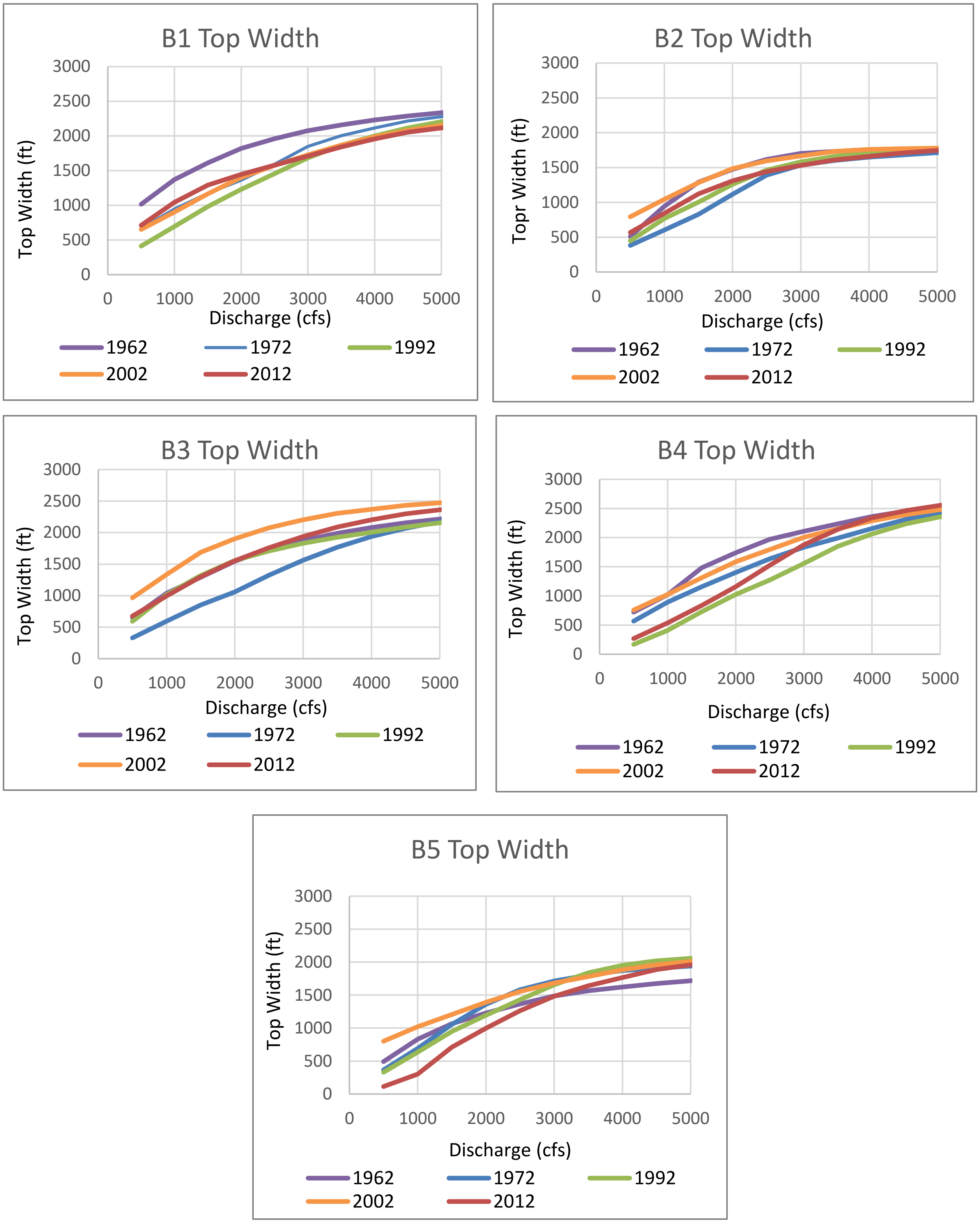

Figure 37: *Average top width for B1 (top left), B2 (top right), B3 (middle left), B4 (middle right), and B5 (bottom) at discharges 500 to 5,000 cfs*

3.2 Width (Defined by Vegetation)

The width of the active channel, defined as the non-vegetated channel, was found by clipping the agg/deg line to the width of the active channel polygon provided by Reclamation's GIS and Remote Sensing Group. The widths of the active channel agg/deg lines were exported from ArcMap for each agg/deg line. Then the average width of each subreach was calculated by averaging the width of all agg/deg lines within the subreach. Aerial photographs and accompanying digital shapefiles were provided for years 1918, 1935, 1949, 1962, 1972, 1985, 1992, 2001, 2002, 2006, 2008, 2012, 2016, and 2019. The results are shown in Figure 38.

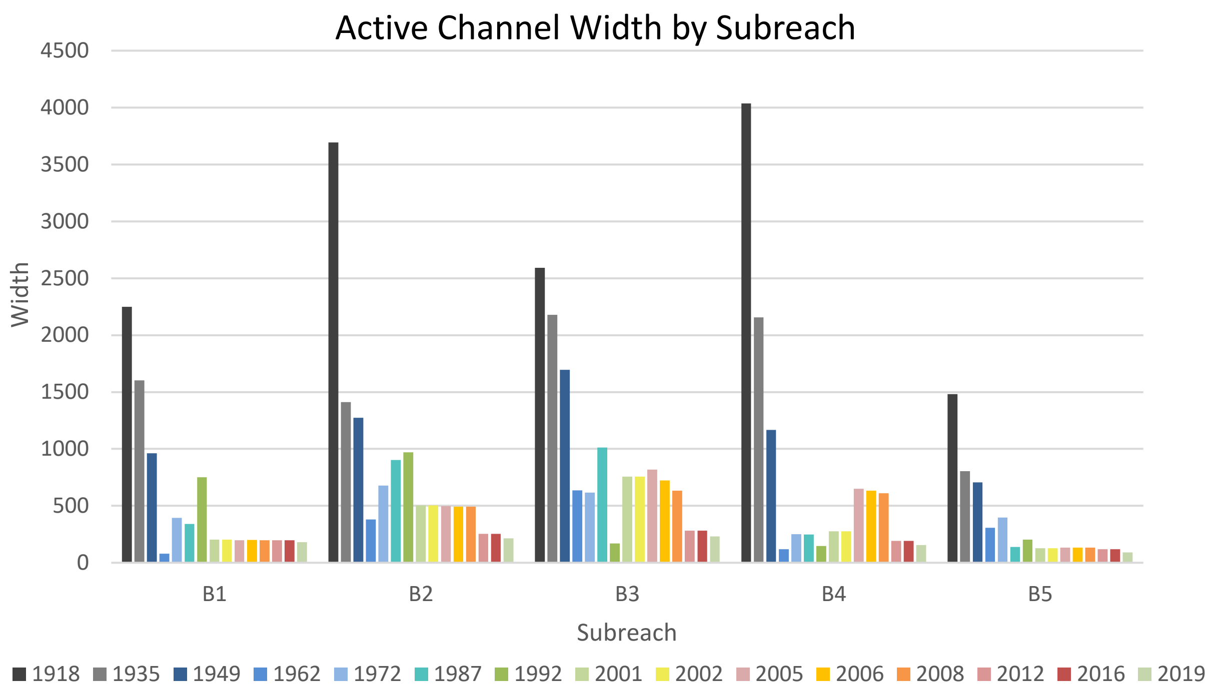

Figure 38 Averaged active channel width by subreach

Throughout the time period of available aerial imagery, the active channel width decreased dramatically, greater than an order of magnitude in difference between 1918 and 2019 for all subreaches. Figure 38 shows that the active channel width in all subreaches was the greatest in 1918 before a sharp decrease in width in the following years. During this time, a reduction in spring/summer baseflows from agricultural diversions in addition to changes in land use such as grazing lead to a dramatic decline in the active channel width of the river between 1918 and 1949 (Scurlock, 1998). An extended period of drought beginning in the 1940s and installation of jetty jacks in the 1950s resulted in additional narrowing of the active channel (Scurlock, 1998). Upstream dams and reservoir storage also lead to a decrease in peak flows throughout this time period. Furthermore, installation of the Low Flow Conveyance Channel reduced the discharges in the Rio Grande by diverting the flow from the 1960s to the 1980s, further decreasing the width as seen in Figure 38. Mowing operations cleared vegetation along the river banks from the 1960s to the 1980s (and into the early 1990s in various locations along the MRG), which played a part in a slight widening of the river between 1972 and 1985, in addition to the increased flows as the period of drought came to an end and operation of the Low Flow Conveyance Channel was stopped

(Makar, 2006). After another period of severe drought from the late 1990s to the late 2000s (though this drought is still on-going), the active channel width of the river has decreased once again and has since remained stable.

3.3 Bed Elevation

The minimum channel bed elevation is used to evaluate the change in the longitudinal profile of the Bosque del Apache reach. The bed elevation of the channel comes from an estimate generated by HEC-RAS, which is based on the discharge and the water surface elevation on the day of the aerial photography. Cross sectional data for 2012 was derived from LiDAR mapping (Varyu, 2013). While the minimum channel elevation points may not be exact, the overall trends can still be identified throughout the Bosque del Apache reach. The minimum channel elevation was obtained at each cross-section from the HEC-RAS geometry files to generate a plot of the bed elevation throughout the reach, as seen in Figure 39.

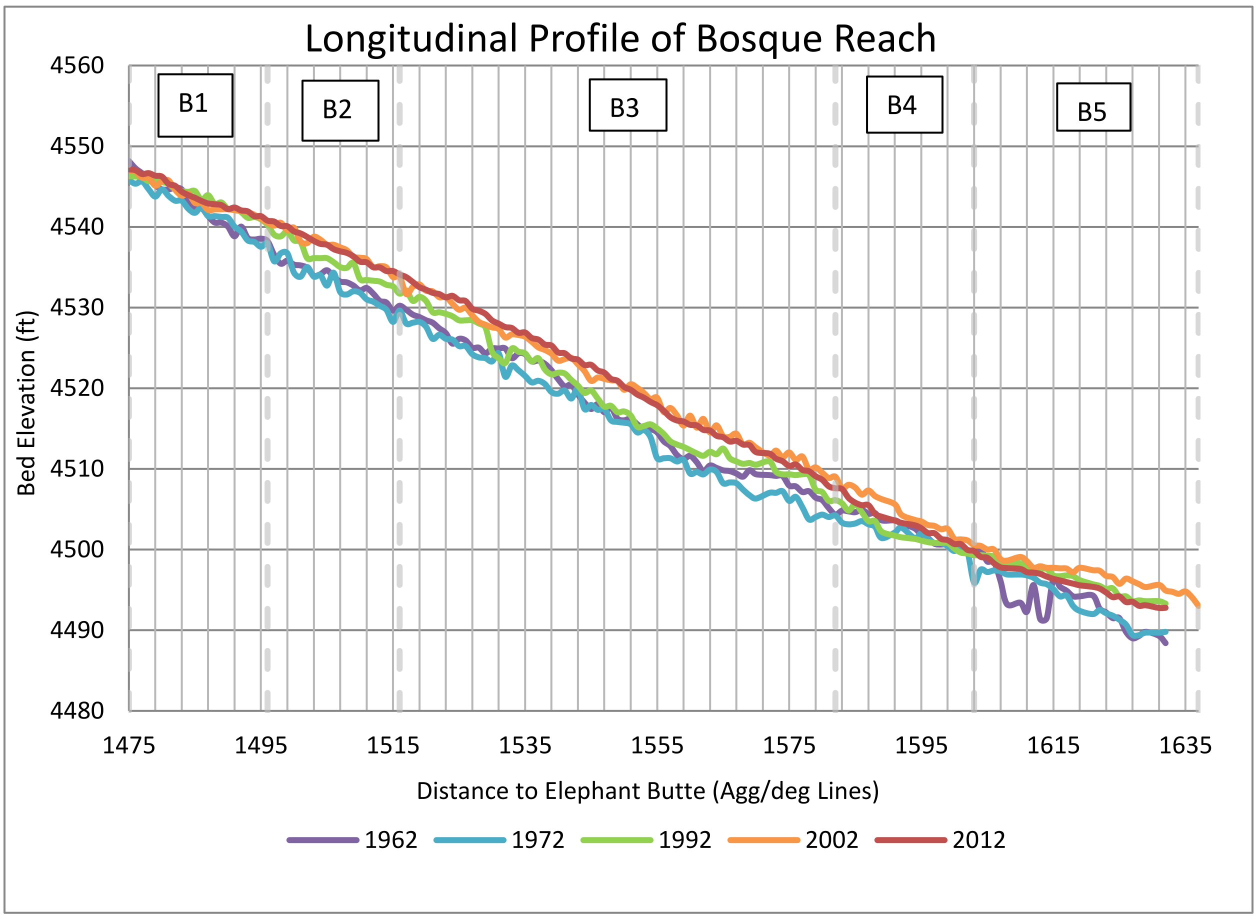

Figure 39 Longitudinal profiles of bed elevation

As shown in Figure 39, the Bosque del Apache reach has shown net aggradation in subreaches B1, B2, and B3 from 1962 to 2012 though these subreaches have undergone cycles of both aggradation and degradation throughout this time period. This deposition of sediment at the upstream end of the Bosque del Apache subreach is consistent with a previous report by Beckwith, which focused on the Escondida reach, just upstream of the Bosque del Apache reach. In their report, the erosion in the upstream portion of the Ecsondida reach had supplied sediment for deposition in the downstream portion of the Escondida reach (Beckwith, 2020). This depositional trend continues into the upstream portion of the Bosque del Apache reach. Figure 39 also shows that between 2002 and 2012 the bed surface elevation has remained stable in subreaches B1, B2, and B3, with small amounts of deposition occurring in 2012 at the end of B3. From subreach B2 to midway through B3, the recent bed surface profile appears to have formed a crown-shaped (convex) profile, which may indicate a local reduction in sediment transport capacity. In subreaches B4 and B5 there is a net trend of aggradation between 1962 and 2012 or lesser magnitude compared to other subreaches, with the filling of deep pool sin subreach B5. Midway through subreach B4 (Agg/Deg Line 1592 to 1606) the bed surface elevation appears to be more stable. This stretch of stable reach appears to occur downstream of two large bends in Subreach 4. After this section the bed elevation becomes more dynamic again as it approaches the end of B5.

Figure 40 shows the main channel aggradation and degradation of each subreach, which was found by first finding the average minimum channel elevation for each subreach and then subtracting the average bed elevation of the earlier year from the later year. A positive number indicates aggradation, and a negative number indicates degradation. This figure visualizes a direct comparison of trends in bed elevation between time intervals within individual subreaches. Both 1962-1972 and 2002-2012 were generally periods of degradation in all subreaches with exceptions in B1, B2 and B5, whereas 1972-1992 and 2002-2012 were periods of aggradation in all subreaches with exception to B1.

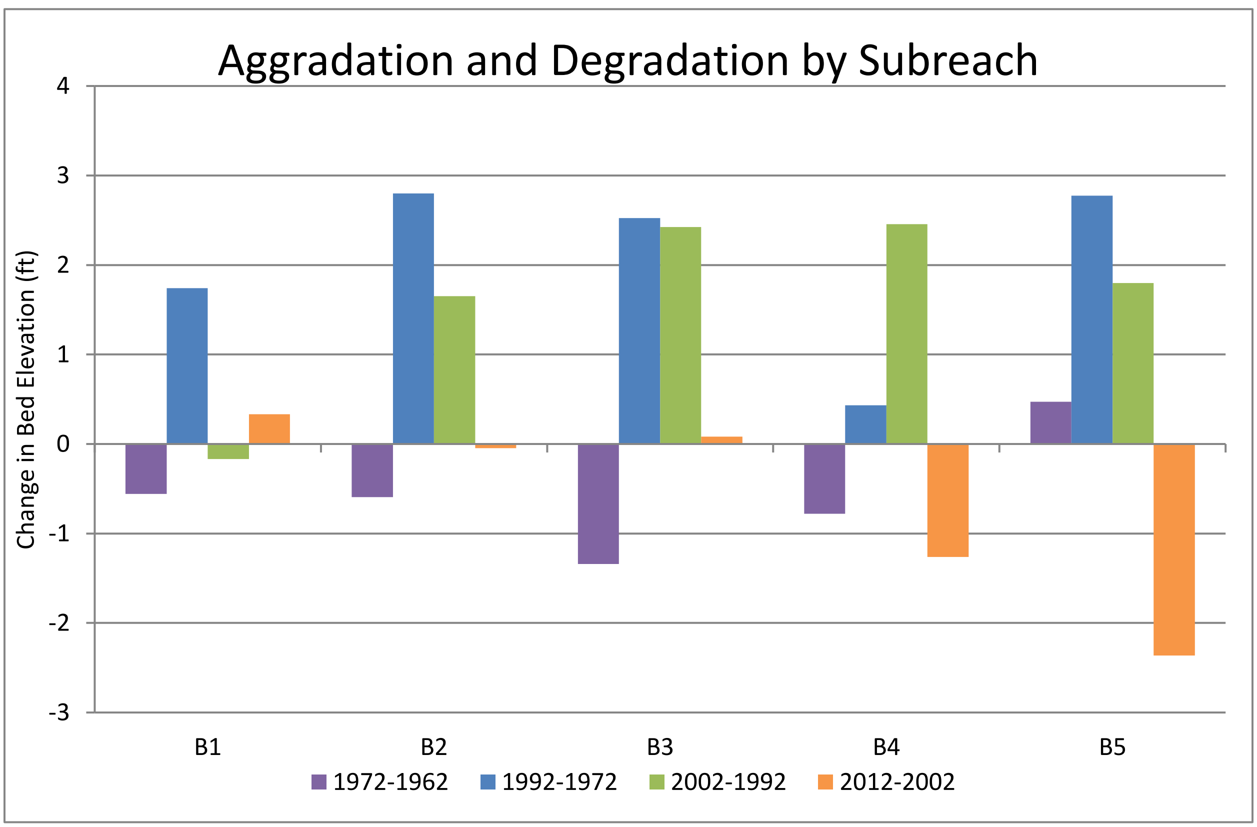

Figure 40 Degradation and Aggradation by subreach

3.4 Bed Material

Bed material samples were collected at various rangelines in the channel. There are bed material samples available for analysis of the Bosque del Apache reach from the years 1990 to 2016. Figure 41 shows the median grain diameter of each sample versus the distance upstream of Elephant Butte Reservoir.

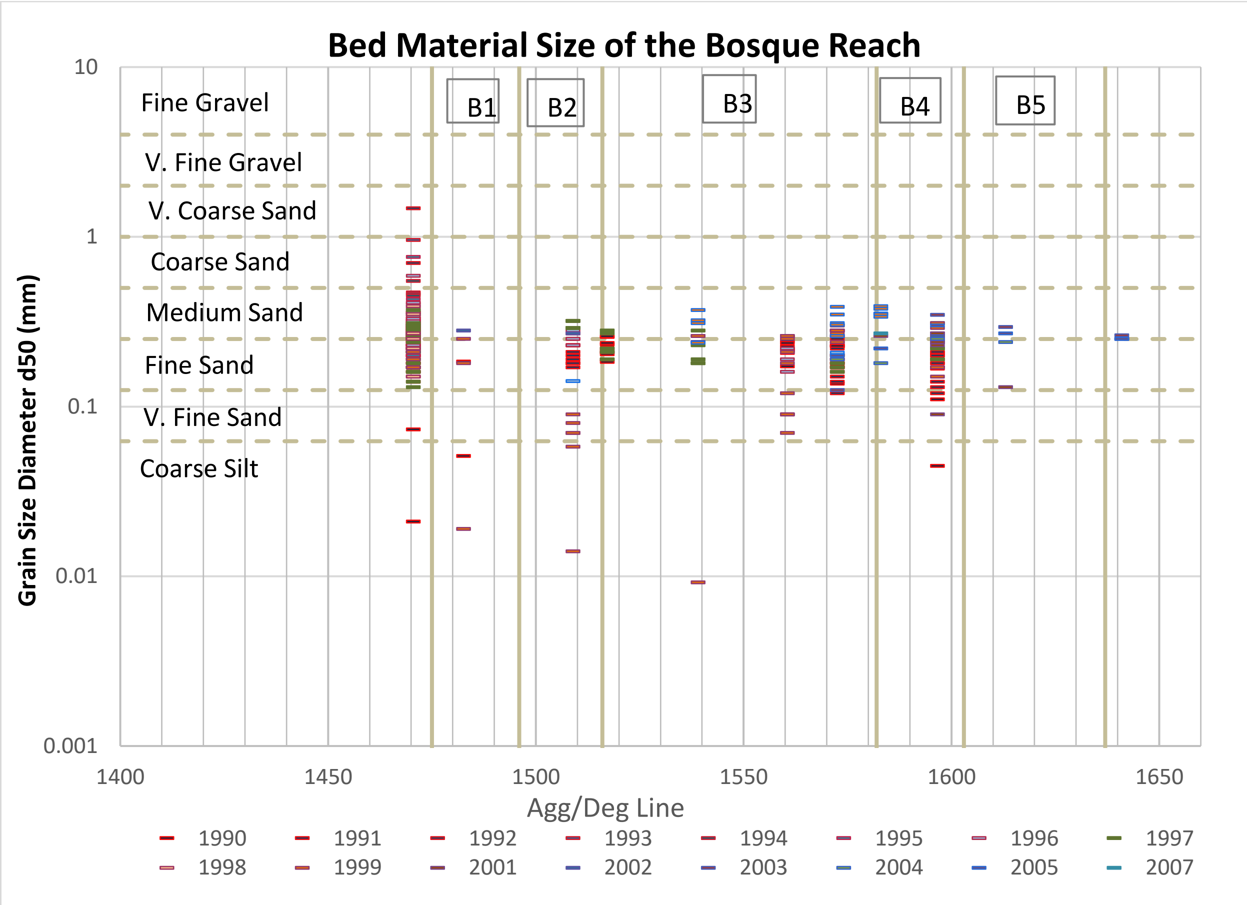

Figure 41 Median grain diameter size of samples taken throughout the Bosque reach

Throughout the reach the median diameter size of the samples is typically between 0.1 millimeter and 1 millimeter. These grain size diameters correspond with classifications of fine sand to coarse sand, emphasizing that the Bosque del Apache reach of the MRG is a sand-bed river.

3.5 Sinuosity

The sinuosity was calculated at each subreach using digitized channel centerlines provided by Reclamation's GIS and Remote Sensing Group. Aerial photographs and accompanying digital shapefiles were provided for the years 1918, 1935, 1949, 1962, 1972, 1985, 1992, 2001, 2002, 2006, 2008, 2012, 2016, and 2019. To analyze the sinuosity of each subreach, the centerlines were split at each subreach boundary. Then, for each subreach, the length of the centerline (channel length) was divided by the valley length (end of centerline to end of centerline) to get the sinuosity value. The results of this analysis are presented in Figure 42.

In subreaches B1, B2, and B5, the channels today exhibit low levels of sinuosity (about or below 1.05). While subreach B1 appears to have maintained the same sinuosity since 1918, B2 and B5 exhibit large declines in sinuosity occurring between 1918-1962 before remaining relatively straight up to 2019. Subreach B3 interestingly showed an increase in sinuosity between 1918-1949 before declining during 1962-2005, and then increasing back to around a sinuosity of 1.13. Subreach B4 is the most sinuous subreach in the Bosque del Apache reach and displayed trends opposite of B1, B2, and B3. In 1918 subreach B4 was almost straight with a sinuosity close to one, then between 1992 and 2005 the sinuosity increased dramatically and has remained moderately high up to 2019.

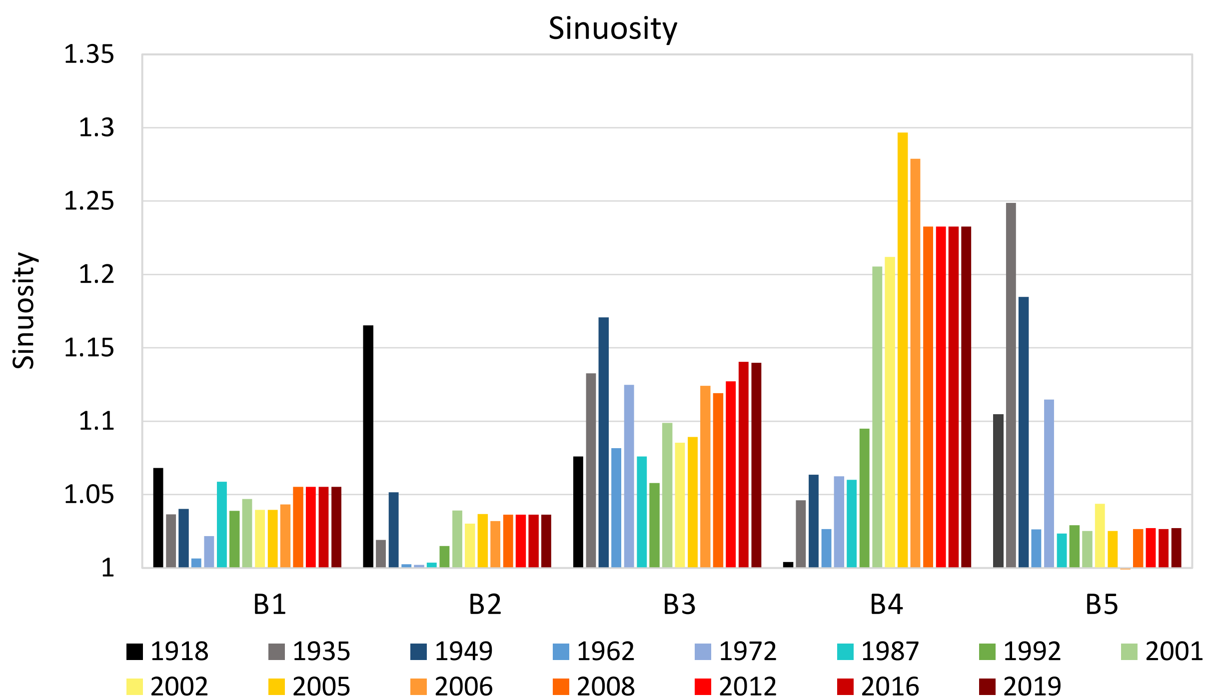

Figure 42 Sinuosity by subreach

3.6 Hydraulic Geometry

Flow depth, velocity, width, wetted perimeter of the main channel, and bed slope are obtained using HEC-RAS 5.0.3 with a discharge of 3,000 cfs, which was selected based on the fact that this discharge represents bankfull conditions with limited likelihood of overbanking (LaForge et al., 2019 and Yang et al., 2019). A discharge of 3,000 cfs has a daily exceedance of 3.7% at the upstream end of the Bosque del Apache reach, a relatively uncommon flow. Therefore, the same hydraulic geometry variables were also analyzed for a discharge more commonly seen in this reach: 1,000 cfs, which has a daily exceedance of about 16%. For the plots of the hydraulic geometry variables, the values were averaged by subreach.

The HEC-RAS results (Figure 43) show a decrease in the wetted top width from the years 1962 to 1972 due to the divergence of flow into the Low Flow Conveyance channel and a period of drought, which matches the findings from section 3.2 Width (Defined by Vegetation). Figure 43 also shows a slight increase in width for most of the Bosque del Apache reach between 1972 and 2002 at 1000 cfs, which is likely from increased discharge values in the MRG and the mowing operations that cleared vegetation along the banks of the MRG. At 3000 cfs 1972 and 1992 demonstrate a similar trend of decreasing widths before increasing by 2002. Between 2002-2012 almost all subreaches again experience a decrease in top width. Generally, all subreaches demonstrate net trends of decreasing top widths over the period of interest, with B1 and B5 representing the greatest decreases.

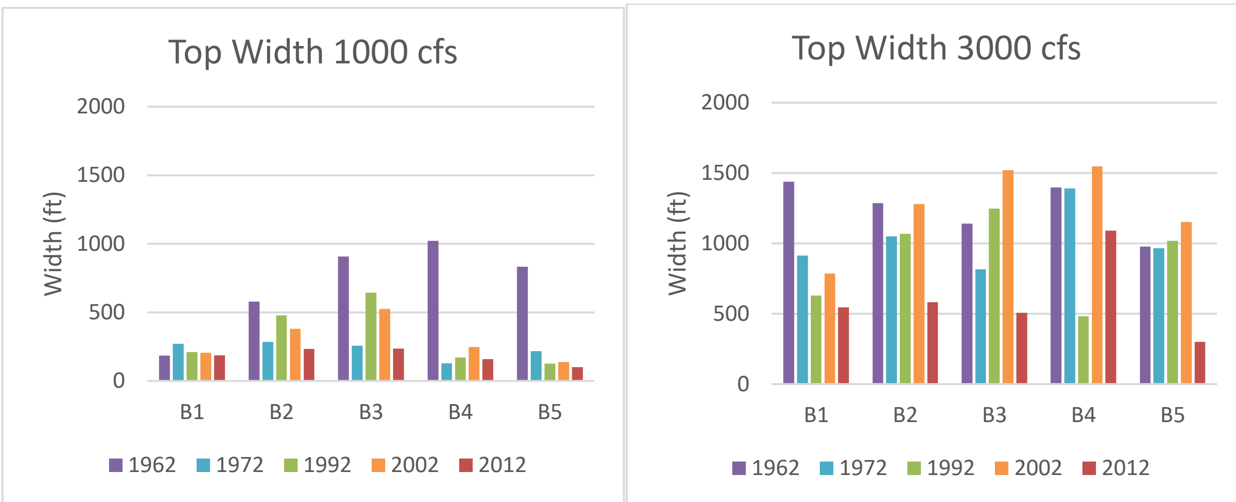

Figure 43 HEC-RAS Wetted top width of channel at 1,000 cfs (left) and 3,000 cfs (right)

Because the upstream end of the Bosque del Apache reach is narrowing, an increase in flow depth would be expected. Figure 44 shows the HEC-RAS calculated hydraulic depths (the cross sectional area divided by wetted perimeter) at discharges of 1,000 cfs and 3,000 cfs. Subreaches B1 and B5 show the greatest increase in hydraulic depth between 1962 and 2012, which corresponds with the decrease in widths. All subreaches appear to generally exhibit trends of increasing hydraulic depth, though subreaches B2, B3, and B4 do exhibit fluctuations in depth between 1972 and 2002 rather than consistent trends. At 1000 cfs, subreaches B2, B3, and B4 has a low range of variation in depth whereas subreach B5 has a larger range of variation.

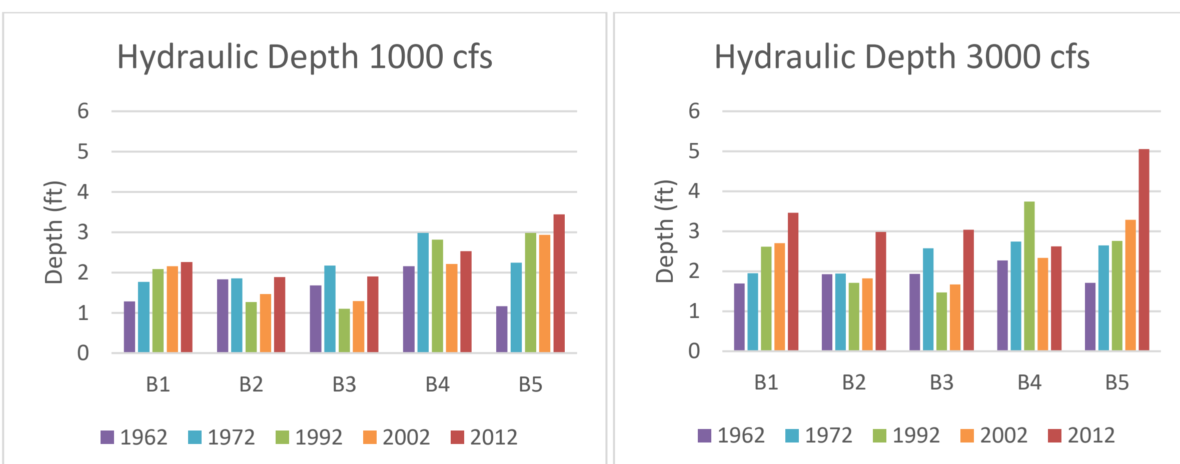

Figure 44 HEC-RAS Hydraulic depth at 1,000 cfs (left) and 3,000 cfs (right)

Figure 45 shows one cross section in Subreach B5. This example shows that although the main channel has aggraded, the banks have aggraded as well. In the downstream end of subreach B5, several cross sections have exhibited this pattern in which the banks are aggrading faster than the main channel, which is another factor leading to an average increase in the hydraulic depth and decrease in width. In the specific cross section shown (Figure 45), it is possible excavation of a sediment plug could explain recent lowering of the main channel bed elevation.

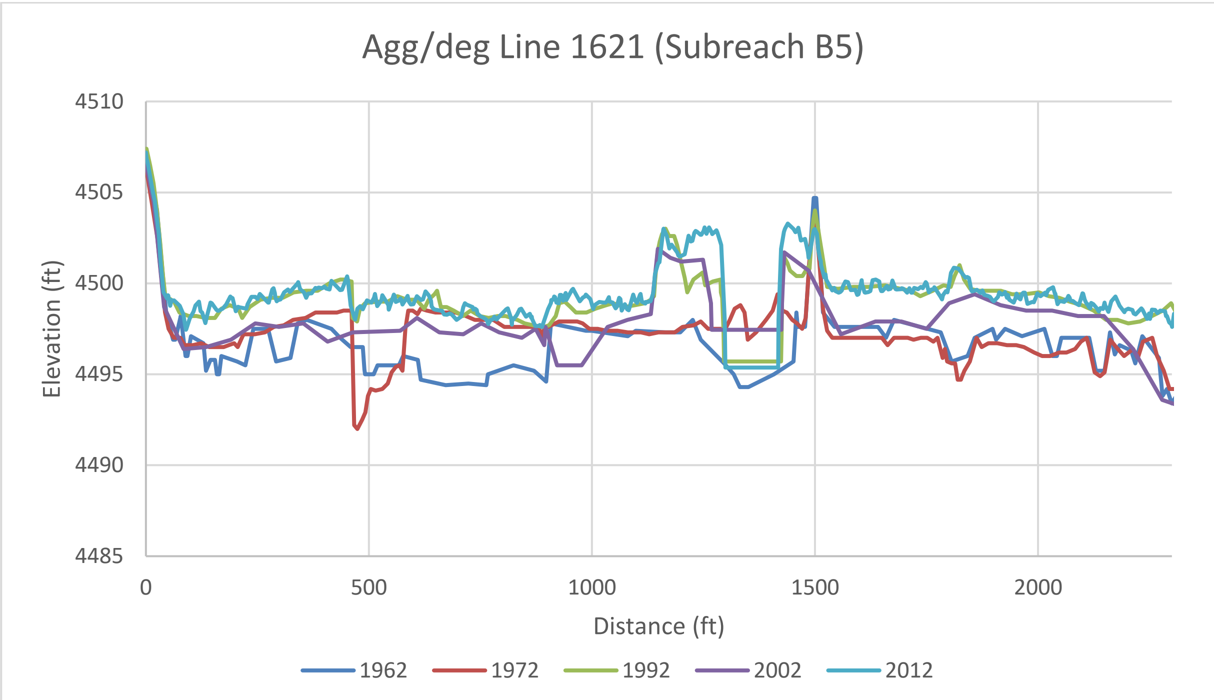

Figure 45 Example cross section indicating that the banks are aggrading in addition to the main channel bed. On average, throughout the reach, there was also a decrease in top wetted width.

The wetted perimeter of the main channel was also obtained from HEC-RAS for each of the years analyzed, as shown in Figure 46. Generally, the wetted perimeter follows a similar trend to the top width before the flood plain is activated. The wetted perimeter obtained is specifically for the main channel and so in instances in which the flood plain is activated, the top width value is much larger than the wetted perimeter. This can be seen in subreach B1 in 1962 at 3000 cfs. Subreaches B1 and B5 exhibit large decreases in wetted perimeter of the main channel between 1962 and 2012 whereas subreaches B2 and B3 exhibit a peak in wetted perimeter in 1992. Subreach B4, shows fluctuations in wetted perimeter from 1962-2012 with no obvious trend.

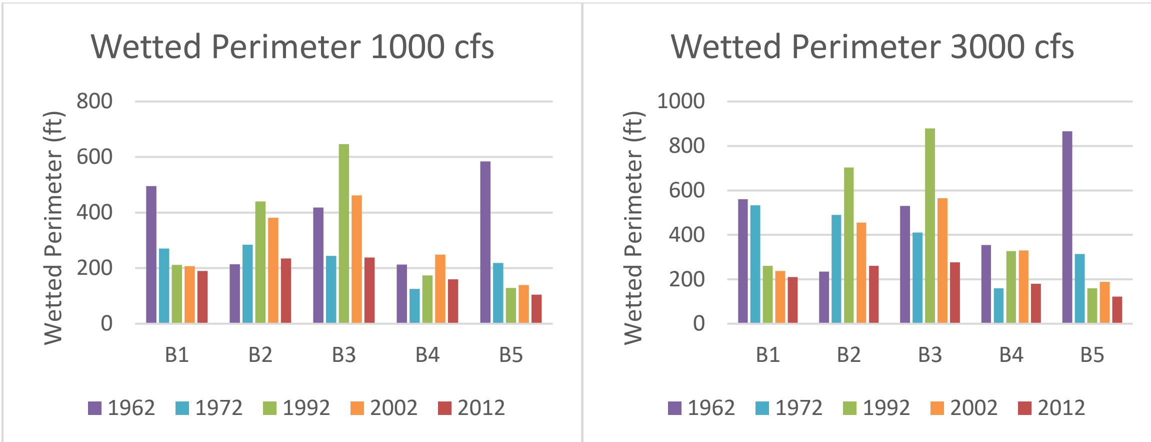

Figure 46 Wetted Perimeter at 1000 cfs (left) and 3000 cfs (right)

The bed slope was calculated using the slope function in Microsoft excel, which returns the slope of a linear regression from given "y" and "x" values. The bed slopes in each reach were calculated using two methods. First, the slopes were found using cross sectional bed slope elevations of the channel thalweg. Second, the slopes were found using the elevation of the water surface slope at 500 cfs in an effort to the reduce the effects of negative channel slopes and provide an estimate similar to the energy slope. A bar chart of the bed slopes is shown in Figure 47. Subreaches B1, B2, and B5 have all exhibited a general decrease in slope between 1962/1972 and 2012. As of 2012, the slope using both methods is above .0006 for B1, about .0007 for B2, about .00075 for B3, about .00065 for B4, and .0005 for B5. Subreach B3 has maintained a very consistent slope (.0007 to .00075), compared to other subreaches. Subreach B4 stands out in comparison to other subreaches as exhibiting a consistent increase in slope during the study period. Changes in flow depth and slope often have an inverse relationship. As slope decreases, the flow depth increases. This trend can be seen in the Bosque del Apache reach, particularly in subreach B1. The bed slope has decreased between the years 1962 and 2012 and the hydraulic depth has increased since 1962.

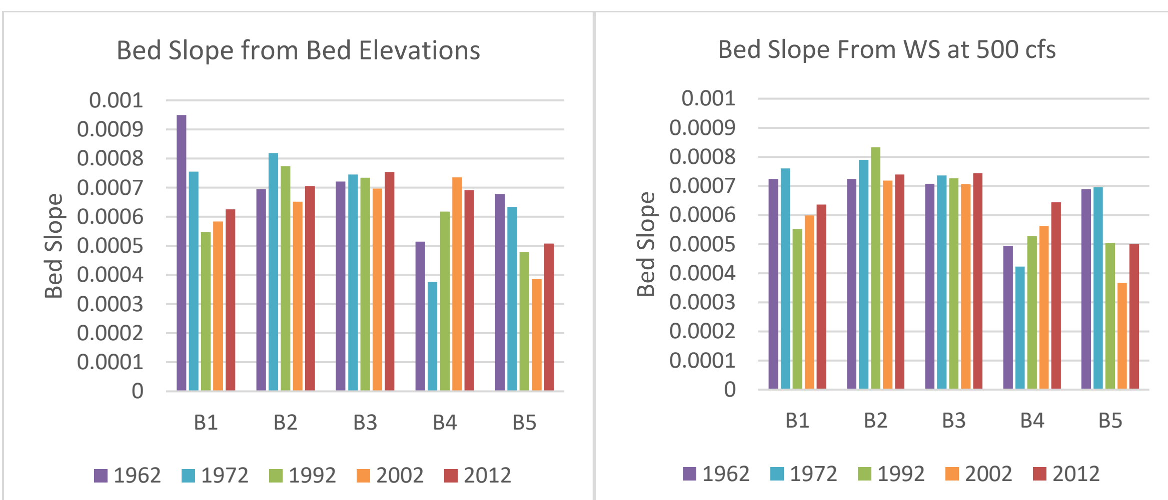

Figure 47 Bed Slope from Bed Elevations and Water Surface at 500 cfs.

3.7 Mid-Channel Bars and Islands

At low flows, the number of mid-channel bars and islands at each agg/deg line is measured from digitized planforms from the aerial photographs provided by the Reclamation. In some locations, multiple channels were present at one agg/deg line due to a vegetated bar or island bifurcating the flow. The number of channels at each agg/deg line were averaged throughout each subreach and the results are presented in Figure 48. A limitation in this analysis is that for some aerial images, it is unsure what time of year they were taken and therefore what the discharge was. The stage of a river can greatly affect the number of visible islands and bars. If the photos were not taken at a consistent discharge, this adds a degree of variability as to whether the bars and islands were due to a variation in stage or a change in channel morphology. This analysis, however, is still helpful in comparing general trends over a longer time period.

In 1918, subreach B2 appeared to be braided with sometimes 2 or more channels but has since decreased to lower averages. All subreaches generally do not have many sand bars or islands however they did appear to peak around in the 1990s and early 2000s across many subreaches. Although there are slight changes by subreach, the average number of mid-channel bars and islands throughout the reach is still only just above 1 for most of the years analyzed. Subreach B5 appeared to consistently be the most single threaded channel throughout the study period.

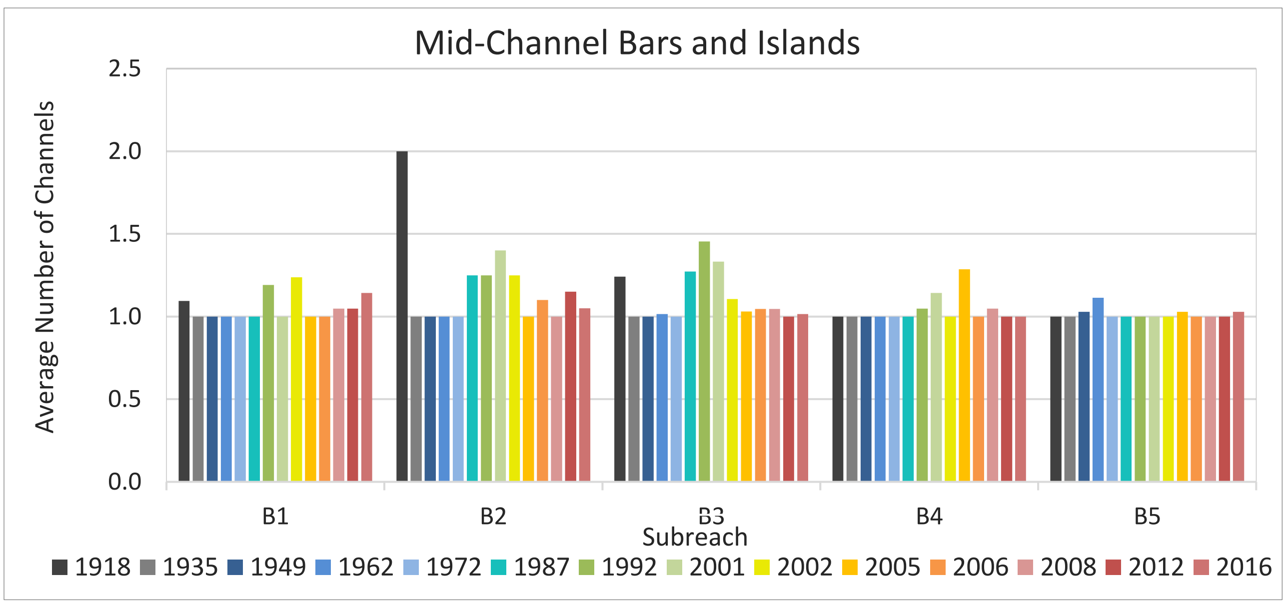

Figure 48 Average number of channels at the agg/deg lines in each subreach

Based on the analysis of the digitized planforms, the 1990s through the early 2000s appear to be more braided, which could be due to lower peak flows unable to wipe out the vegetation and re-work bars and islands. As peak flows begin to increase in the mid-2000s, the number of braided channels and bars decreases. Figure 49 shows an aerial photograph in 1992, just after an increase in the number of bars and islands, compared to the year 2012. After 1992, the number of bars and islands decreased. The aerial photographs show that vegetation has encroached on the channel and side channels have been eliminated by 2012.

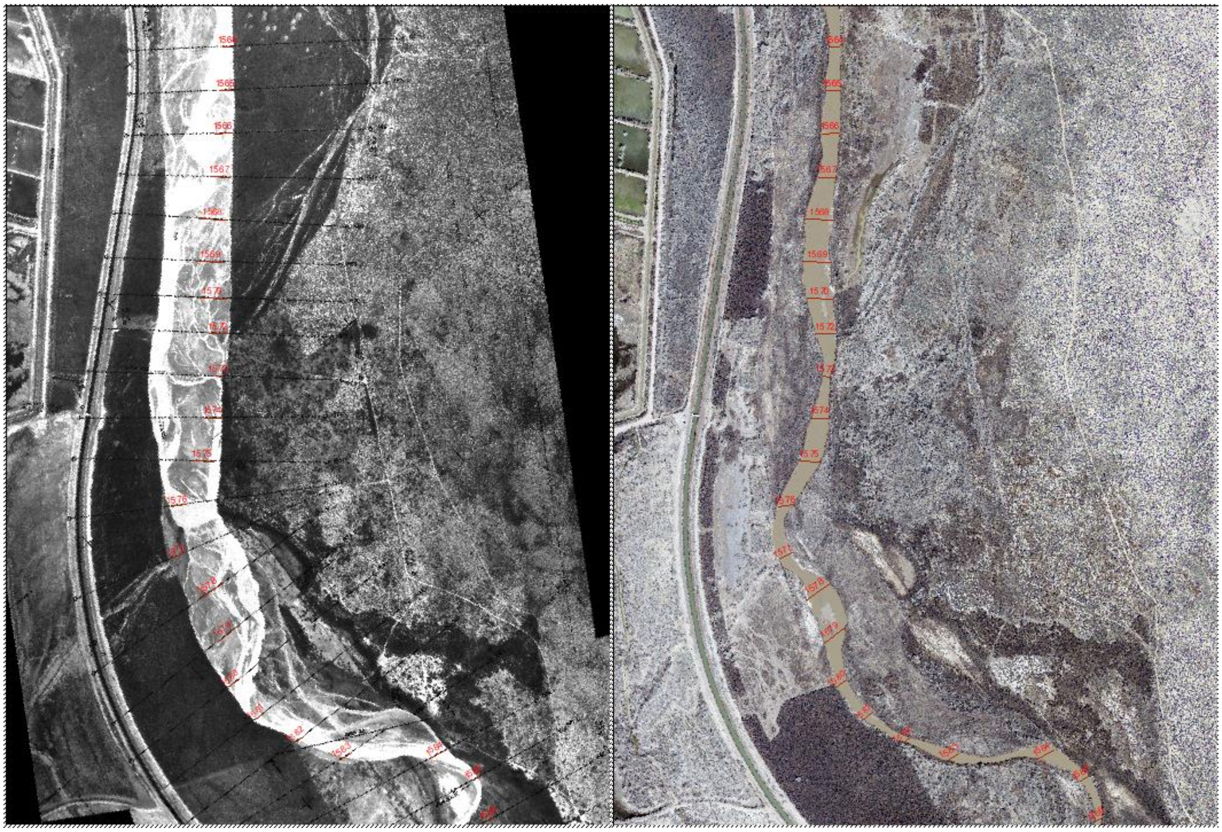

Figure 49 Digitized planform and aerial photograph of subreach B3 when multiple mid-channel bars and islands were present in 2002 (left) and in 2012 (right) after a reduction of mid-channel bars and islands.

3.9 Channel Response Models

The Julien and Wargadalam (JW) equations were used to predict the downstream hydraulic geometry of rivers (Julien and Wargadalam, 1995). These equations were based on empirical analysis of over 700 single-threaded rivers and channels, and predicted the width and depth likely to result from a given discharge, grain size and slope:

$$h = 0.2Q^{\frac{2}{6m+5}}D_s^{\frac{6m}{6m+5}}S^{\frac{-1}{6m+5}}$$
$$W = 1.33Q^{\frac{4m+2}{6m+5}}D_s^{\frac{-4m}{6m+5}}S^{\frac{-1-2m}{6m+5}}$$

Where $m = 1/\left[2.3\log\left(\frac{2h}{D_s}\right)\right]$, h is the flow depth, W is the channel width, Q is the flow discharge, D_s is the median grain size, and S is the slope. A discharge of 3,000 cfs, the same discharge as in the previous HEC-RAS analysis, was used. The values for slope and grain size were obtained from 3.6 Hydraulic Geometry and 3.4 Bed Material, respectively. The D_{50} of subreach 5 was not available for the selected years of interest but were instead substituted with close years with available data as described in Table 4. The results are compared to the observed active channel widths (from the GIS analysis of the digitized planforms) in Table 4 and plotted in Figure 50. The percent difference was calculated as:

$$\text{Percent Difference} = 100 * \left(\frac{\text{predicted width} - \text{observed width}}{\text{observed width}}\right)$$

Table 4 Julien Wargadalam channel width prediction

Year	Subreach	D_s (mm)	Slope	Predicted Width (ft)	Observed Width (ft)	Percent difference
1992	B1	0.225	0.0005	271.5	213.9	26.92
	B2	0.206	0.0008	249.0	750.0	-66.81
	B3	0.184	0.0007	251.9	969.9	-74.03
	B4	0.180	0.0006	263.0	168.3	56.25
	B5	0.236*	0.0005	276.2	146.7	88.30
2002	B1	0.260	0.0006	265.3	199.2	33.15
	B2	0.260	0.0007	254.9	493.7	-48.37
	B3	0.263	0.0007	253.1	724.0	-65.04
	B4	0.280	0.0007	253.4	633.4	-59.99
	B5	0.255*	0.0005	275.8	132.9	107.54
2016	B1	0.208	0.0006	261.9	198.4	32.00
	B2	0.168	0.0007	254.7	254.8	-0.03
	B3	0.183	0.0007	251.6	281.2	-10.55
	B4	0.239	0.0007	258.6	191.8	34.80
	B5	0.210*	0.0005	269.4	119.1	126.20

*For 1992, there were no grain size data available for B2, B3, B4, and B5, so data from 1991 were used in replacement. For 2002, there were no grain size data available for B5, so the 2001 data was used. For 2016, there were no grain size data for subreach B5, so the 2005 data was used.

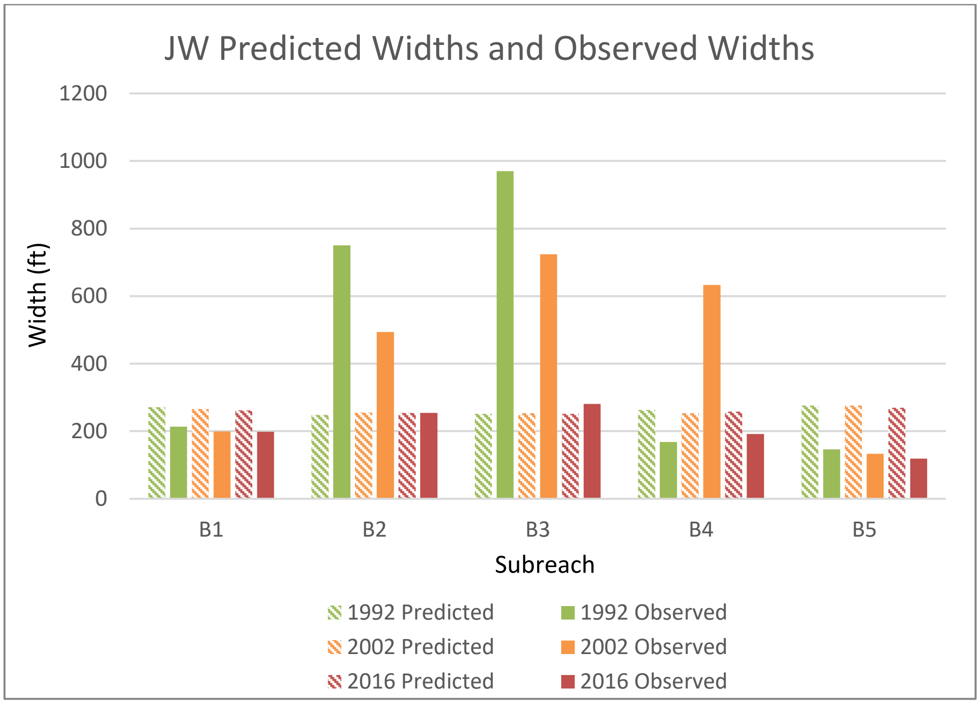

Figure 50 Julien and Wargadalam predicted widths and observed widths of the channel

The predicted widths are generally wider in subreaches B1, B4, and B5 and generally narrower in subreaches B2 and B3. The JW equations predict that the channel width for all subreaches will eventually narrow to around 250 to 270 feet. When calculating the predicted width of the river, the bankfull discharge was used when in reality, varying discharges would be occurring in the river. This could lead to the greater variability in the observed width values.

3.10 Geomorphic Conceptual Model

Massong et al. (2010) developed a channel planform evolution model for the Rio Grande based on historic observations. The sequence of planform evolution is outlined in Figure 51. Stage 1 describes a large channel with a high sediment load and large floods, which results in an active channel with constantly changing bars and dunes and little vegetation encroachment. The evolution from dunes to islands and bars transitions the river into Stage 2. As the islands and bars are stabilized by vegetation, they begin to act like floodplains indicating that the river is transitioning to Stage 3. The sediment transport capacity then becomes the determining factor of the future course of the river to either an aggrading river (stages A4-A6) or a migrating river (stages M-4 to M-8). A deficiency in sediment transport capacity, meaning the sediment supply is exceeding the transport capacity, leads to aggradation in the main channel and the flow eventually shifts onto the lower surrounding floodplain. When the sediment transport capacity exceeds the sediment supply, bank material erodes both laterally and vertically, leading to a meandering river. Transition between the M stages and the A stages can occur, but a reset to a Stage 1 requires a large, prolonged flood (Massong et al., 2010).

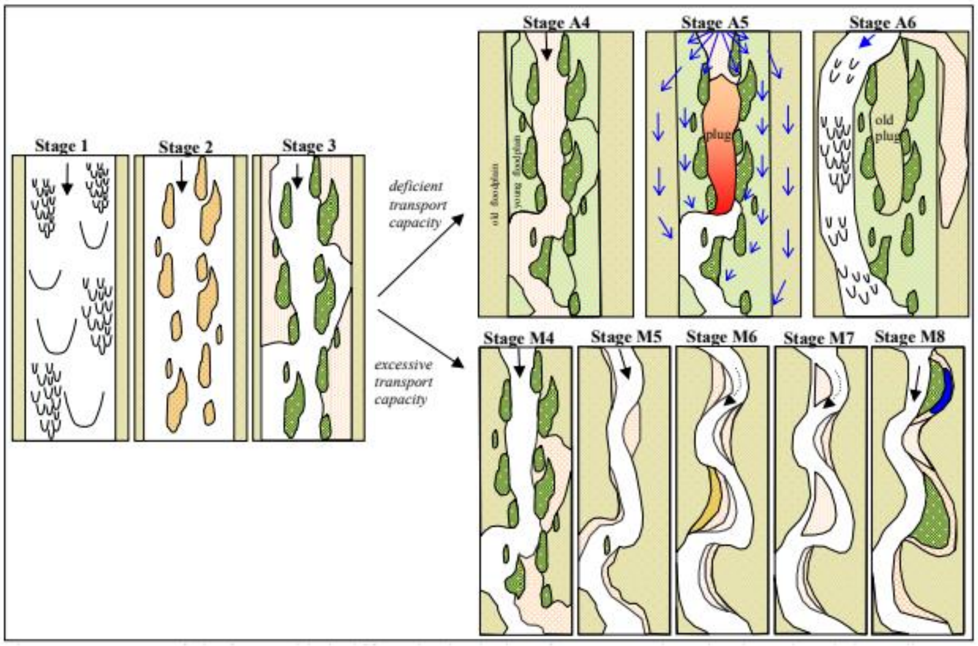

Figure 51: Planform evolution model from Massong et al. (2010). The river undergoes stages 1-3 first and then continues to stages A4-A6 or stages M4-M8 depending on the sediment transport capacity.

Comparisons between channel shifts and the channel slope of the MRG have indicated that transitions into the aggrading reach cycle have a slope of less than 0.0007 ft/ft, while transitions through the migrating reach stages have a slope greater than 0.0009 ft/ft (Massong 2010). The Bosque del Apache reach has had slopes that ranged between 0.0004 and 0.0009, which has resulted in a river that can transition into either the aggrading or migrating reach stages. Though as of 2012, four out of five subreaches have average slopes less than 0.0007 ft/ft, indicating they are in an aggrading reach cycle.

Figure 52 and Figure 53 show the evolution of the channel in the first subreach using a representative cross section of B1 along with aerial photos throughout history. The river's discharge is unknown at the time of the photos.

Subreach B1 has aggraded and narrowed between 1962 and 2012, while the main channel appears to have developed a more uniform cross section. This corresponds with the findings in section 3.3, which shows a net increase in bed elevation for this portion of the reach. The sediment supply exceeds the sediment transport capacity in this subreach, leading to deposition.

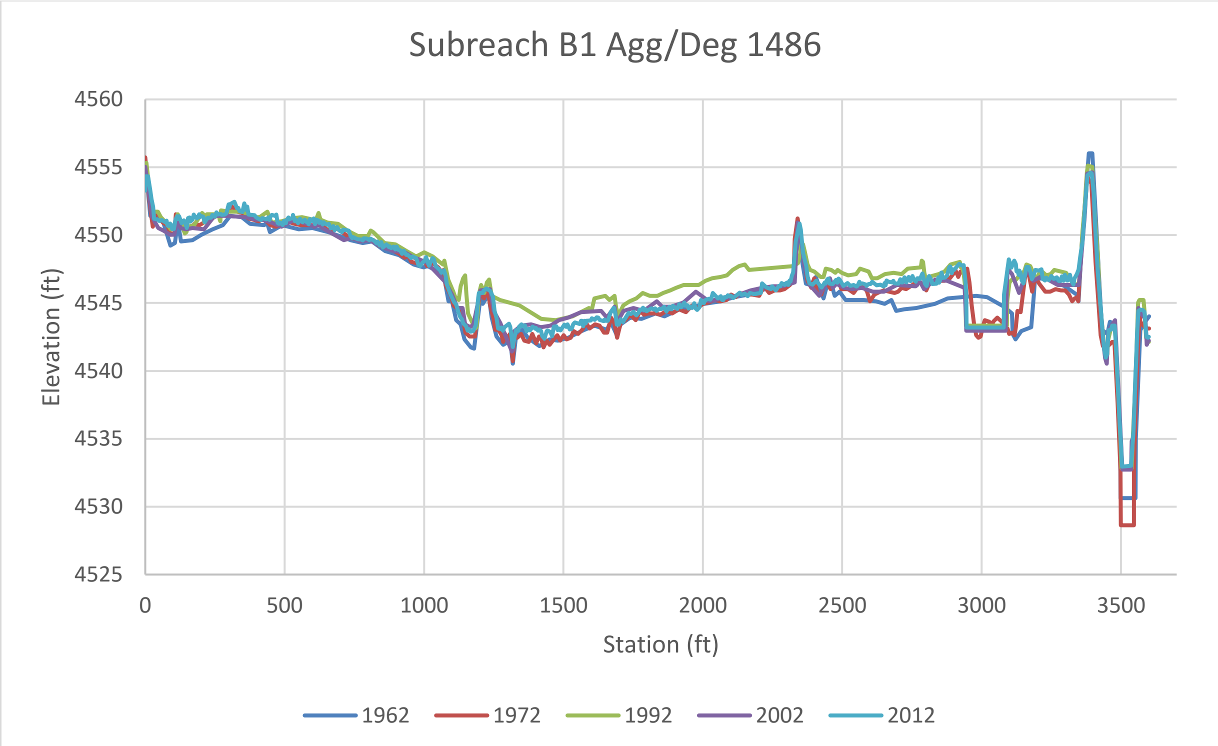

Figure 52: Channel evolution of a representative cross section from subreach B1. Deep channel on far right of plot represents low flow conveyance channel.

Between 1972 and 1992, subreach B1 appears to have shifted from Stage 1/Stage 2 to Stage A4 (Figure 50). As seen in the arial imagery, vegetation had established itself on the floodplain and encroached on the banks of the river. No lateral migration of the channel was observed, just the further establishment of a riparian forest close to the main channel. The cross-section profile is shown in Figure 52 and a side by side view of the cross section and aerial imagery is shown in Figure 53.

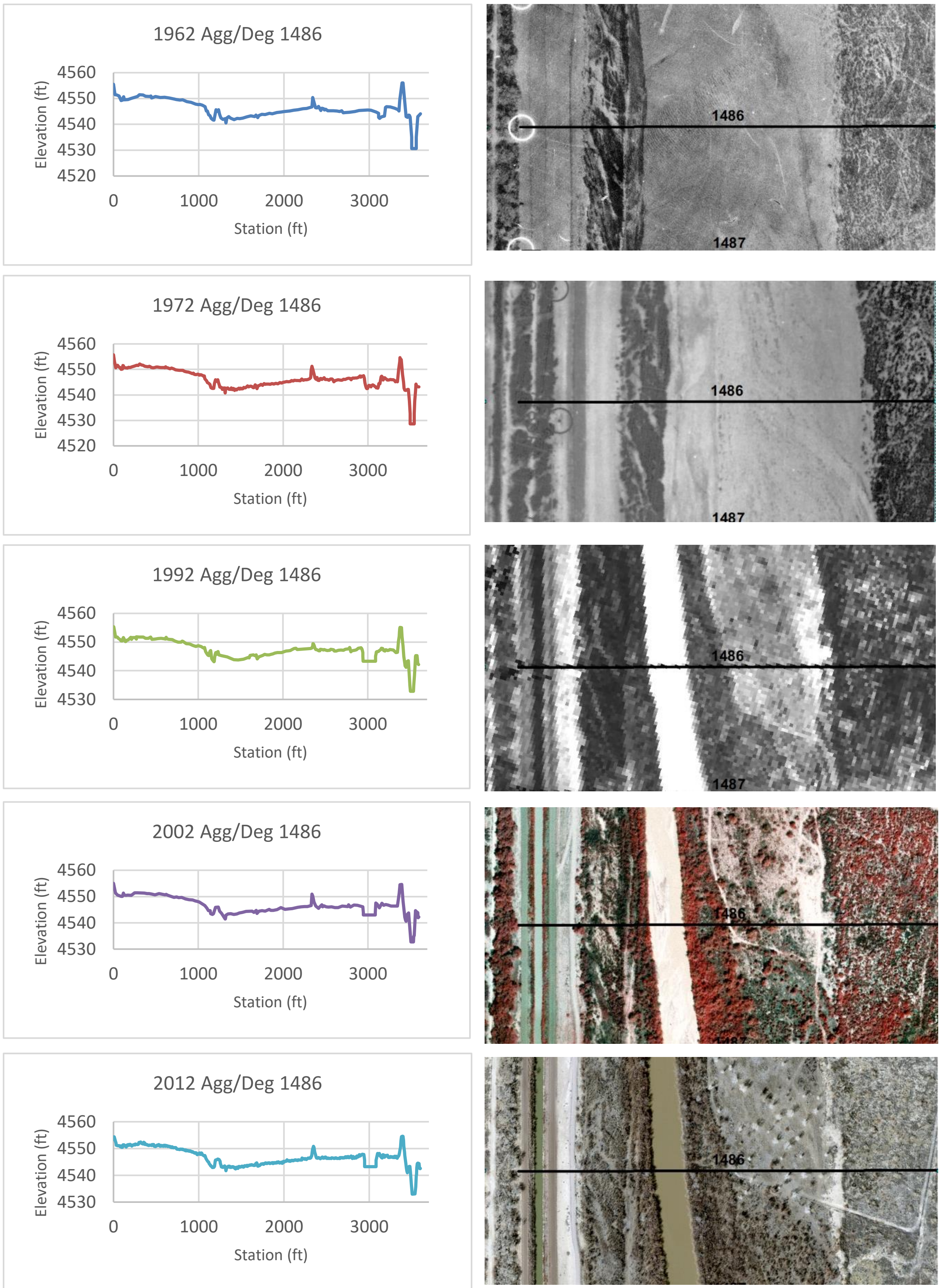

Figure 53: Subreach B1: historical cross section profiles and corresponding aerial images

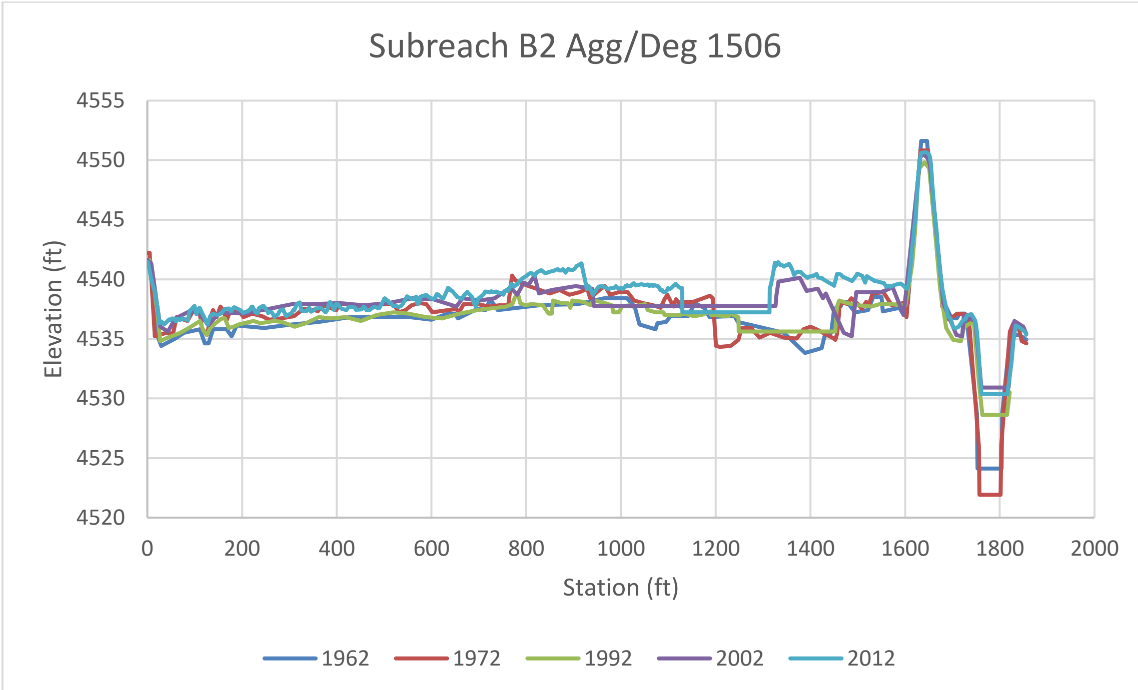

Figure 54: Channel evolution of a representative cross section from subreach B2. Deep channel on far right of plot represents low flow conveyance channel.

Subreach B2 appears to be currently transitioning from stage 3 to stage A4. The transition between these two stages is not necessarily discrete but is characterized by deposition within the main channel (Massong, 2010). In Figure 54, the bed elevation for the majority of the cross section is shown to increase. However, in 2012 the main channel appears to be increasing faster than its surrounding floodplain. Eventually this aggradation will lead to superelevation of the channel above its floodplain is indicative of stage A4.

In Figure 55, between 1962 and 1992, the channel can be seen transitioning from stage 1 to stage 2 as the sandbars become more stable and start to develop vegetation in 1992. Between 1992 and 2002 the channel appears to still be moderately wide with the main channel appearing to shift southeastward. However, between 2002 and 2012, vegetation appears to further encroach on the channel, narrowing it and resulting in the development of a wider floodplain. Figure 55 shows the cross-section profile for the various years along with a corresponding aerial image of the river.

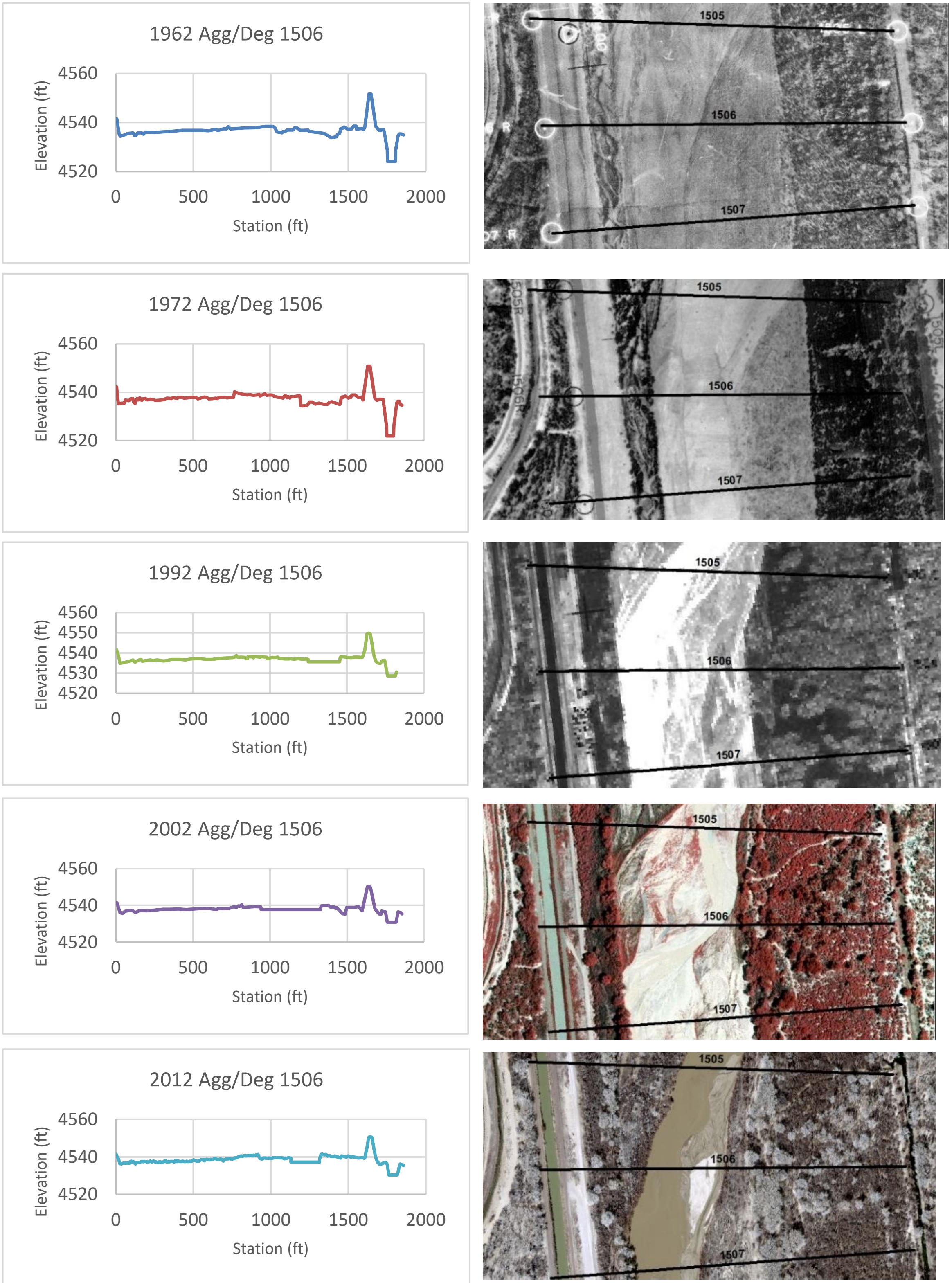

Figure 55: Subreach B2: historical cross section profiles and corresponding aerial images

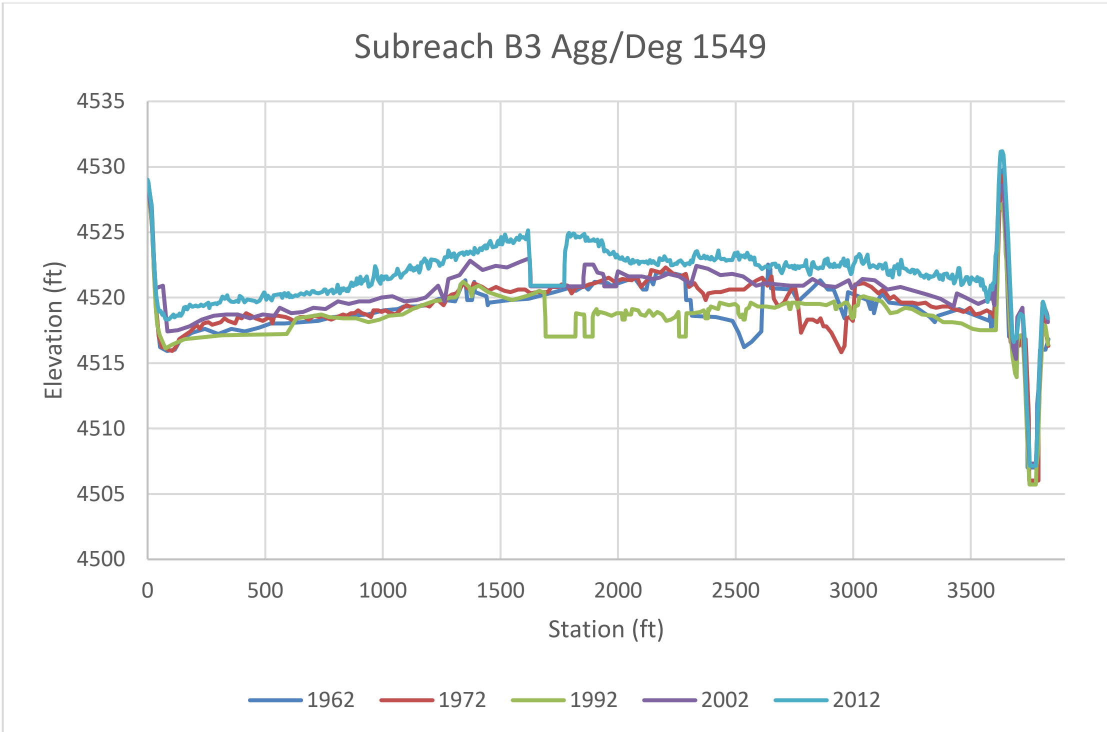

Figure 56*: Channel evolution of a representative cross section from subreach E3. Deep channel on far right of plot represents low flow conveyance channel.*

Subreach B3 is characterized by high amounts of deposition within the main channel and on the floodplain, though as seen in 2012, the main channel is aggrading much faster than the floodplain, resulting in channel perching. This is shown in comparison of cross sections in Figure 56. Between 1992 and 2012 the channel has increased in elevation by approximately 5 feet. A superelevated channel over its floodplain is indicative of the subreach in stage A4. At such high levels of perching, the channel is likely to eventually transition between A4 and A5, forming a sediment plug. In fact, in 2008 a sediment plug had formed in the channel beginning at agg/deg line 1547 as shown in Figure 57 following high discharges that summer (Shrimpton, 2012). The resulting plug was then excavated in the fall to create a pilot channel and return the flow to the main channel. A cross section just upstream of the selected cross section, agg/deg 1548, is provided in Figure 58 to demonstrate the formation of a sediment plug in this same area again in 2019.

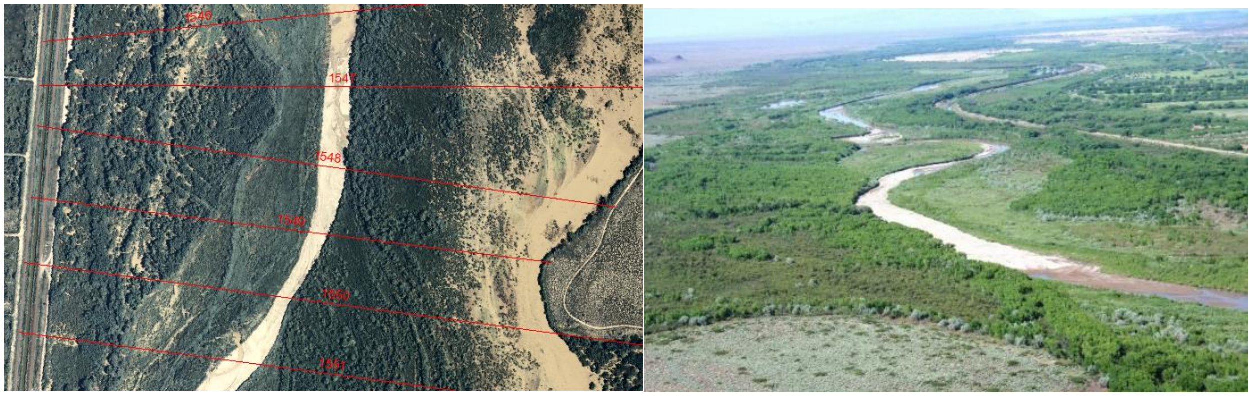

Figure 57: Aerial photos of 2008 Bosque del Apache plug

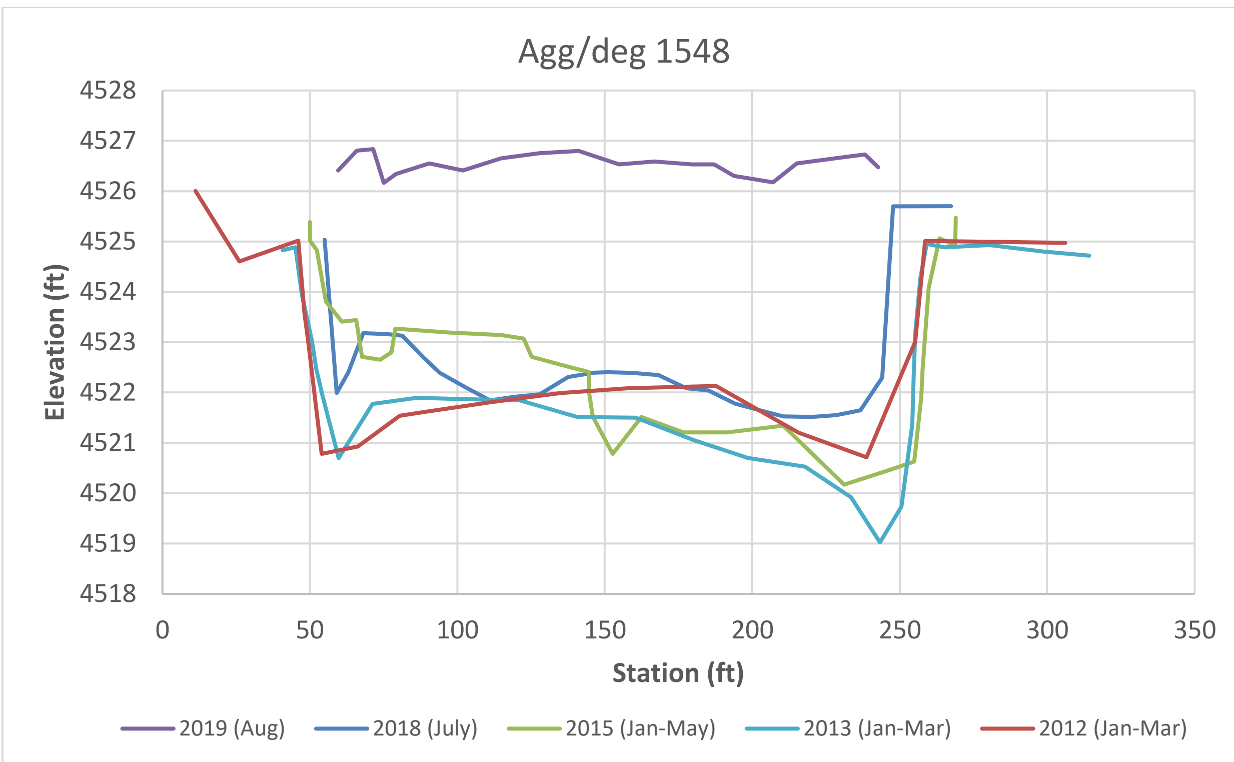

Figure 58: Cross section of 2019 sediment plug at agg/deg 1548, data from Nathan Holste (pers. comm.)

In Figure 59, the river can be seen shifting from stage 1 to stage 2/stage 3 between 1962 and 1992. As the sand bars became more stable and vegetation became more established, sediment began to deposit and the river then shifted from stage 3 to stage A4 between 2002 and 2012. As described above, in 2008 the river had transitioned into stage A5, forming a sediment plug, however this plug was manually excavated reverting this subreach back to stage A4 before a new channel could become established. Figure 59 shows the cross-section profile for the various years along with a corresponding aerial image of the river.

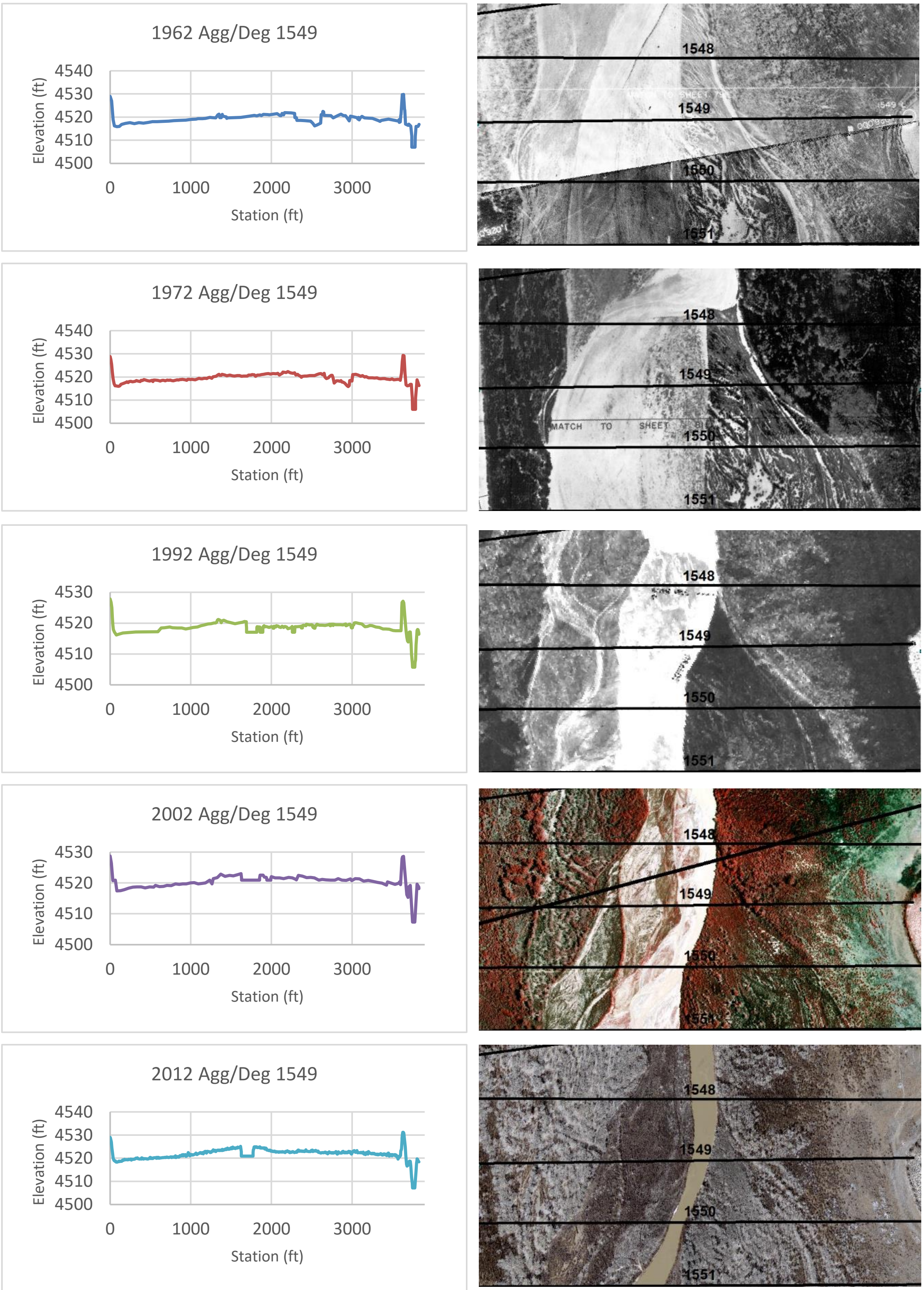

Figure 59: Subreach B3: historical cross section profiles and corresponding aerial images

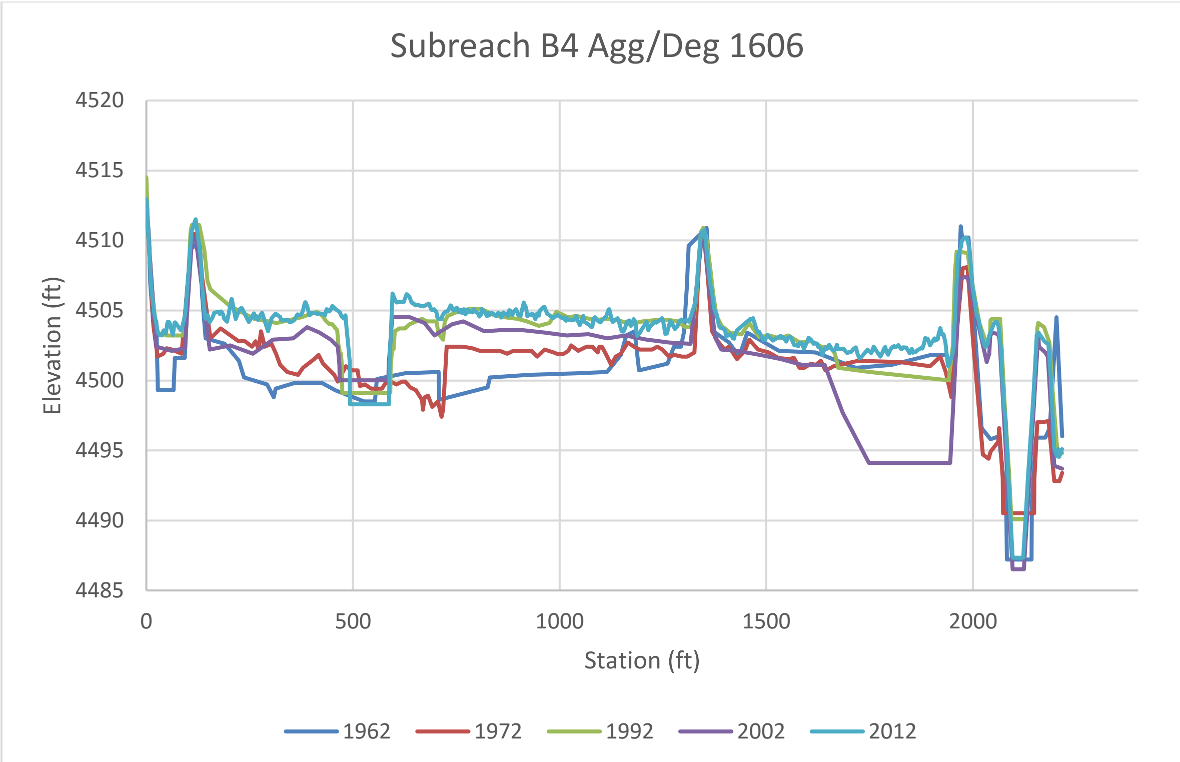

Figure 60: Channel Evolution of a representative cross section of subreach B4. Deep channel on far right of plot represents low flow conveyance channel.

Figure 60 shows the comparison of cross sections at agg/deg line 1606 overtime. A gradual trend of channel perching can be seen with large amounts of aggradation occurring between 1972 and 1992. While the rate of aggradation appears to have slowed in recent years, it can still be observed close to the main channel such as in 2012. The banks of the main channel are above the floodplain, indicating perching and that subreach B4 is currently in stage A4. In Figure 61, the aerial photos of the cross section at various times and their corresponding cross sections are shown. From the photos, the channel transitioned from a multithreaded channel in 1962 to a narrow single channel in 1992. Between 1992 and 2012 the planform of the main channel has hardly changed, except for possibly becoming narrower from encroaching vegetation.

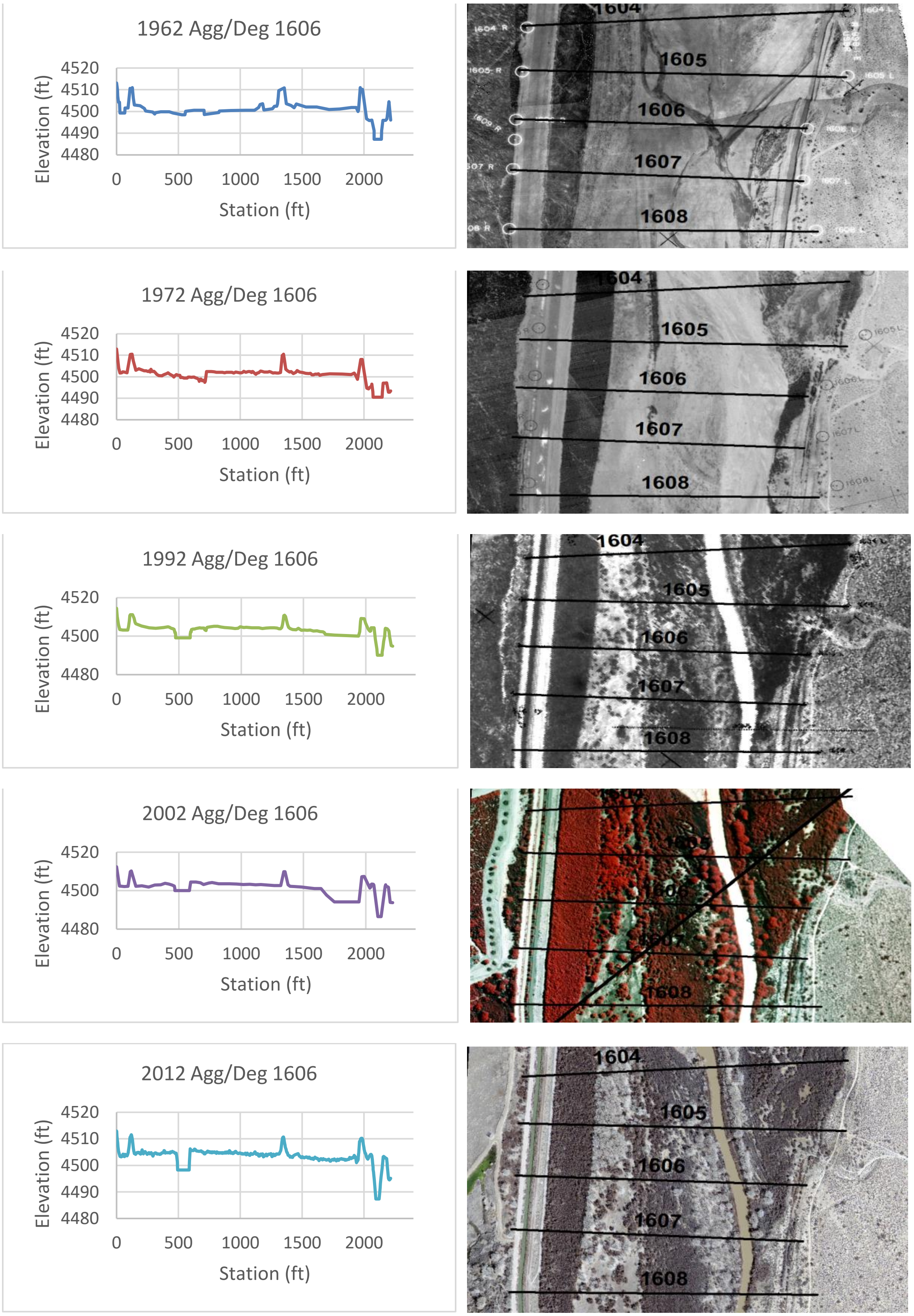

Figure 61: Subreach B4: historical cross section profiles and corresponding aerial images

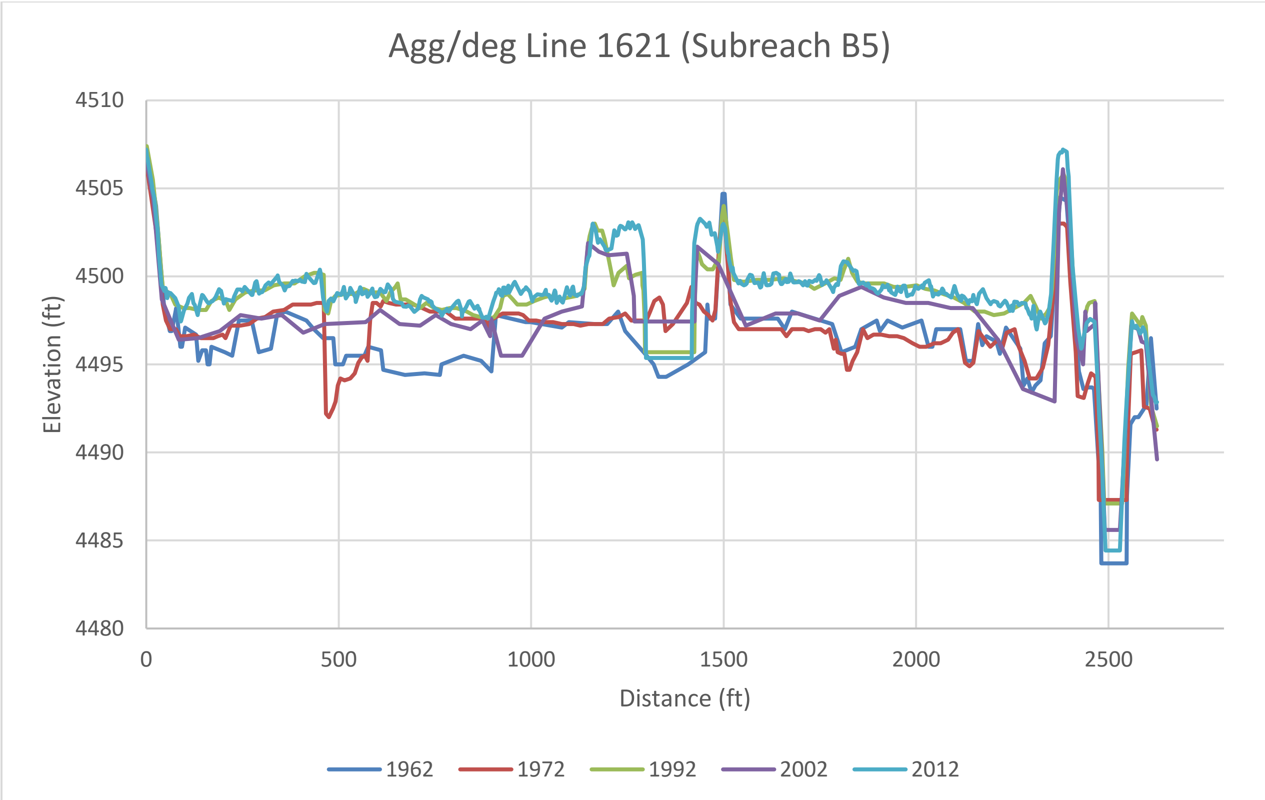

Figure 62: Channel evolution of a representative cross section of subreach E5. Deep channel on far right of plot represents low flow conveyance channel.

Figure 62 shows the comparison of cross sections at agg/deg line 1621 over time. Here a clear trend of channel perching can be seen, beginning in 1992 and becoming more extreme with every following decade. This channel perching indicates that subreach B5 is in stage A4. In Figure 63, the aerial photos of the cross section at various times and their corresponding cross sections are shown. From the photos, little change can be seen to the channel's planform other than narrowing between 1962 and 1972.

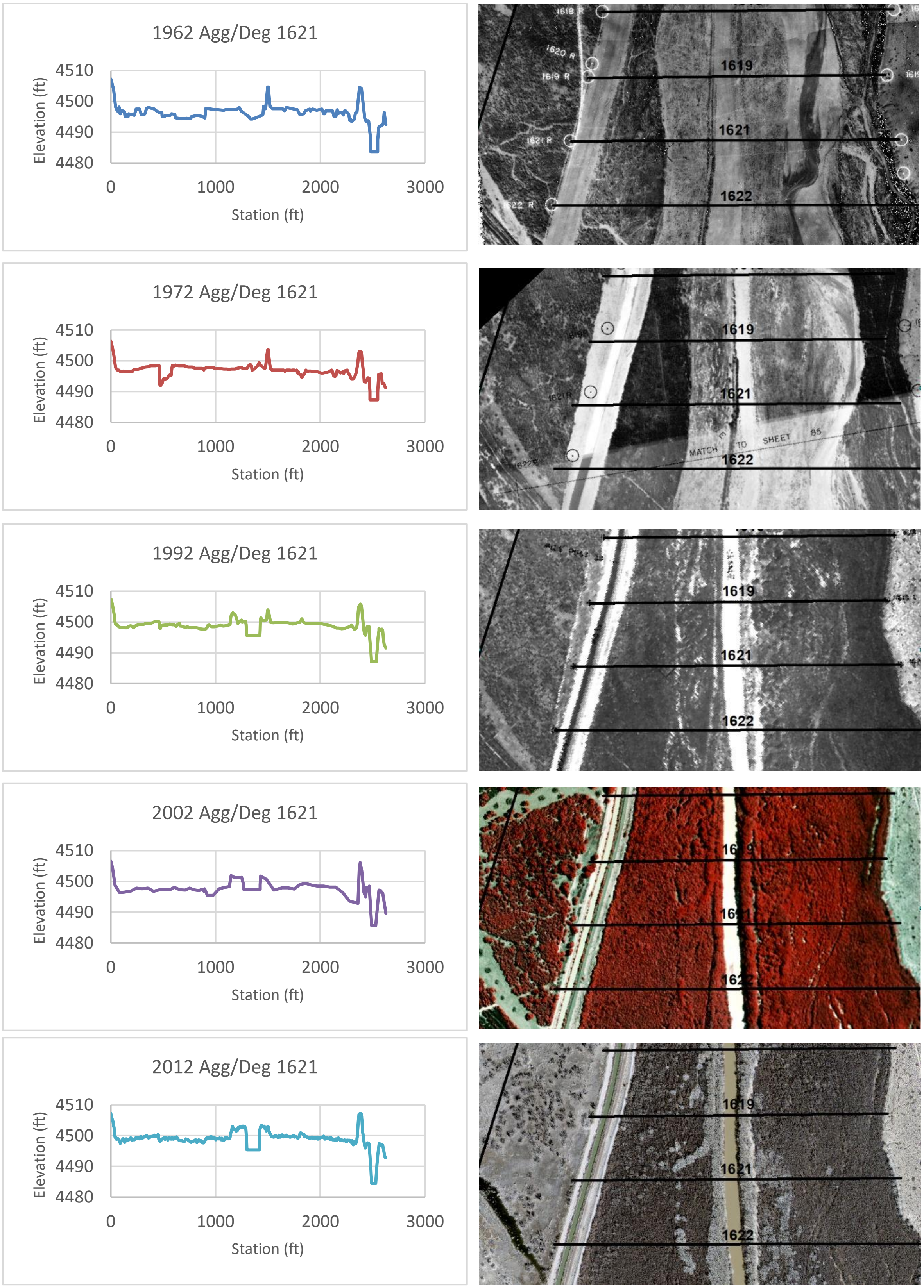

Figure 63: Subreach B5: historical cross section profiles and corresponding aerial images

4. HEC-RAS Modeling for Silvery Minnow Habitat

The Rio Grande Silvery Minnow (RGSM or silvery minnow) is an endangered fish species that is native to the Middle Rio Grande. Currently, it occupies only about seven percent of its historic range (U.S. Fish and Wildlife Service, 2010). It was listed on the Endangered Species List by the US Fish and Wildlife Service in 1994.

One of the most important aspects of silvery minnow habitat is the connection of the main channel to the floodplain. Spawning is stimulated by peak flows in late April to early June. These flows should create shallow water conditions on the floodplains, which is ideal nursery habitat for the silvery minnow (Mortensen et al., 2019). Silvery minnows prefer specific velocity and depth ranges depending on the life stage that the fish is in. Table 5 outlines these velocity and depth guidelines. Fish population counts are available from prior to 1993 to the present. Therefore, analysis of silvery minnow habitat will not begin prior to 1992. In preparation for the process linkage report, figures relating the geomorphology of the river and RGSM habitat availability are included in Appendix F.

Table 5 Rio Grande Silvery Minnow habitat velocity and depth range requirements (from Mortensen et al., 2019)

	Velocity (cm/s)	Depth (cm)
Adult Habitat	<40	>5 and <60
Juvenile Habitat	<30	>1 and <50
Larvae Habitat	<5	<15

4.1 Modeling Data and Background

The data available to develop these models varies year by year. Cross section geometry was available for the years 1962, 1972, 1992, 2002, and 2012. In 2012, additional LiDAR data of the floodplain was available, which allowed the development of a terrain for RAS-Mapper. Therefore, RAS-Mapper was used in 2012 only, while comparisons across years are done using 1-D techniques.

HEC-RAS distributes water by adding water to a cross section from the lowest elevation up. Much of the MRG is perched, so this can lead to inaccurate predictions of the flow distribution within the cross section, overpredicting water in the floodplains, therefore overpredicting hydraulically suitable habitat. Computational levees were used in HEC-RAS to keep the water contained in the channel until bankfull is reached. At the discharge that this occurs, the computational levees were removed to allow water to spill out onto the floodplains. The computational levees are removed at the same discharge throughout the entire reach. This method is described by Holste (2020) and uses a capability in HEC-RAS that determines the “left levee freeboard” and “right levee freeboard” which is the difference between water surface elevation and computational levee elevation. A negative value indicates an overtopping discharge. A sensitivity analysis was completed to determine the percentage of cross sections that should be overtopped before removing the top of bank points in HEC-RAS. For this analysis, when 25% of the cross sections in the reach were experiencing overtopping, signifying 25% had reached bankfull discharge, the computational levees were removed, allowing water to inundate the floodplains. The results from the levee freeboard analysis are shown in Figure 64.

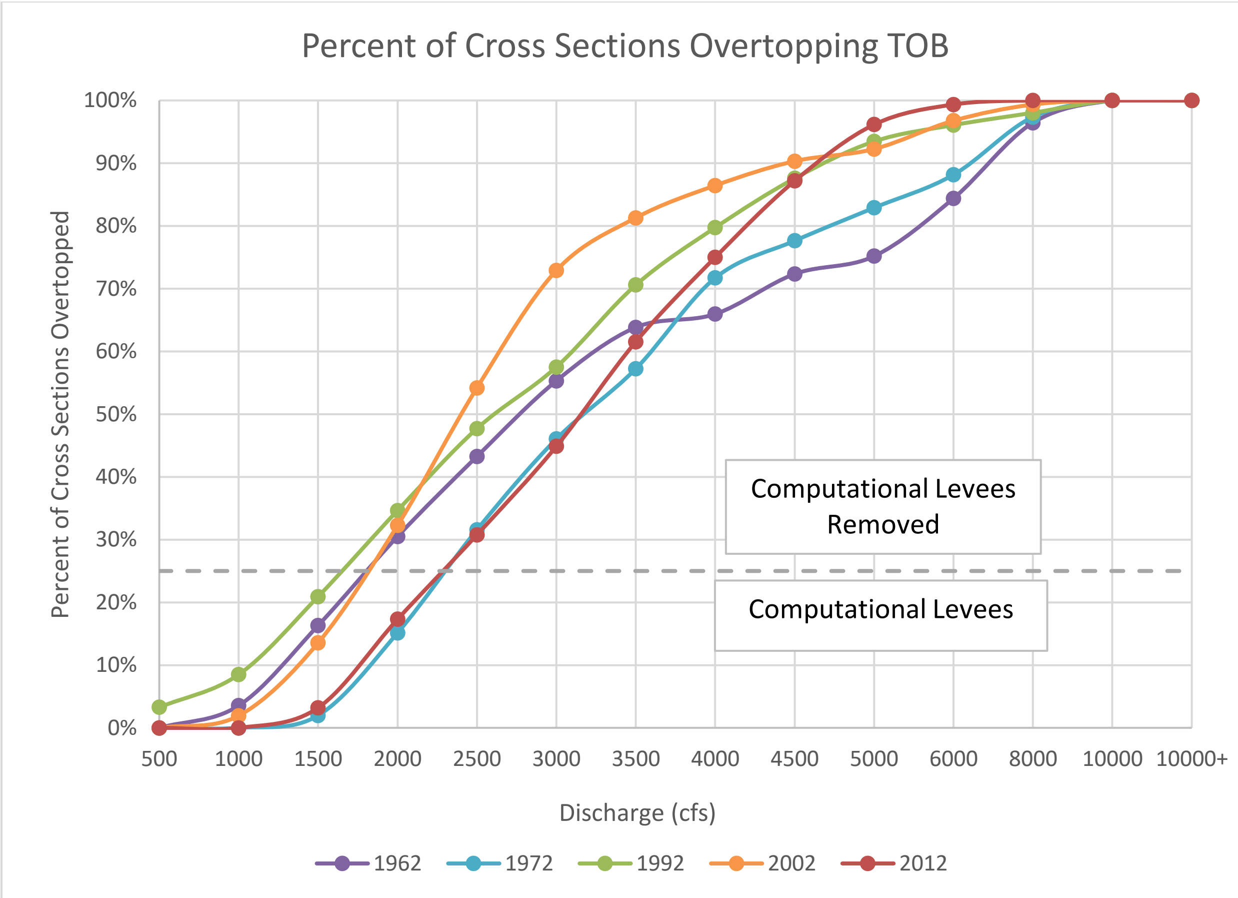

Figure 64: Comparing the overbanking discharge values at various years. The dashed line (indicating 25% of cross sections in a reach experiencing overbanking) determines the discharge at which computational levees are removed for habitat analysis.

4.2 Width Slices Methodology

Without a terrain for 2002 and 1992, additional methods had to be considered to determine a metric of fish habitat. HEC-RAS has the capability to perform a flow distribution analysis to calculate the laterally varying velocities, discharges, and depths throughout a cross section as described in chapter 4 of the HEC-RAS Hydraulic Reference Manual (US Army Corps of Engineers, 2016). HEC-RAS allows each cross-section to be divided into up to 45 slices. Because the RGSM relies heavily on floodplains for habitat (due to higher velocities and depths in the main channel) and the floodplains contain more variability than the main channel, 20 width slices were assigned in each floodplain and 5 width slices in the channel. An example of the flow distribution in a cross-section is shown in Figure 65. The velocity and depth of each slice were analyzed to determine the total width at each agg/deg line that meets the RGSM larval, juvenile, and adult criteria. Because the agg/deg lines are spaced approximately 500 feet apart, the hydraulically suitable widths were multiplied by 500 feet to obtain an area of hydraulically suitable habitat per length of river. For areas outside of the main channel, a Manning's roughness of 0.1 was and for inside the main channel, a Manning's roughness of 0.025 was used.

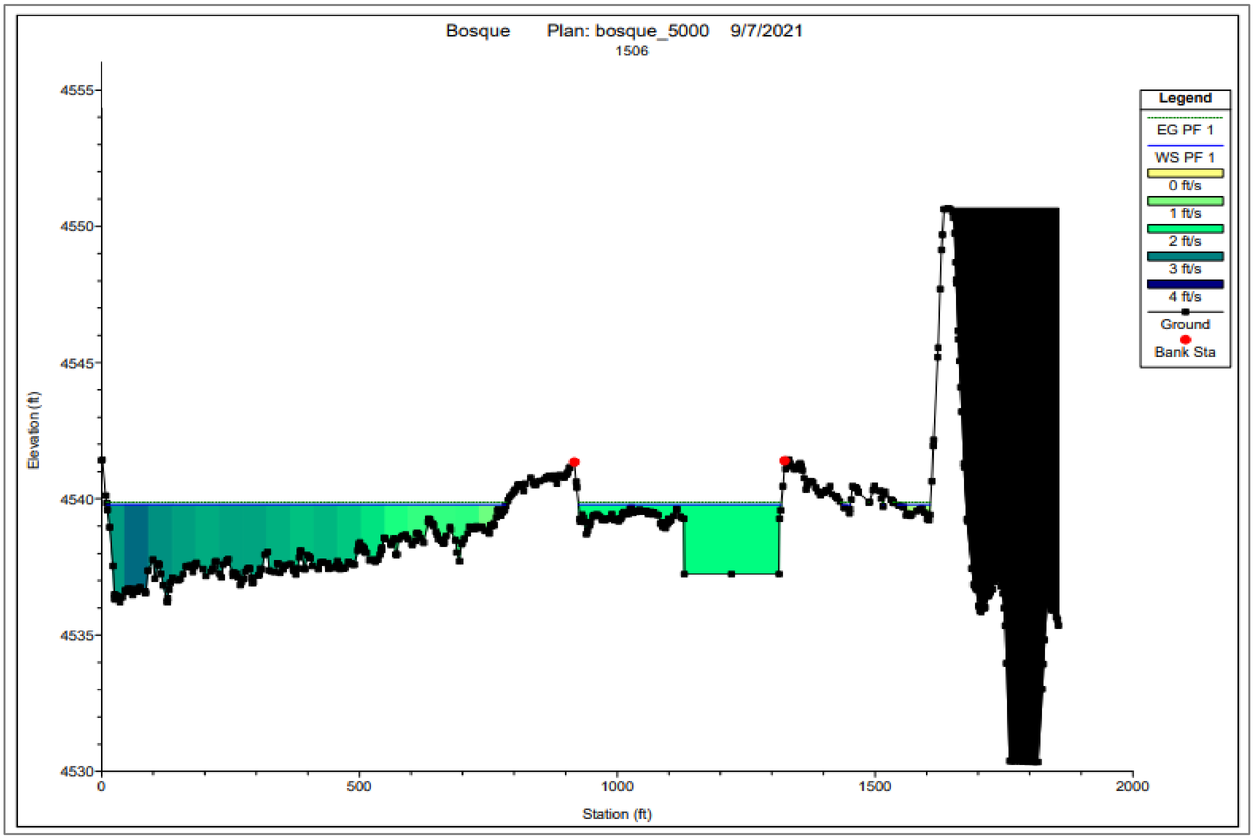

Figure 65: Cross-section at a discharge of 5,000 cfs with flow distribution from HEC-RAS of 20 vertical slices in the floodplains and 5 vertical slices in the main channel. The blue and green slices are small enough that the discrete color changes look more like a gradient.

4.3 Width Slices Habitat Results

The width slices method was first used to analyze the habitat availability throughout the Bosque del Apache reach at a reach scale for the years of 1962, 1972, 1992, 2002 and 2012. For the discharges at which the water is contained in the main channel, there is less habitat availability. At low discharges, 1500 cfs and below, there is generally little available habitat for the RGSM at all life stages because flow is confined to the main channel. For all life stages, low discharge habitat has decreased between 1962 and 2012. As the discharge increases past 2500 cfs, the velocities and depths increase making the main channel less hydraulically suitable for the RGSM but increasing overall habitat on the floodplains. This is displayed by Figures 66 to 68.

Depending on the year, discharges of 2000 cfs to 3000 cfs appear to activate the floodplains of the reach, representing a large increase in available habitat for the RGSM. The channel appears to overbank at lower discharges (2000 cfs) in 1962 and 2002, at 2500 cfs in 1992, 1972, and 2012. Across all life stages, available habitat appears to peak in 2012. 2012 represents the year with the most available habitat across all life stages and all discharges.

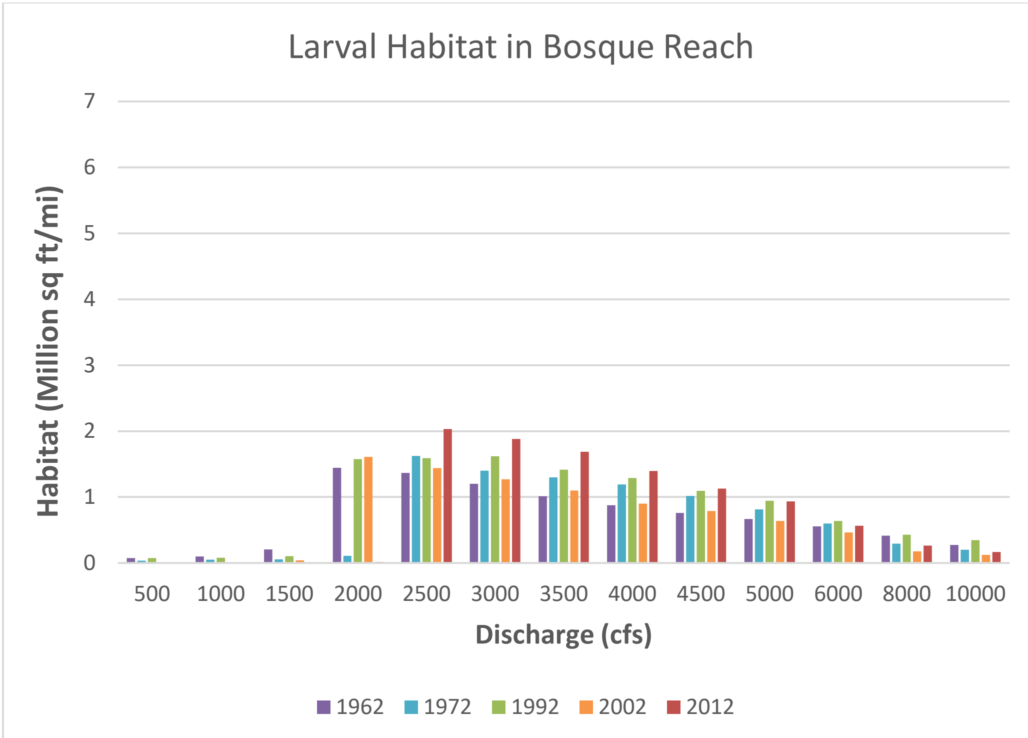

Figure 66: Larval RGSM habitat availability throughout the Bosque del Apache reach

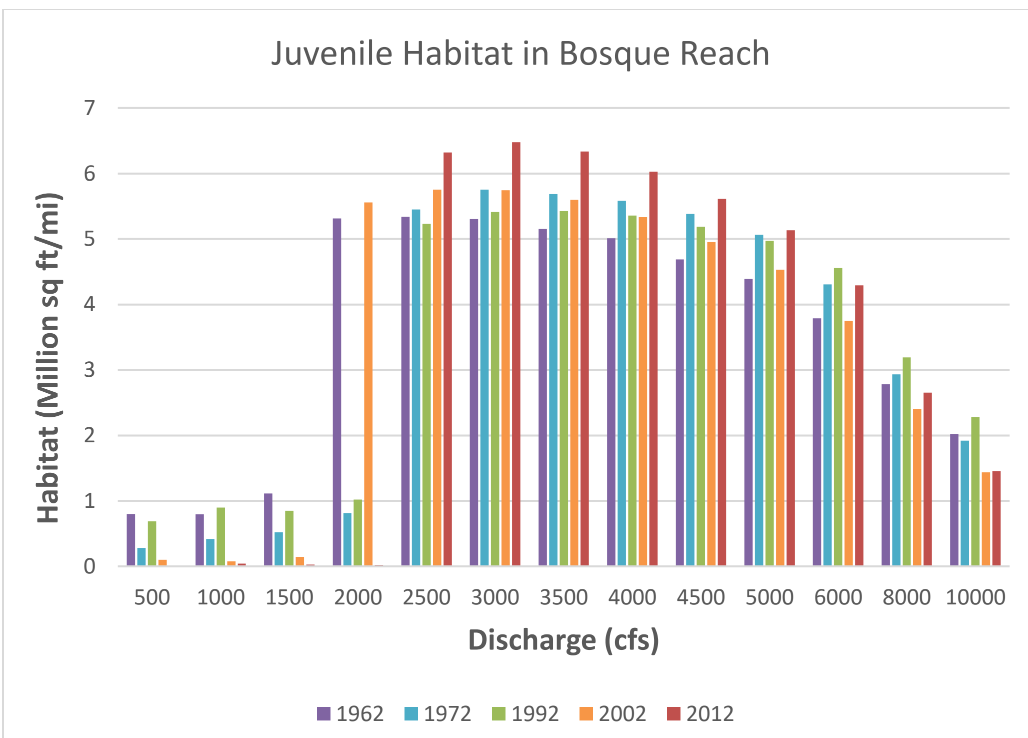

Figure 67: Juvenile RGSM habitat availability throughout the Bosque del Apache reach

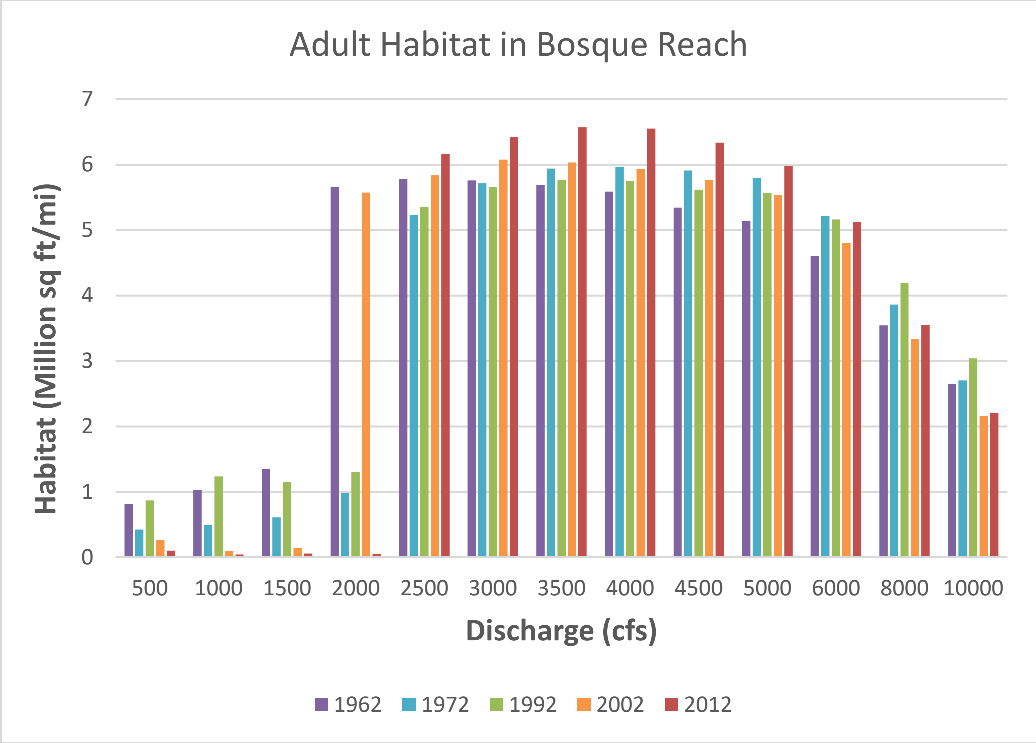

Figure 68: Adult RGSM habitat availability throughout the Bosque del Apache reach

The width slices method was also used to analyze the habitat availability throughout the Bosque del Apache reach at a subreach level. Based on this method, subreach B3 had the greatest amount of possible habitat at higher discharge and lower discharges while subreaches B3, B4, and B5 provided the second most habitat at higher discharges. Additional bar charts for all subreaches are in Appendix D.

Stacked habitat bar charts were also created to portray the spatial variation of hydraulically suitable habitat throughout the Bosque del Apache reach. Bar charts displaying units of habitat area were created for 1962, 1972, 1992, 2002, and 2012. To convert to an area, these values would be multiplied by 500 ft. There is little available habitat at the lower discharges for the year 2012, so first a plot of 2012 habitat is shown up to 3,000 cfs in Figure 69. The full stacked habitat chart for 2012 is shown in Figure 70, and the other years are included in Appendix D.

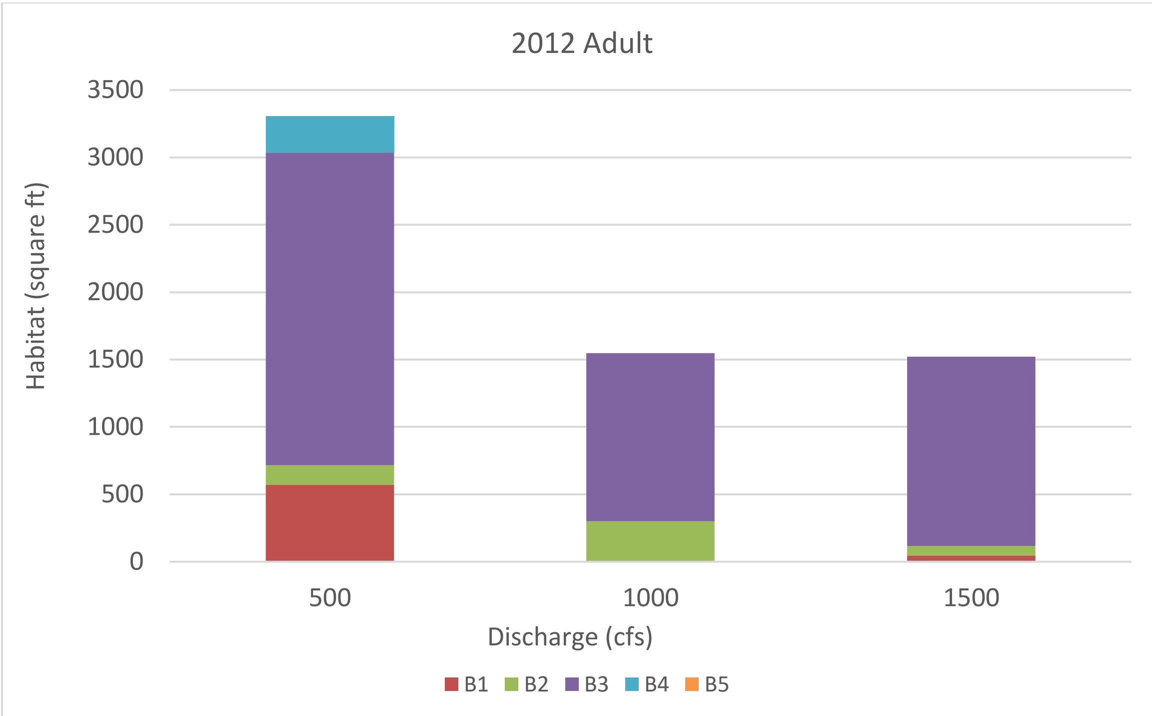

Figure 69: Stacked habitat charts to display spatial variations of habitat throughout the Bosque del Apache reach in 2012

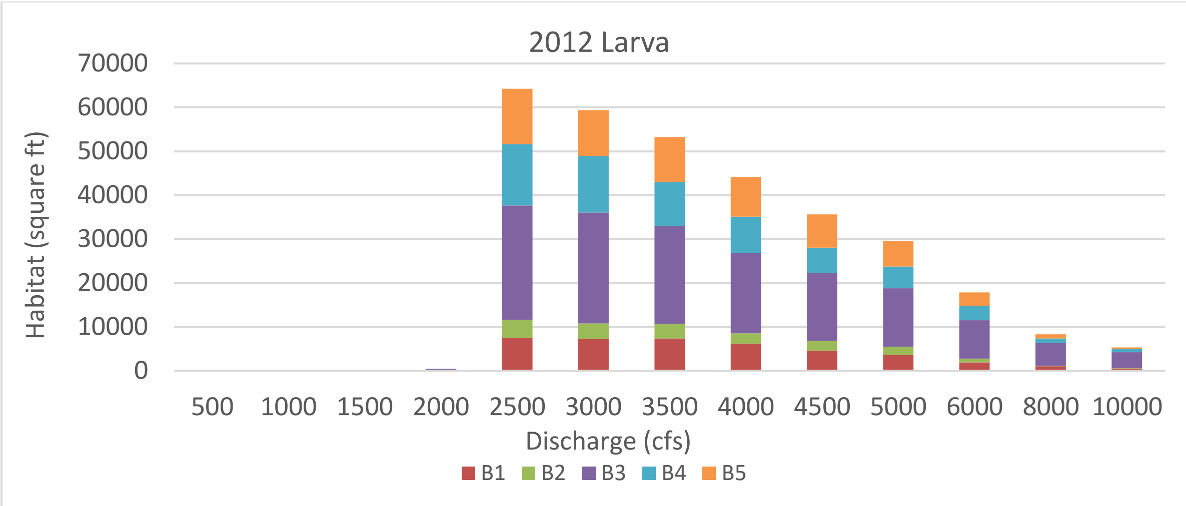

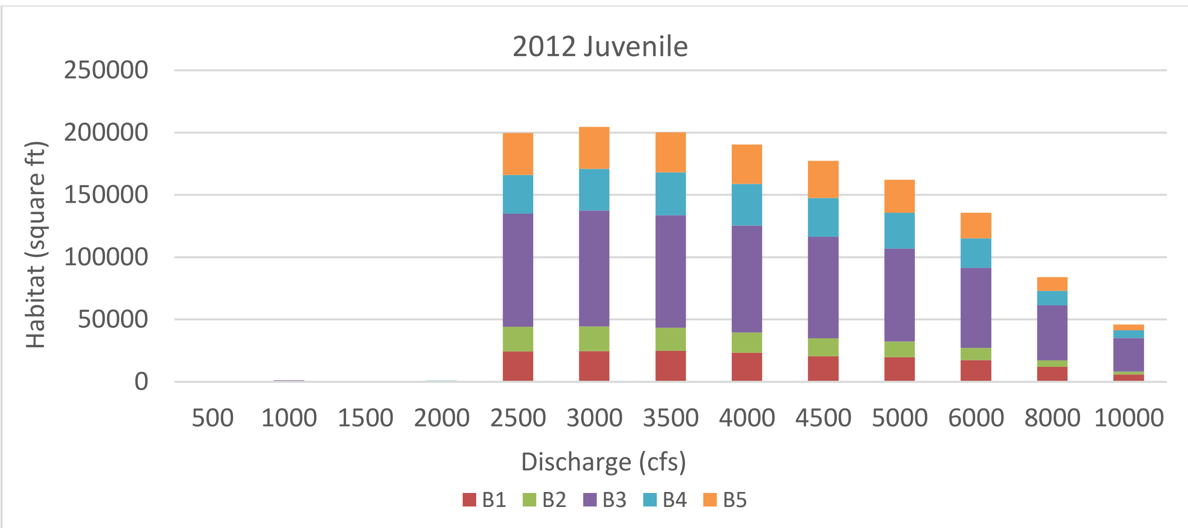

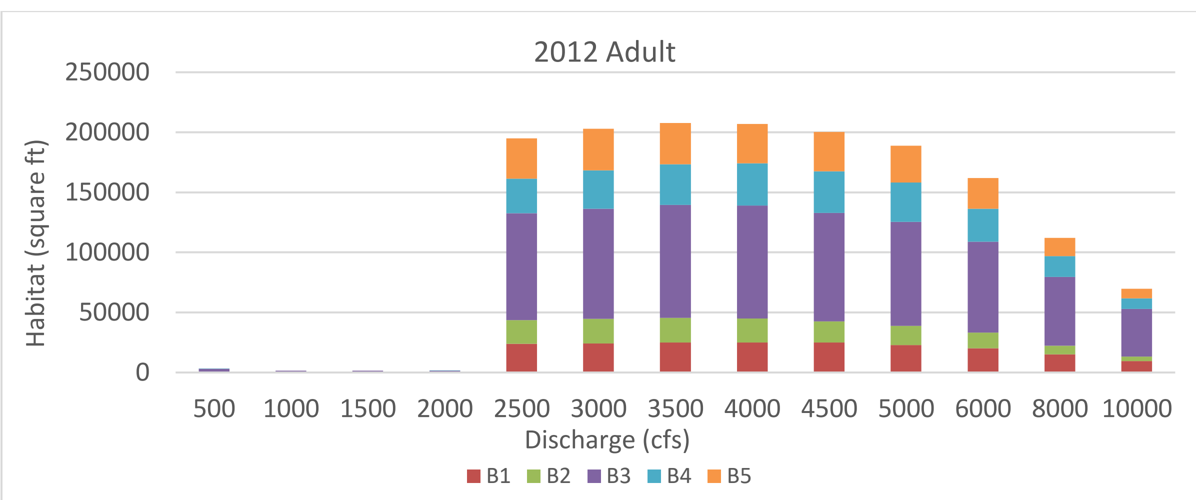

Figure 70: Stacked habitat charts to display spatial variations of habitat throughout the Bosque del Apache reach in 2012

4.4 RAS-Mapper Methodology

RAS-Mapper was used to present the 1-D habitat estimates in a pseudo two-dimensional (2-D) visualization. RAS-Mapper overlays the water onto a prescribed terrain and interpolates the water surface elevation to create an estimate of the location of water inundation, which can then be used to predict locations of hydraulically suitable habitat.

The HEC-RAS geometry data that was necessary for the RAS-Mapper analysis (geo-referenced cross-sections and a LiDAR surface to generate a terrain) was available only for the year 2012. Therefore, only 2012 results were processed in RAS-Mapper. The original 2012 LiDAR data were used to develop a raster on ArcMap software which could be imported as a terrain in RAS-Mapper. The RAS-Mapper application distributes the water throughout the terrain, interpolating between the cross-sections, which results in a more accurate understanding of where water is present in a channel. RAS-Mapper will also predict the flow depth and velocity at a given discharge. ArcMap's "ModelBuilder" feature was used to combine the RAS-Mapper generated rasters for velocity and depth, so the RGSM depth and velocity criteria could be applied to identify the areas of suitable habitat. The results were used to create maps that show the areas of hydraulically suitable habitat for each life stage of the RGSM.

4.5 RAS-Mapper Habitat Results in 2012

While the width slice method quantitatively determined areas with increased potential for habitat, RAS-Mapper was used to spatially depict these areas of potential RGSM habitat throughout the MRG and display the results on a map of the river. The hydraulically suitable habitat for each life stage was mapped at discharges of 1,500 cfs, 3,000 cfs, and 5,000 cfs, which have daily exceedance probabilities of around 11%, 4%, and 0.08%, respectively. The habitat maps for the reach at these discharges are available in Appendix E.

At 1,500 cfs, flow is confined to the main channel limiting suitable habitat in all subreaches. While there are very small portions of habitat available in the upper subreaches B1, B2, and B3, there is virtually no habitat available in subreaches B4 and B5. At 3,000 cfs the virtual levees are removed and the flow overtops the banks of the main channel. At this discharge, the amount of potential habitat drastically increases for juvenile and adult life stages of the RGSM across all subreaches. Larval habitat does not appear in large amounts but is instead very isolated to the edges of some inundated areas. At 5,000 cfs the inundated areas appear very similarly to the 3,000 cfs maps with differences in the distribution of suitable habitat now located closer to the edges of floodplains as the stage has increased. The differences between habitat maps at 1,500 cfs and 3,000 are demonstrated in Figure 71.

At the higher discharges the perching of the main channel becomes very apparent, as seen in Figure 71 and more clearly in the larger maps Appendix E. On these maps, levees bordering the main channel separate the main channel from the floodplains. These levees could therefore pose issues for the Silvery Minnow's ability to return to the main channel after high flows have receeded. Because the perching is not isolated but ubiquitous throughout the reach, actual habitat areas could be overrepresented.

Although a discharge of 5,000 cfs may not be commonly seen throughout the Bosque del Apache reach, maps at this discharge still provide the opportunity to examine possible areas that are more likely to meet the velocity and depth criteria for the RGSM. This can help in identifying which areas may have hydraulically suitable habitat that are connected to the main channel due to backwater or natural formation of pools and which subreaches contain habitat that may be found suitable but are not connected to the main channel. Both instances may be beneficial for the future of the RGSM, but different approaches may be needed in planning restoration efforts.

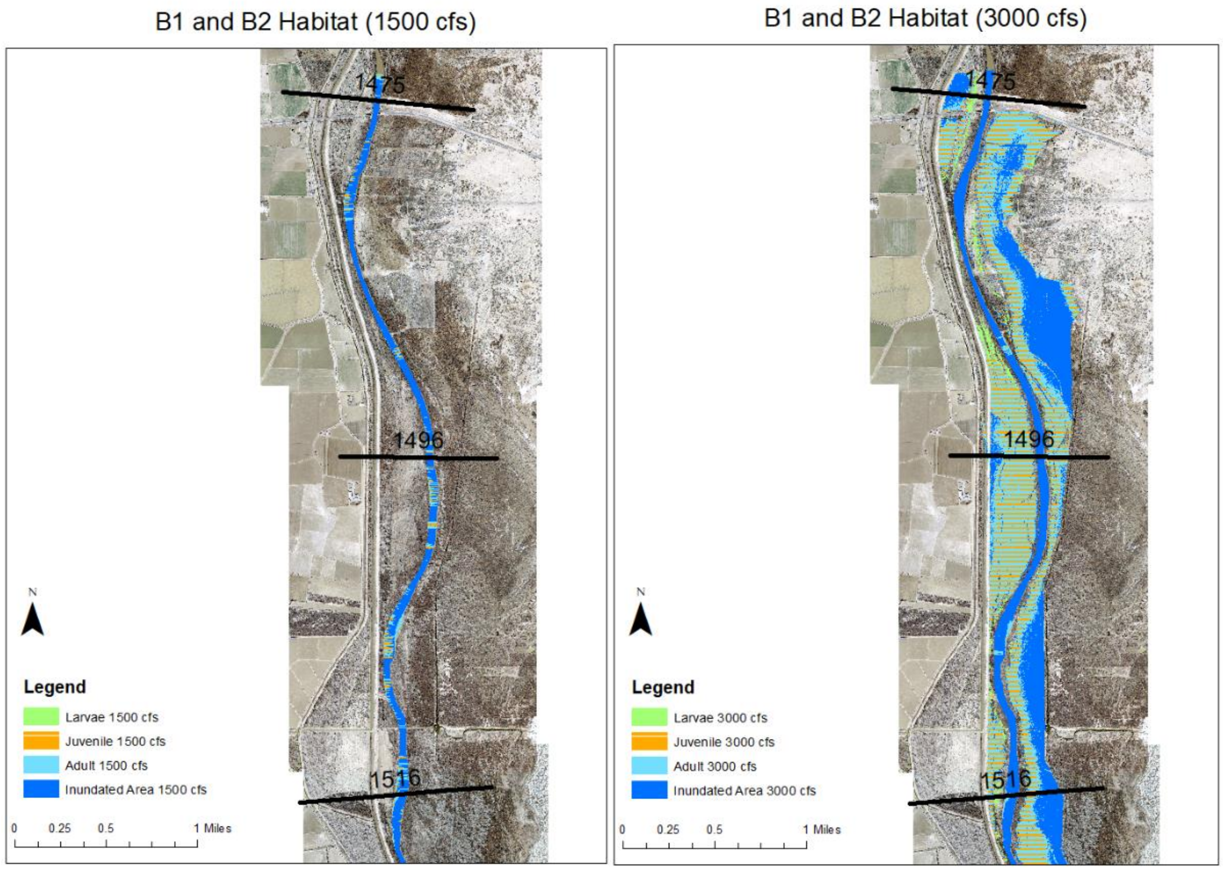

Figure 71: Habitat maps for subreaches B1 and B2 at 1500 cfs and 3000 cfs

4.6 Disconnected Areas

RAS-Mapper provides the opportunity to identify areas that likely meet the velocity and depth requirements of the RGSM at specified discharges. RAS-Mapper may also be beneficial for identifying areas throughout the reach that may contain water but fail to remain connected to the main channel. These may be possible areas of focus for restoration efforts.

By connecting several of these disconnected areas, the Silvery Minnow may gain a great amount of possible habitat. Figure 72 shows one instance of a disconnected area in the Bosque del Apache reach. The disconnected area is emphasized in the red square. It is possible to see that the main channel is deeper (darker blue) yet the floodplains and low-lying areas may become inundated at higher flows. The disconnected areas could identify problem areas for the RGSM by indicating that there are areas where fish may become stranded in months when the river contains less water and disconnected areas form. Conversely, these areas could become possible restoration sites leading to an increase in hydraulically suitable RGSM habitat.

After calculating the velocity and depth distribution, these disconnected areas often meet the depth and velocity criteria of the RGSM. However, the lack of connectivity eliminates the possibility of RGSM habitat. Figure 72 for example predicts that the shown disconnected areas would be hydraulically suitable for the RGSM extensively for the adult and juvenile life stages, and even show small areas that may support the larval life stage as well.

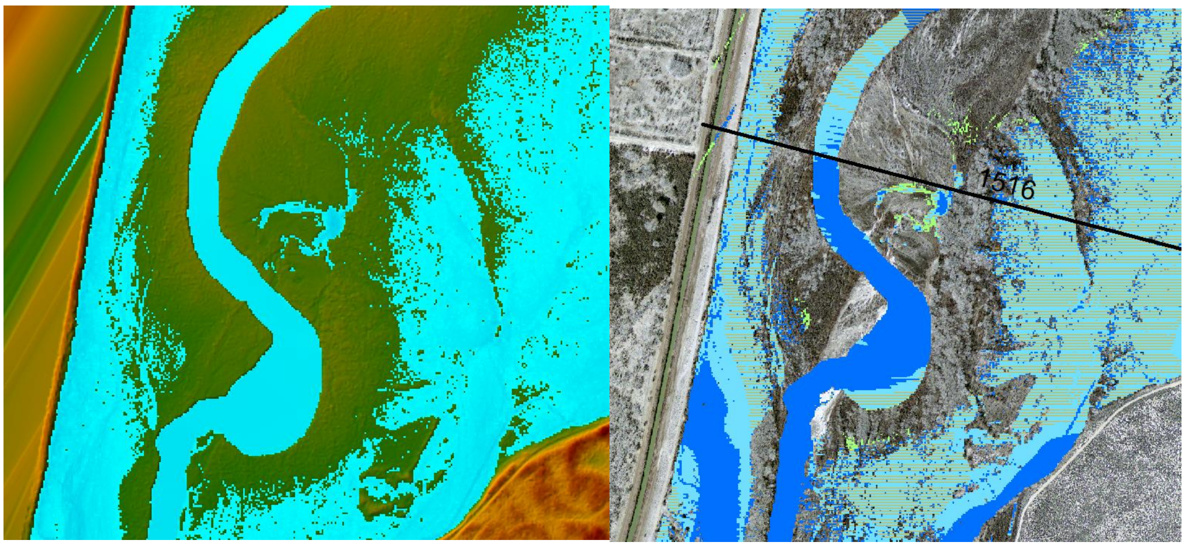

Figure 72: Inundated area disconnected from main channel (left) and habitat map (right) showing hydraulically suitable habitat for RGSM adult (green), juvenile (yellow cross hatch), and larvae (orange)

5. Bosque Del Apache Reach Synthesis

In the Bosque Del Apache Reach, the channel morphology is influenced by upstream reservoir construction, flow diversions, and periods of drought and high annual flow volumes. Changes in flow peaks, annual flow volume, and sediment supply have influenced channel width, depth, and velocity. The flow and sediment drivers have caused changes in bed elevation, which has altered the discharge at which flows overbank the channel and access the floodplain. In this section, results presented throughout the report are synthesized to link the effects of the geomorphic drivers (sediment and water supply) with the observed changes in channel morphology.

To understand the underlying processes driving the changes to the Bosque Del Apache Reach, first the trends in the hydrology of the river must be examined. As shown in Section 2, there have been changes in mean daily peak flow and annual flow volume. Figure 18 shows the cumulative annual discharge in the Bosque Del Apache Reach from 1949 to present, and the discharge trends during this time can be divided into three distinct periods. Most notably, the first period (late 1940s to late 1970s) was a time of low annual flow volume. During the period from 1949 to 1978 the annual flow volume was significantly less than from 1979 to 1999. Then from 2000 to the present (2021) annual flow volume was lower. The periods when flow exceeded 5,000 cfs for the greatest number of days are consistent with the cumulative annual flow volume (Figure 25). During the period from 1949 to 1978 there were very few days when flows were greater than 5,000 cfs. Conversely, from 1979 to about 1999 there were a larger number of days with higher flows. Since 2000, there were not many days above 5,000 cfs, although 2008, 2017, and 2019 also had relatively large, long duration, spring runoff events. The Escondida and San Antonio gages had relatively short period of records for use in this synthesis. It is evident from the San Marcial Gage raster hydrographs of daily discharge (Figures 12 and 13) that there were several large peaks over 10,000 cfs in the early 1900s up until about 1942. Peak flow decreased during the period from 1943 to the present due to a combination of upstream dams and drought. After the high flow year in 1942, peak flows have commonly been near or below 5,000 cfs. Although annual flow volumes are large between 1979 and 1999, the peak flow magnitude is much smaller than events in the early 1900s. Annual flow volumes and peak flow magnitudes have both been low during the current drought from 2000 to the present, with the 2005 spring runoff event being the most notable exception.

Sediment loads in the Bosque Del Apache Reach have also changed over the period recorded by the gages. From 1957 (when data are first available) to 1982, sediment loads were higher on an annual basis than from 1982 to the present. The change after 1982 is most likely because of closure of Cochiti Dam in 1975 and the time lag required for effects to propagate downstream.

These changes to the hydrology and sediment drivers of lower peak flows, lower annual flow volumes, and lower sediment loads have resulted in channel narrowing, increased mean flow depth, and decreased wetted perimeter. All sub-reaches show that the active channel width, determined using the channel vegetated bank lines (Figure 38) was greatest in 1918 before a sharp decrease in 1935 and 1949, most likely due to changes in peak flow and some change in sediment supply (Scurlock, 1998). The narrowing between 1949 and 1962 is attributed to Reclamation's channelization during a period of drought. The width increase between 1972 and 1992 in sub-reaches B1 and B2, and the increase between 1972 and 1987 in sub-reach B3, is attributed to bankline destabilizing vegetation clearing. The vegetation clearing during the 1960s and 1970s enabled subsequent high flows in the early and mid-1980s to erode a wider channel. Using HEC-RAS results for 3,000 cfs, 1972 and 1992 demonstrate a similar trend of decreasing widths before increasing by 2002 (Figure 35). Between 2002-2012 the top width decreased for nearly all sub-reaches. The relatively large spring runoff flow event in 2005 did not widen the channel, likely because of the combined effects of vegetation stabilizing the banks and the smaller flow energy compared to previous historical events. Generally, all sub-reaches demonstrate net trends of decreasing top widths over the period from 1962 to 2012. The expected increase in hydraulic depth occurred (Figure 44) over this same time period when the channel narrowed. Between 1962 and 2012, the channel wetted perimeter decreased (Figure 46) as a result of channel narrowing. Although there are periods of degradation for certain subreaches, the bed elevation has been increasing, with the highest bed elevation occurring in 2012 for the upstream subreaches and in 2002 for the downstream subreaches. The increased hydraulic depth during a period of bed aggradation illustrates that the rate of sediment deposition on the banks has been higher than sediment deposition on the bed. Overall, during this same time period bed slope has decreased. Channel narrowing, bed aggradation, bankline deposition and a flatter slope indicate that the river system is not transporting the sediment supplied from upstream, even though this supply has decreased since 1982. The reduction in transport capacity caused by channel perching, reduced peak flows, and reduced flow volumes have a larger effect than the reduced suspended sediment supply. Additionally, there is a discontinuity between the seasonal timing of sediment supply and transport. Most of the sediment is delivered to the system from summer monsoon events, while most of the energy to transport sediment is available during spring runoff events (Figure 30 and 31).

Large peak flow events are an important factor in the channel morphology of the Bosque Del Apache Reach. As shown in Figure 32, monsoonal thunderstorms during the summer months serve as the primary mechanism for delivering large quantities of sediment to this Reach. Even though large discharges occur during the spring months, these flows are controlled by dam releases, which are typically sediment starved. Conversely, summer thunderstorms cause runoff from arroyos to enter the river, carrying with it large amounts of sediment. Consequently, much of the geomorphic changes to the river likely happen during these events. Field observations from the Bureau of Reclamation (Nathan Holste, pers. comm.) indicate that monsoon events typically cause sediment deposition and the formation of new bank-attached bars, while channel erosion typically occurs during larger spring runoff events if there is not a sediment plug.

From Figure 32, large discharges of suspended sediment correlate with large monsoonal events. The 2013 summer thunderstorms provide a clear example of this. This event had a high suspended sediment concentration, delivering approximately 66% of the total suspended sediment measured that year. 2014 and 2018 are also good examples this characteristic stair-stepping pattern with large jumps in suspended sediment occurring between June and September. Some years, such as 2017, have more gradual patterns. However, even in 2017, a large sediment discharge event occurred in September that accounted for approximately 35% of the total annual suspended sediment load.

As described in Section 3.3, the bed elevation of the river has undergone alternating cycles of aggradation and degradation. However, generally, the Bosque Del Apache Reach has been experiencing net aggradation since 1962. From agg/deg line 1590-1605 the bed elevation appears to be less sensitive to change. This point in the Reach is just downstream of two large bends and is where the river begins to dramatically narrow and straighten. While it is possible that differences in bed sediment composition, such as a clay deposit, could make this portion of the Reach less sensitive to aggradation and degradation, without subsurface sediment sampling in this location, the cause is unknown. Upstream from agg/deg line 1590 and in sub-reaches B2 and B3 the main channel bed has been raising (Figure 39). A depositional riverbed causes more sediment to flow into the floodplain resulting in sediment deposition in the riparian zone forming "natural levees". This creates a main channel that is "perched" above the valley floor (Figure 45). Channel perching is present in all subreaches of the Bosque Del Apache reach but is most pronounced in areas with the largest bed elevation increases. Most channel perching has occurred in subreaches B2 and B3 (Figure 39). Conversely, in the portion of the channel that has had limited changes in bed elevation (Agg/deg 1590-1605), there is little to no channel perching. In Subreach B5 (agg/deg line 1605 to 1637) the river bed aggraded between 1972 and 2002, then degraded back to the 1992 profile between 2002 and 2012. The aggradation is a result of reservoir water surface elevation increase while the degradation is a result of reservoir water surface elevation decrease (Sperry, et al. 2022).

Table 6 summarizes the hydrology, sediment, and geomorphic trends between 1962 and 2012. While the Bosque Reach has generally been experiencing aggradation, the channel has been simultaneously narrowing (Figure 42), and the slope has been generally flattening (Figure 47), with the exception of subreach B4. At the same time the bank height has been changing as a result of natural levee development. The narrow width and flatter slope are indications of peak flow reduction and reduced sediment load, but due to the effects of channel perching, aggradation and plug formation have ensued. Sinuosity across most subreaches has decreased with the exception of subreach B4.

Table 6 Geomorphic trends overtime by subreach

	Period	Hydrology	Suspended Sediment	Change in Bed Elevation	Change in Width	Change in Slope	Change in Sinuosity	Change in Bank Height
Subreach B1	1962-1972	Dry; low volumes and peaks	High	None	Increase	Decrease	Slight Increase	Increase
	1972-1992	Wet; high volumes and moderate peaks	High (1972 – 1982) then low (1983 – 1992)	Increase	Increase	Decrease	Slight Increase	Decrease
	1992-2002	Average; high then low volumes, moderate peaks	Moderate	None	Decrease	Increase	None	Decrease
	2002-2012	Dry; low volumes and peaks	Moderate	Slight Increase	None	Increase	Slight Increase	Increase
Subreach B2	1962-1972	Dry; low volumes and peaks	High	None	Increase	Increase	None	Increase
	1972-1992	Wet; high volumes and moderate peaks	High (1972 – 1982) then low (1983 – 1992)	Increase	Increase	Decrease	Slight Increase	Decrease
	1992-2002	Average; high then low volumes, moderate peaks	Moderate	Increase	Decrease	Decrease	Slight Increase	Decrease
	2002-2012	Dry; low volumes and peaks	Moderate	None	Decrease	Increase	Slight Increase	Increase
Subreach B3	1962-1972	Dry; low volumes and peaks	High	Decrease	None	None	Increase	Increase
	1972-1992	Wet; high volumes and moderate peaks	High (1972 – 1982) then low (1983 – 1992)	Increase	Decrease	None	Decrease	Decrease
	1992-2002	Average; high then low volumes, moderate peaks	Moderate	Increase	Increase	None	Increase	Decrease
	2002-2012	Dry; low volumes and peaks	Moderate	None, Slight Inc/Dec	Decrease	Slight Increase	Increase	Increase

Subreach B4	1962-1972	Dry; low volumes and peaks	High	Decrease	Increase	None	Increase	Increase
	1972-1992	Wet; high volumes and moderate peaks	High (1972 – 1982) then low (1983 – 1992)	Slight Decrease	Decrease	Increase	Increase	Increase
	1992-2002	Average; high then low volumes, moderate peaks	Moderate	Increase	Increase	Increase	Increase	Decrease
	2002-2012	Dry; low volumes and peaks	Moderate	Increase	Decrease	Decrease	Slight Increase	Increase
Subreach B5	1962-1972	Dry; low volumes and peaks	High	Increase	Increase	Slight Decrease	Increase	Decrease
	1972-1992	Wet; high volumes and moderate peaks	High (1972 – 1982) then low (1983 – 1992)	Increase	Decrease	Decrease	Decrease	Decrease
	1992-2002	Average; high then low volumes, moderate peaks	Moderate	Increase	Decrease	Decrease	Slight Increase	Decrease
	2002-2012	Dry; low volumes and peaks	Moderate	Decrease	None	Increase	Slight Decrease	Increase

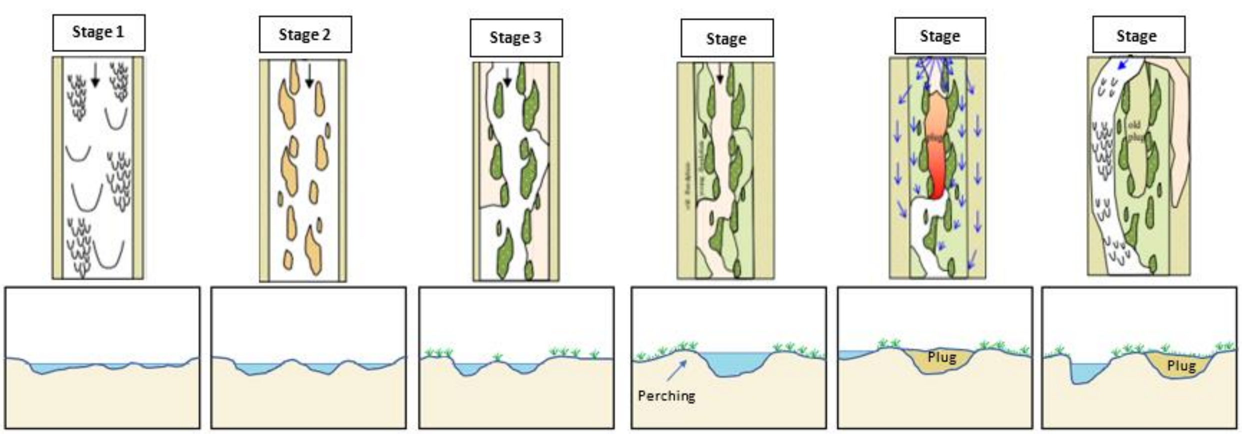

Figure 73: Top Row: Original Massong planforms; Second Row: Typical cross sections in the Bosque Del Apache Reach.

Using the Massong et al. (2010) classification system for these sub-reaches, coupled with the agg/deg cross section data, has enabled representative typical cross sections to be developed for Stage 1,2, and 3 and stages A4 A5 and A6 (Figure 73). These typical cross section depictions can serve as a helpful aid to visualize the different cross sections found within the Bosque Del Apache reach and demonstrate the rationale behind their classification. Stages one through three show a wide and braided channel that progressively becomes more vegetated and less braided. In stage 3, the channel corridor narrows as vegetation establishes. In the aggrading stage A4 there is an excess sediment supply and as a result, sediment is deposited on the riverbanks, eventually resulting in channel perching. The channel continues to narrow and perch until an eventual threshold is reached in which a sediment plug is formed, blocking the main channel (A5). In this stage flow is diverted to the floodplain. By stage A6 a new channel is established and the old channel is abandoned. These cross-section depictions based on measured agg/deg data enables the Massong et al. (2010) classification system to be expanded to provide a more complete three-dimensional description of the channel stages.

HEC-RAS modeling was completed to evaluate habitat for the RGSM. One of the most important aspects of RGSM is the connection of the main channel to the floodplain. In general, flows that go over bank and access the floodplain results in significant habitat availability. The general trends for all sub-reaches are that significant habitat was available at 1500 cfs in 1962, 3,000 cfs in 1972, 2500 cfs in 1992, 1500 cfs in 2002, and 2,000 cfs in 2012. The bed incision between 1962-1972 resulted in higher flows being needed for minnow habitat, aggradation from 1972 to 2002 resulted in suitable minnow habitat at lower flows, and the small change between 2002 and 2012 resulted in slightly higher flows for significant overbanking, but not as high as 1972. Minnow habitat and the associated link to geomorphology and hydraulics will be further discussed in a separate process linkage report.

6. Conclusions

The Bosque del Apache reach, spanning about 16 miles from the US 380 Bridge near San Antonio, New Mexico to the southern boundary of BNWR was analyzed for hydrologic, hydraulic and geomorphic trends between 1918 and 2021. HEC-RAS and GIS were used to find geomorphic and river characteristics such as sinuosity, width, bed elevation and other hydraulic parameters. Hydraulically suitable RGSM habitat was determined quantitatively and spatially throughout the reach.

Major findings include:

- The hydrograph for the Bosque del Apache reach has become less varied and flashy since the 1950's due to diversions and damming of the MRG. Higher flows appear to return to the channel in the 1970s, possibly due to the San Juan-Chama project. Beginning in the late 1990s, the number of zero flow days as well as the average flow amounts had decreased at the San Marcial gage.
- While spring snowmelt typically brings the largest increases in the discharge volumes in the Bosque del Apache reach, summer thunderstorms have a greater impact on the amount of suspended sediment transported. Strong monsoonal storms led to flooding of the MRG in September of 2013, resulting in large increases in both cumulative discharge and sediment. On September 17th, 2013, the San Antonio gage reached a peak discharge of 6,310 cfs with suspended sediment reaching 403,000 tons per day on September 14th. Several severe thunderstorms between July 27th and August 5th of 2014 also resulted in flooding of the MRG with a peak discharge of about 1,860 cfs on August 5th with suspended sediment transport of

285,000 tons per day on Aug 5th. In 2013, the sediment concentration peaked around 71,000 mg/L where in 2014 concentrations peaked at 78,000 mg/L.

- The channel has narrowed significantly in the Bosque del Apache reach between 1918 and 1972 by a range of differences between 1084 feet and 3014 feet. In subreaches B2, B3, and B4, a second round of narrowing appears to have occurred between 2008 and 2012. These subreaches have since remained stable at widths between 150 ft and 250 ft, which is close to the predicted widths by the JW equations ~250 ft. Subreaches B1 and B5 had reached stability in 2002 and have remained at 180 and 100 ft respectively.
- All subreaches have experienced net aggradation between 1962 and 2012. This trend is most pronounced in subreach B3 with a bed increase up to 6 ft. In subreaches B4 and B5 the increase in bed elevation is less pronounced and even appears to have begun degrading between 2002 and 2012.
- Cross sections in all subreaches indicate that the bank elevation is aggrading faster than the bed elevation, thus forming natural levees and perching.
- The majority of grain diameter measurements from 1991 to 2002 did not significantly change and are classified as fine to medium sand.
- Sinuosity has remained low and stable for subreaches B1, B2, and B5 at or below 1.05 in 2019. However, sinuosity appears to be increasing in subreach B3, which is moderately sinuous at 1.14 in 2019. Subreach B4 has a slightly higher sinuosity at 1.23 which has remained stable since 2001.
- Through observation of the cross-sectional profiles and historical aerial imagery, all subreaches appear to be in the aggrading stage of Massong's classification, A4.
- The bankfull discharges in 1972 and 2012 were approximately 500 cfs higher than all other years.
- While the width slices method shows a relatively significant area of hydraulically suitable habitat for most of the reach, the RAS-mapper habitat maps show that much of the habitat has very limited connectivity to the main channel due to channel perching.

7. Bibliography

Holste, N. (2020) “One-Dimensional Numerical Modeling of Perched Channels.” U.S. Bureau of Reclamation, Denver, CO.

Beckwith, T and Julien, P.Y (2020) *“Middle Rio Grande Escondida Reach Report:Morpho-dynamic Processes and Silvery Minnow Habitat from Escondida Bridge to US-380 Bridge (1918-2018.)”* Colorado State University, Fort Collins, CO.

Bovee, K.D., Waddle, T.J., and Spears, J.M. (2008). “Streamflow and endangered species habitat in the lower Isleta reach of the middle Rio Grande.” *U.S. Geological Survey Open-File Report 2008-1323*.

Doidge, S and Julien, P.Y. (2019). Draft Report. *Middle Rio Grande San Acacia Reach: Morphodynamic Processes and Silvery Minnow Habitat from San Acacia Diversion Dam to Escondida Bridge*, Colorado State University, Fort Collins, CO.

Glasser, L.S. (1998). *San Juan-Chama Project*, Bureau of Reclamation, Albuquerque, NM.

Greimann B. and N. Holste (2018). *Analysis and Design Recommendation of Rio Grande Width,* Technical Report. SRH-2018-24, Sedimentation and River Hydraulics Group Technical Service Center, US Bureau of Reclamation, Denver, Colorado, 20p.

Julien, P.Y. (2002). *River Mechanics*, Cambridge University Press, New York

Julien, P. Y., and Wargadalam, J. (1995). “Alluvial channel geometry: theory and applications.” *Journal of Hydraulic Engineering*, American Society of Civil Engineers, 121(4), 312–325.

Klein, M., Herrington, C., AuBuchon, J., and Lampert, T. (2018a). *Isleta to San Acacia Geomorphic Analysis*, U.S. Bureau of Reclamation, Reclamation River Analysis Group, Albuquerque, New Mexico.

Klein, M., Herrington, C., AuBuchon, J., and Lampert, T. (2018b). *Isleta to San Acacia Hydraulic Modeling Report*, U.S. Bureau of Reclamation, Reclamation River Analysis Group, Albuquerque, New Mexico.

LaForge, K., Yang, C.Y., Julien, P.Y., and Doidge, S. (2019). Draft Report. *Rio Puerco Reach: Hydraulic Modeling and Silvery Minnow Habitat Analysis*, Colorado State University, Fort Collins, CO.

Larsen, A. (2007). *Hydraulic modeling Analysis of the Middle Rio Grande-Escondida Reach, New Mexico*. M.S thesis, Civil Engineering Department, Colorado State University, Fort Collins, CO.

Makar, P., Massong, T., and Bauer, T. (2006). “Channel Widths Change Along the Middle Rio Grande, NM.” *Joint 8th Federal Interagency Sedimentation Conference, Reno, NV, April 2 -April6, 2006.*

Massong, T., Paula, M., and Bauer, T. (2010). “Planform Evolution Model for the Middle Rio Grande, NM.” *2nd Joint Federal Interagency Conference, Las Vegas, NV, June 27 - July 1, 2010*.

MEI. (2002). *Geomorphic and Sedimentologic Investigations of the Middle Rio Grande between Cochiti Dam and Elephant Butte Reservoir*, Mussetter Engineering, Inc., Fort Collins, CO, 220 p.

Mortensen, J.G., Dudley, R.K., Platania, S.P., and Turner, T.F. (2019). *Rio Grande Silvery Minnow Habitat Synthesis,* University of New Mexico with American Southwest Ichthyological Researchers, Albuquerque, NM.

Mortensen, J.G., Dudley, R.K., Platania, S.P., White, G.C., and Turner, T.F., Julien, P.Y., Doidge, S, Beckwith, T., Fogarty, C. (2020). *Linking Morpho-Dynamics and Bio-Habitat Conditions on the*

Middle Rio Grande: Linkage Report 1- Isleta Reach Analyses. Submitted to the U.S. Bureau of Reclamation, Albuquerque, New Mexico.

Paris, A., Anderson, K., Shah-Fairbank S., P. Julien, (2011). "Bosque Reach - Arroyo de las Cañas to the South Boundary of the Bosque del Apache: Hydraulic Modeling Analysis 1962-2008". Fort Collins, CO, Colorado State University.

Pinson, A.O., Scissons, S.K., Brown, S.W., Walther, D.E. (2014). *Post Flood Report: Record Rainfall and Flooding Events during September 2013 in New Mexico, Southeastern Colorado and Far West Texas*, U.S. Army Corps of Engineers, Albuquerque, New Mexico.

Posner, A. J. (2017). Draft report. *Channel conditions and dynamics of the Middle Rio Grande River*, U.S. Bureau of Reclamation, Albuquerque, New Mexico.

Scurlock, D. (1998). "From the Rio to the Sierra: an environmental history of the Middle Rio Grande Basin." *General Technical Report RMRS-GTR-5. Fort Collins, CO: US Department of Agriculture, Forest Service, Rocky Mountain Research Station, 440 p.*

Shah-Fairbank, S. C., Julien, P. Y., and Baird, D. C. (2011). "Total sediment load from SEMEP using depth-integrated concentration measurements." Journal of Hydraulic Engineering, 137(12), 1606–1614.

Sperry, J., Schied, A., Julien, P.Y (2022) *"Middle Rio Elephant Butte Reach Report: Morpho-dynamic Processes and Silvery Minnow Habitat from the Southern Boundary of the Bosque Del Apache National Wildlife Refuge to The Elephant Butte Reservoir"* Colorado State University, Fort Collins, CO, 179p.

U.S. Bureau of Reclamation. (2012). "Middle Rio Grande River Maintenance Program - Comprehensive Plan and Guide." Albuquerque Area Office, Albuquerque, New Mexico, 202p.

U.S. Fish and Wildlife Service. (2007). "Rio Grande Silvery Minnow (Hybognathus amarus)." Draft Revised Recovery Plan, Albuquerque, New Mexico, 174 p.

Varyu, D. (2013). *Aggradation / Degradation Volume Calculations: 2002-2012*. U.S. Department of the Interior, Bureau of Reclamation, Technical Services Center, Sedimentation and River Hydraulics Group. Denver, CO.

Varyu, D. (2016). *SRH-1D Numerical Model for the Middle Rio Grande: Isleta Diversion Dam to San Acacia Diversion Dam*. U.S. Department of the Interior, Bureau of Reclamation, Technical Services Center, Sedimentation and River Hydraulics Group. Denver, CO.

Yang, C.Y. (2019). *The Sediment Yield of South Korean Rivers*, Colorado State University, Fort Collins, CO.

Yang, C.Y. and Julien, P.Y. (2019). "The ratio of measured to total sediment discharge." *International Journal of Sediment Research*, 34(3), pp.262-269.

Yang, C.Y., LaForge, K., Julien, P.Y., and Doidge, S. (2019). Draft Report. *Isleta Reach: Hydraulic Modeling and Silvery Minnow Habitat Analysis*, Colorado State University, Fort Collins, CO.

Appendix A

Cumulative Plots used in the Subreach Delineation, Aerial Imagery with Agg/deg Line Labels

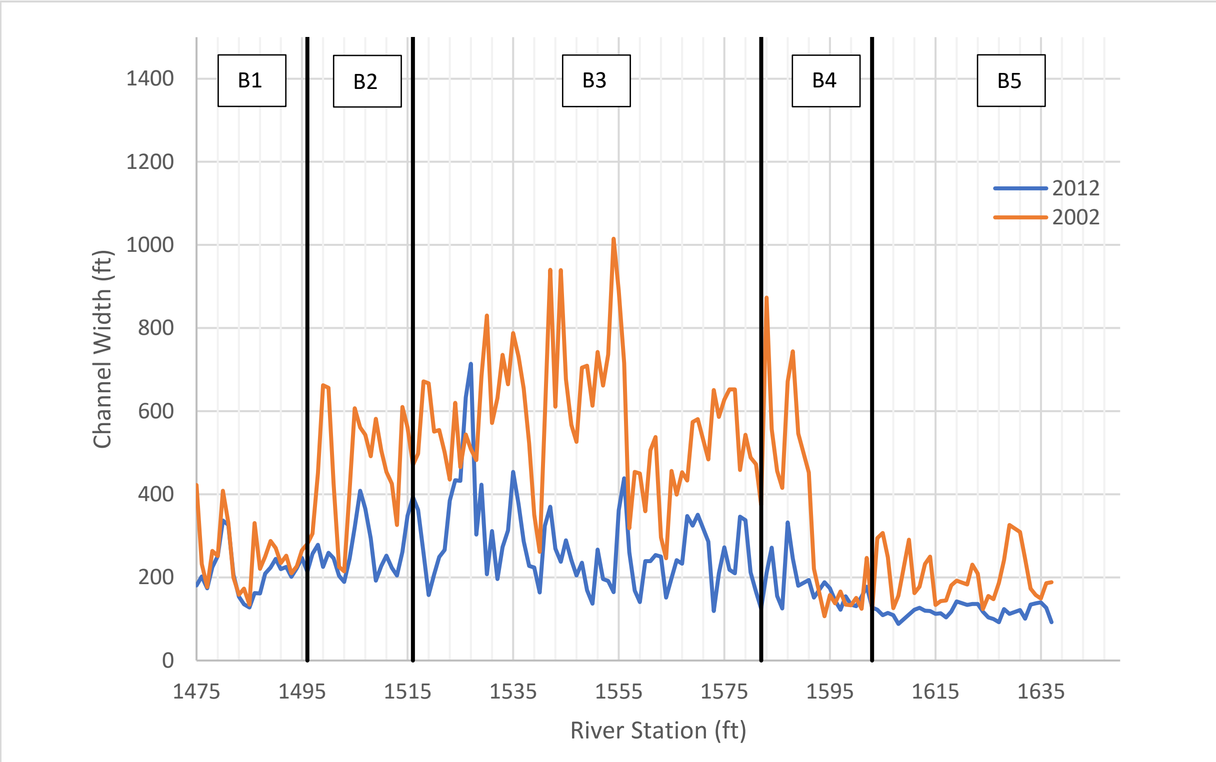

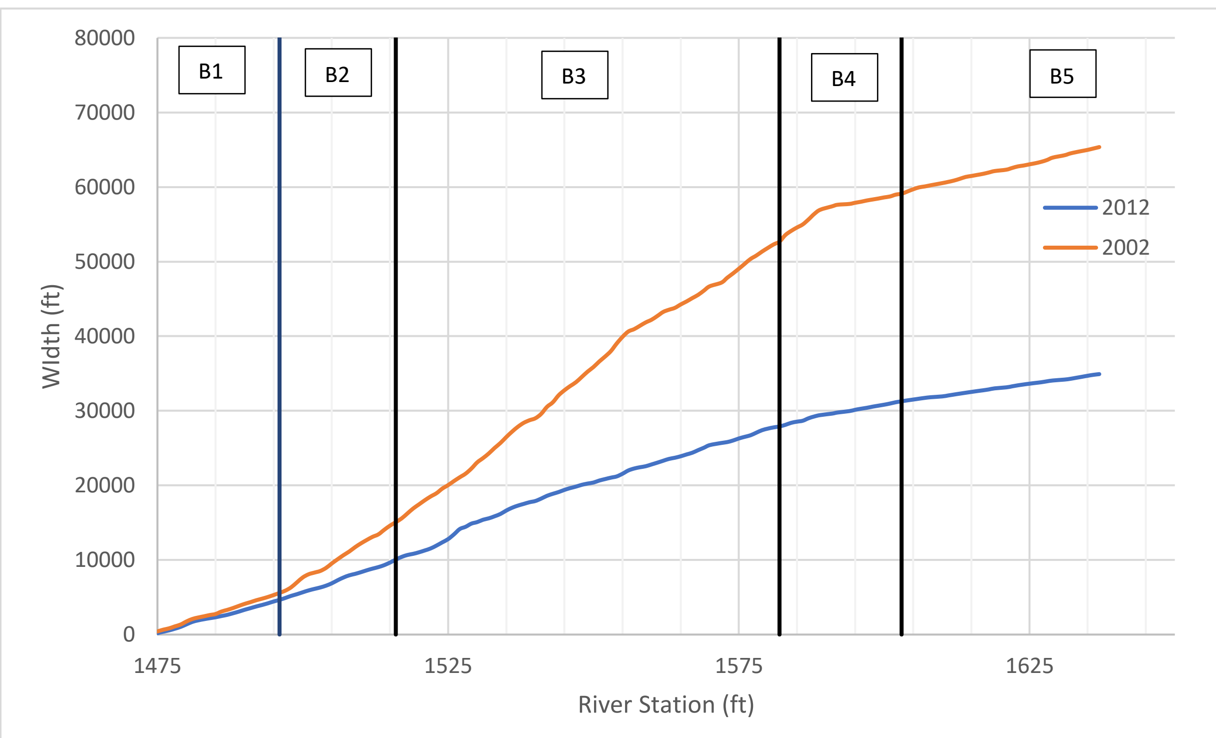

Figure A- 1 Width (top) and cumulative width (bottom) throughout the Bosque reach for the years 2002 (orange) and 2012 (blue).

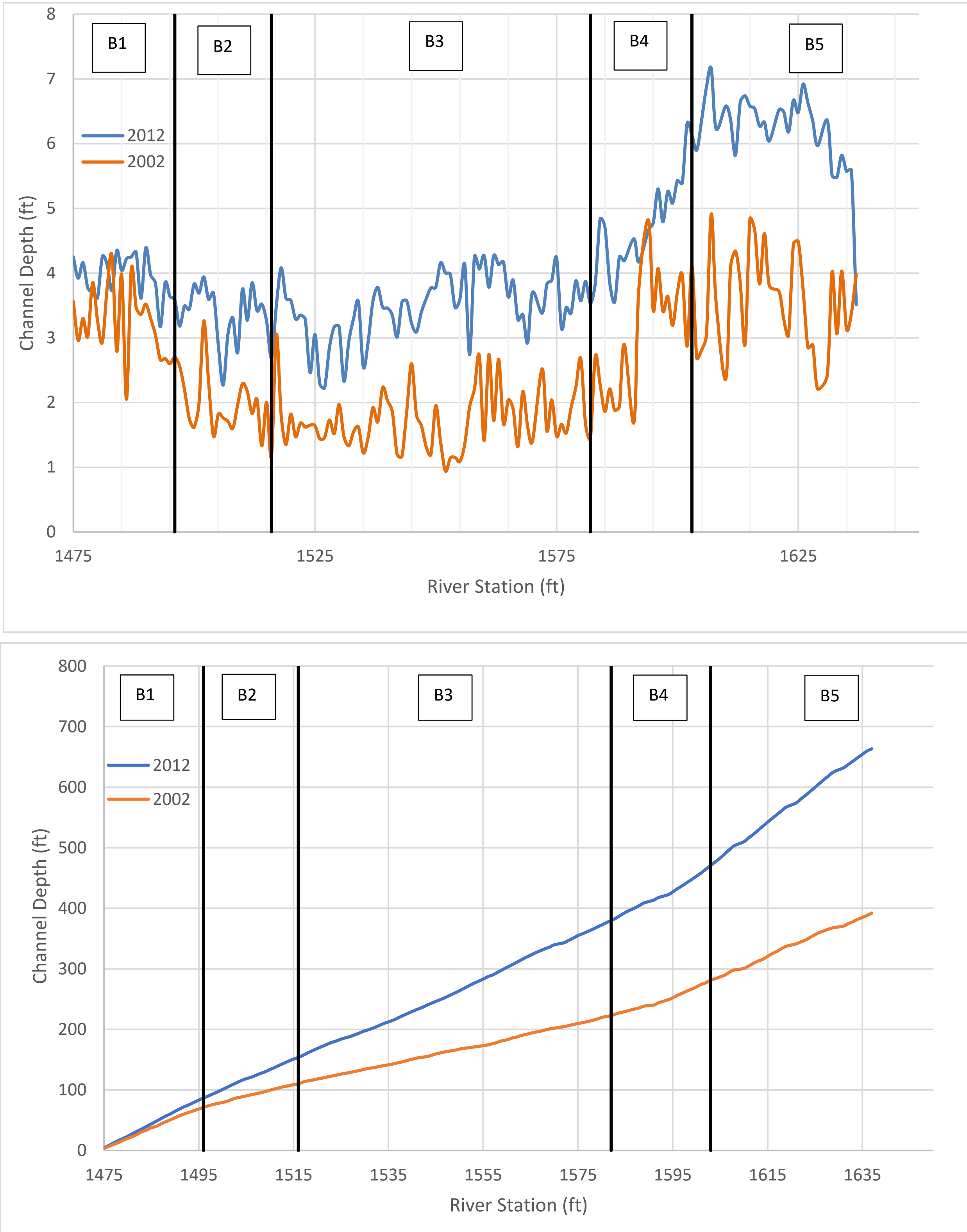

Figure A- 2 Depth (top) and cumulative depth (bottom) throughout the Bosque reach for the years 2002 (orange) and 2012 (blue).

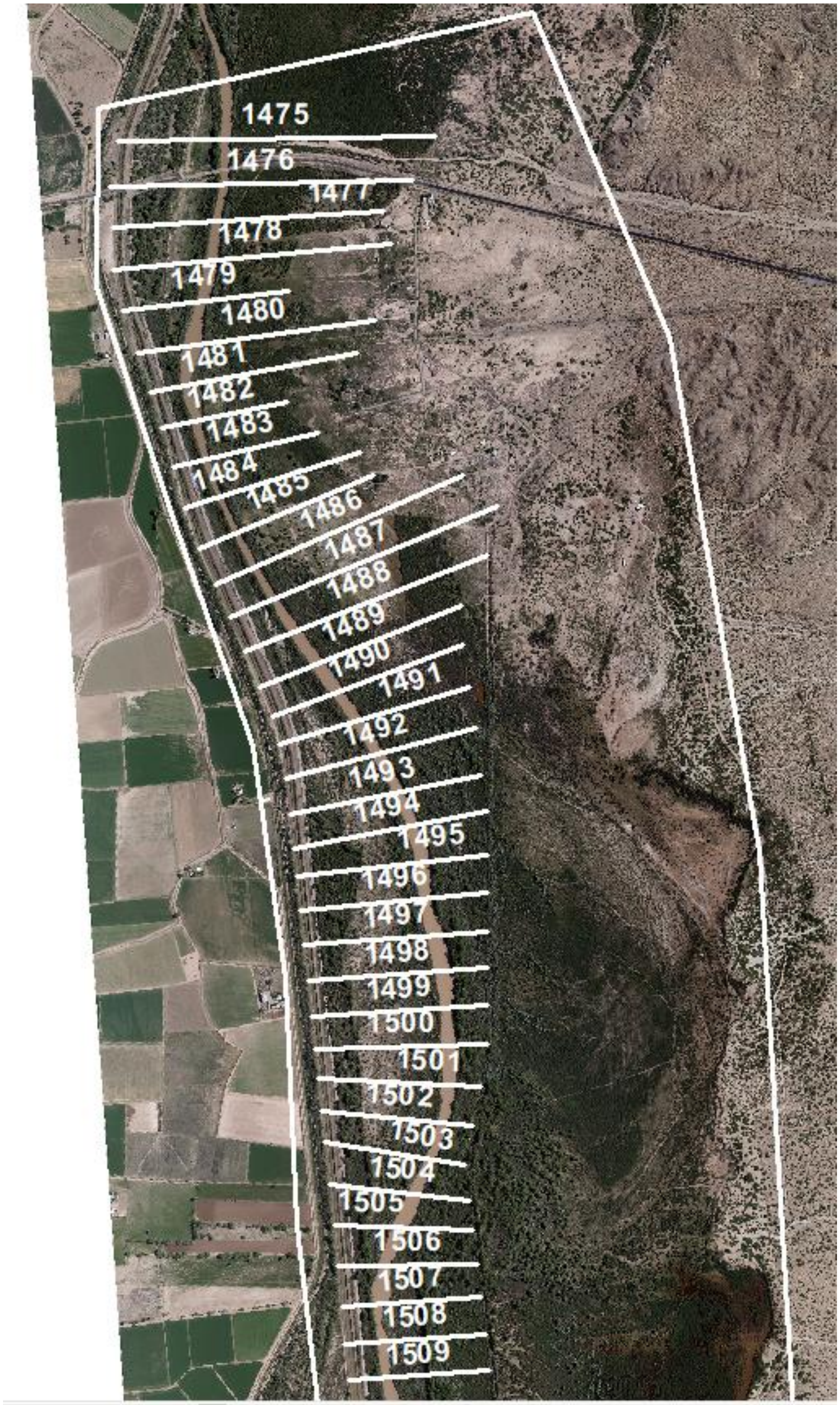

Figure A- 3 Aerial imagery with agg/deg line labels (Google Earth)

Figure A- 4 Aerial imagery with agg/deg line labels (Google Earth)

Figure A- 5 Aerial imagery with agg/deg line labels (Google Earth)

Figure A- 6 Aerial imagery with agg/deg line labels (Google Earth)

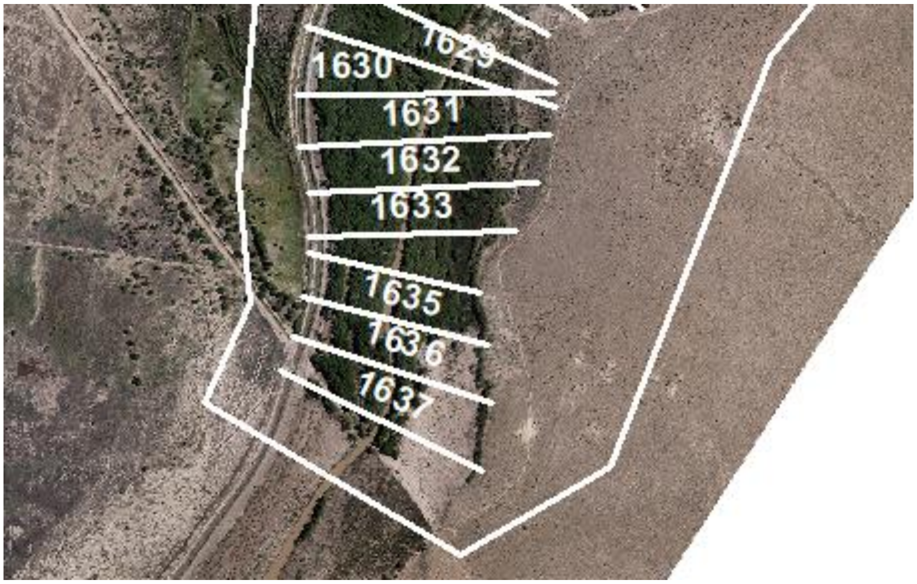

Figure A- 7 Aerial imagery with agg/deg line label (Google Earth)

Appendix B

Total Sediment Load using SEMEP Analysis

The Series Expansion of Einstein Procedure (SEMEP) was used in this study to estimate the total sediment load in the Middle Rio Grande (Yang, C.Y. 2019). The method was developed at CSU with the procedure detailed in Shah-Fairbank et al. (2011) as a function of shear velocity u_* and fall velocity ω. In this report, SEMEP is applied at three stations on the Rio Grande, at San Acacia gage 08354900, as well as Albuquerque and Bernardo at gages 08330000 and 08332010. The number of field samples calculated by the SEMEP are 306, 211, and 173, respectively, at gages 08330000, 08332010, and 08354900. For these stations, the values of u_*/ω range from 1.5 to 37,600. According to Shah-Fairbank et al. (2011), SEMEP performs accurately when $u_*/\omega > 5$, so good results are expected from this application.

It can be seen in Figure B-1 that the SEMEP predictions and total sediment load measurements fall close to the 45-degree line of perfect agreement. Figure B-1 also shows the prediction errors between SEMEP calculations and measurements as a function of u_*/ω. The mean absolute percent difference is 27%. Figure B-2 shows the sediment rating curves for total sediment discharges at gage 08354900.

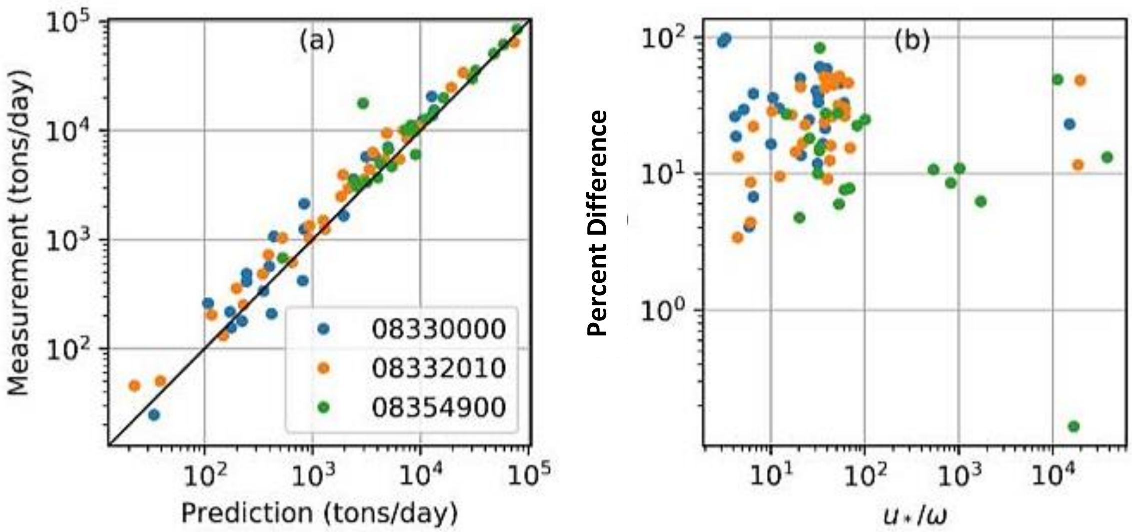

Figure B- 1 Comparison between predicted and measured total sediment load (left) and percent difference vs u/w (right)*

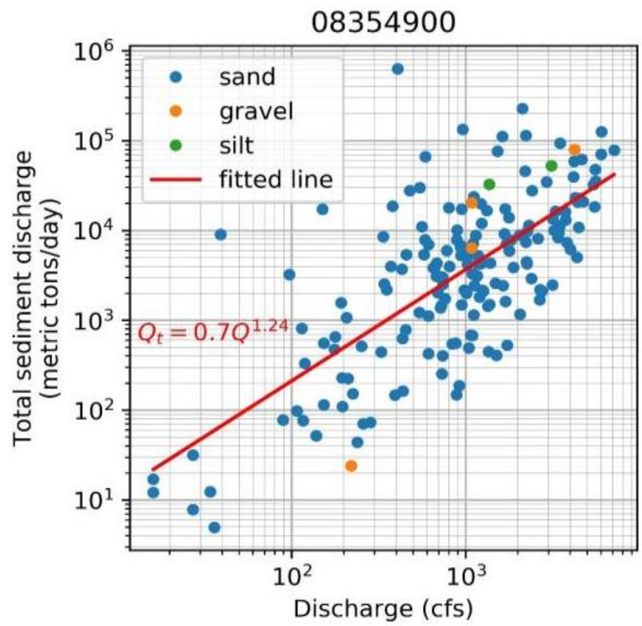

Figure B- 2 Total sediment rating curve at the San Acacia gage

The ratio of measured to total sediment discharge is a function of flow depth h, grain size d_s, and Rouse number Ro (Ro = $\omega/2.5u_*$) according to SEMEP (Shah-Fairbank et al. 2011; Yang and Julien 2019). In addition, the ratio of suspended to total sediment discharge is a function of the ratio h/d_s and Ro. The calculated ratio Q_m/Q_t and the ratio Q_s/Q_t are plotted with the analytical solutions in Figure B-3 for the San Acacia gaging stations, where Q_m is the measured sediment discharge, Q_t is the total sediment discharge, and Q_s is the suspended sediment discharge. As expected, when the value of Ro is low (Ro < 0.3), the ratio Q_s/Q_t is close to 100% during floods when h/d_s > 100. These ratios are also in good agreement with the theory for both sands and gravels.

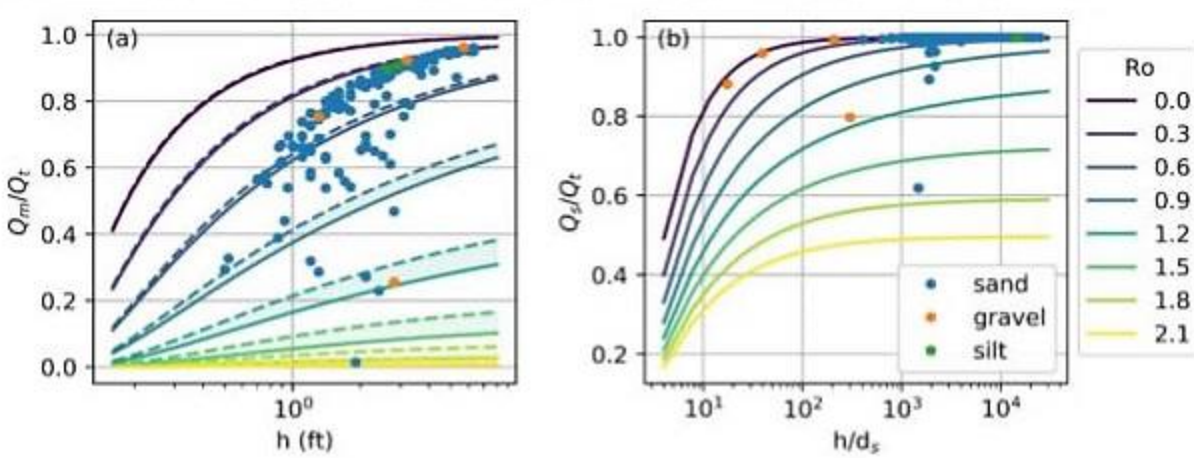

Figure B- 3 the ratio of measured to total sediment discharge vs depth; and (b) the ratio of suspended to total sediment discharge vs h/ds at the San Acacia gage

Appendix C

Wetted Top Width Plots

Wetted Top Width Plots

In section 3.1, the cross-section moving averaged top width was plotted for all agg/deg lines in the Bosque del Apache reach. Figures B-1 and B-2 show each cross-section top width plotted against the agg/deg lines rather than the moving average at discharges of 1,000 cfs and 3,000 cfs.

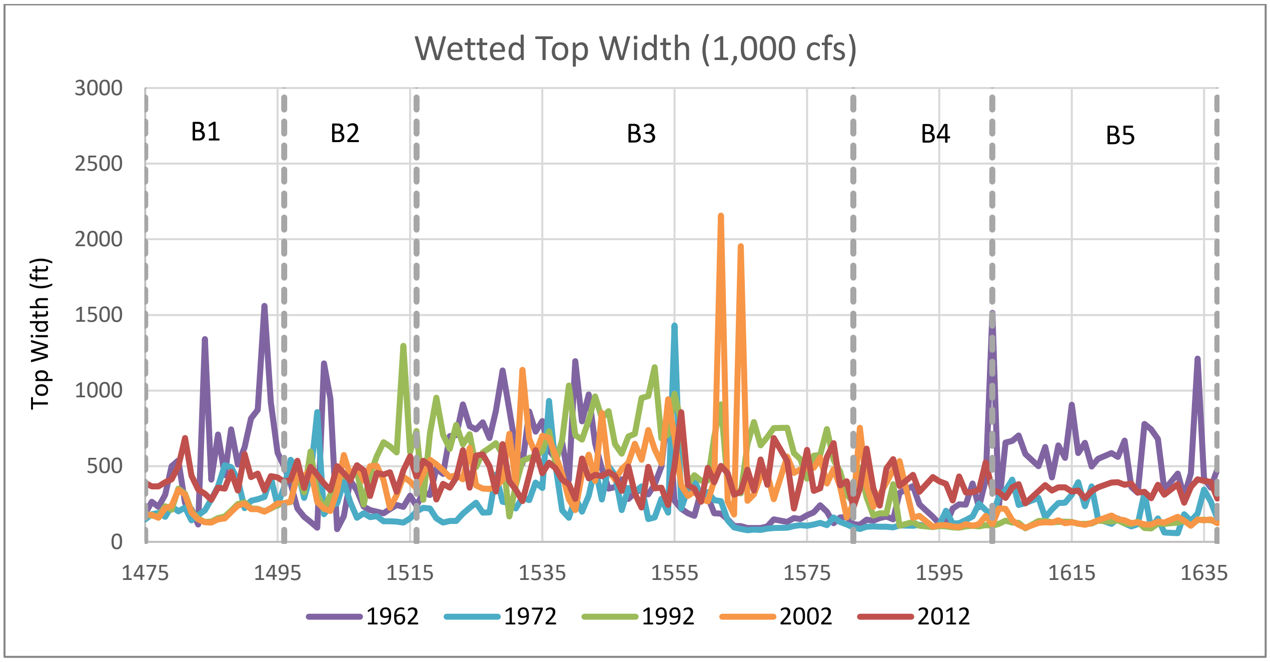

Figure C- 1 Wetted top width at each agg/deg line throughout the Bosque del Apache reach at a discharge of 1,000 cfs

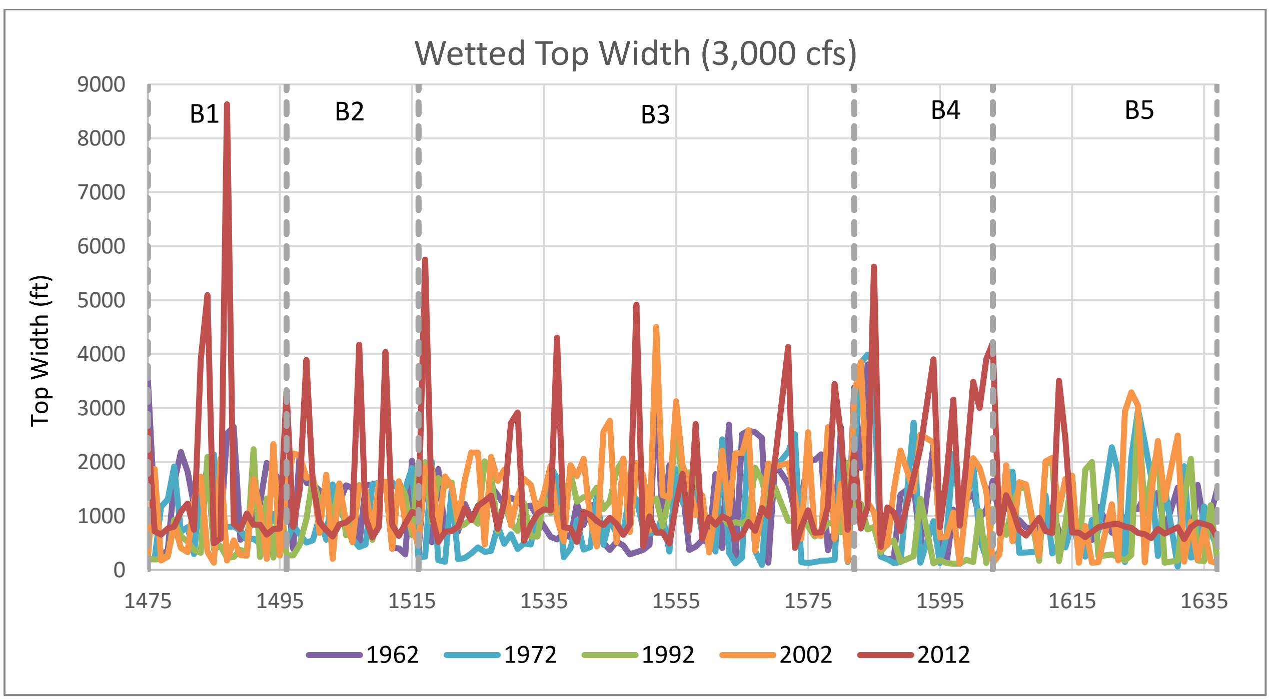

Figure C- 2 Wetted top width at each agg/deg line throughout the Bosque del Apache reach at a discharge of 3,000 cfs

Appendix D

Additional Figures from Habitat Analyses

(Habitat Charts by Subreach, Spatially Varying Habitat Charts, Habitat Curves)

Width Slices: Habitat Bar Charts

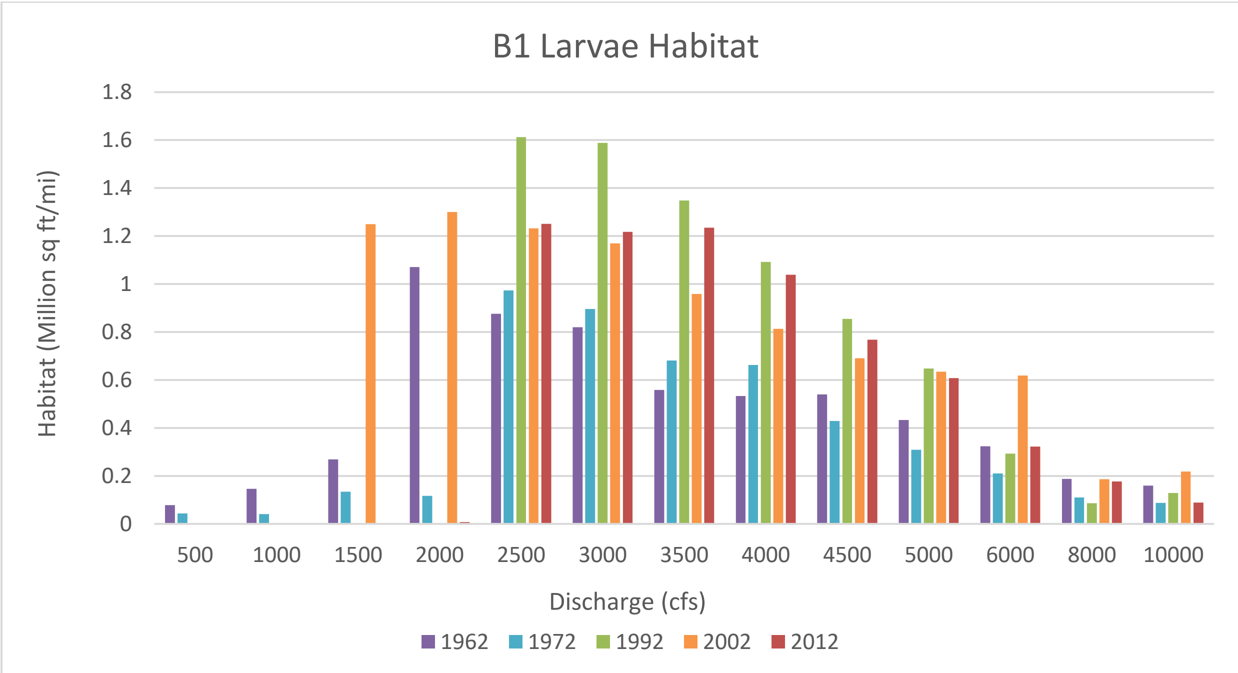

Figure D- 1 Subreach B1 larva habitat

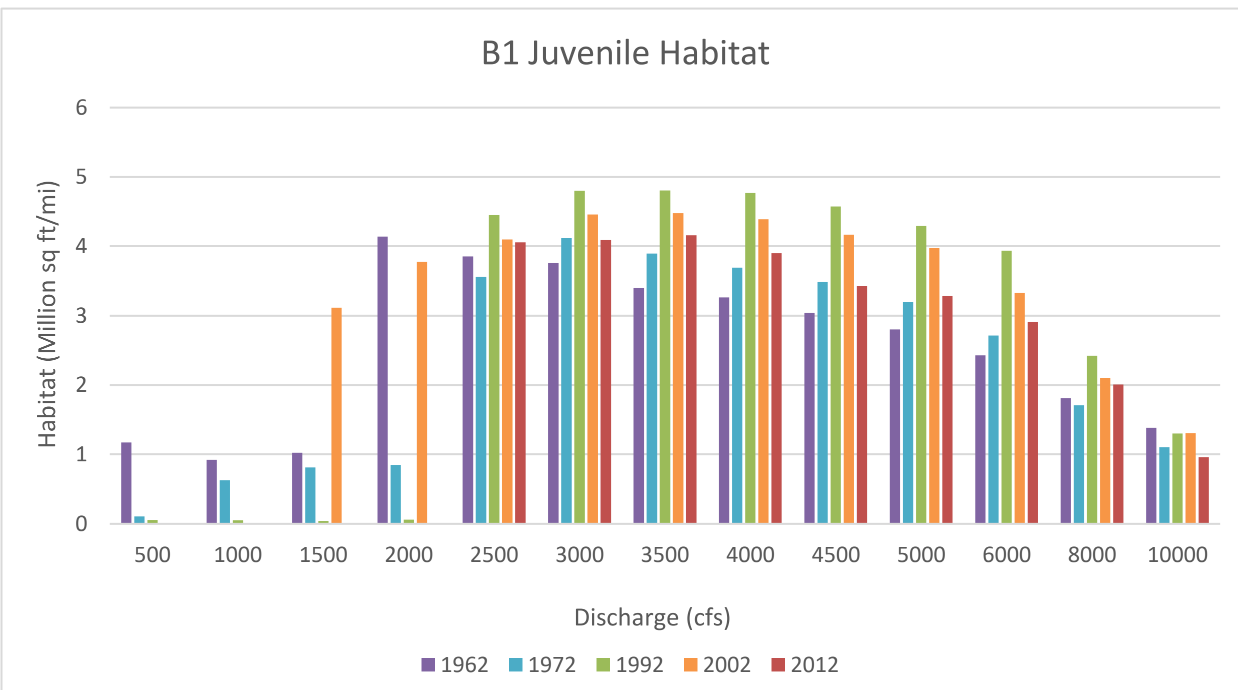

Figure D- 2 Subreach B1 juvenile habitat

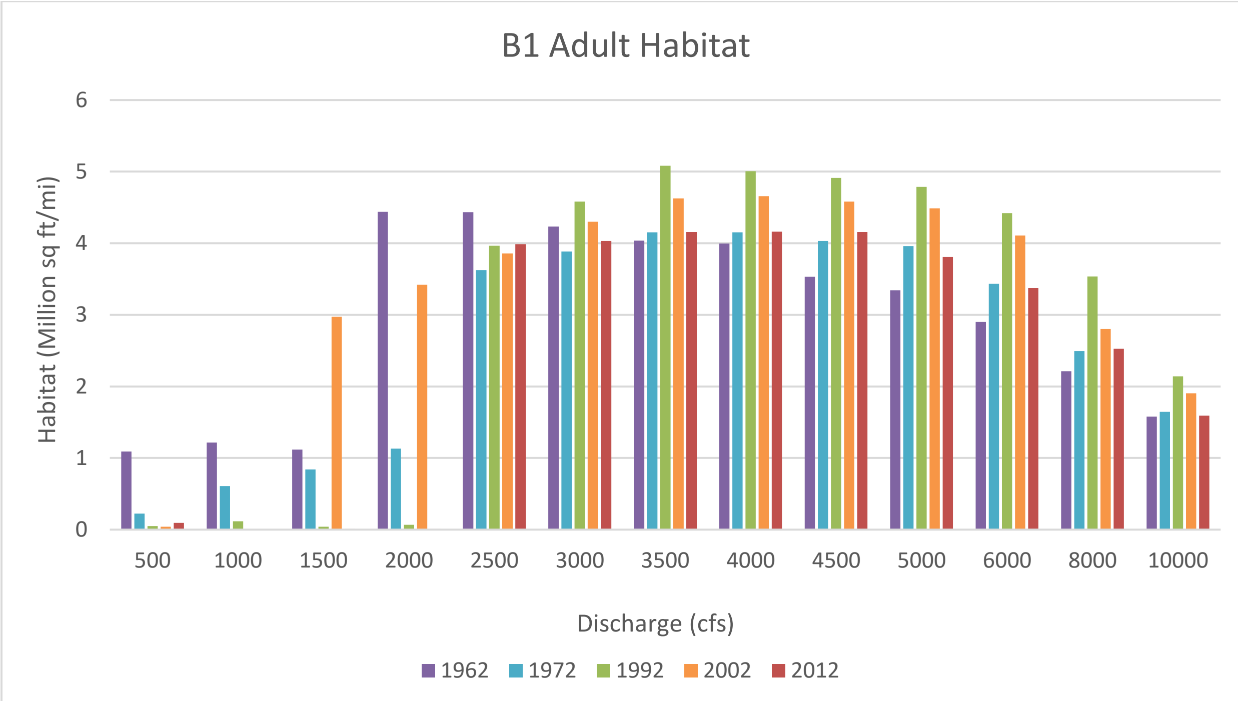

Figure D- 3 Subreach B1 adult habitat

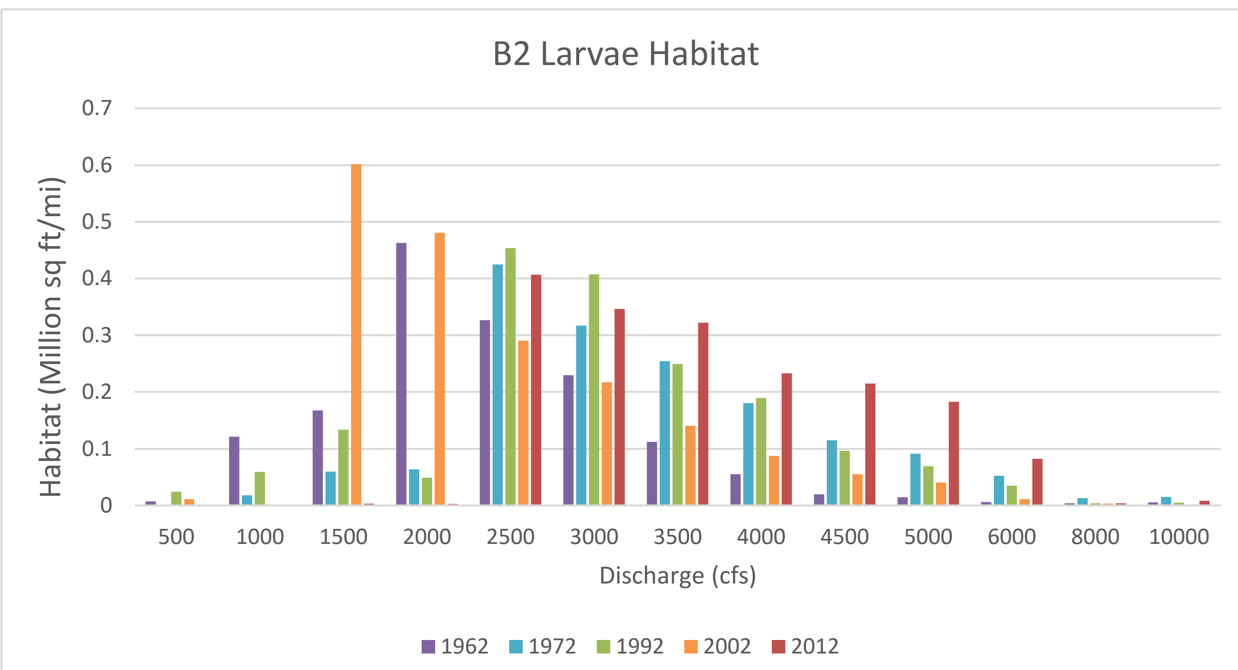

Figure D- 4 Subreach B2 larva habitat

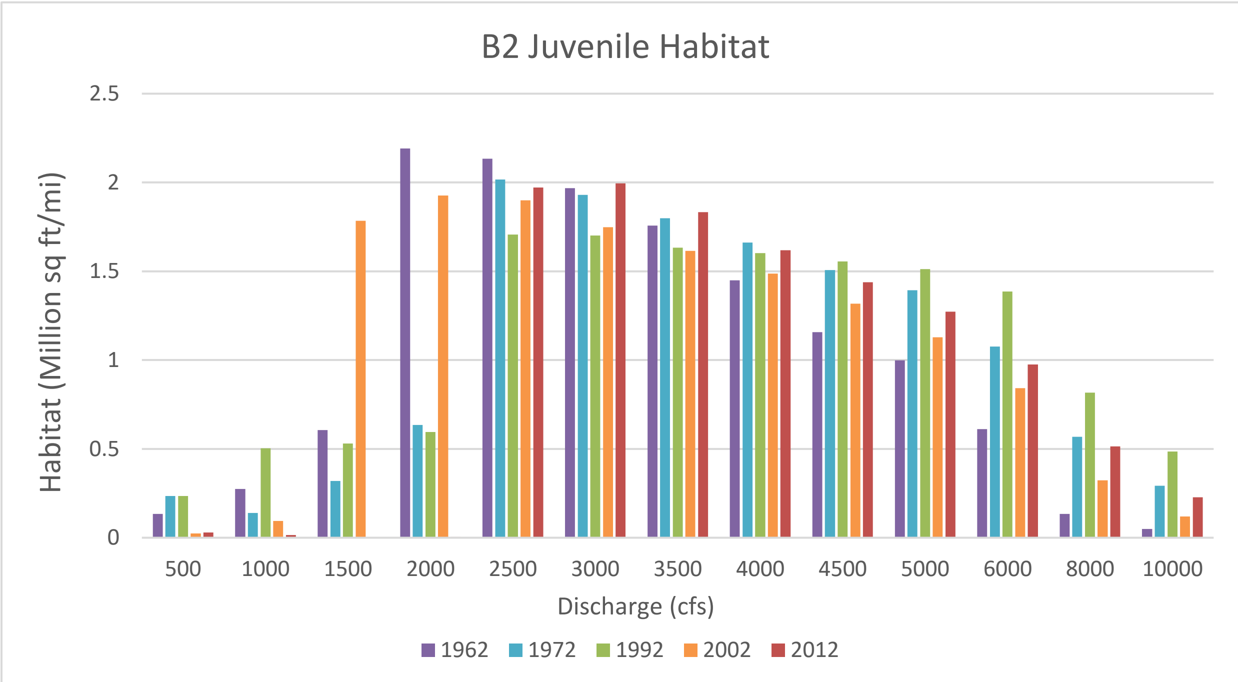

Figure D- 5 Subreach B2 juvenile habitat

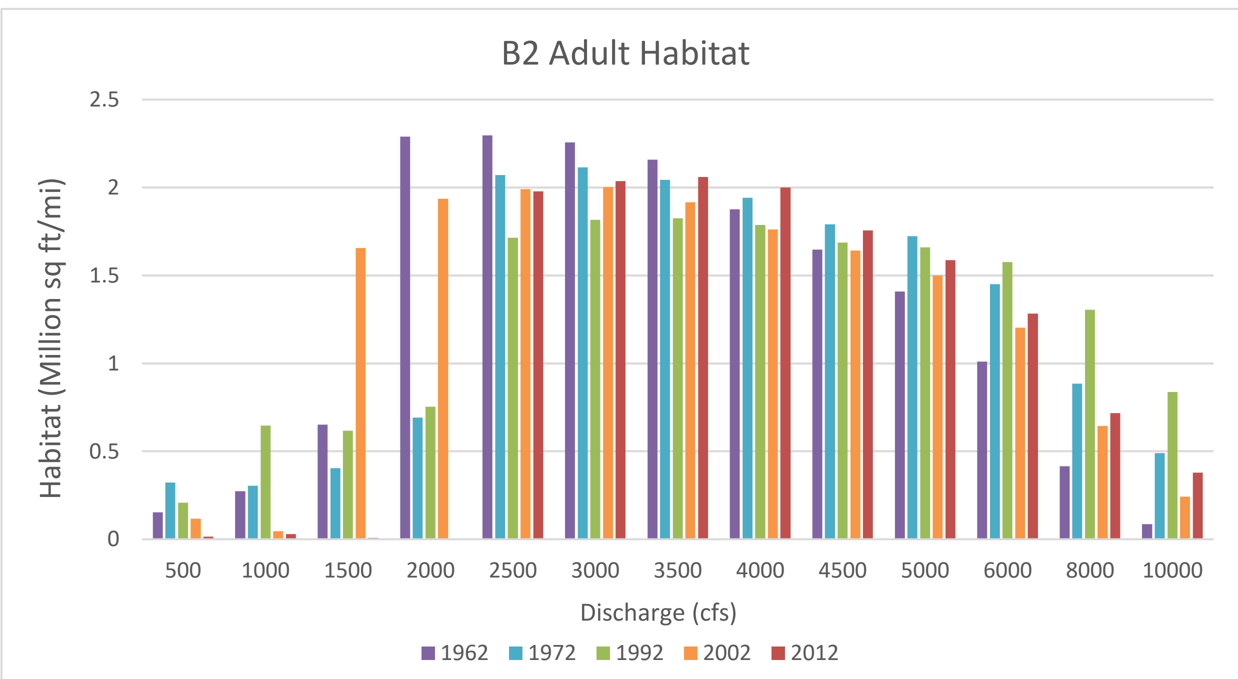

Figure D- 6 Subreach B2 adult habitat

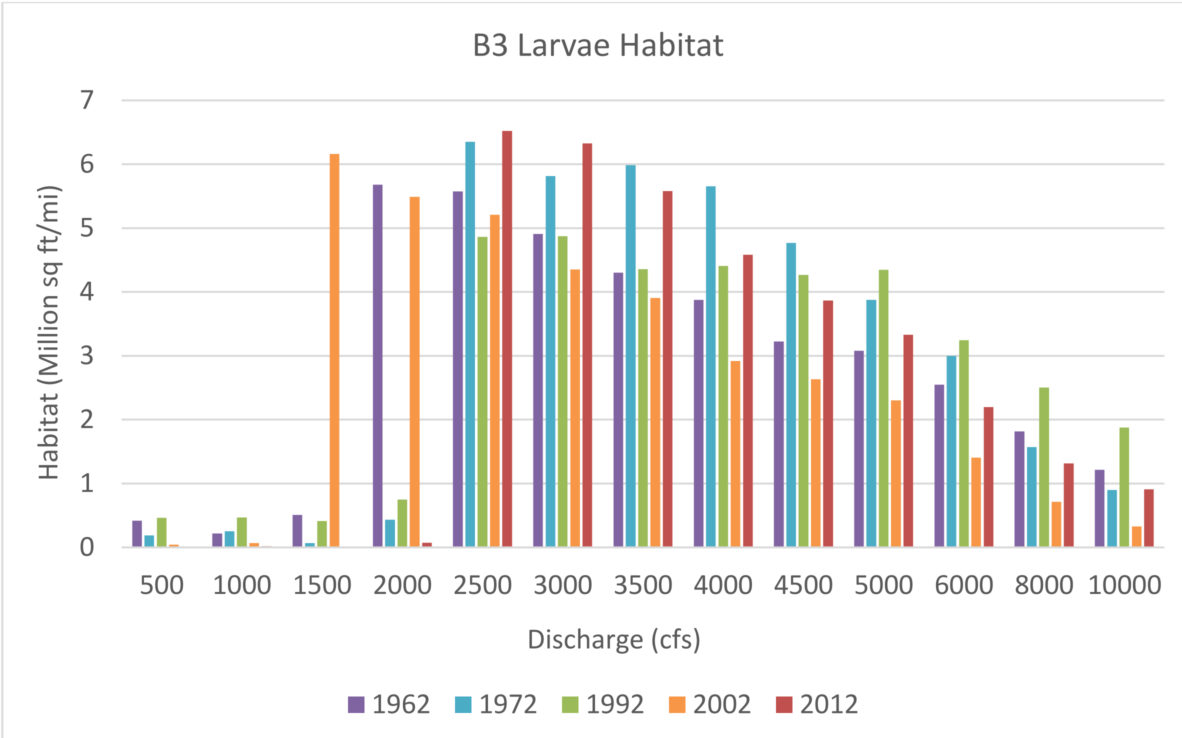

Figure D- 7 Subreach B3 Larva Habitat

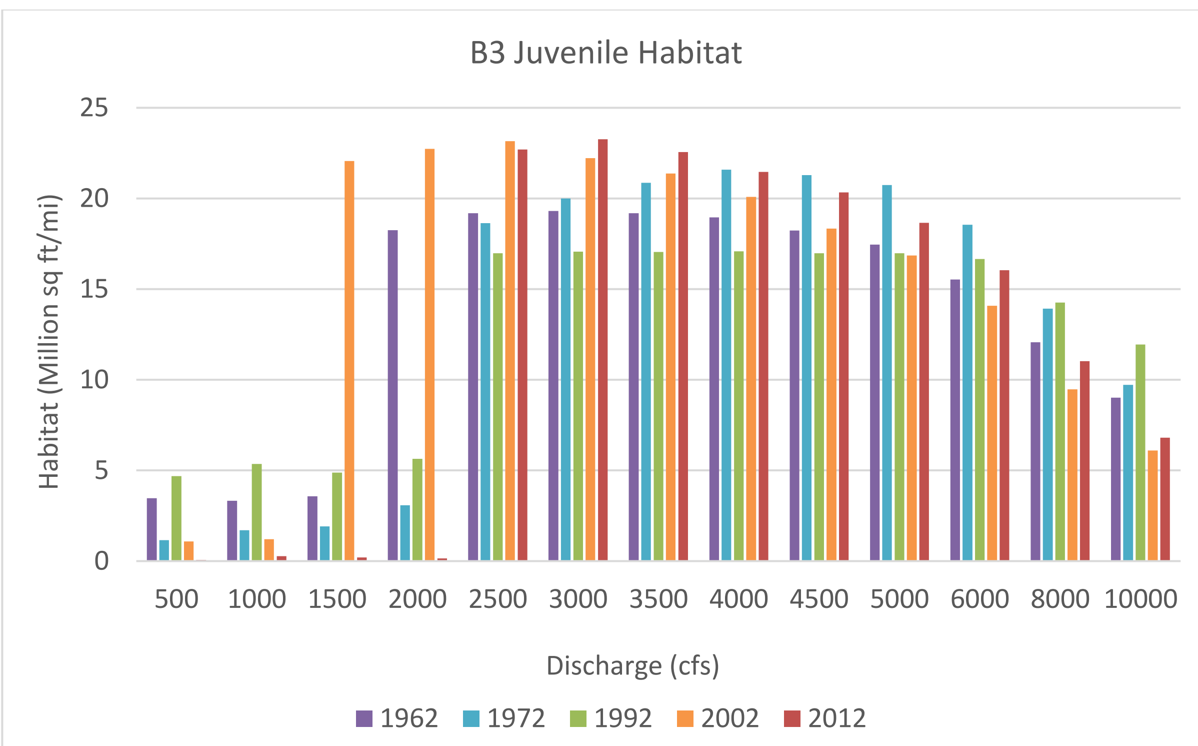

Figure D- 8 Subreach B3 Juvenile Habitat

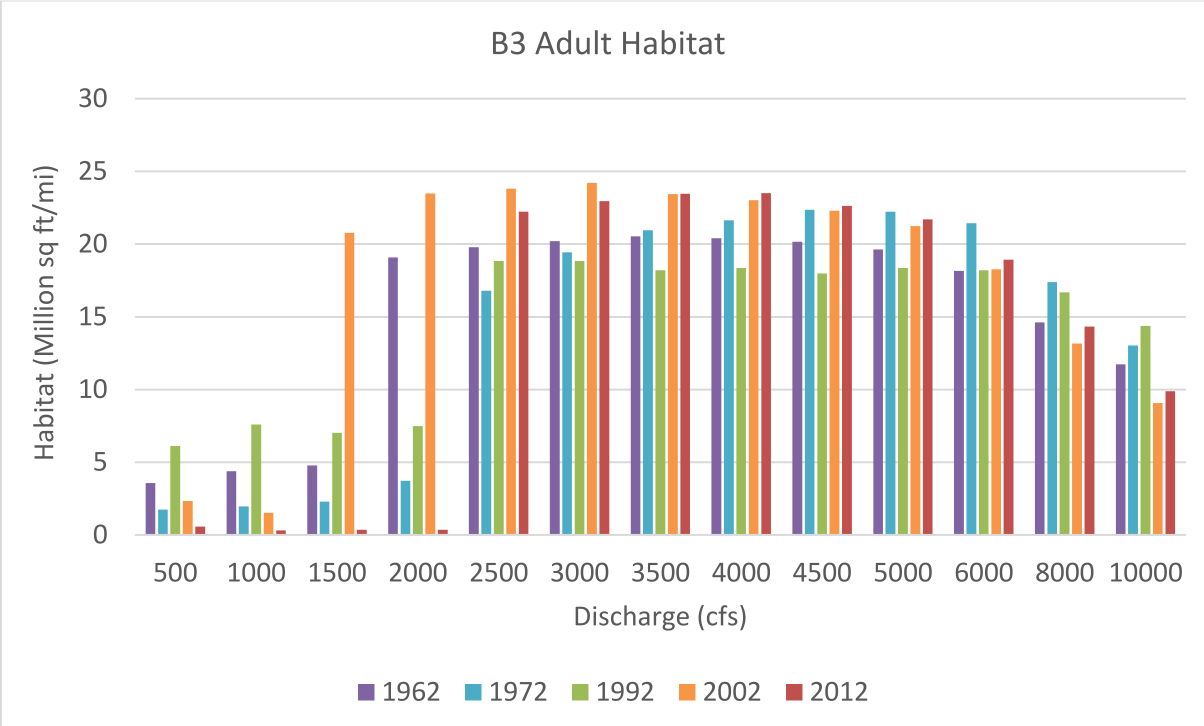

Figure D- 9 Subreach B3 Adult Habitat

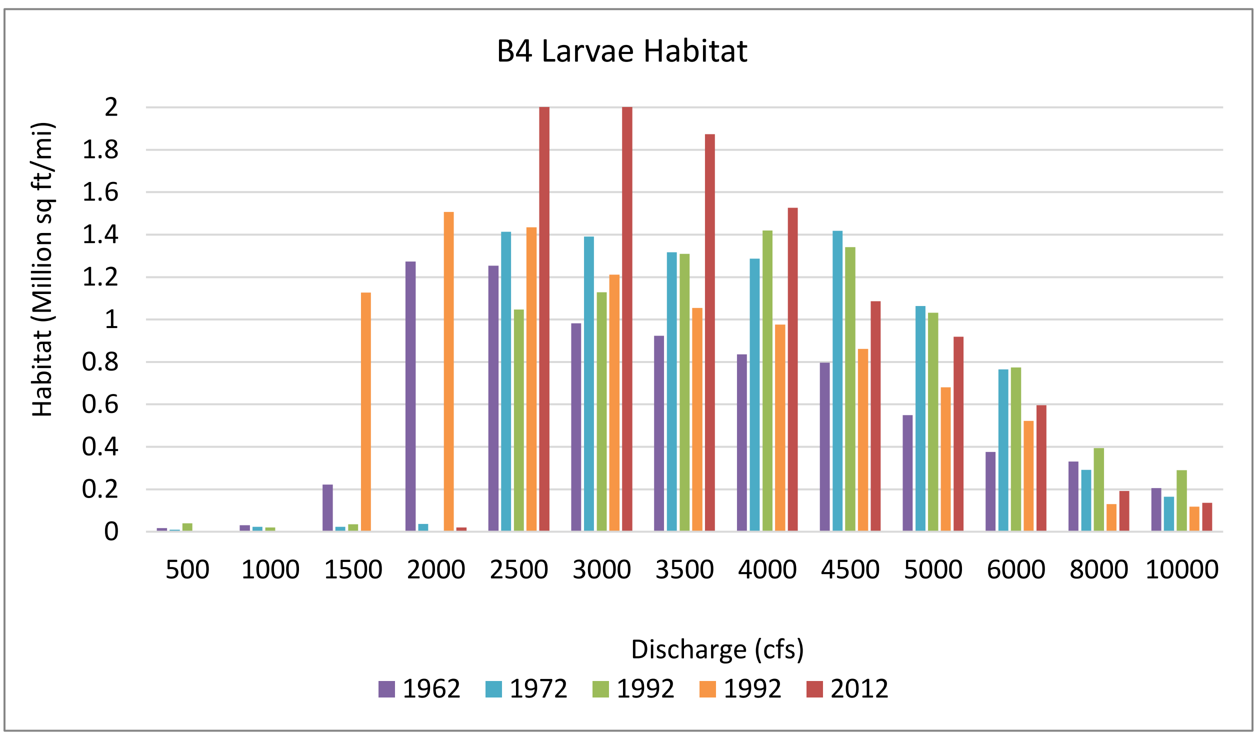

Figure D- 10 Subreach B4 Larva Habitat

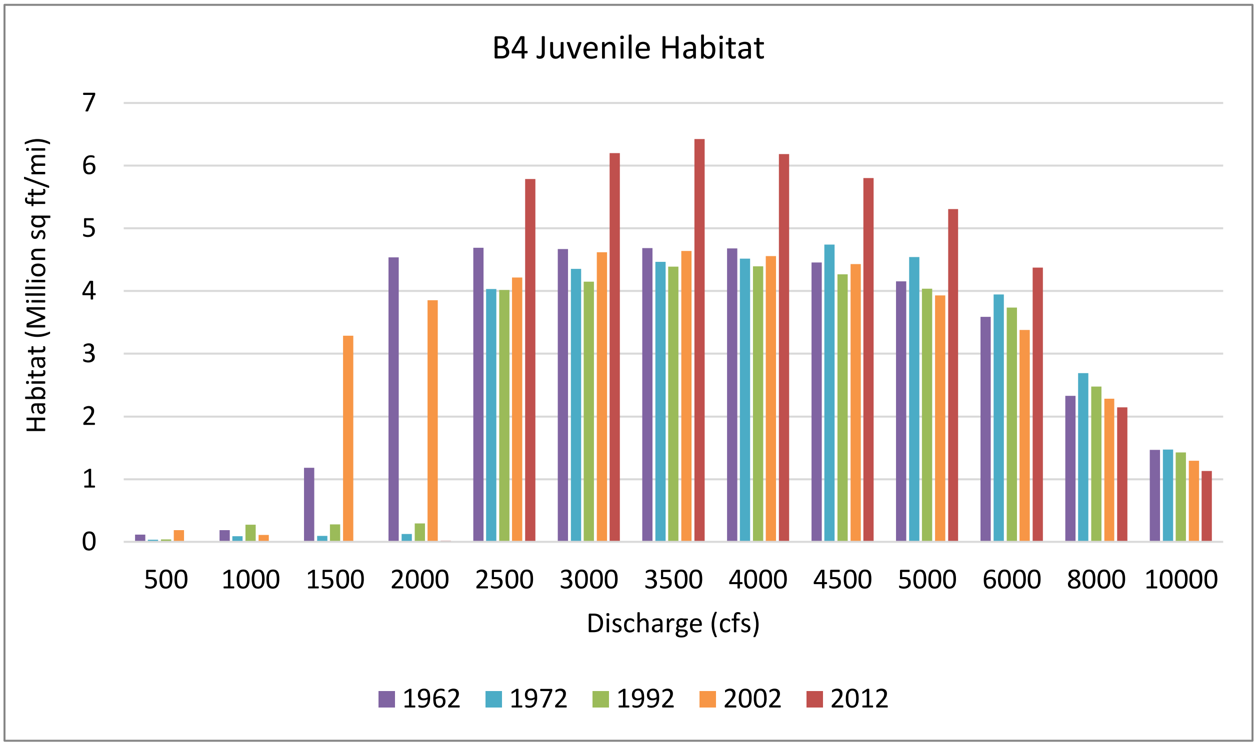

Figure D- 11 Subreach B4 Juvenile Habitat

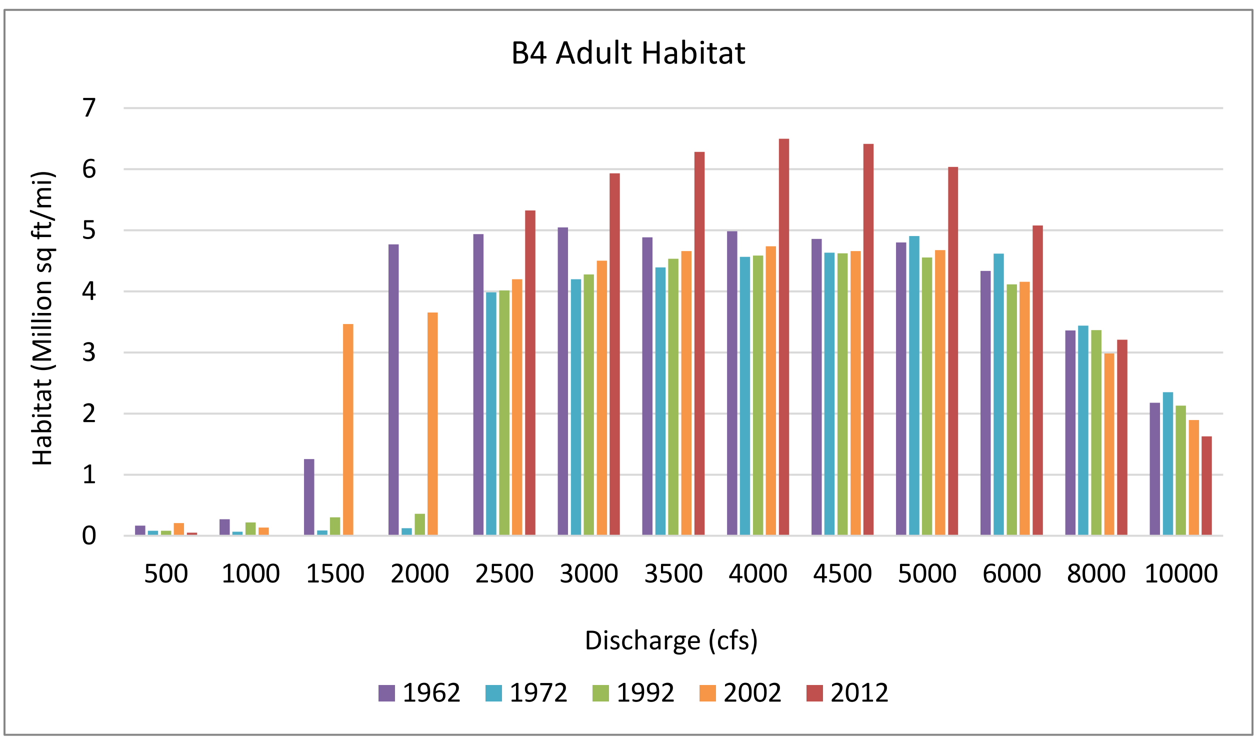

Figure D- 12 Subreach B4 Adult Habitat

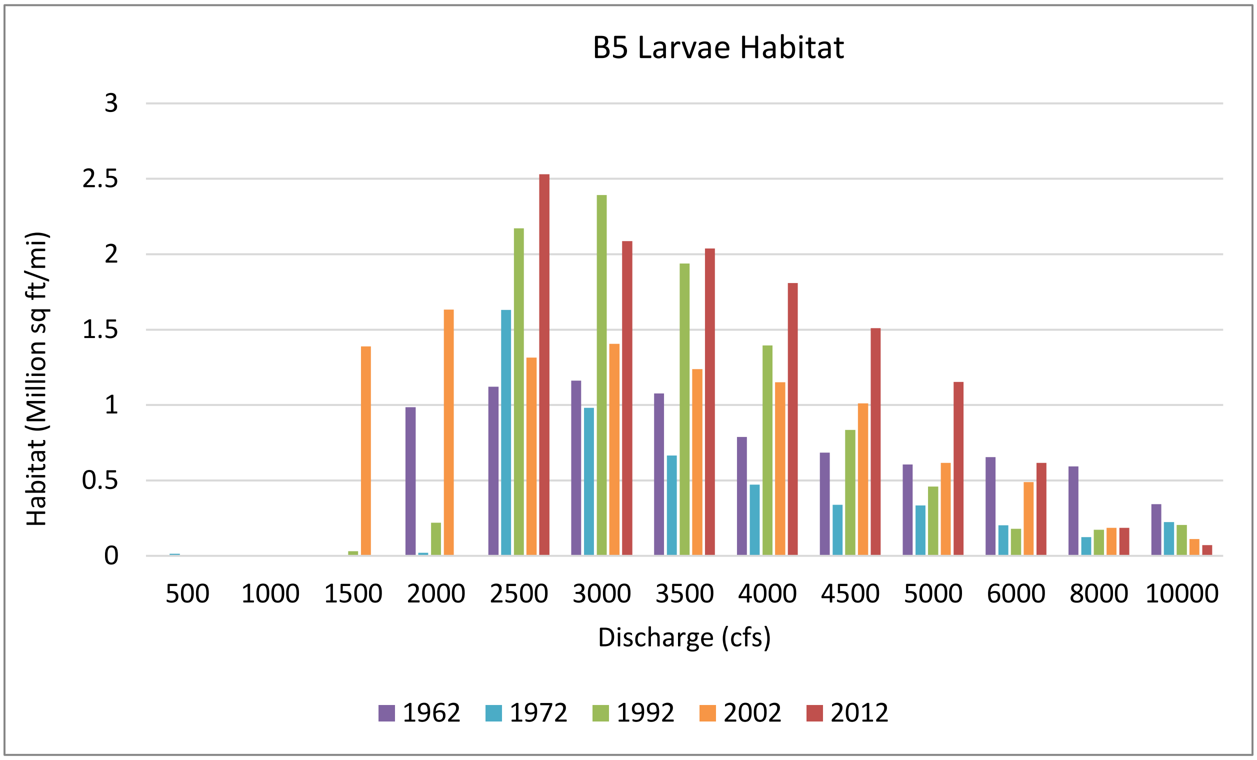

Figure D- 13 Subreach B5 Larva Habitat

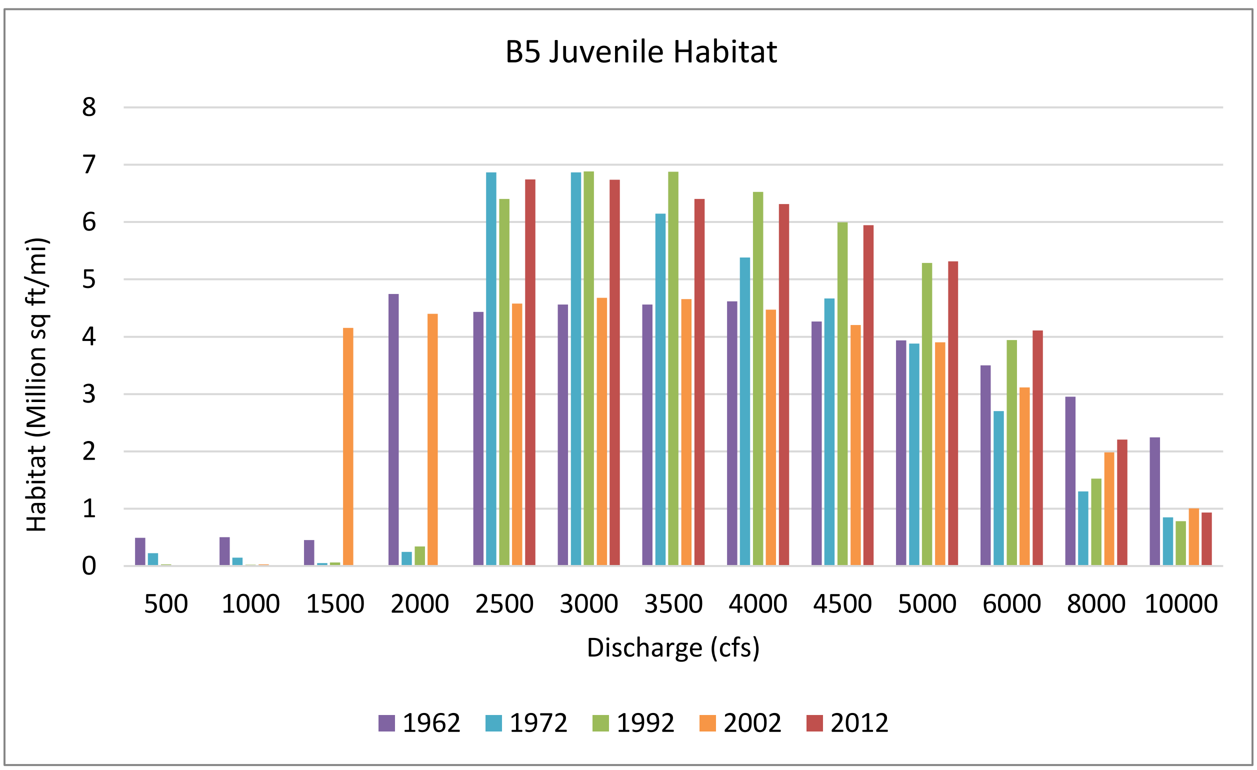

Figure D- 14 Subreach B5 Juvenile Habitat

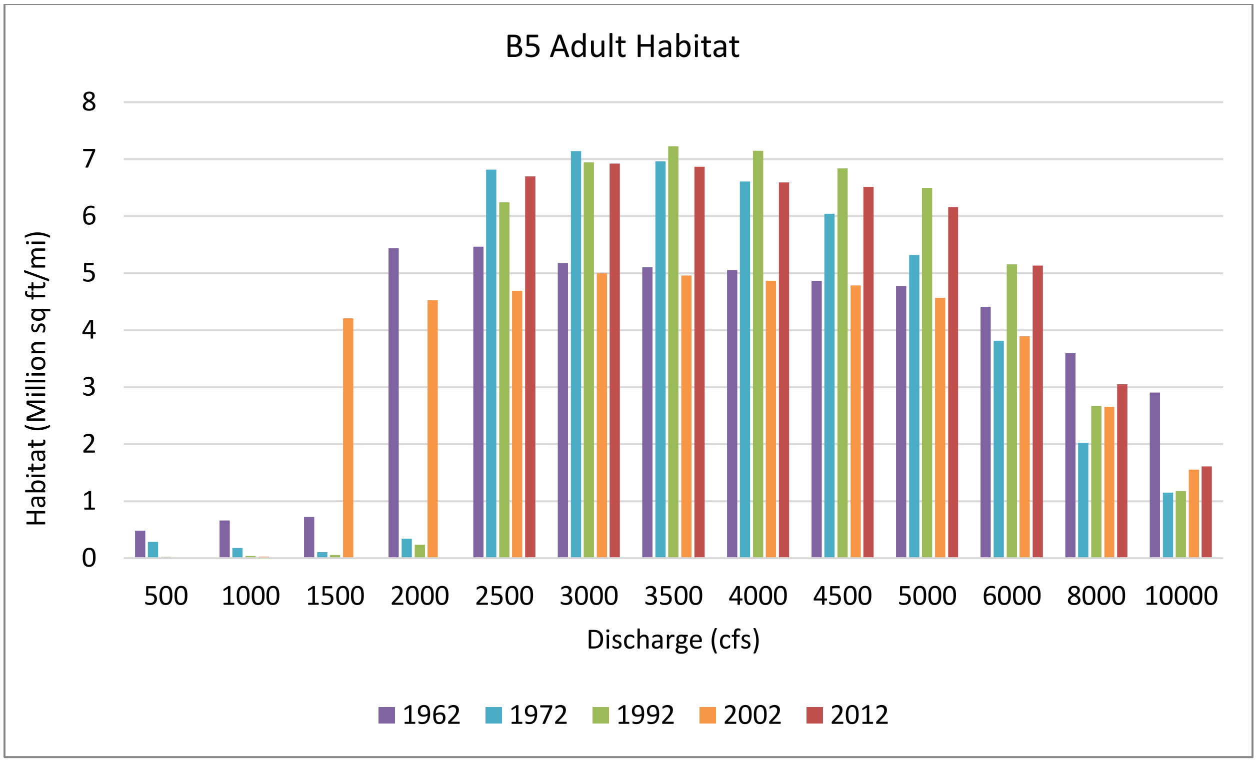

Figure D- 15 Subreach B5 Adult Habitat

Stacked Habitat Chart

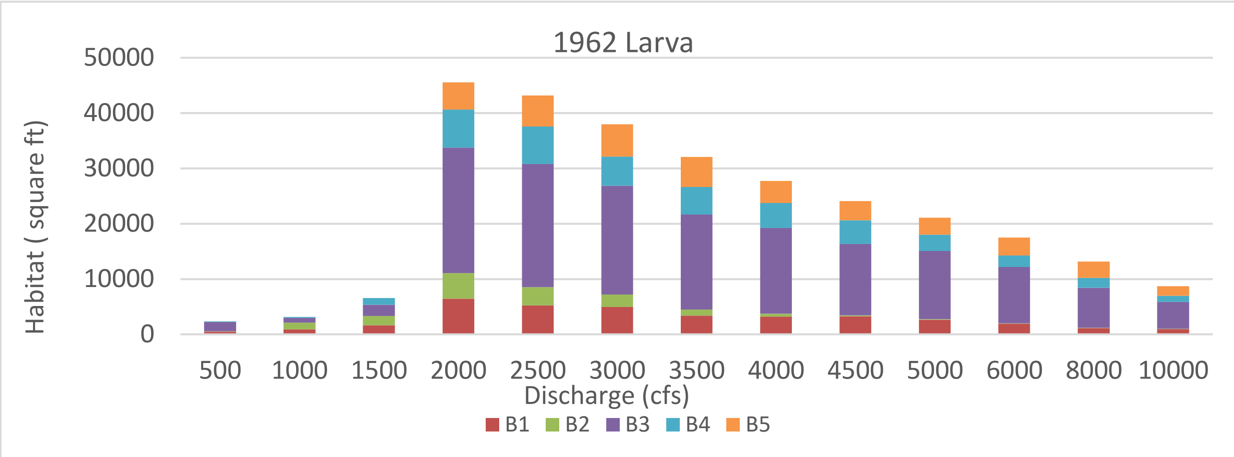

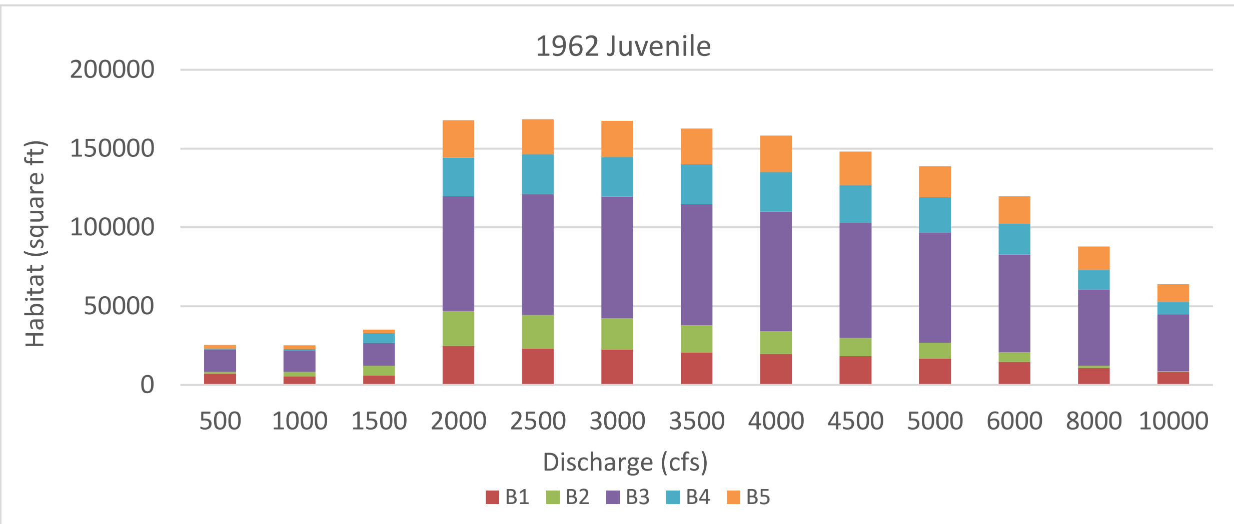

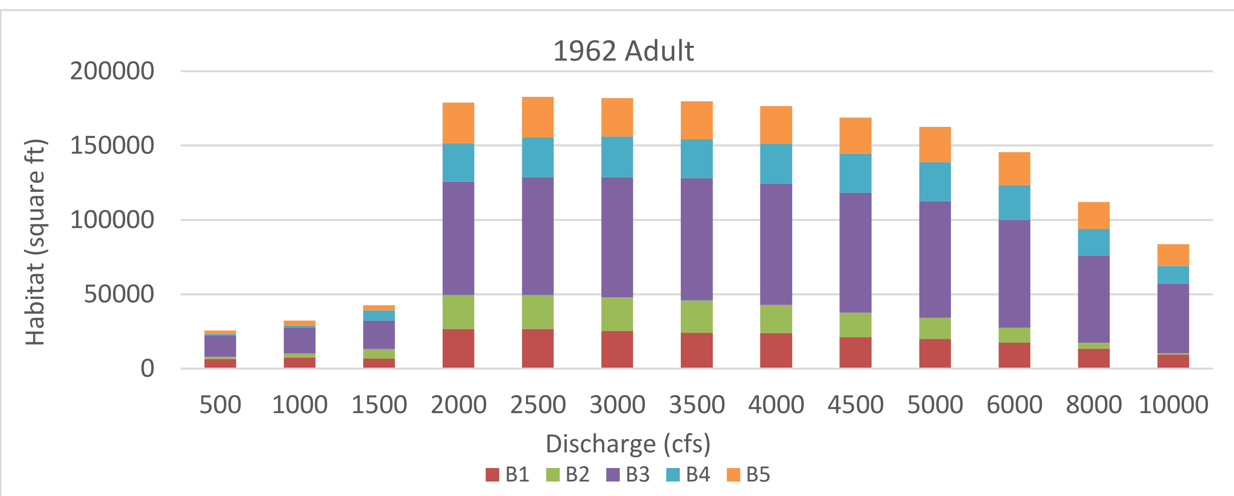

Figure D- 16 Stacked habitat charts to display spatial variations of habitat throughout the Bosque del Apache reach in 1962

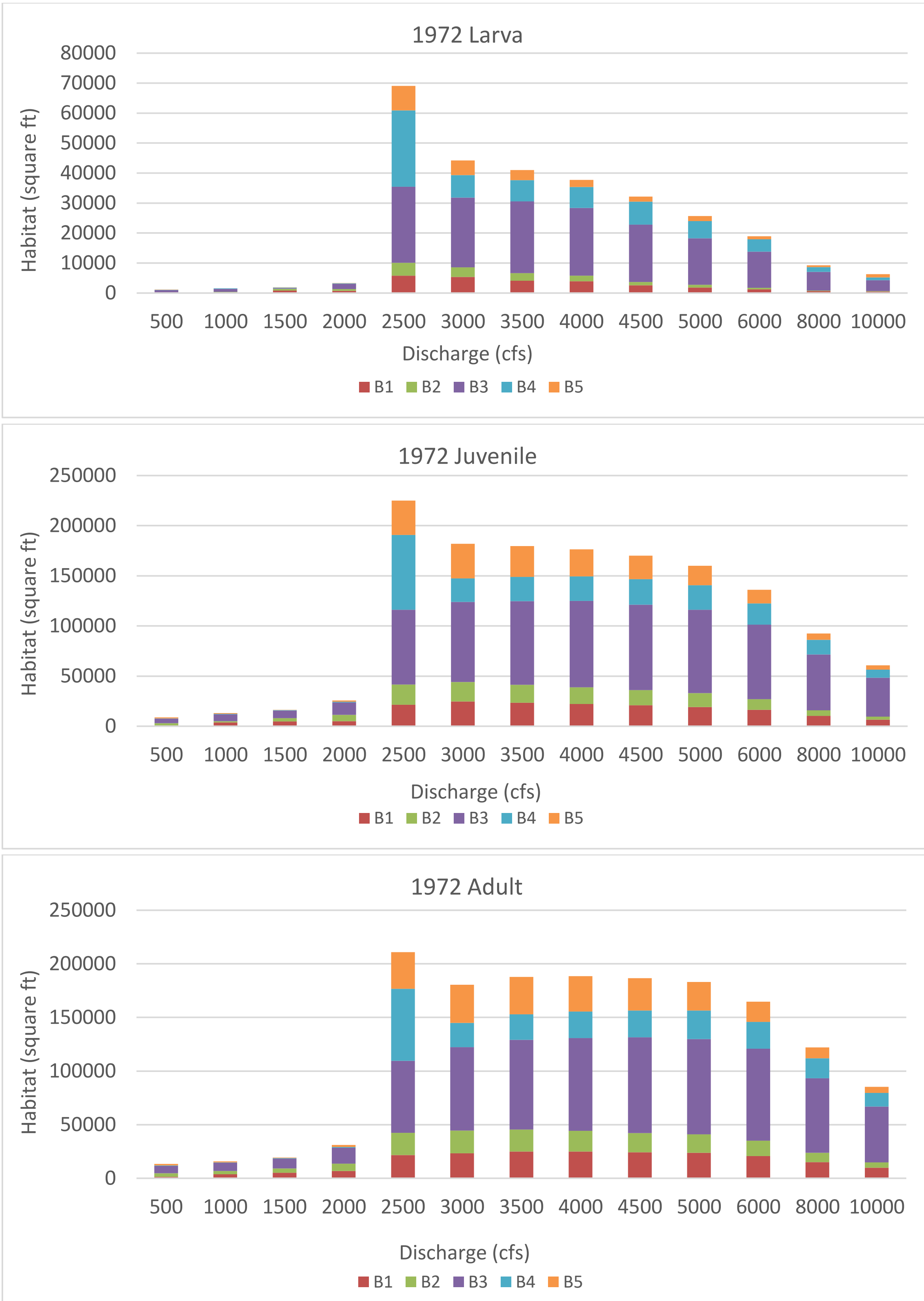

Figure D- 17 Stacked habitat charts to display spatial variations of habitat throughout the Bosque del Apache reach in 1972.

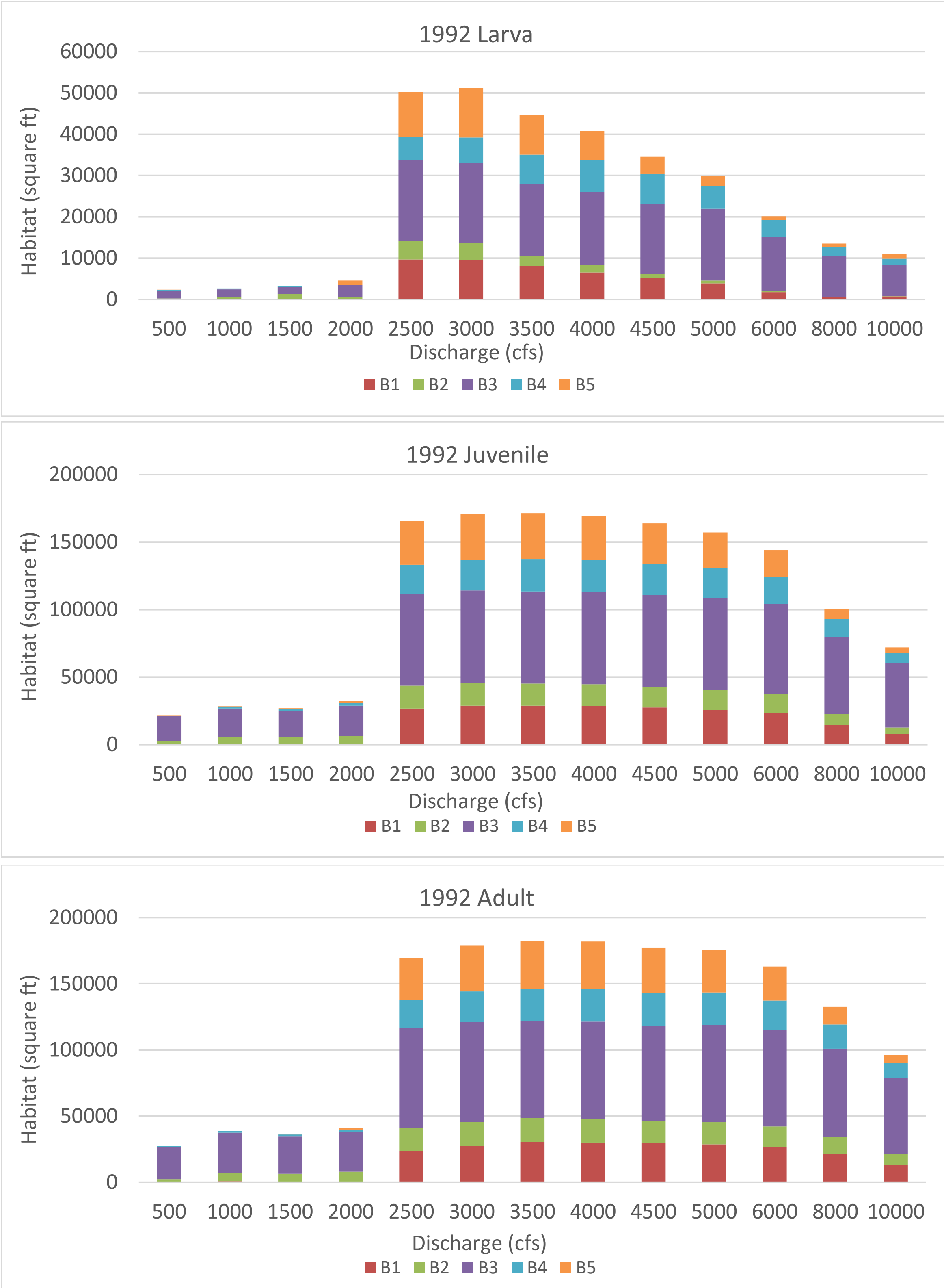

Figure D- 18 Stacked habitat charts to display spatial variations of habitat throughout the Bosque del Apache reach in 1992

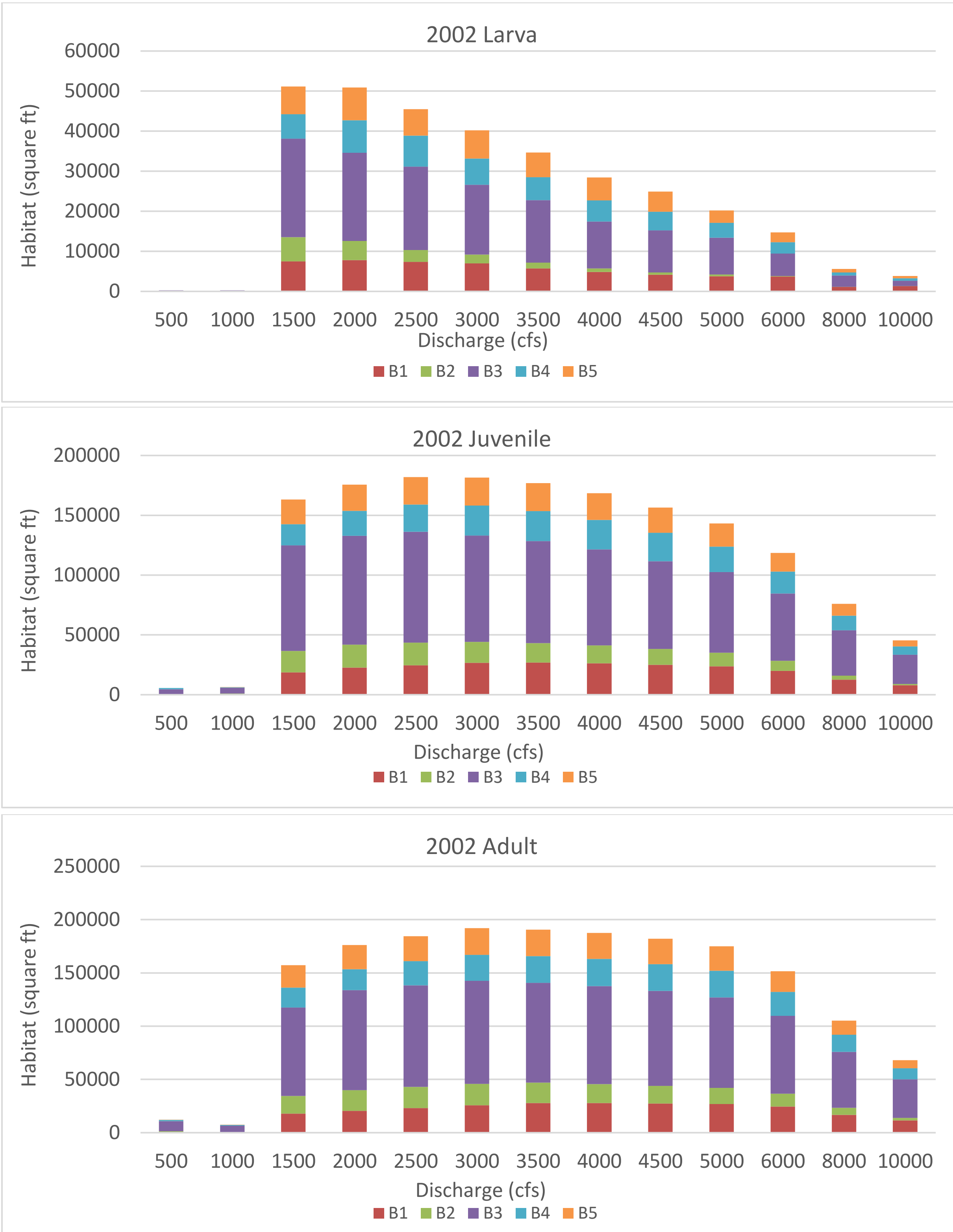

Figure D- 19 Stacked habitat charts to display spatial variations of habitat throughout the *Bosque del Apache* reach in 2002

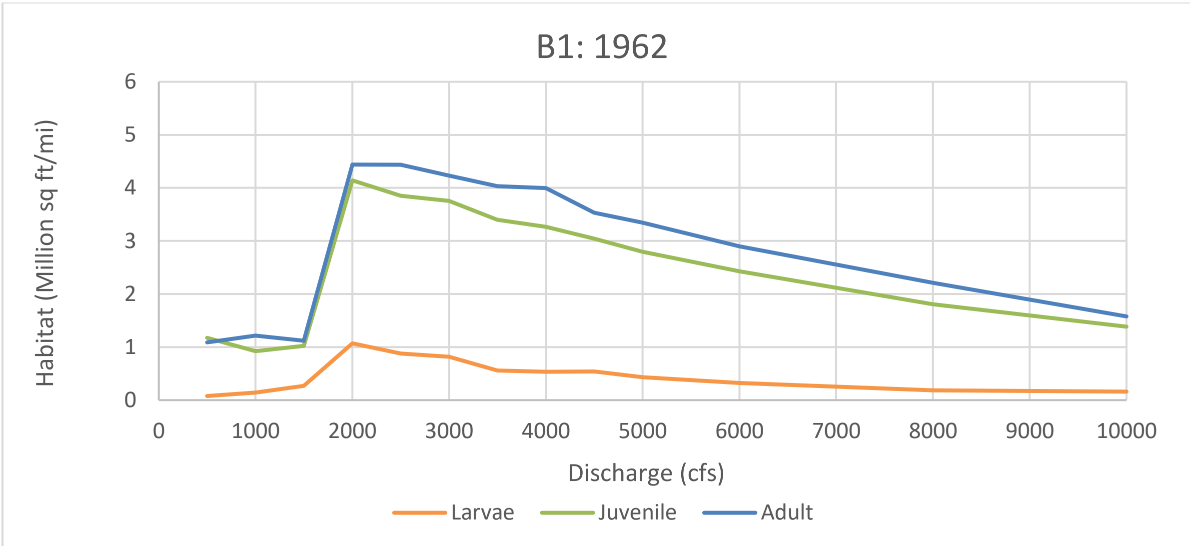

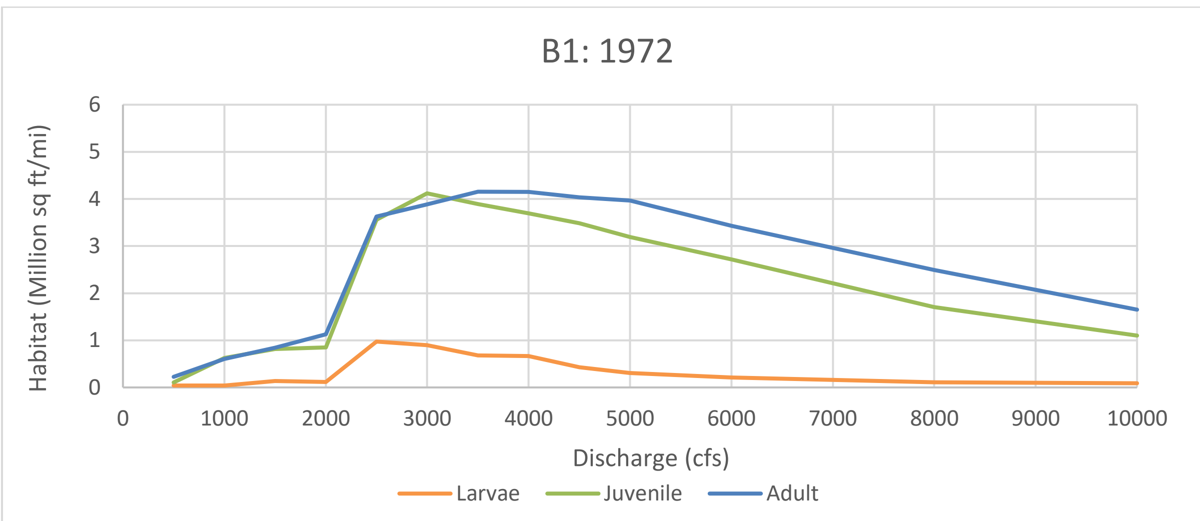

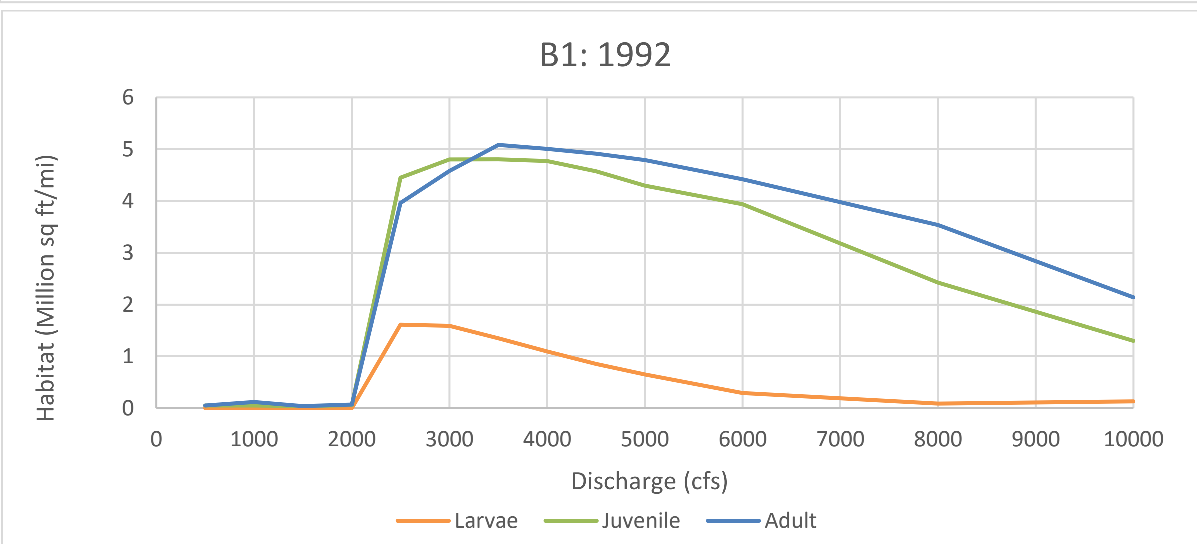

Figure D- 20 Life stage habitat curves for subreach B1 at the years 1962 (top), 1972 (middle), and 1992 (bottom).

Figure D- 21 Life stage habitat curves for subreach B1 for the years 2002 (top) and 2012 (bottom).

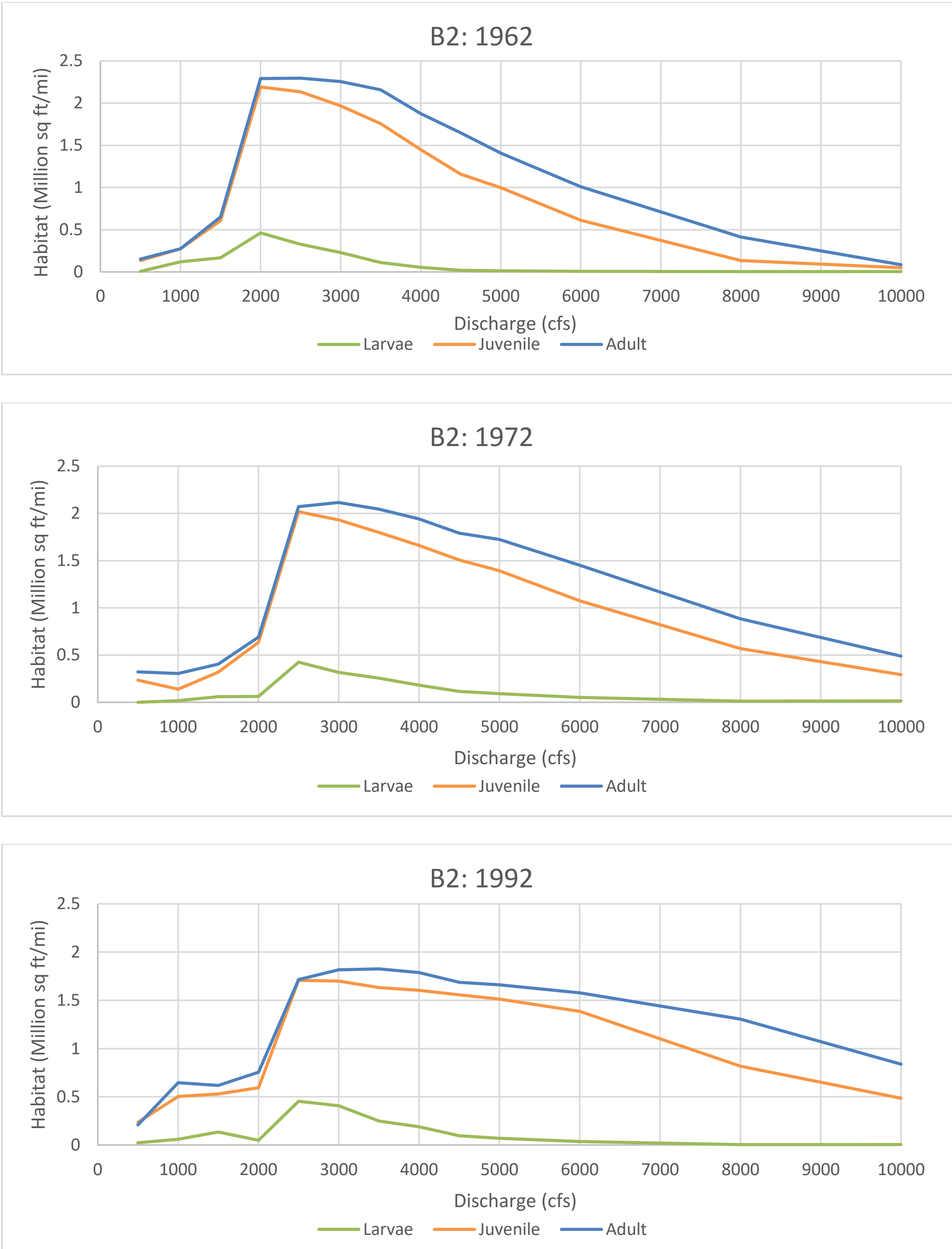

Figure D- 22 Life stage habitat curves for subreach B2 at the years 1962 (top), 1972 (middle), and 1992 (bottom).

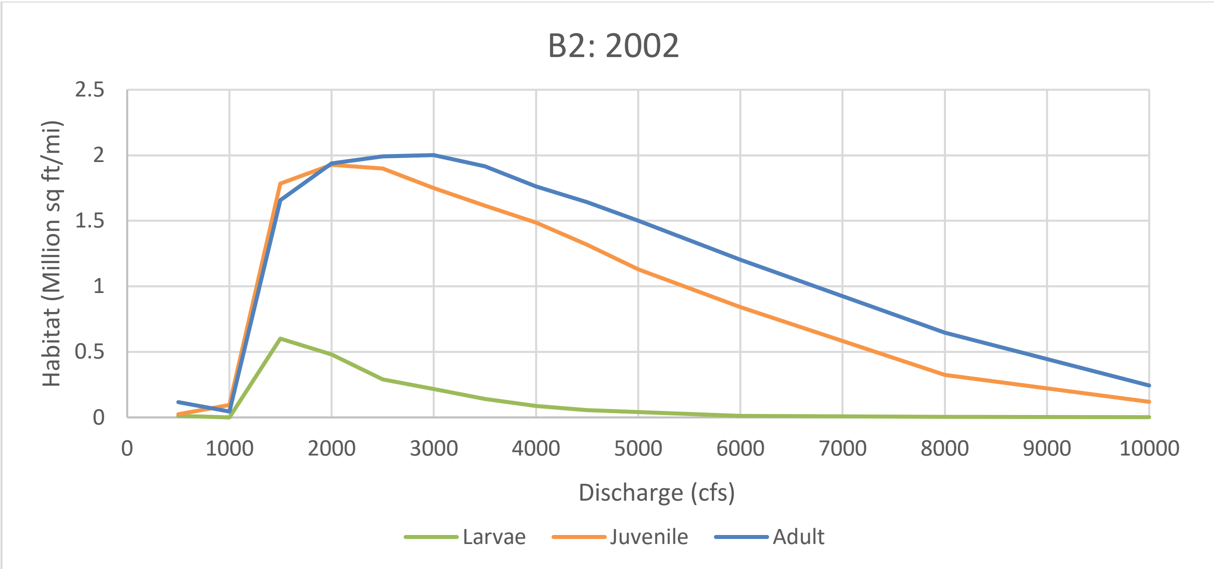

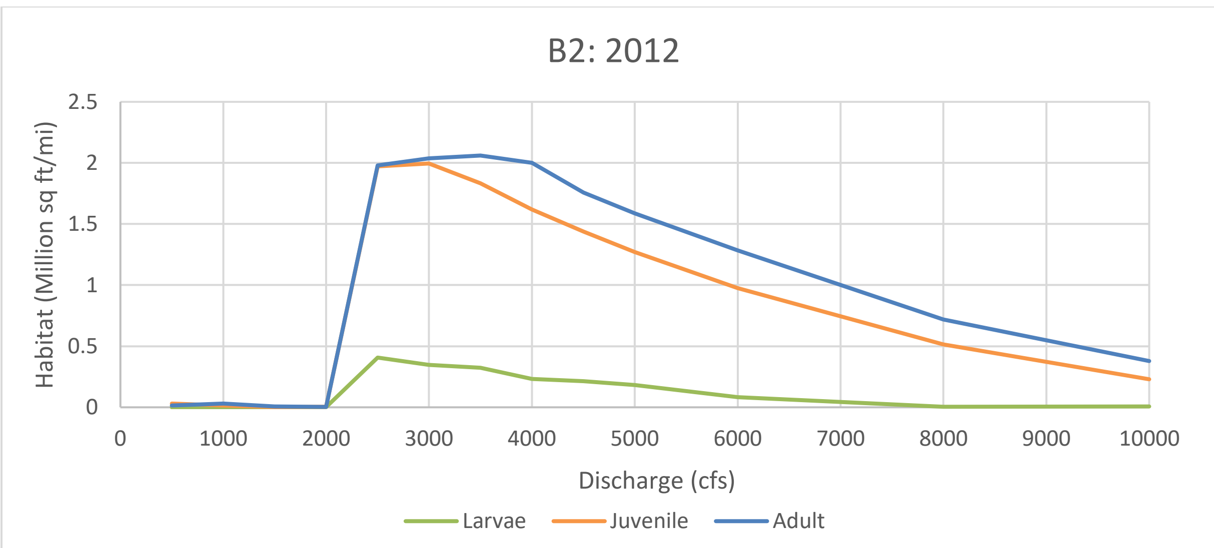

Figure D- 23 Life stage habitat curves for subreach B2 for the years 2002 (top) and 2012 (bottom).

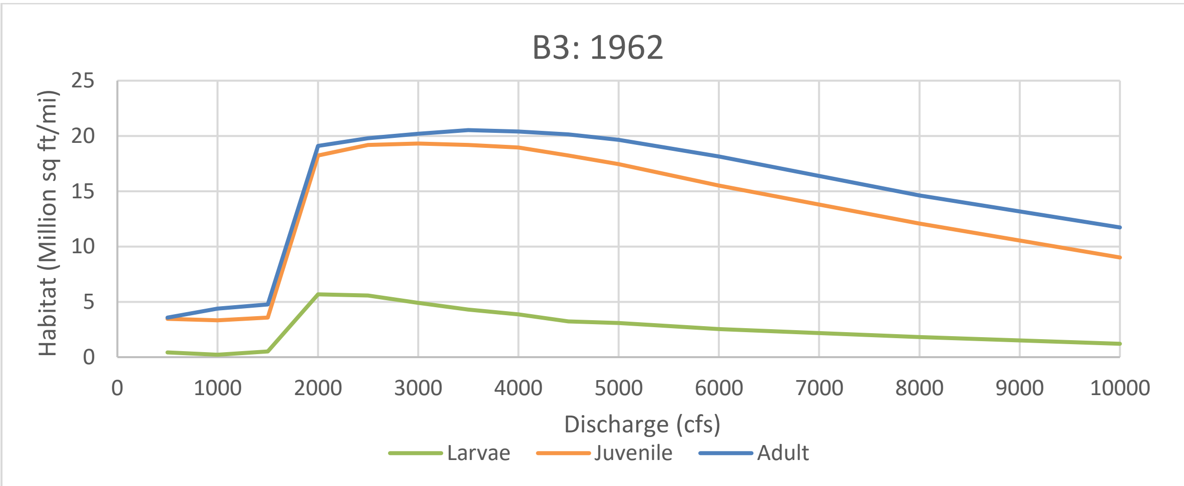

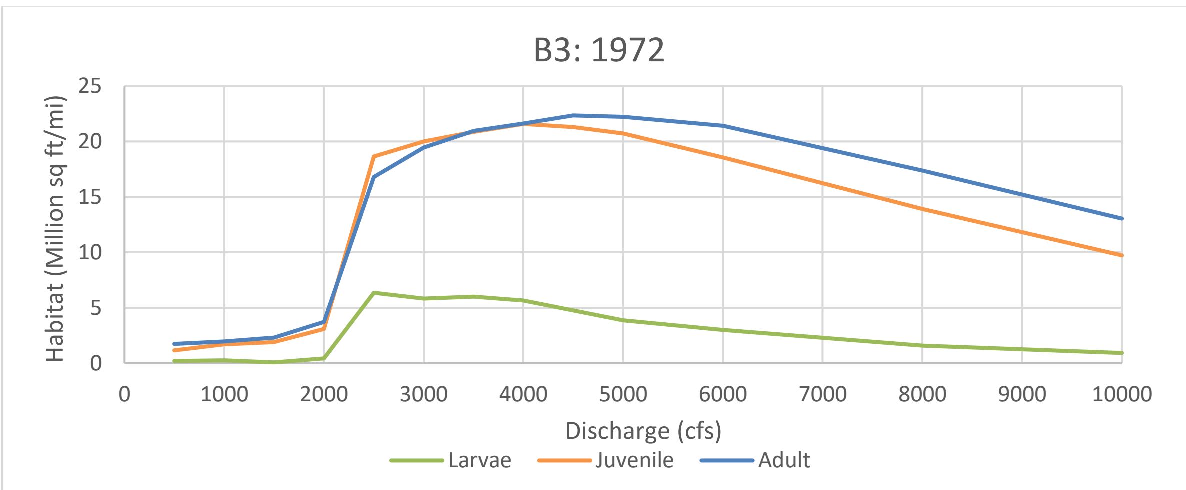

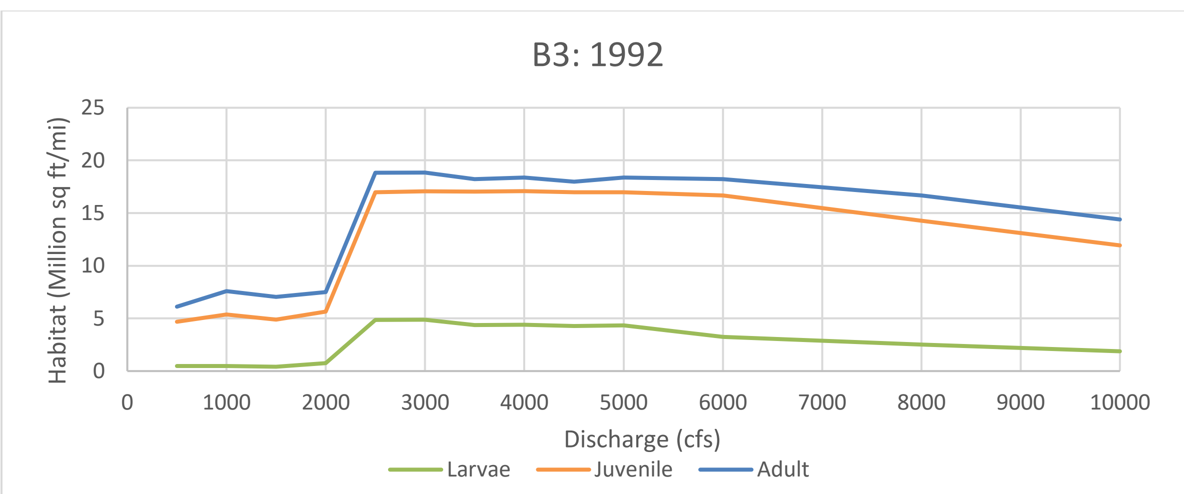

Figure D- 24 Life stage habitat curves for subreach B3 at the years 1962 (top), 1972 (middle), and 1992 (bottom)

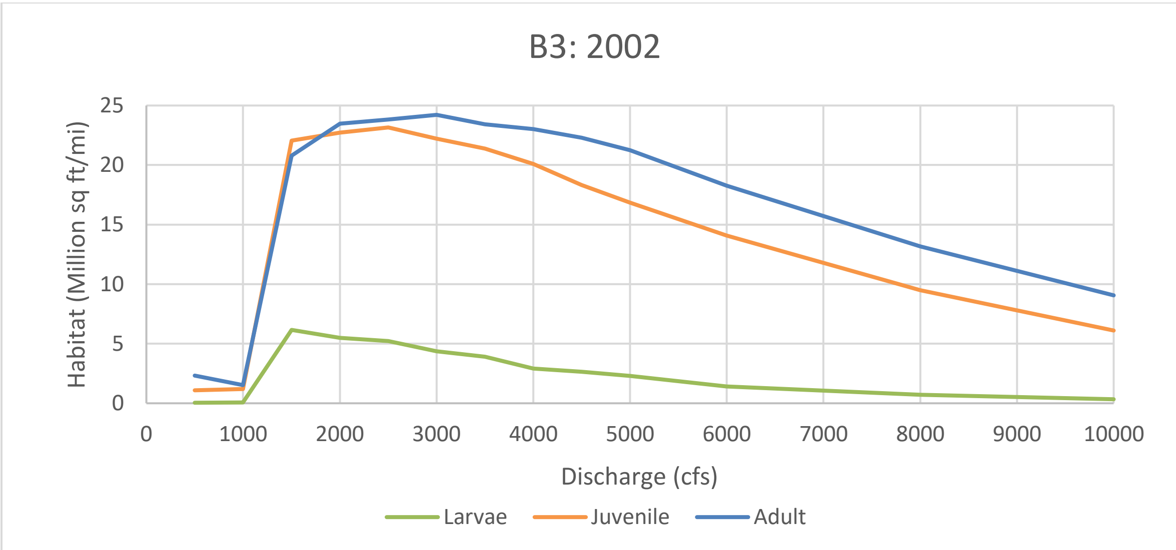

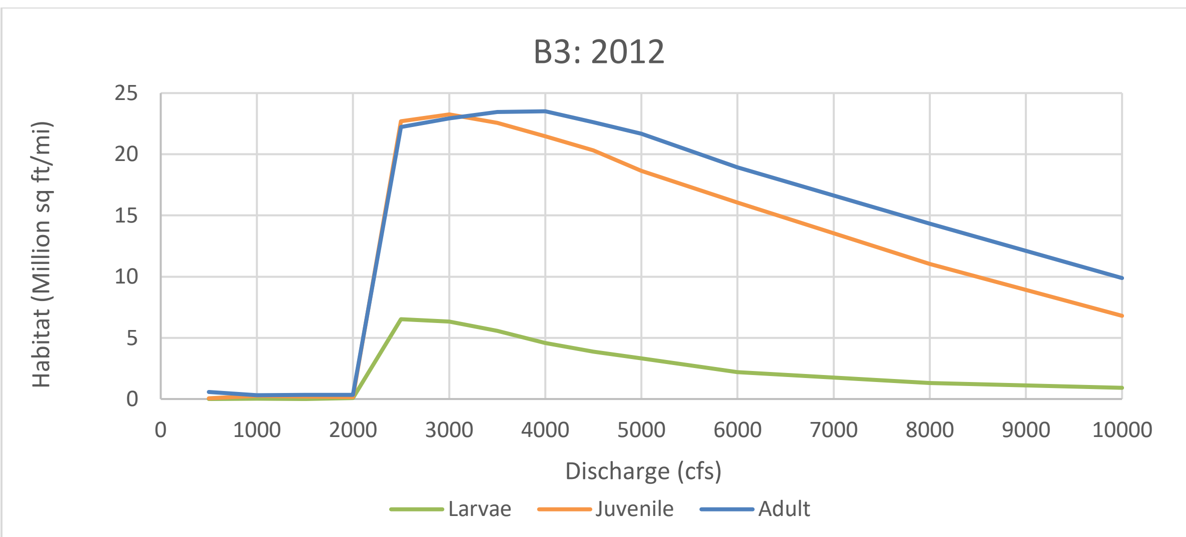

Figure D- 25 Life stage habitat curves for subreach B3 for the years 2002 (top) and 2012 (bottom)

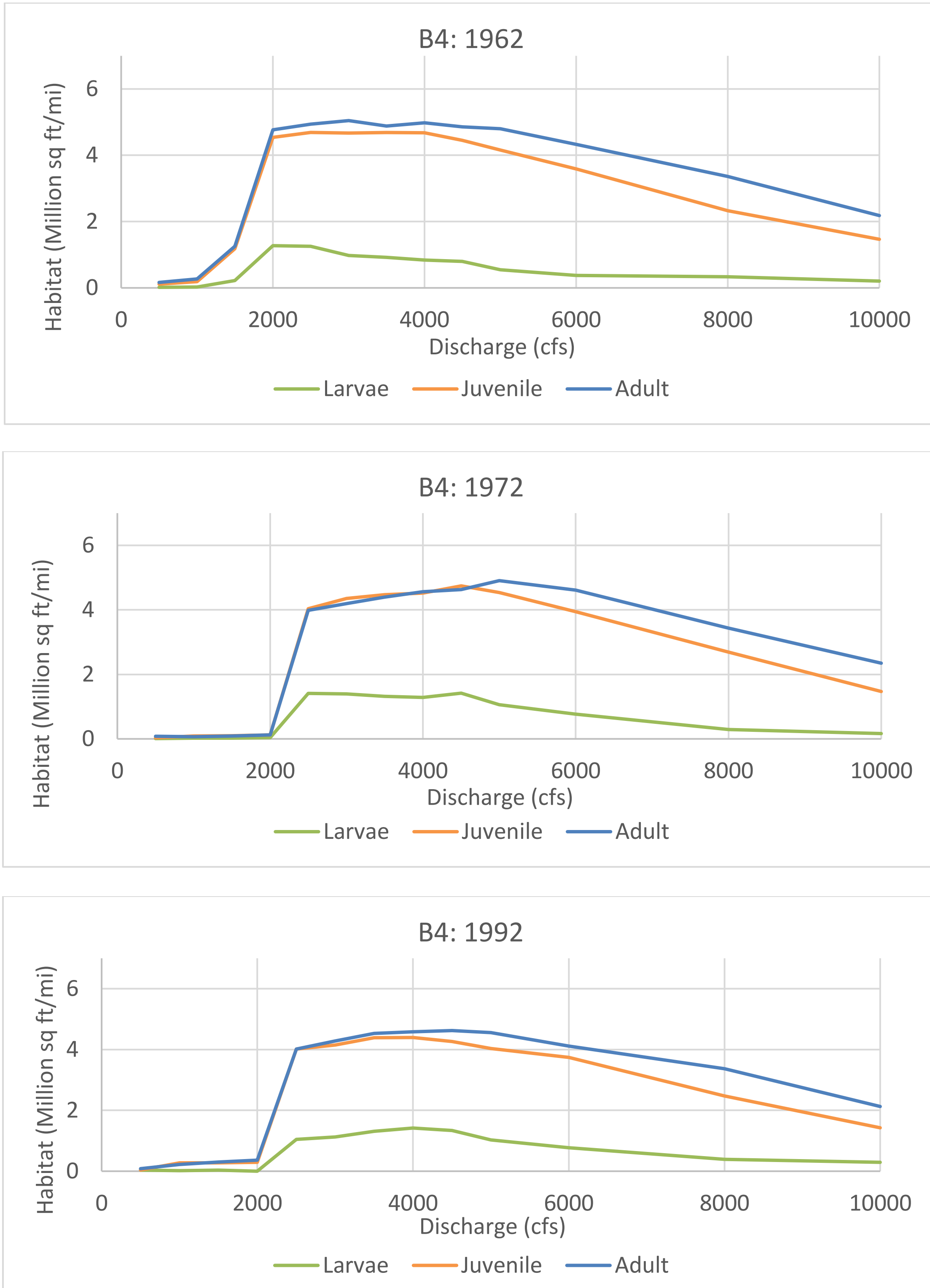

Figure D- 26 Life stage habitat curves for subreach B4 at the years 1962 (top), 1972 (middle), and 1992 (bottom).

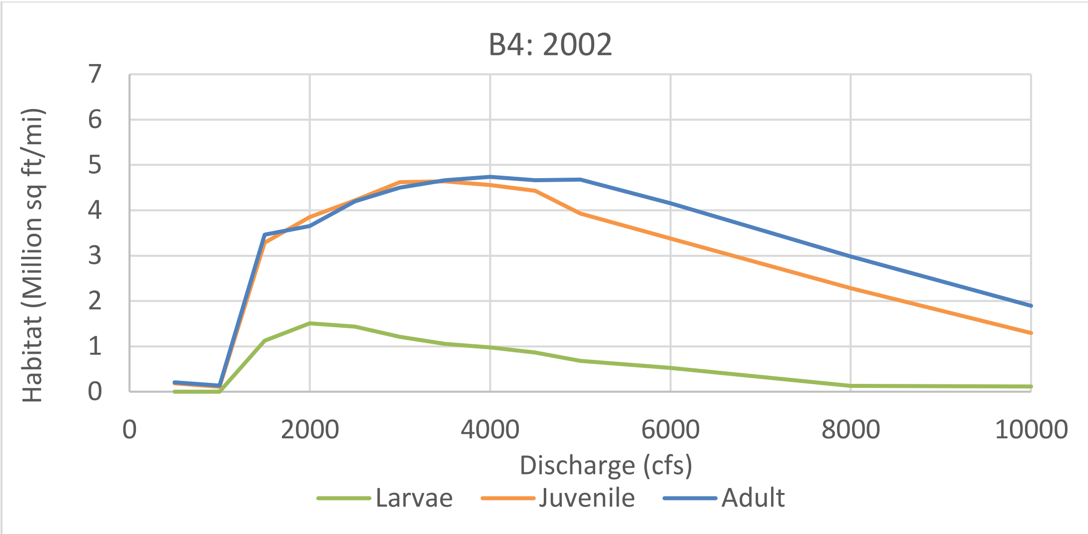

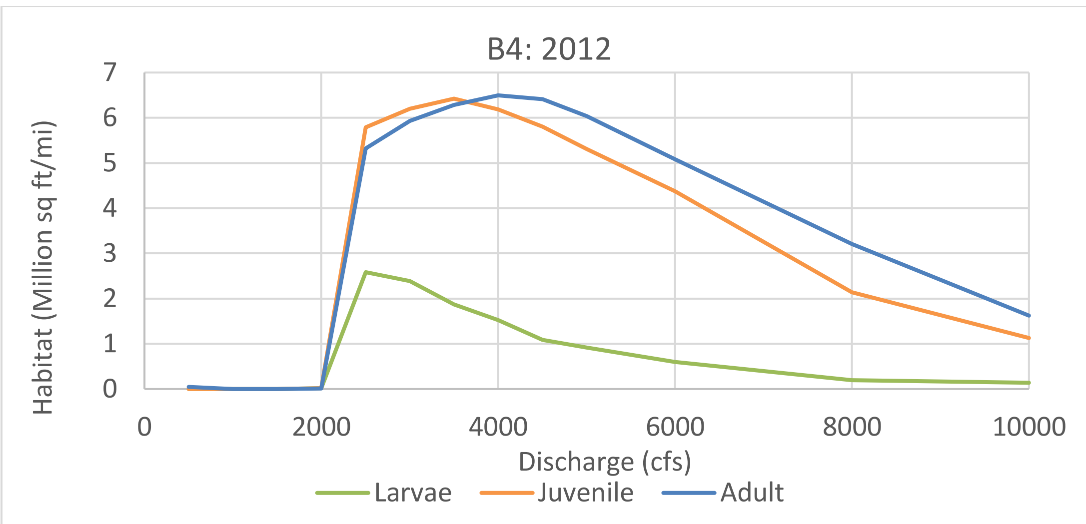

Figure D- 27 Life stage habitat curves for subreach B4 for the years 2002 (top) and 2012 (bottom).

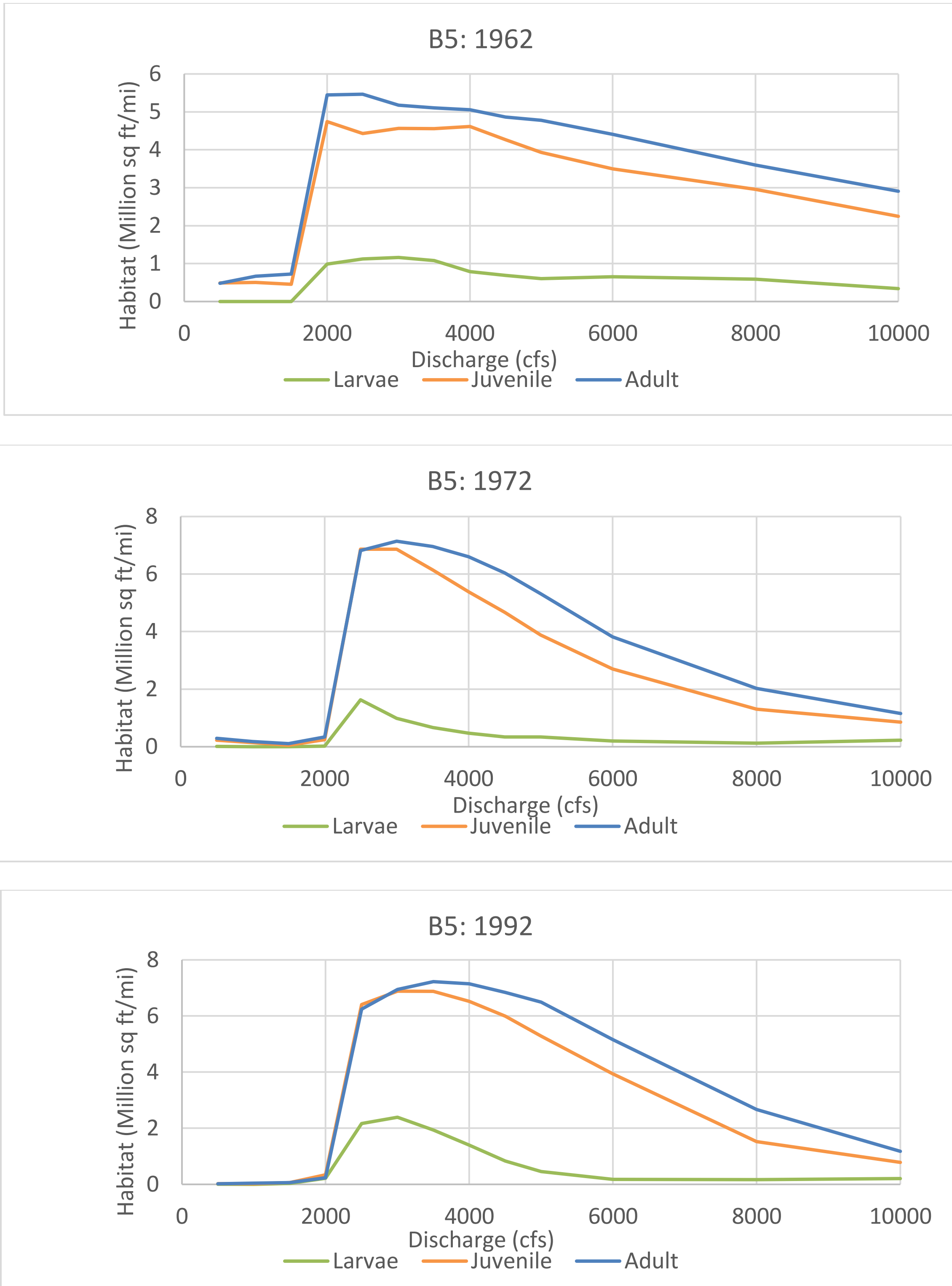

Figure D- 28 Life stage habitat curves for subreach B5 at the years 1962 (top), 1972 (middle), and 1992 (bottom).

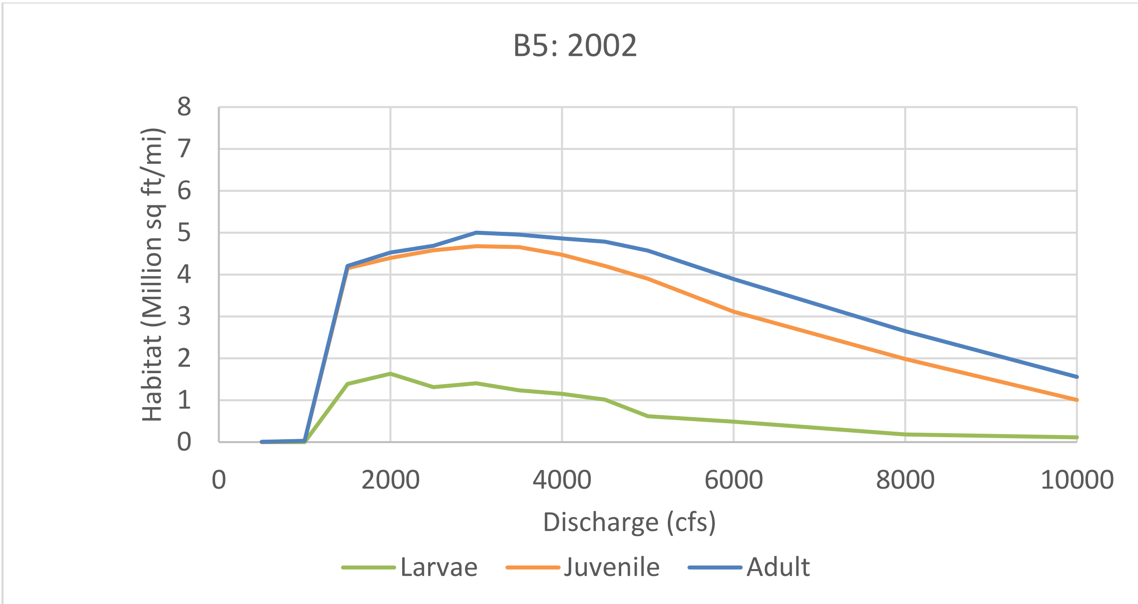

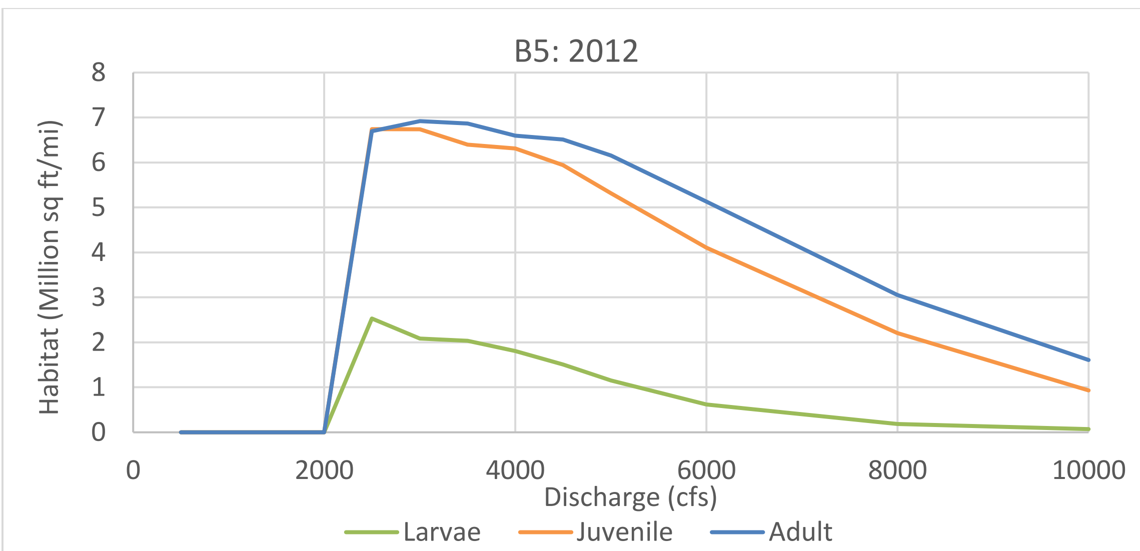

Figure D- 29 Life stage habitat curves for subreach B5 for the years 2002 (top) and 2012 (bottom).

Appendix E

Habitat Maps, Table of Disconnected Areas of Hydraulically Suitable Habitat

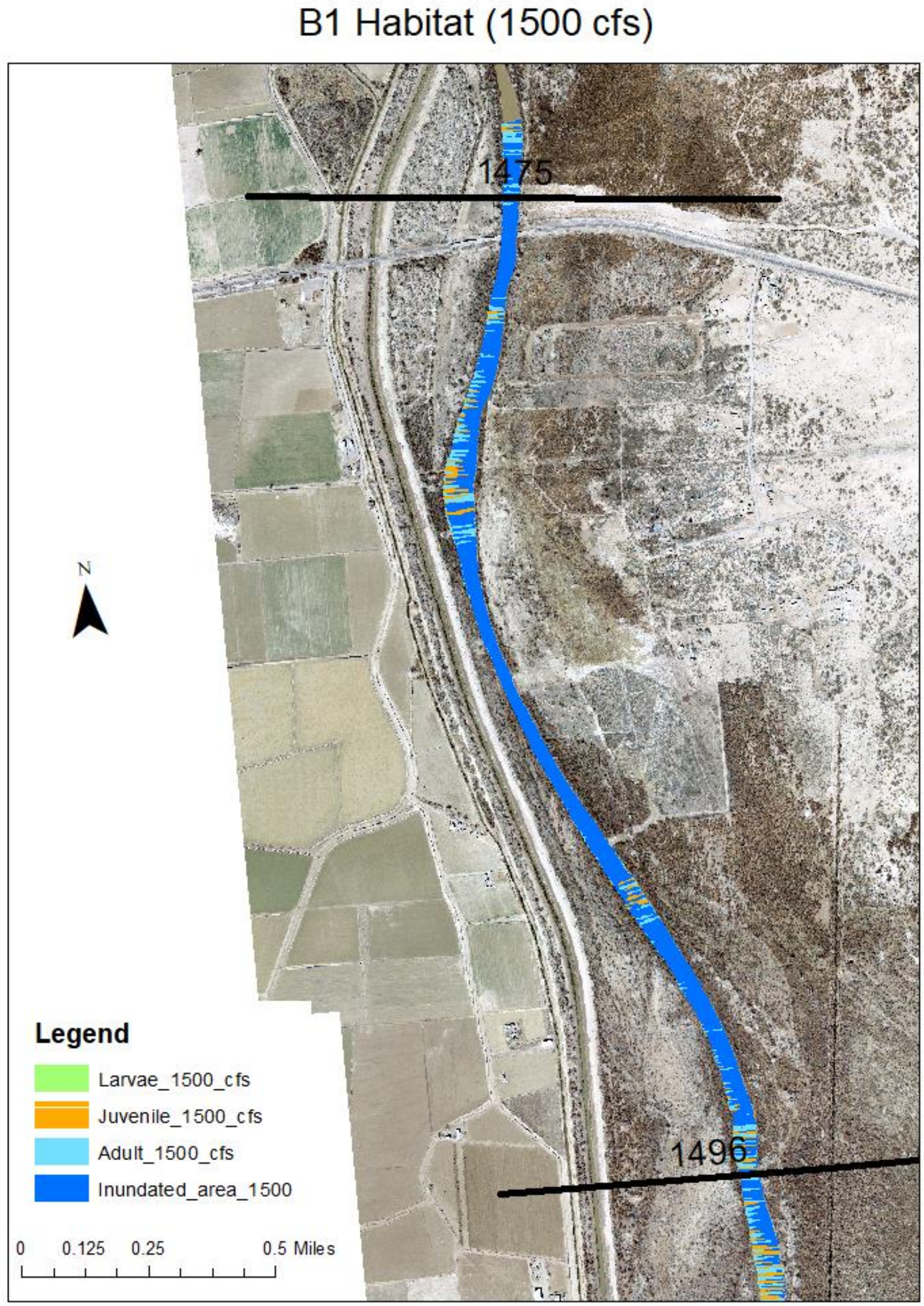

Figure E- 1 RGSM Habitat in subreach B1 at 1500 cfs with hydraulically suitable areas labeled for larvae (green), juvenile (orange), and adult (light blue) and unsuitable inundated areas in dark blue.

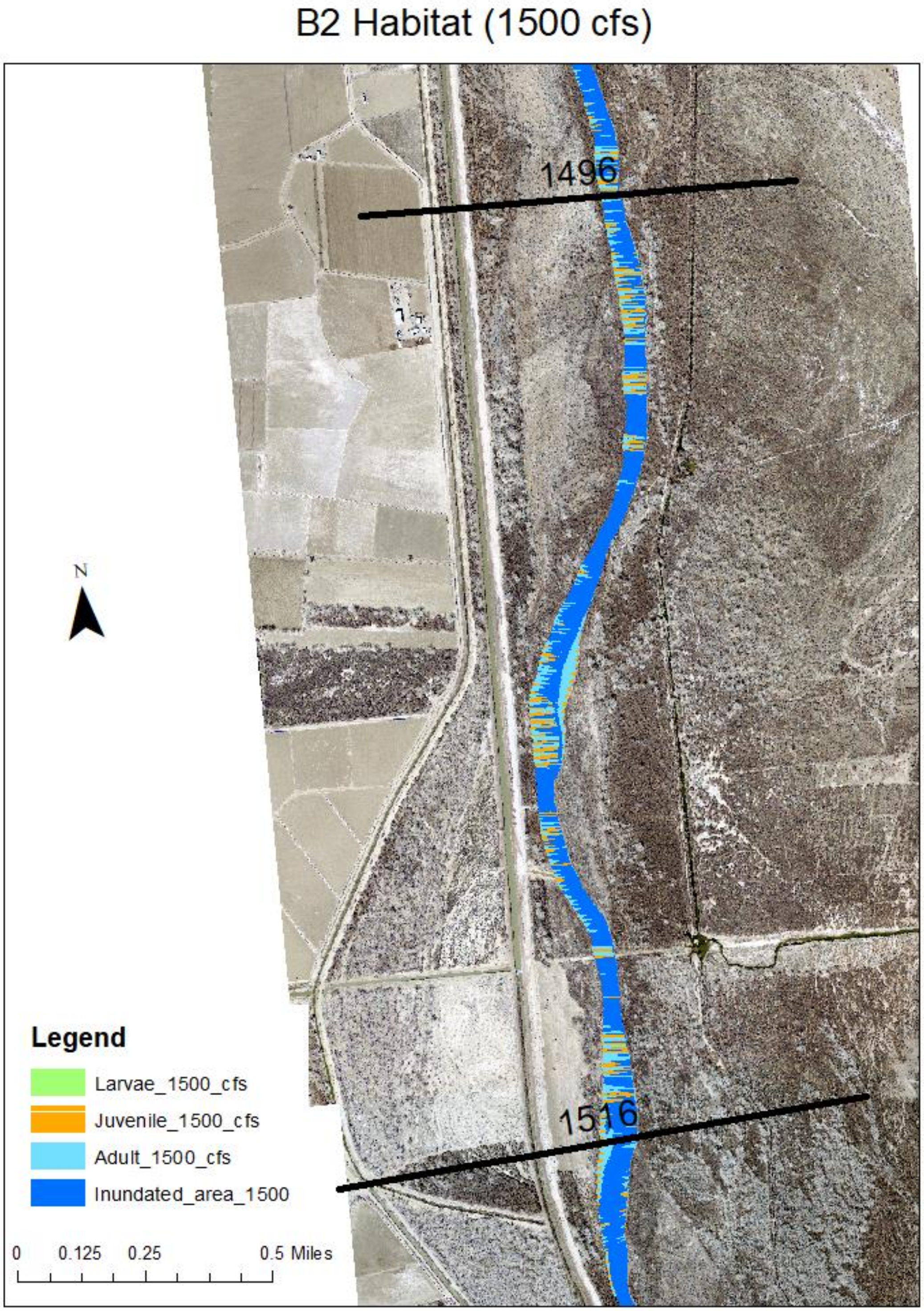

Figure E- 2 RGSM Habitat in subreach B2 at 1500 cfs with hydraulically suitable areas labeled for larvae (green), juvenile (orange), and adult (light blue) and unsuitable inundated areas in dark blue.

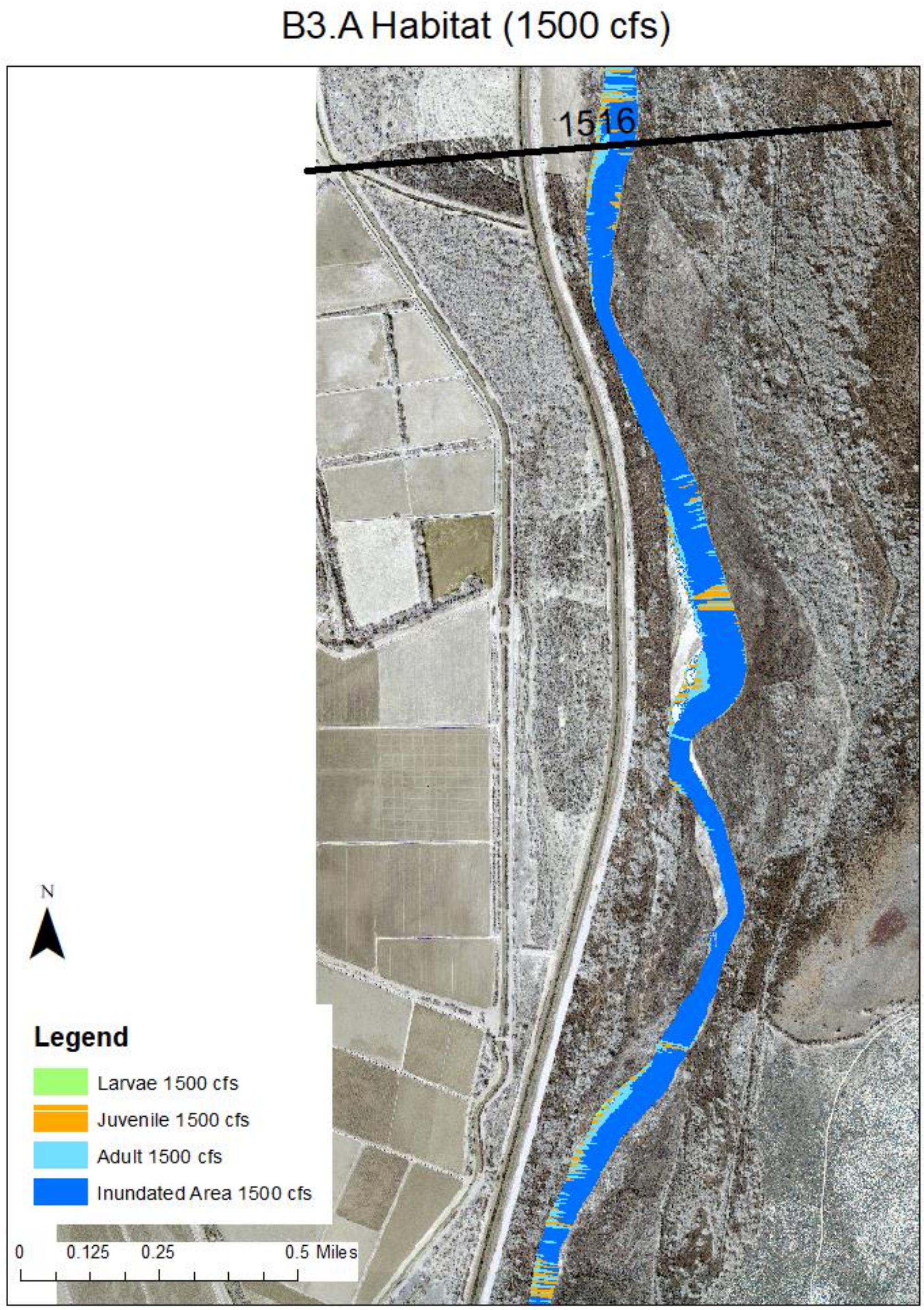

Figure E- 3 RGSM Habitat in subreach B3.A at 1500 cfs with hydraulically suitable areas labeled for larvae (green), juvenile (orange), and adult (light blue) and unsuitable inundated areas in dark blue.

B3.B Habitat (1500 cfs)

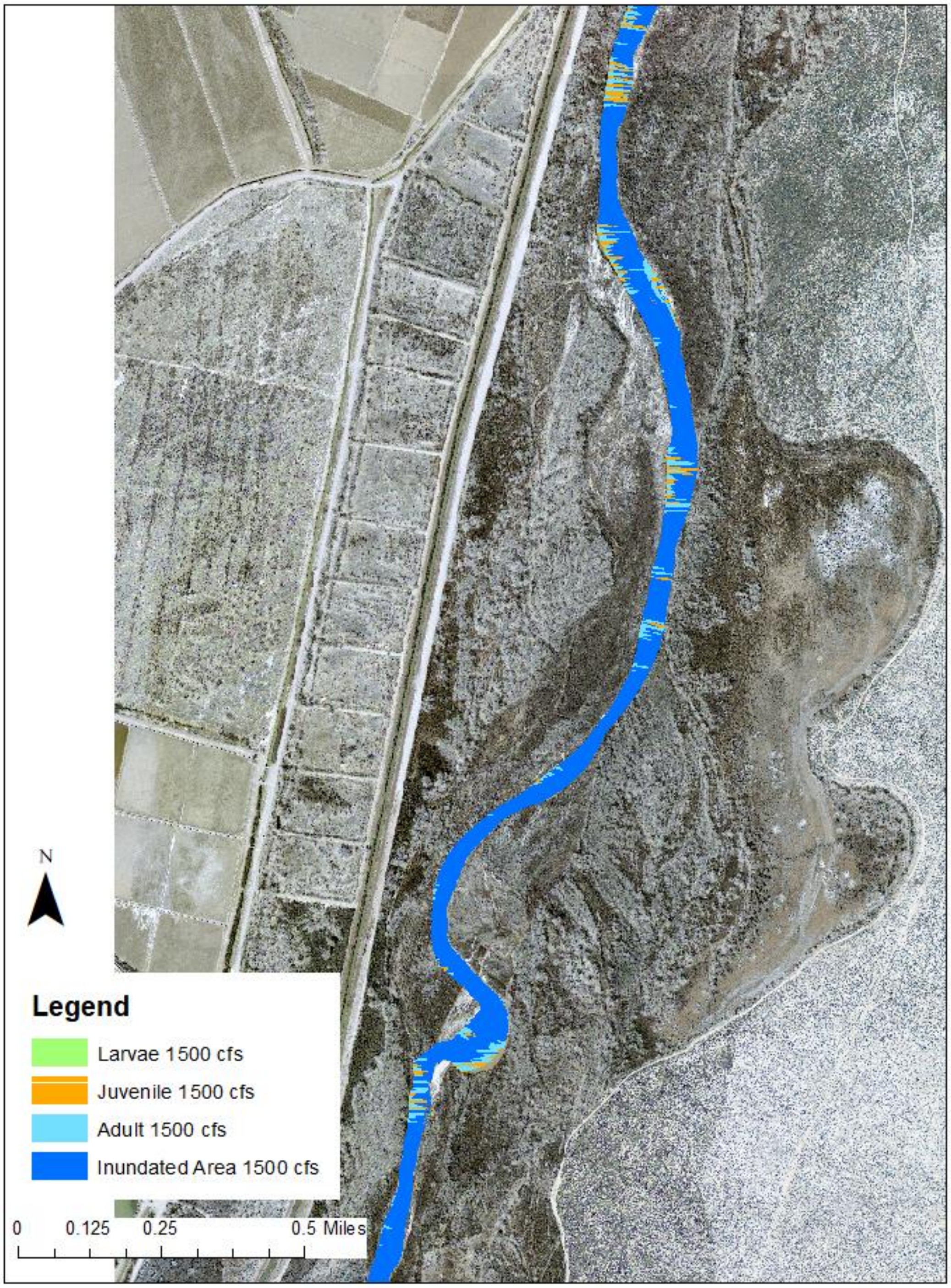

Figure E- 4 RGSM Habitat in subreach B3.B at 1500 cfs with hydraulically suitable areas labeled for larvae (green), juvenile (orange), and adult (light blue) and unsuitable inundated areas in dark blue.

Figure E- 5 RGSM Habitat in subreach B3.C at 1500 cfs with hydraulically suitable areas labeled for larvae (green), juvenile (orange), and adult (light blue) and unsuitable inundated areas in dark blue.

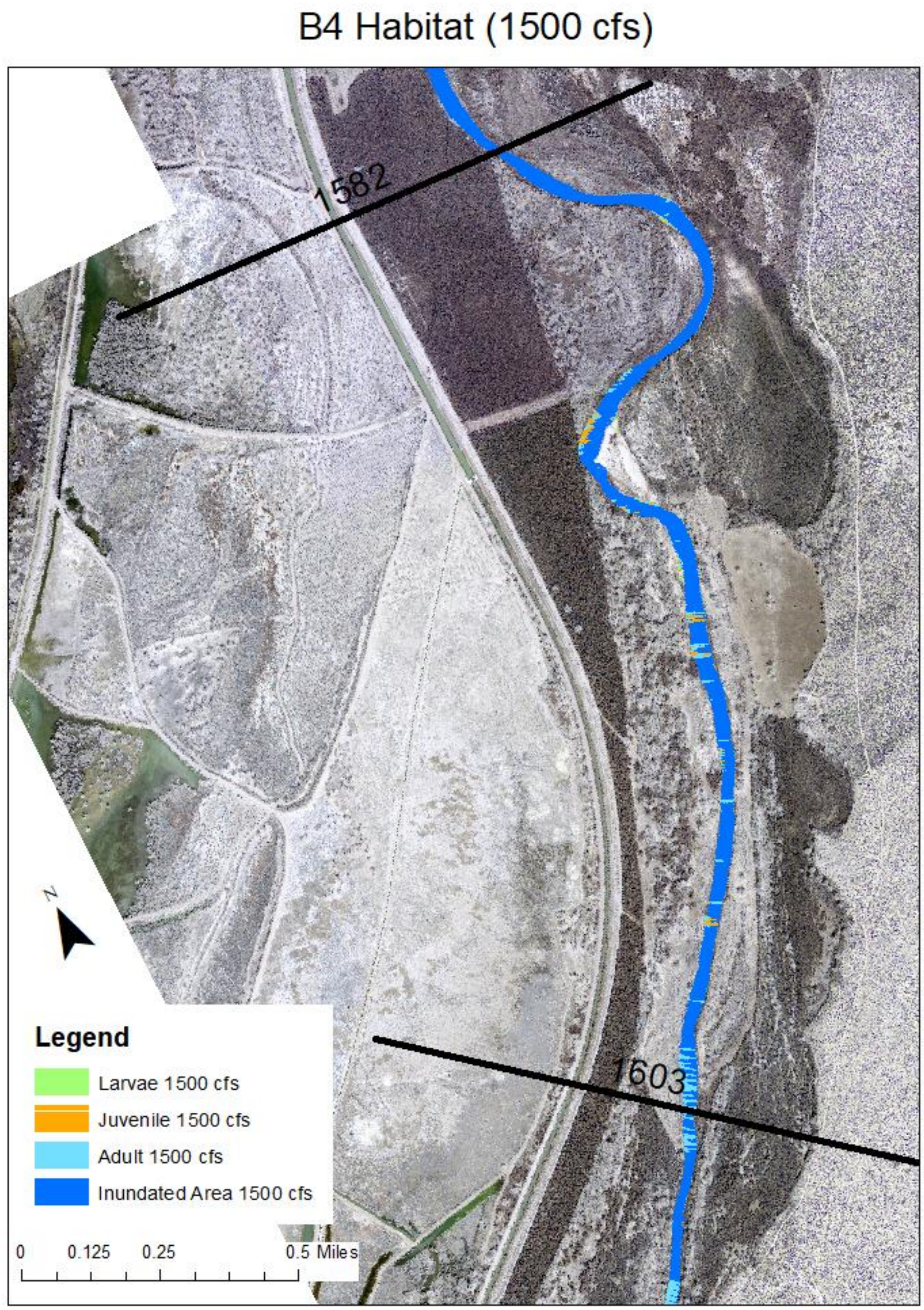

Figure E- 6 RGSM Habitat in subreach B4 at 1500 cfs with hydraulically suitable areas labeled for larvae (green), juvenile (orange), and adult (light blue) and unsuitable inundated areas in dark blue.

B5.A Habitat (1500 cfs)

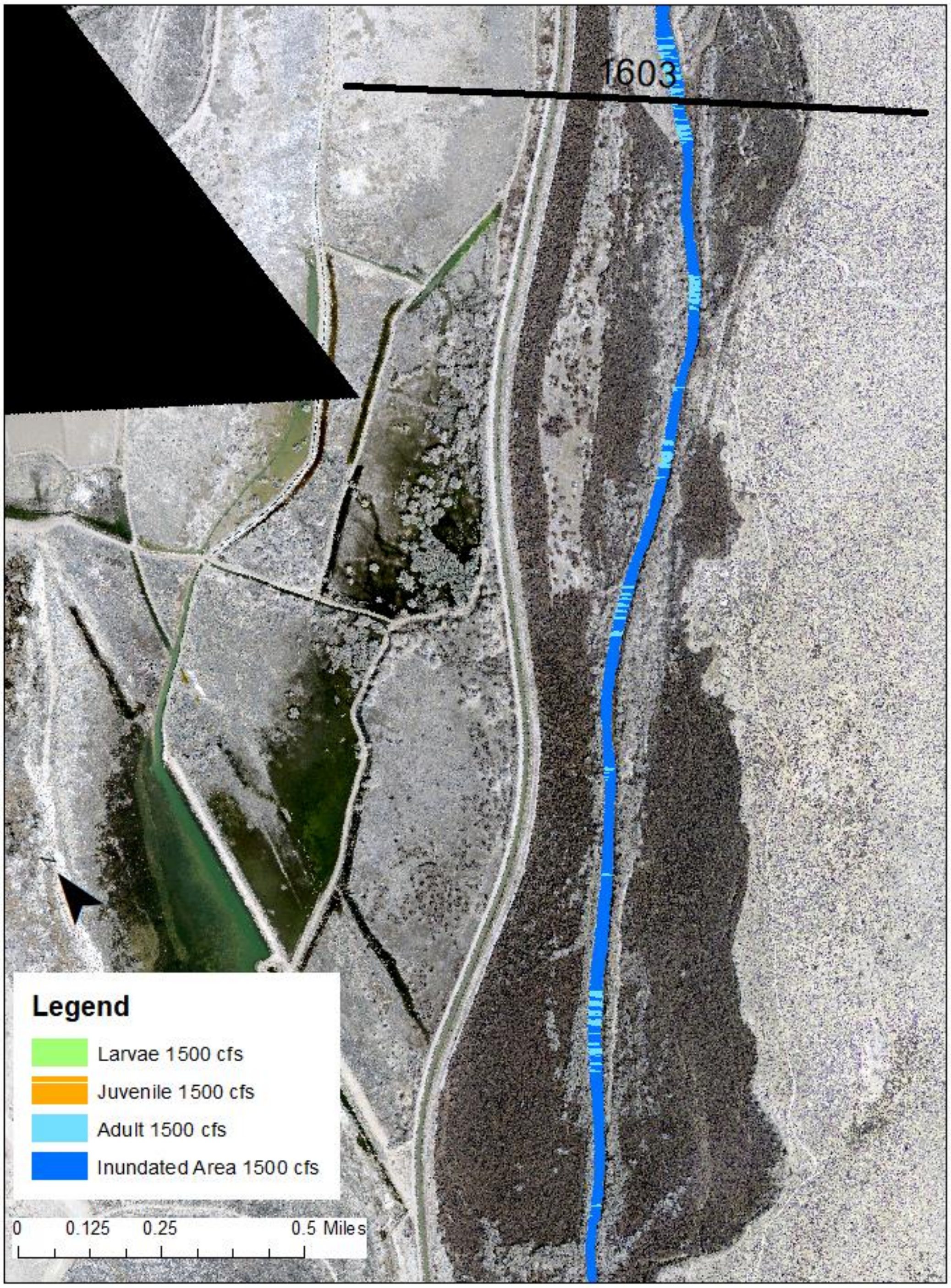

Figure E- 8 RGSM Habitat in subreach B5.A at 1500 cfs with hydraulically suitable areas labeled for larvae (green), juvenile (orange), and adult (light blue) and unsuitable inundated areas in dark blue.

B5.B Habitat (1500 cfs)

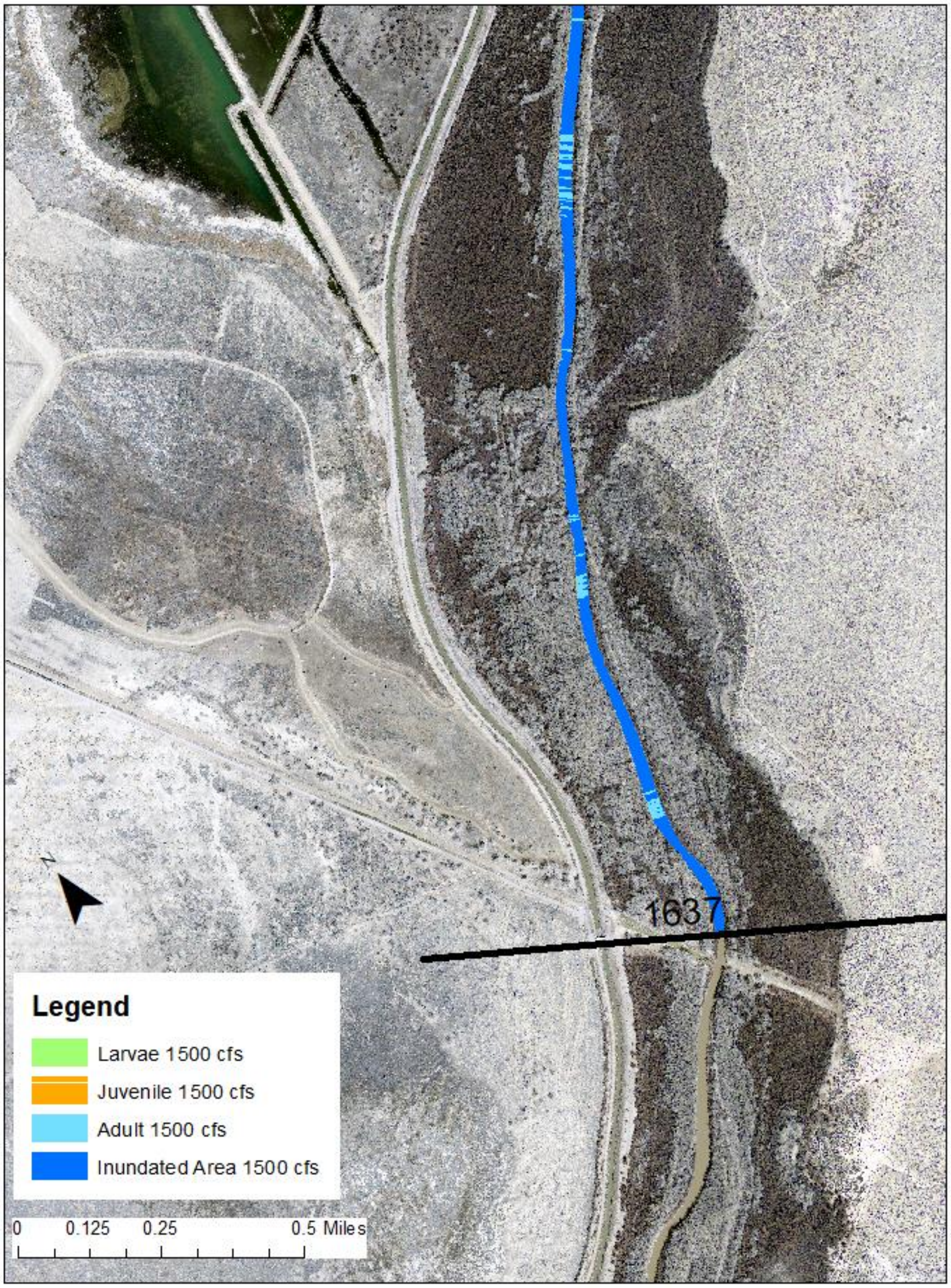

Figure E- 9 RGSM Habitat in subreach B5.B at 1500 cfs with hydraulically suitable areas labeled for larvae (green), juvenile (orange), and adult (light blue) and unsuitable inundated areas in dark blue.

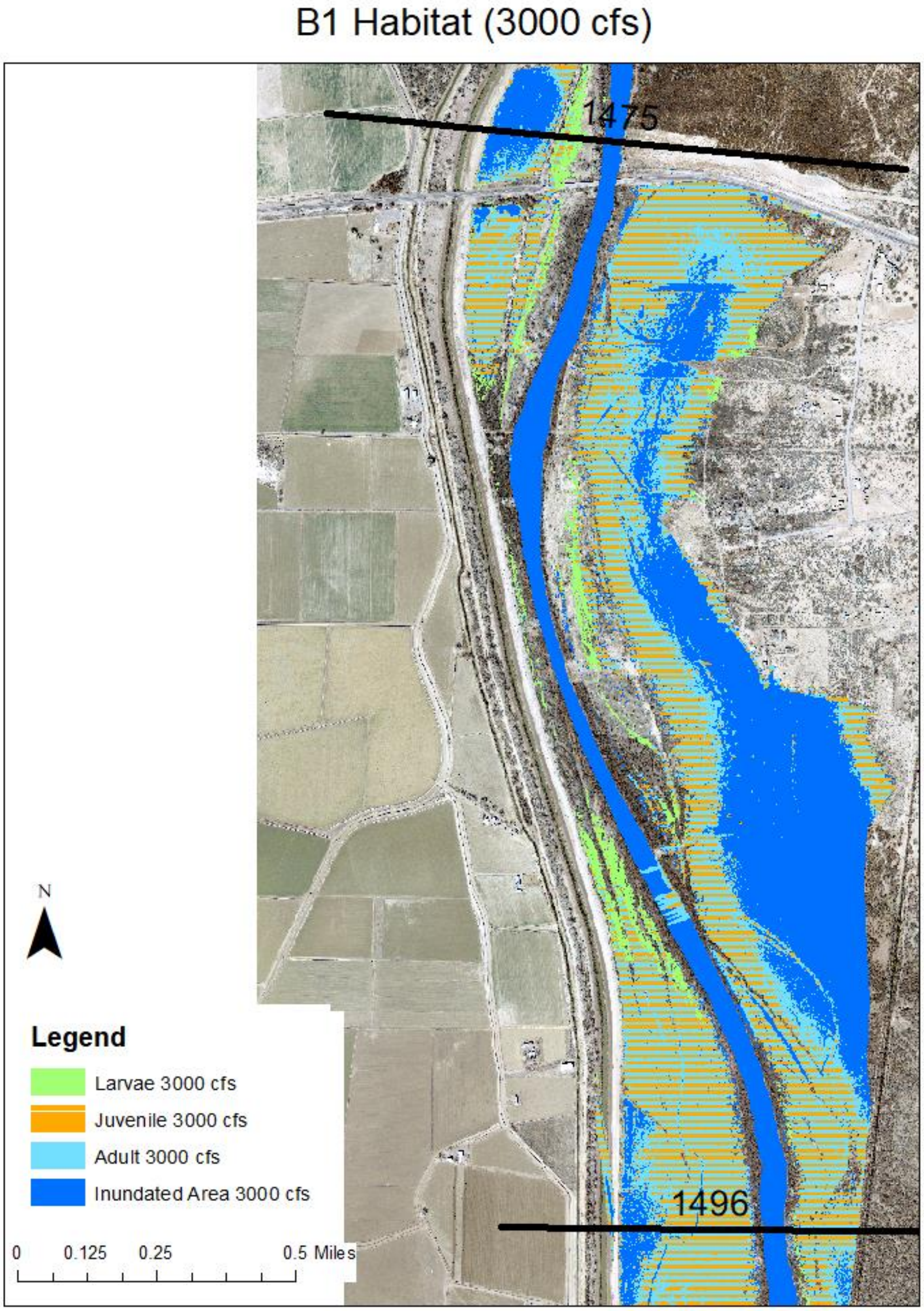

Figure E- 10 RGSM Habitat in subreach B1 at 3000 cfs with hydraulically suitable areas labeled for larvae (green), juvenile (orange), and adult (light blue) and unsuitable inundated areas in dark blue.

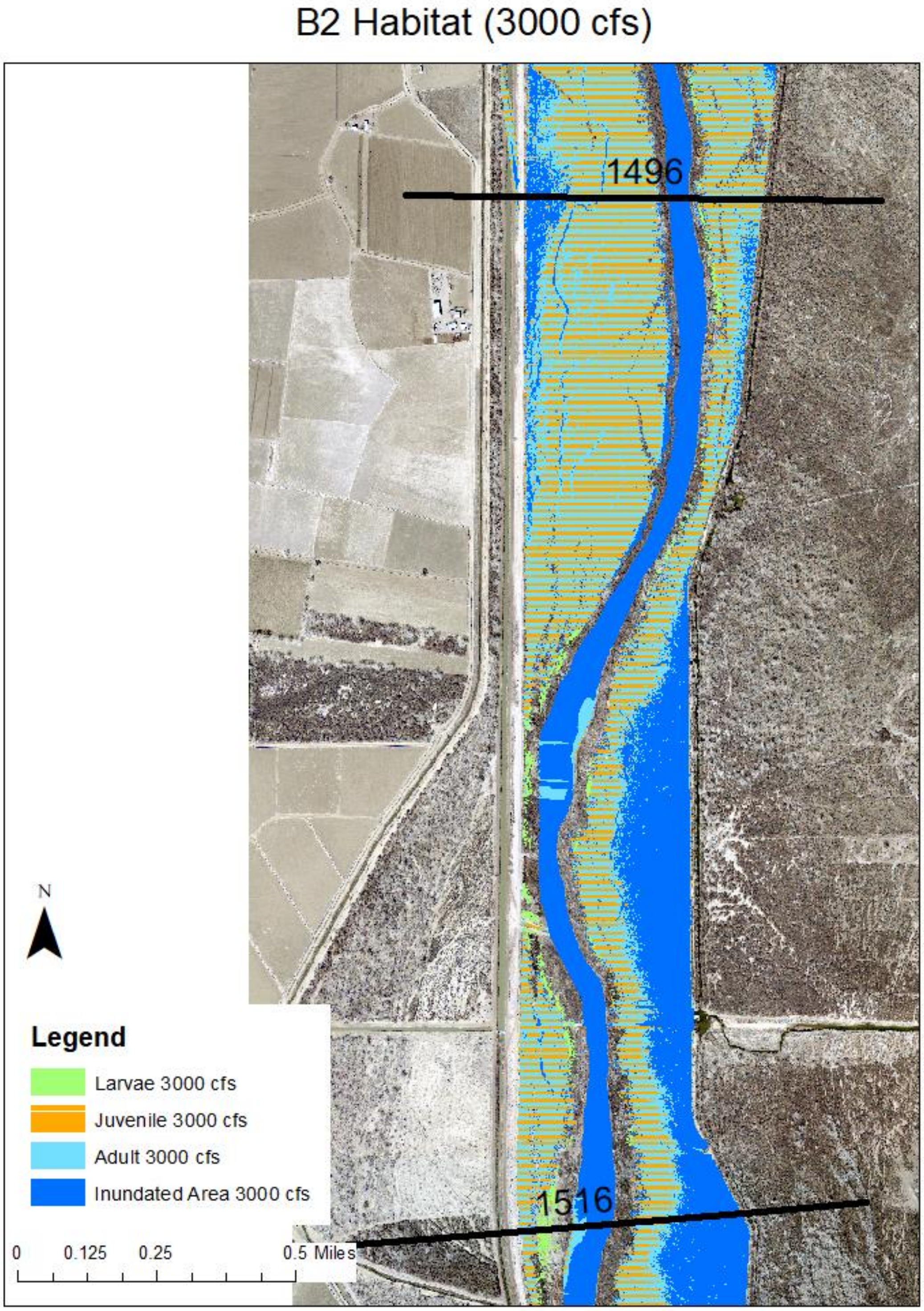

Figure E- 12 RGSM Habitat in subreach B2 at 3000 cfs with hydraulically suitable areas labeled for larvae (green), juvenile (orange), and adult (light blue) and unsuitable inundated areas in dark blue.

B3.A Habitat (3000 cfs)

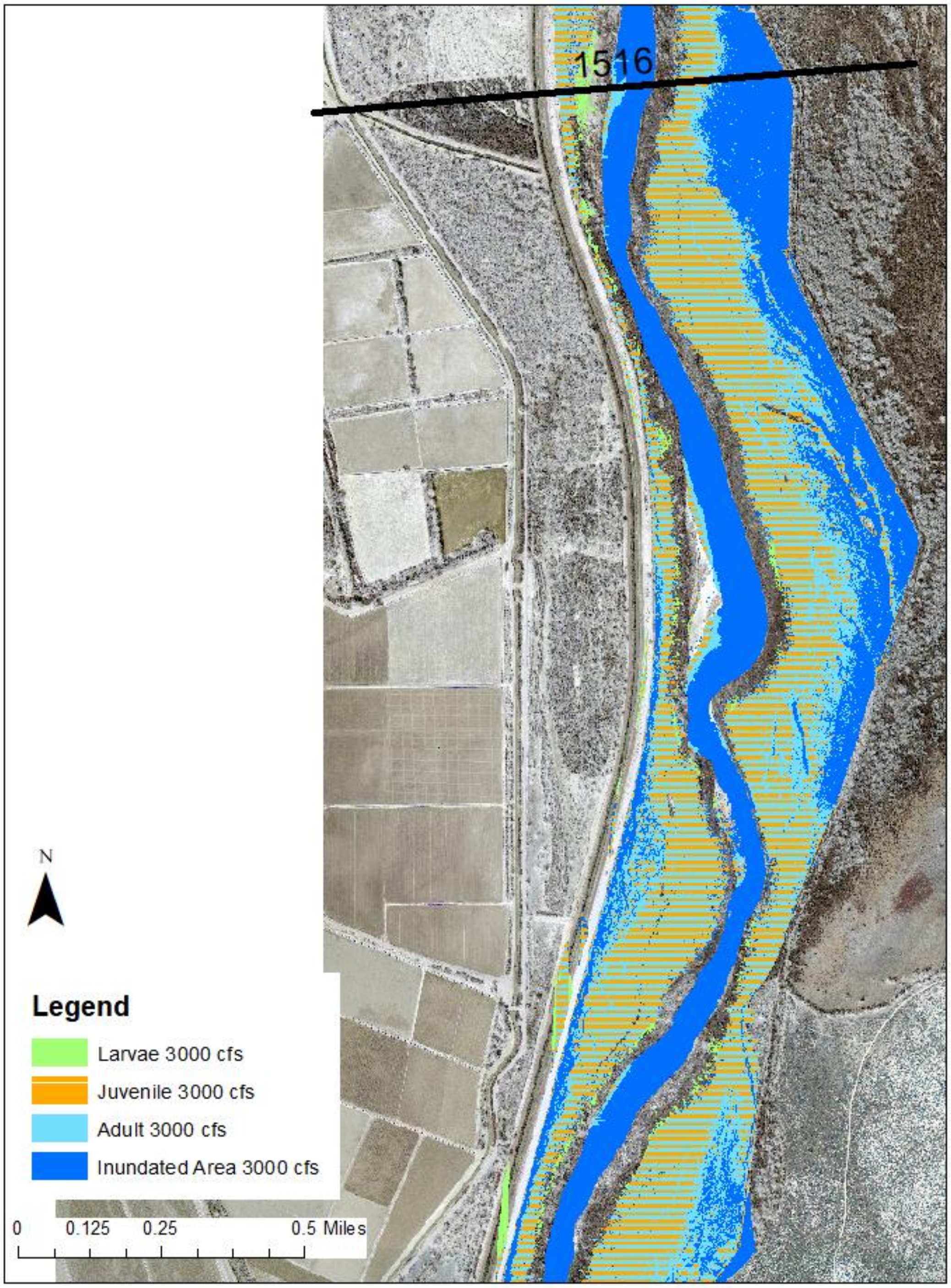

Figure E- 13 RGSM Habitat in subreach B3.A at 3000 cfs with hydraulically suitable areas labeled for larvae (green), juvenile (orange), and adult (light blue) and unsuitable inundated areas in dark blue.

B3.B Habitat (3000 cfs)

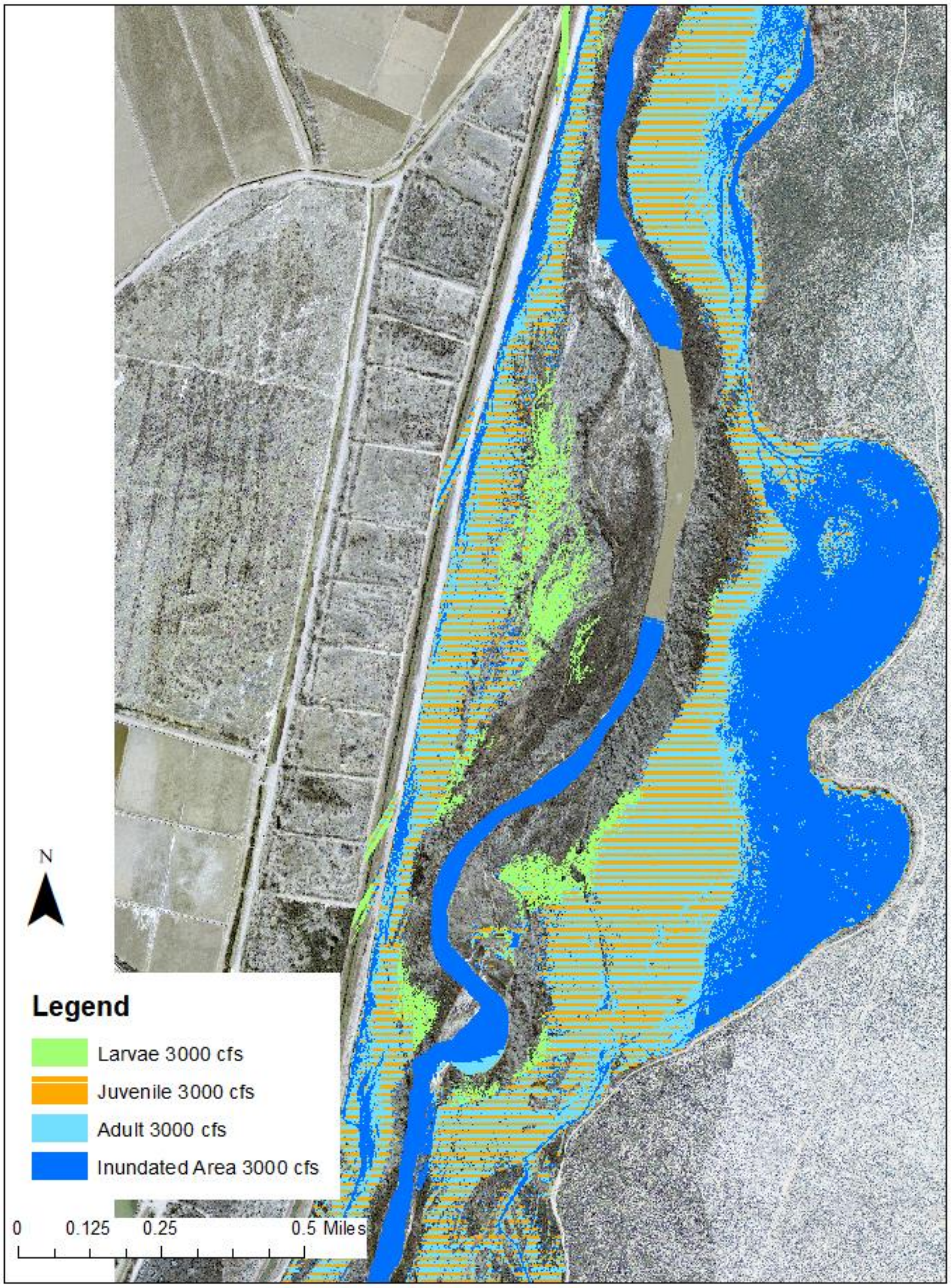

Figure E- 15 RGSM Habitat in subreach B3.B at 3000 cfs with hydraulically suitable areas labeled for larvae (green), juvenile (orange), and adult (light blue) and unsuitable inundated areas in dark blue.

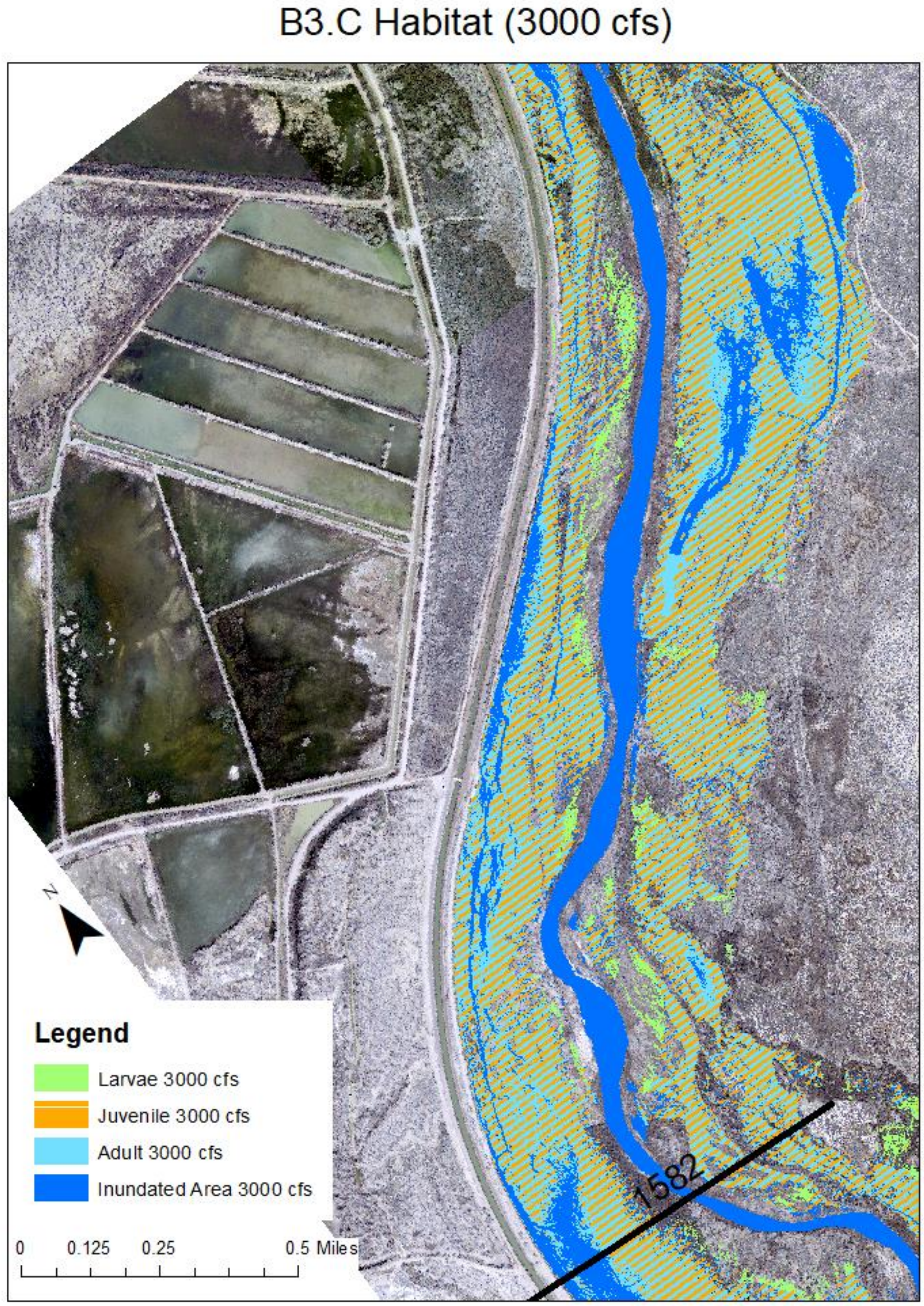

Figure E- 16 RGSM Habitat in subreach B3.C at 3000 cfs with hydraulically suitable areas labeled for larvae (green), juvenile (orange), and adult (light blue) and unsuitable inundated areas in dark blue.

B4 Habitat (3000 cfs)

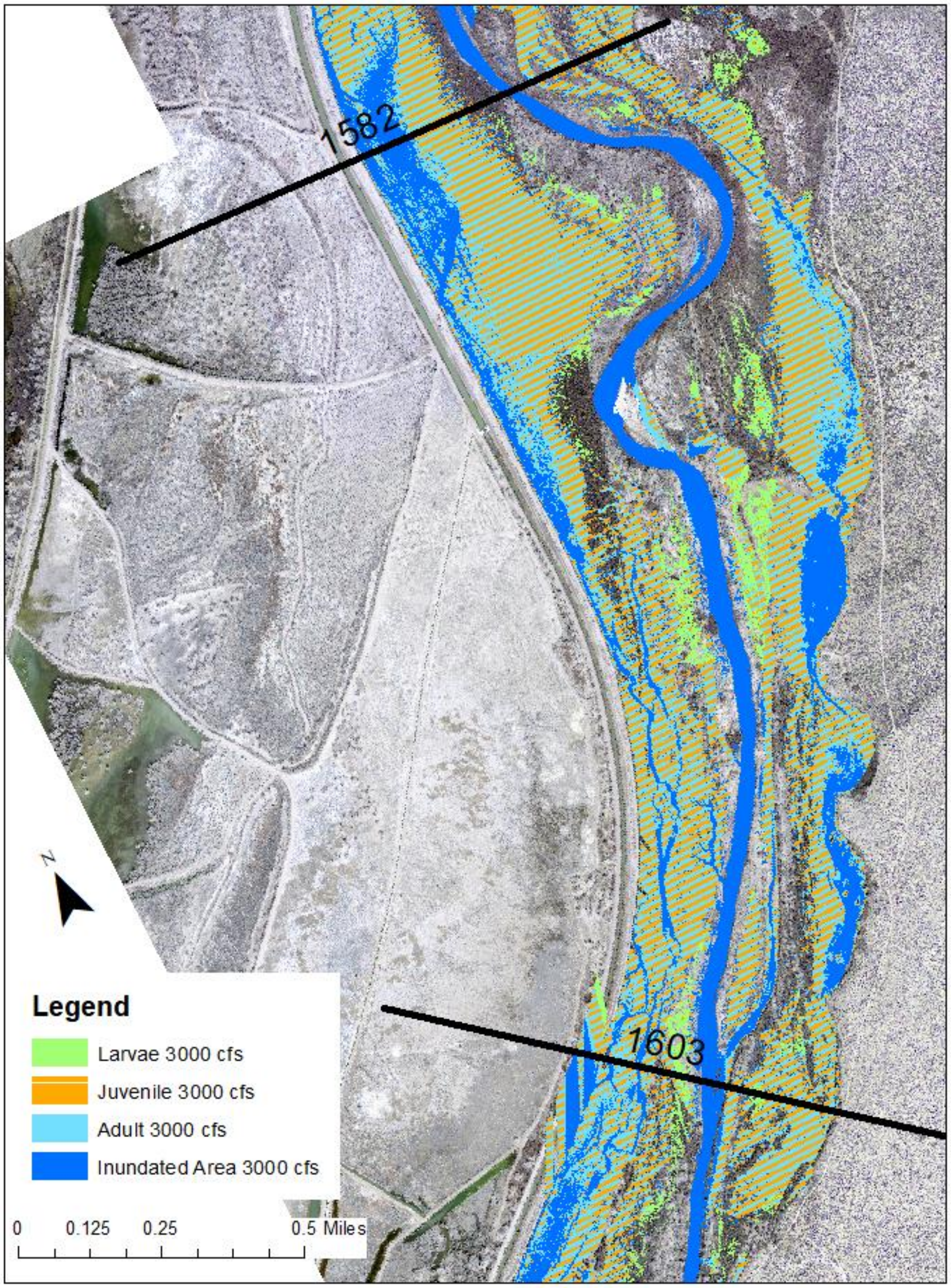

Figure E- 17 RGSM Habitat in subreach B4 at 3000 cfs with hydraulically suitable areas labeled for larvae (green), juvenile (orange), and adult (light blue) and unsuitable inundated areas in dark blue.

B5.A Habitat (3000 cfs)

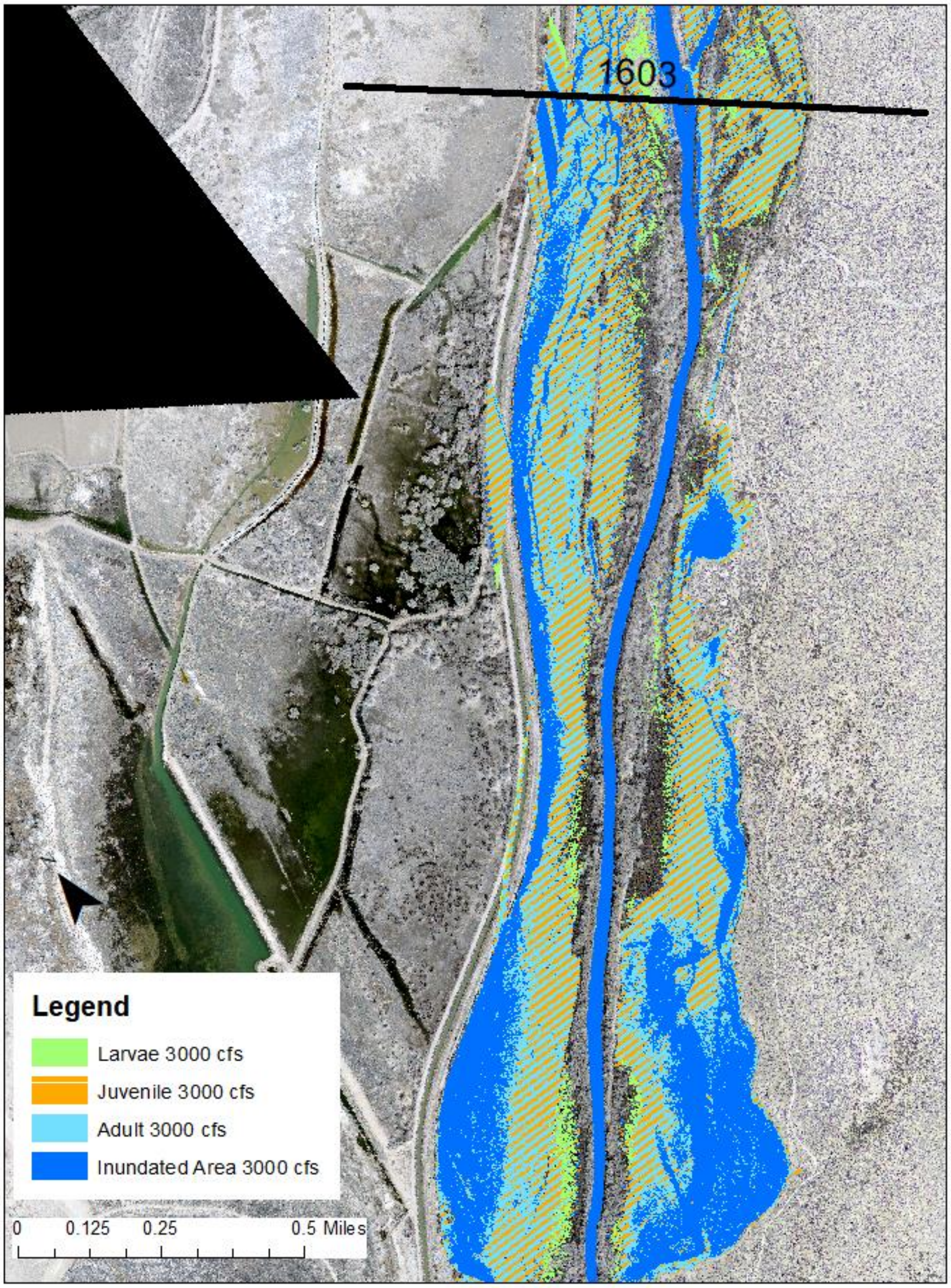

Figure E- 18 RGSM Habitat in subreach B5.A at 3000 cfs with hydraulically suitable areas labeled for larvae (green), juvenile (orange), and adult (light blue) and unsuitable inundated areas in dark blue.

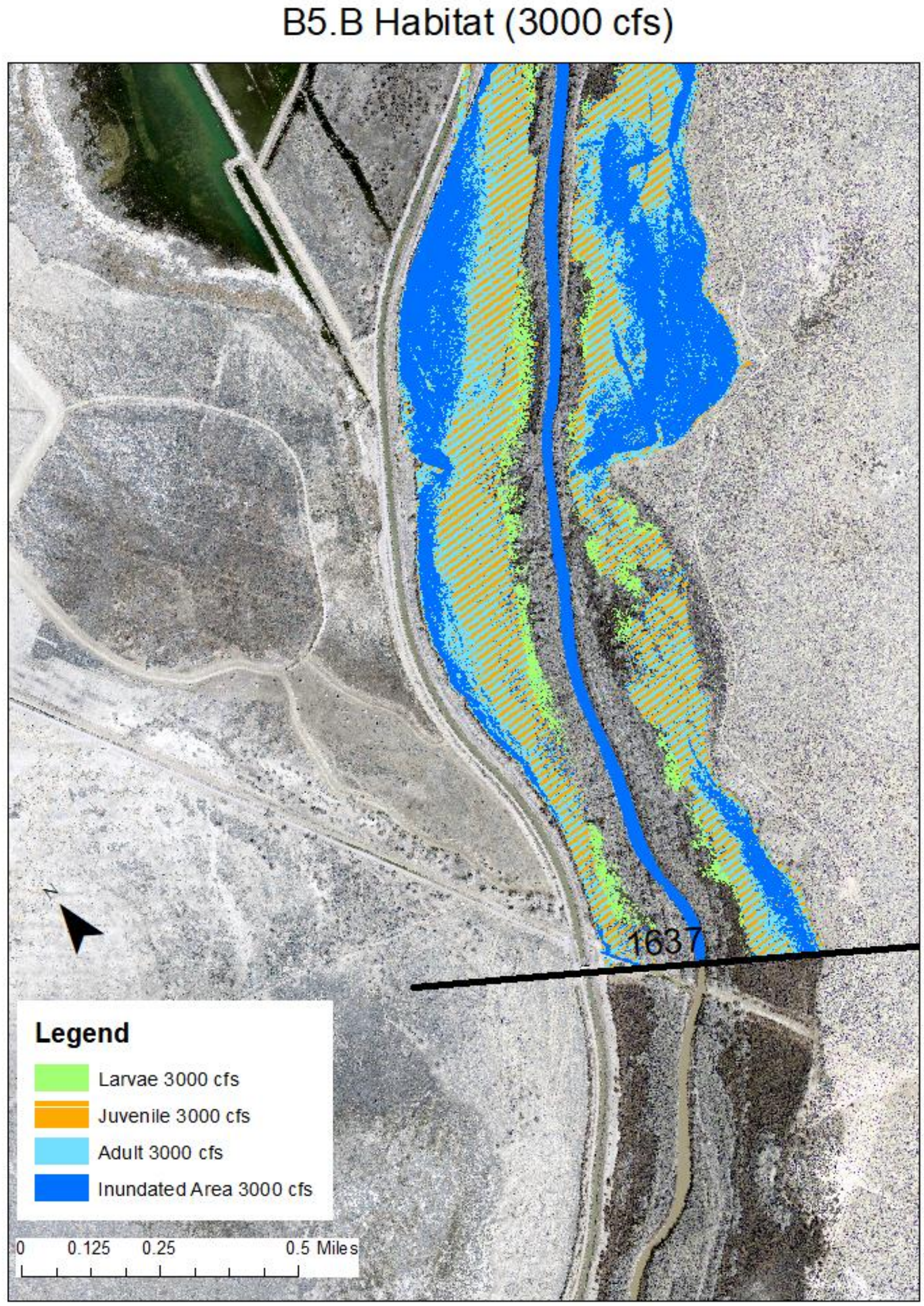

Figure E- 19 RGSM Habitat in subreach B5.B at 3000 cfs with hydraulically suitable areas labeled for larvae (green), juvenile (orange), and adult (light blue) and unsuitable inundated areas in dark blue.

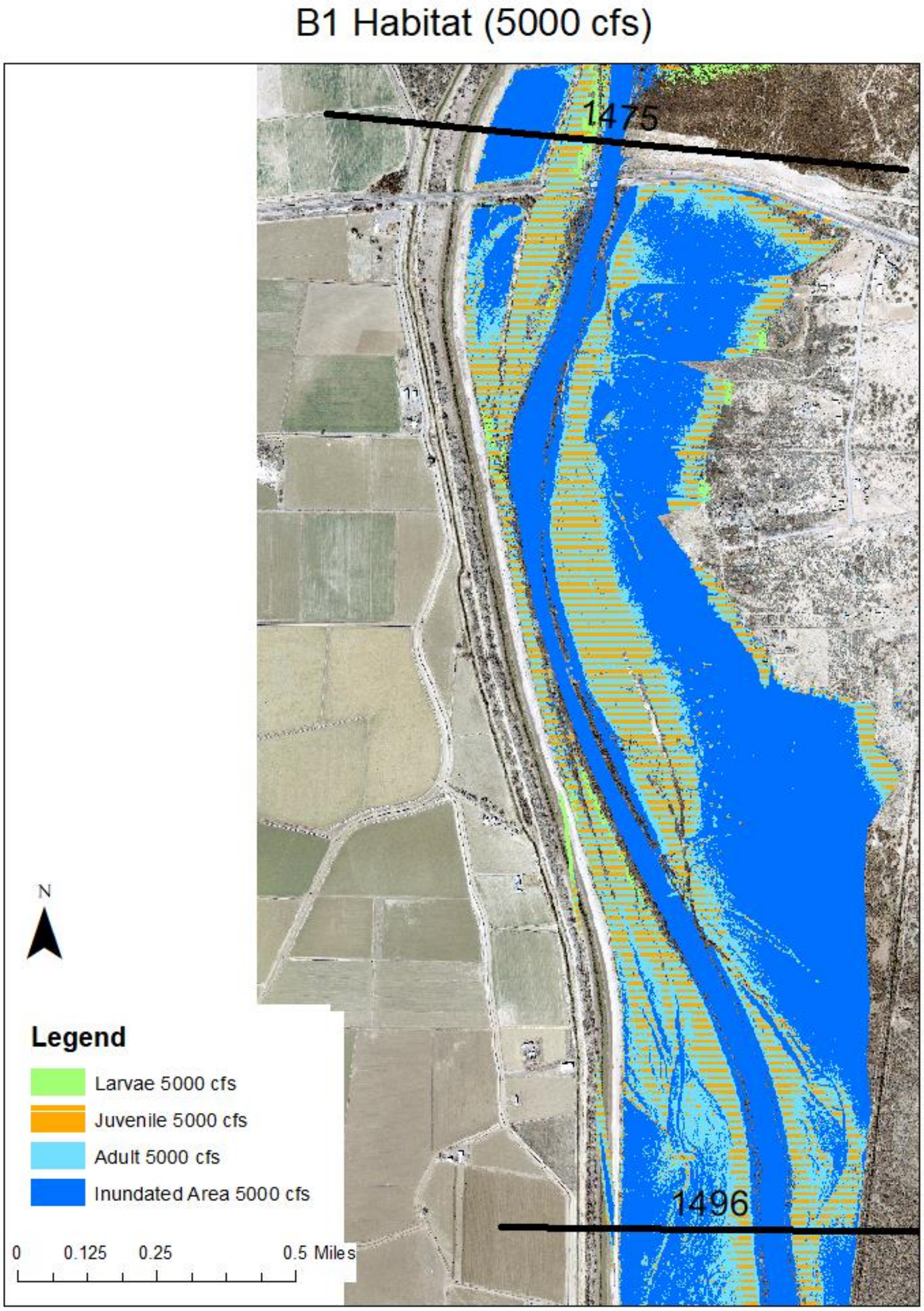

Figure E- 20 RGSM Habitat in subreach B1 at 5000 cfs with hydraulically suitable areas labeled for larvae (green), juvenile (orange), and adult (light blue) and unsuitable inundated areas in dark blue.

B2 Habitat (5000 cfs)

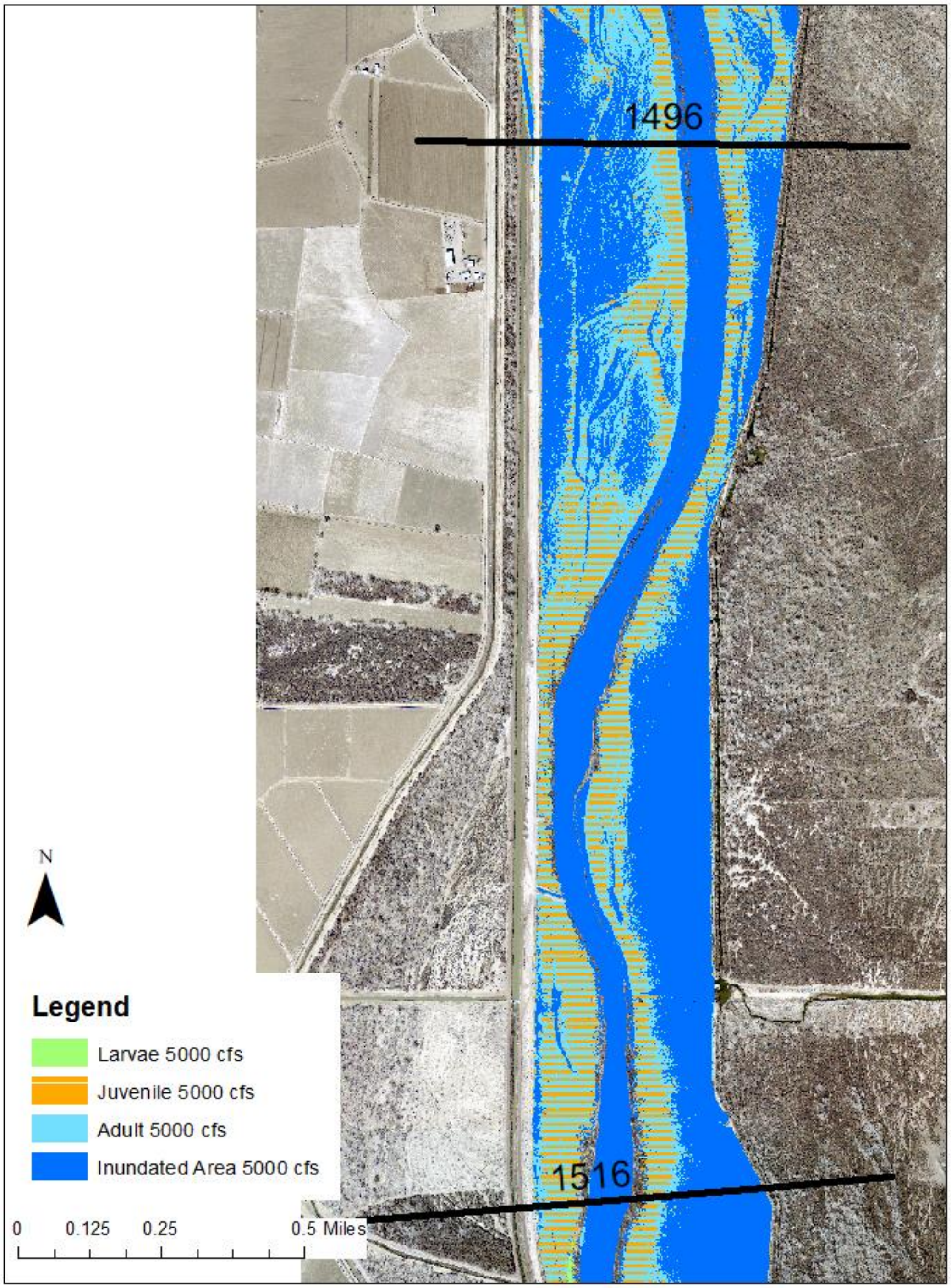

Figure E- 22 RGSM Habitat in subreach B2 at 5000 cfs with hydraulically suitable areas labeled for larvae (green), juvenile (orange), and adult (light blue) and unsuitable inundated areas in dark blue.

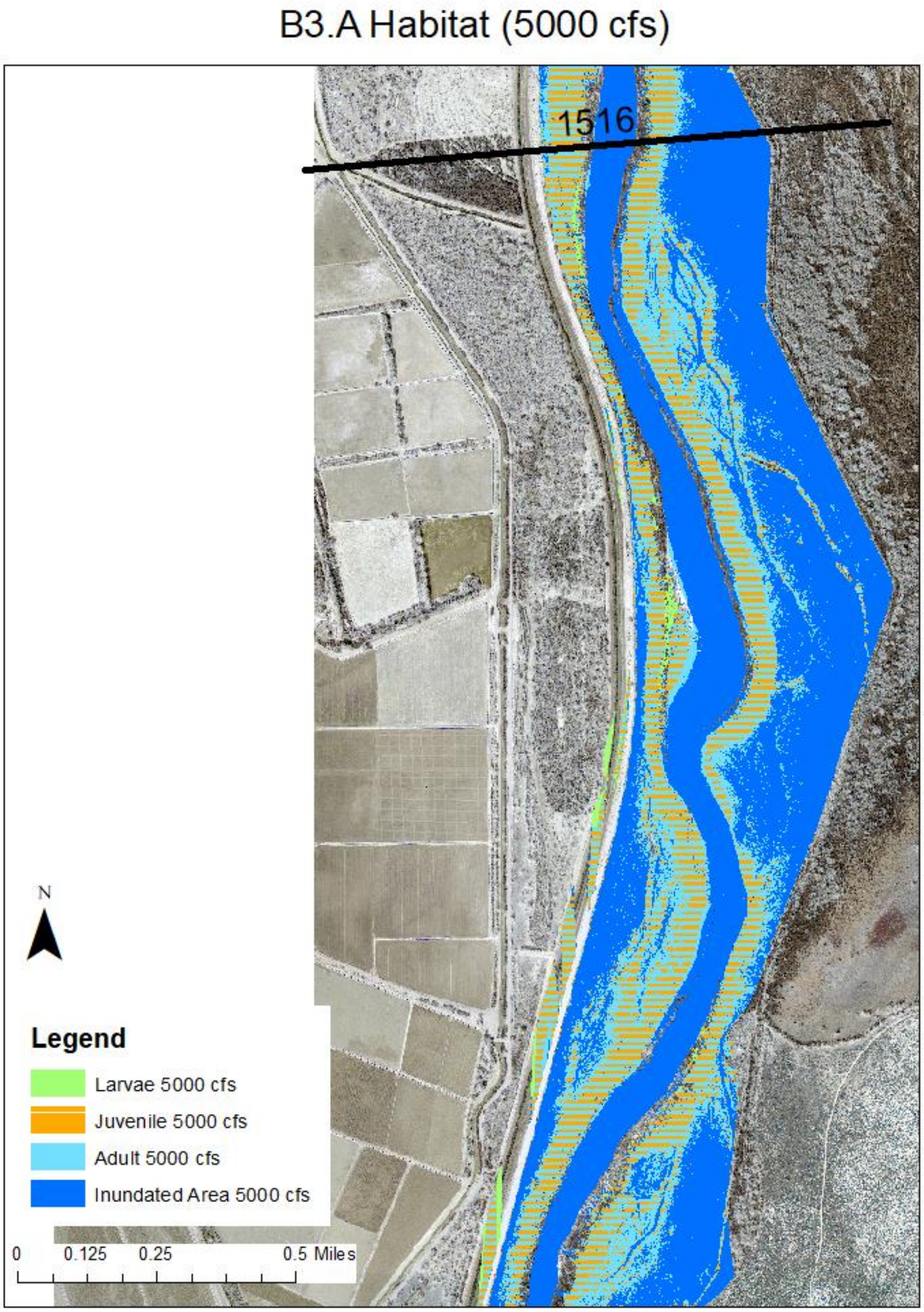

Figure E- 23 RGSM Habitat in subreach B3.A at 5000 cfs with hydraulically suitable areas labeled for larvae (green), juvenile (orange), and adult (light blue) and unsuitable inundated areas in dark blue.

B3.B Habitat (5000 cfs)

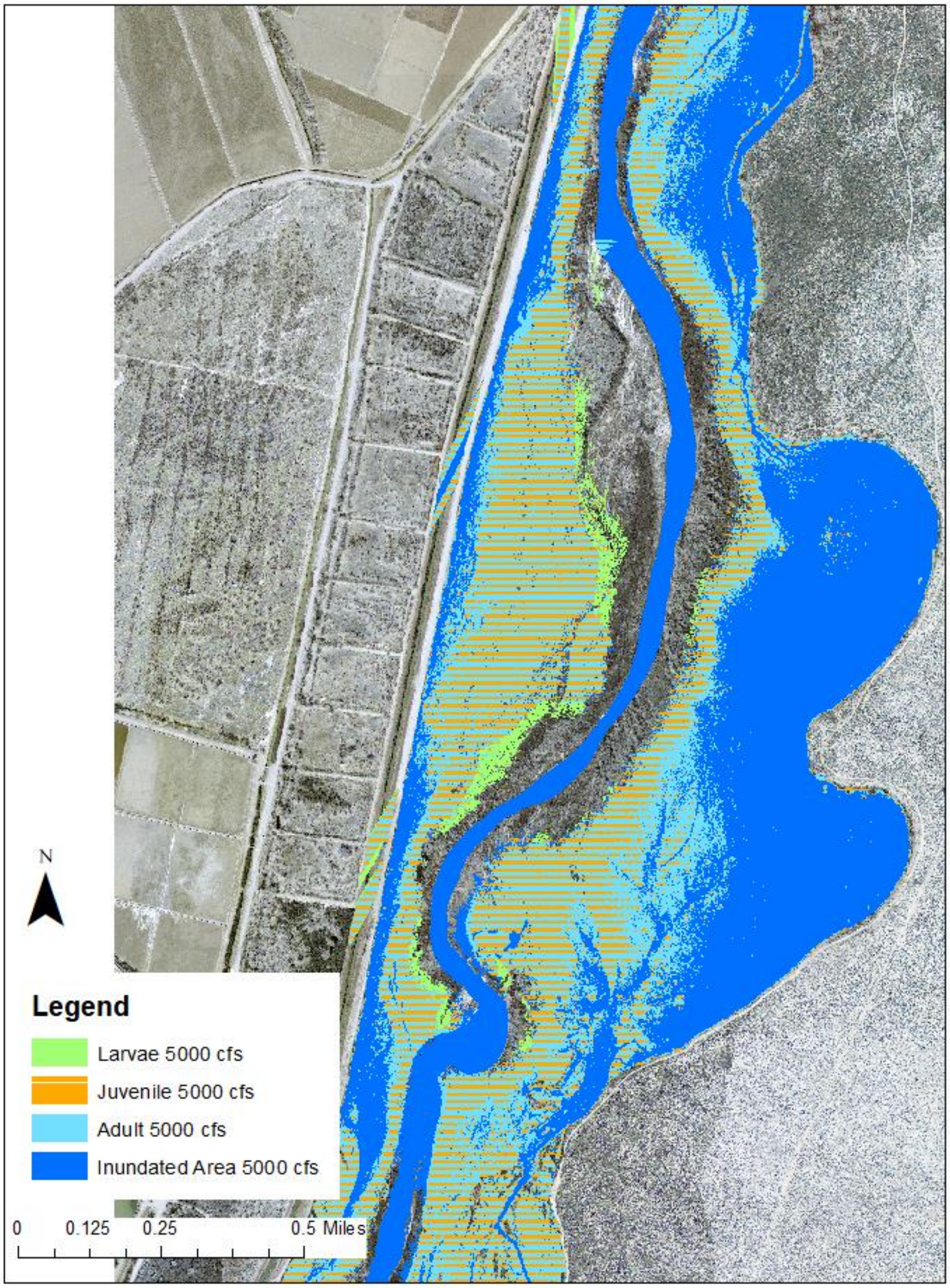

Figure E- 24 RGSM Habitat in subreach B3.B at 5000 cfs with hydraulically suitable areas labeled for larvae (green), juvenile (orange), and adult (light blue) and unsuitable inundated areas in dark blue.

B3.C Habitat (5000 cfs)

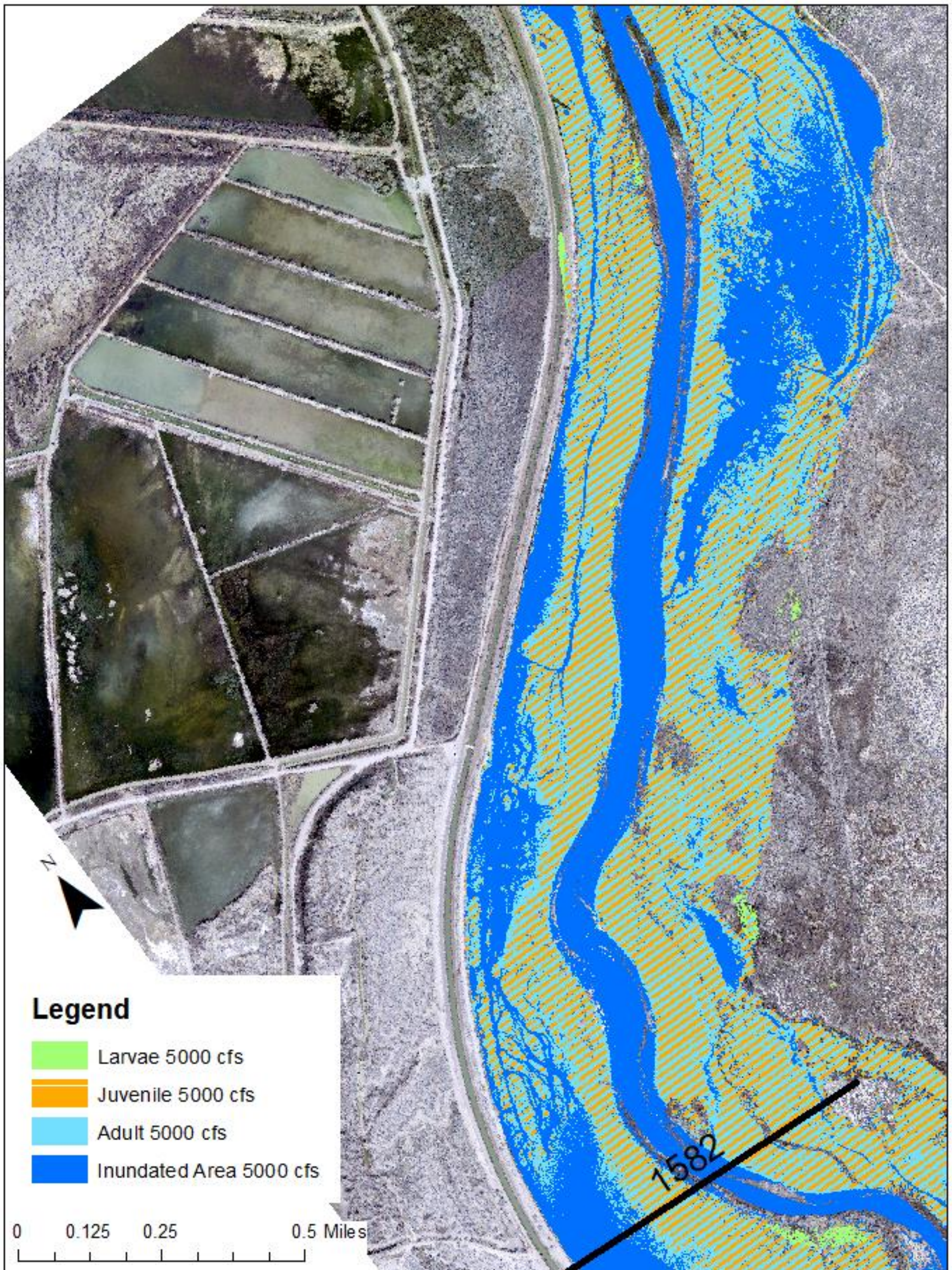

Figure E- 25 RGSM Habitat in subreach B3.C at 5000 cfs with hydraulically suitable areas labeled for larvae (green), juvenile (orange), and adult (light blue) and unsuitable inundated areas in dark blue.

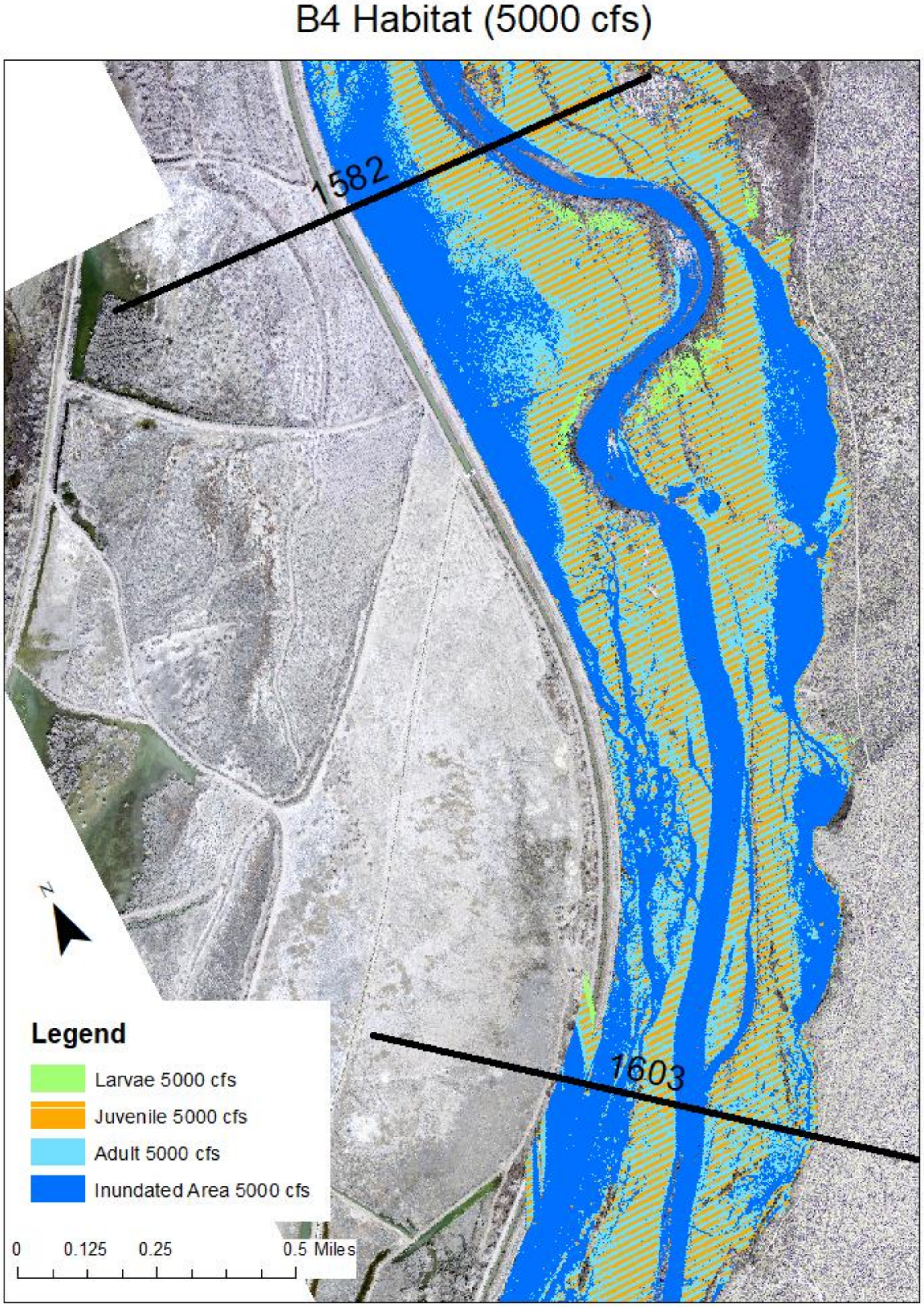

Figure E- 26 RGSM Habitat in subreach B4 at 5000 cfs with hydraulically suitable areas labeled for larvae (green), juvenile (orange), and adult (light blue) and unsuitable inundated areas in dark blue.

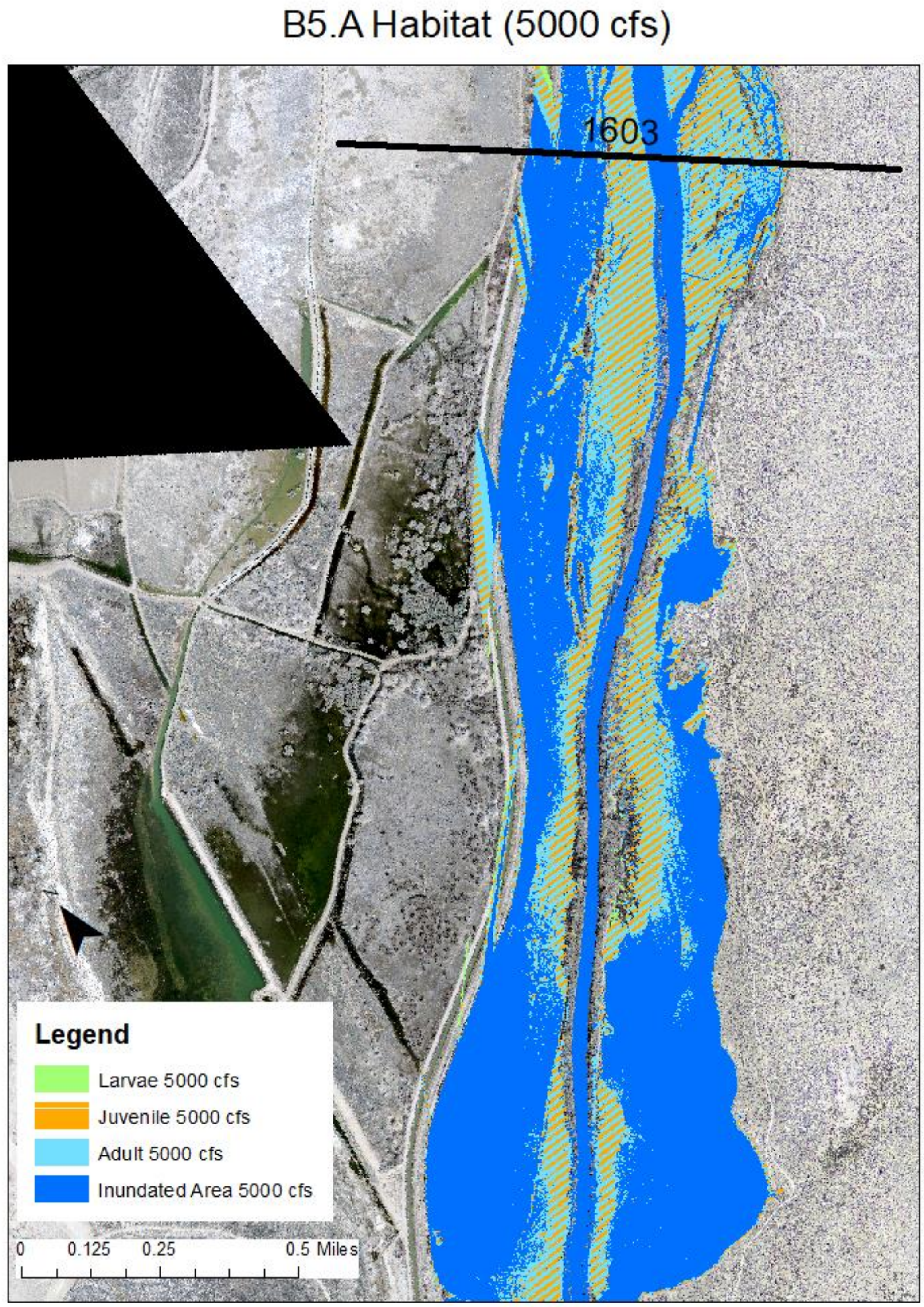

Figure E- 27 RGSM Habitat in subreach B5.A at 5000 cfs with hydraulically suitable areas labeled for larvae (green), juvenile (orange), and adult (light blue) and unsuitable inundated areas in dark blue.

B5.B Habitat (5000 cfs)

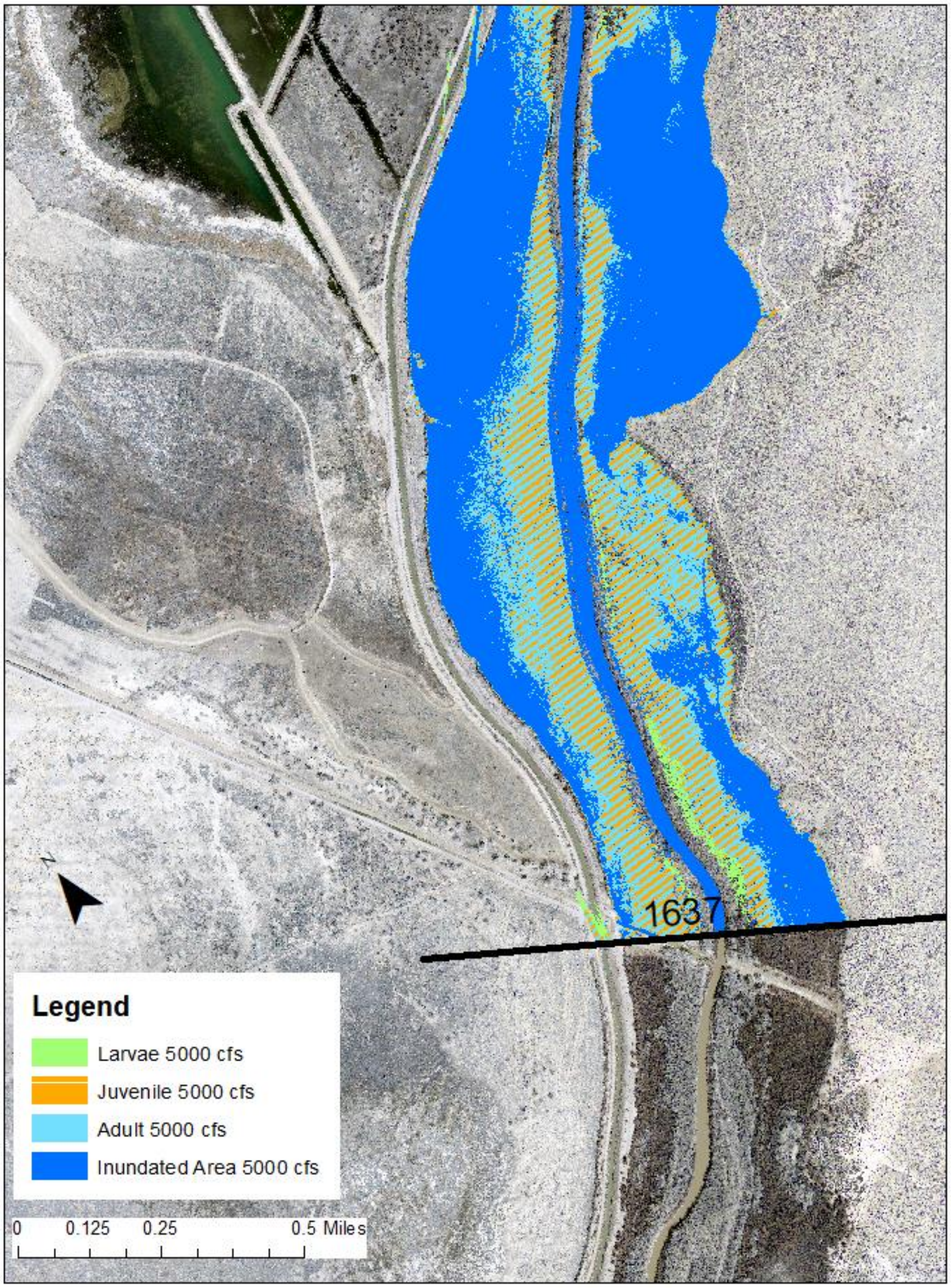

Figure E- 28 RGSM Habitat in subreach B5.B at 5000 cfs with hydraulically suitable areas labeled for larvae (green), juvenile (orange), and adult (light blue) and unsuitable inundated areas in dark blue.

Appendix F

Geomorphology/Habitat Connection Figures for Process Linkage Report

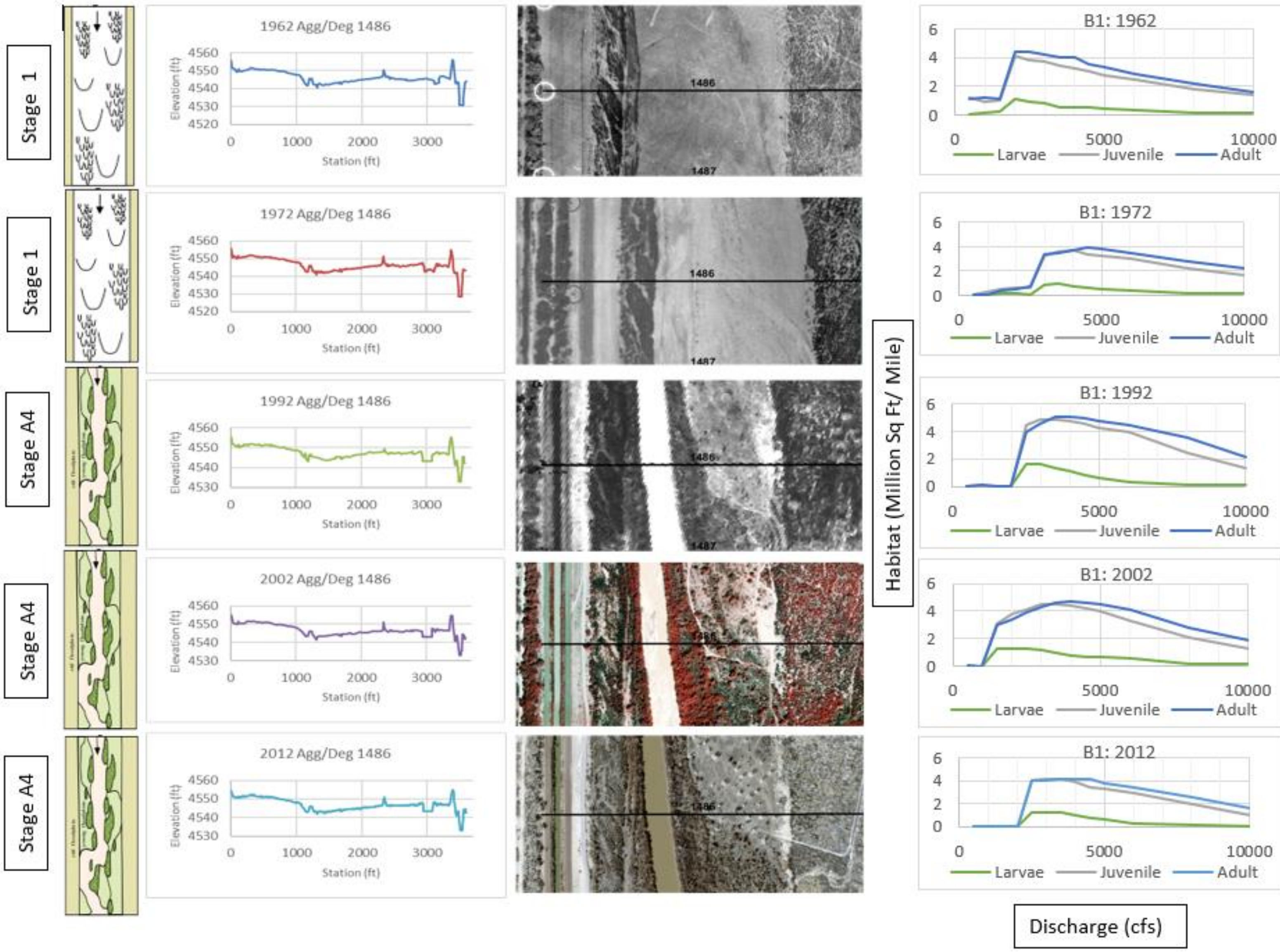

Figure F- 1 Geomorphology and habitat connections collage for subreach B1

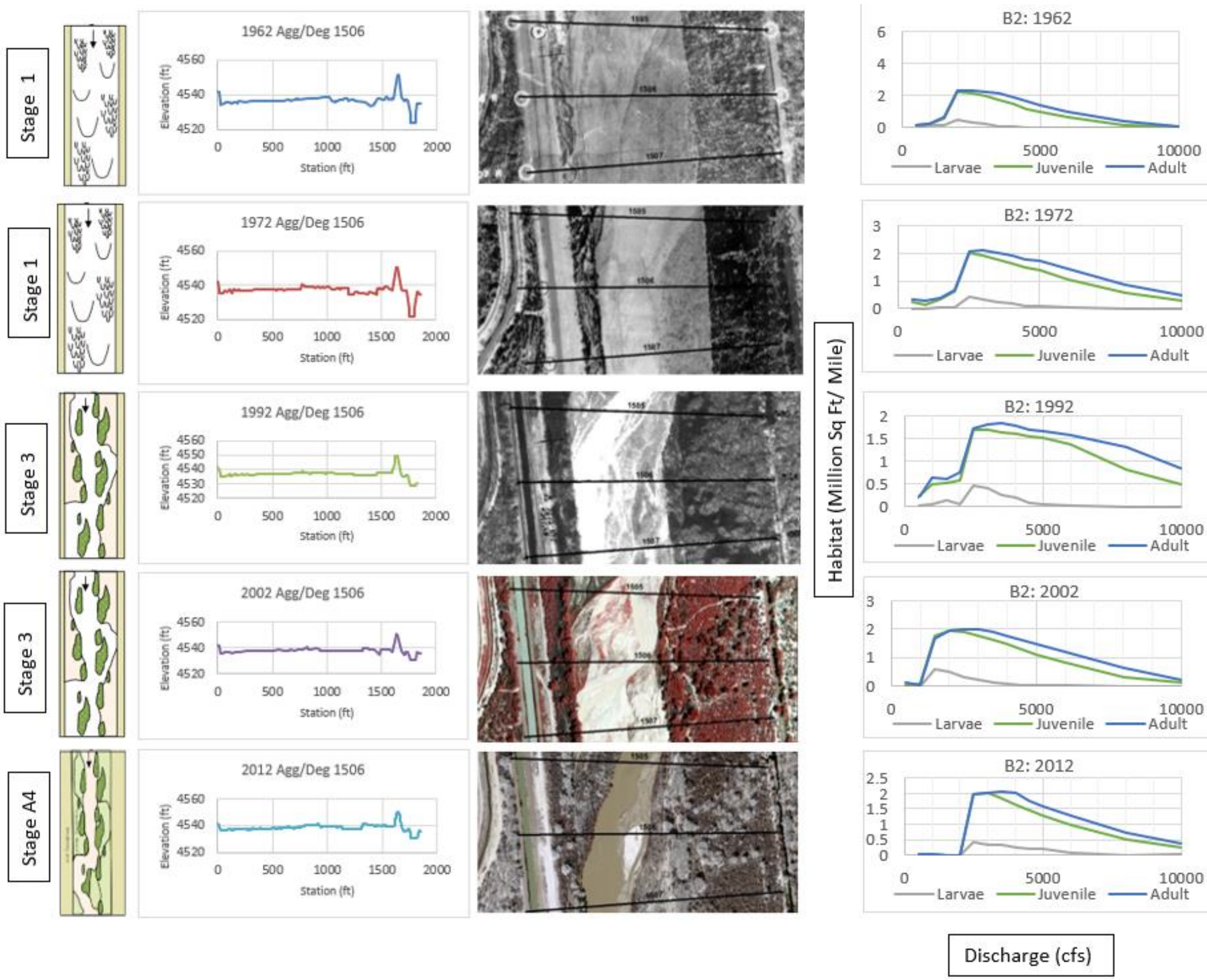

Figure F- 2 Geomorphology and habitat connections collage for subreach B2

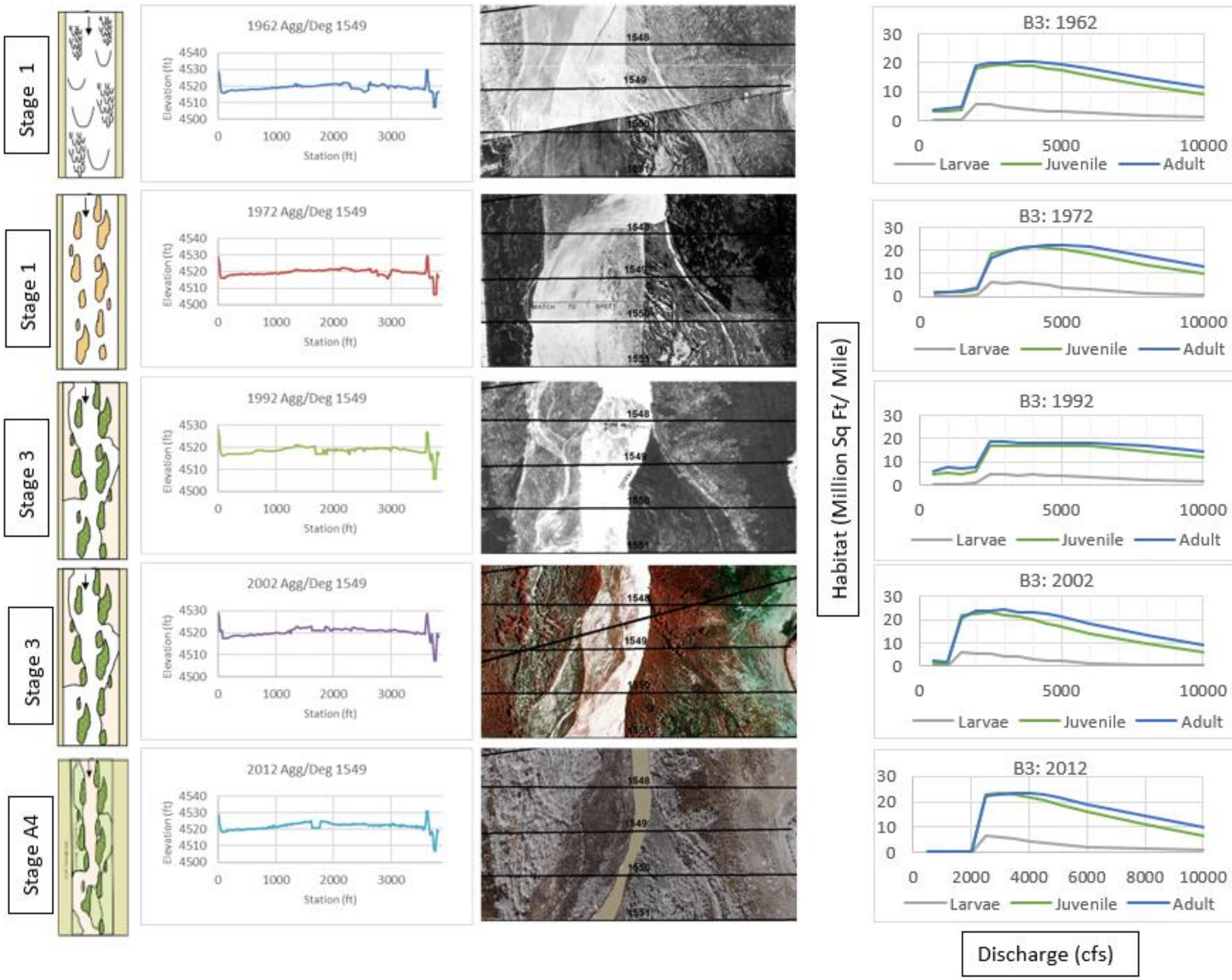

Figure F- 3 Geomorphology and habitat connections collage for subreach B3

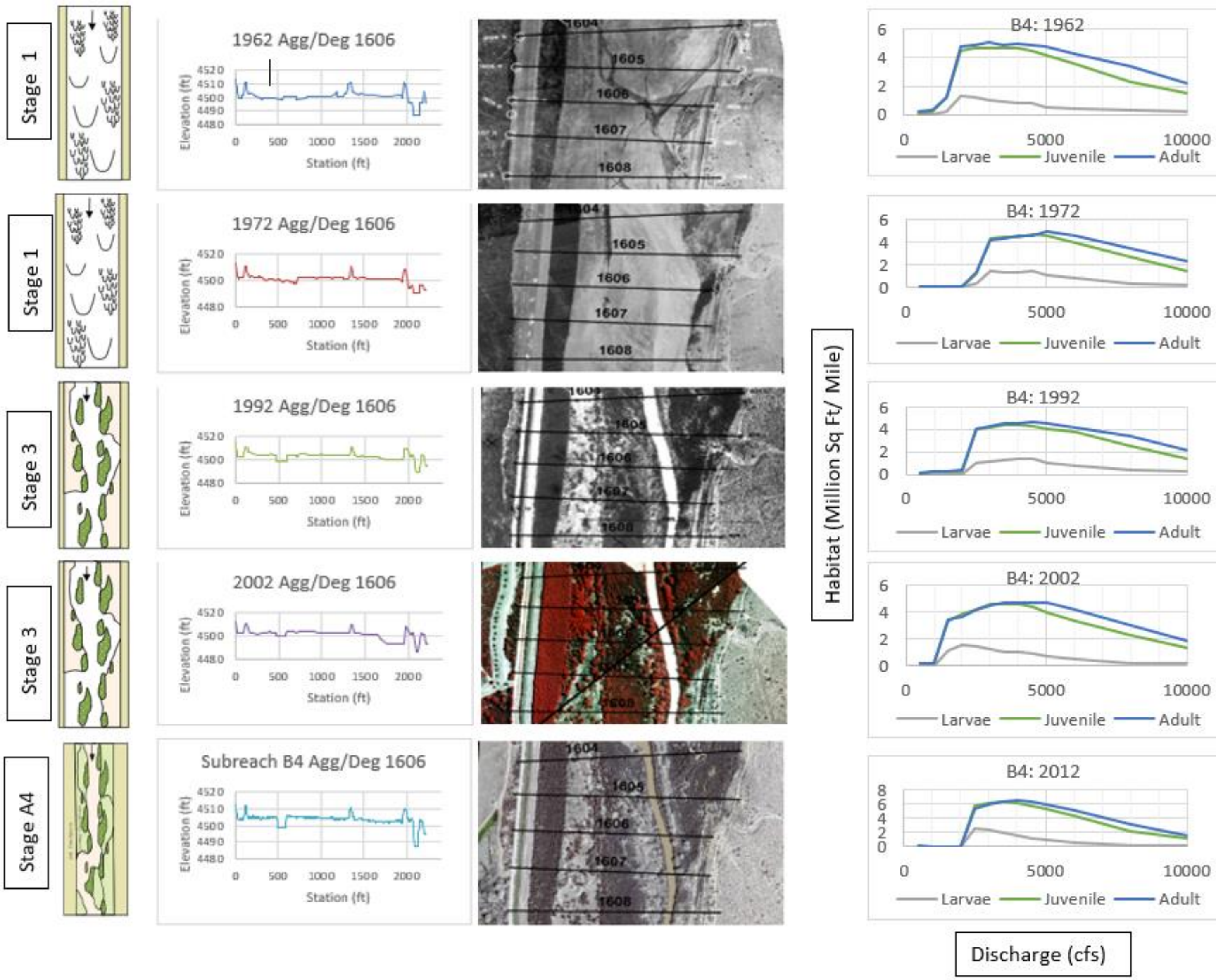

Figure F- 4 Geomorphology and habitat connections collage for subreach B4

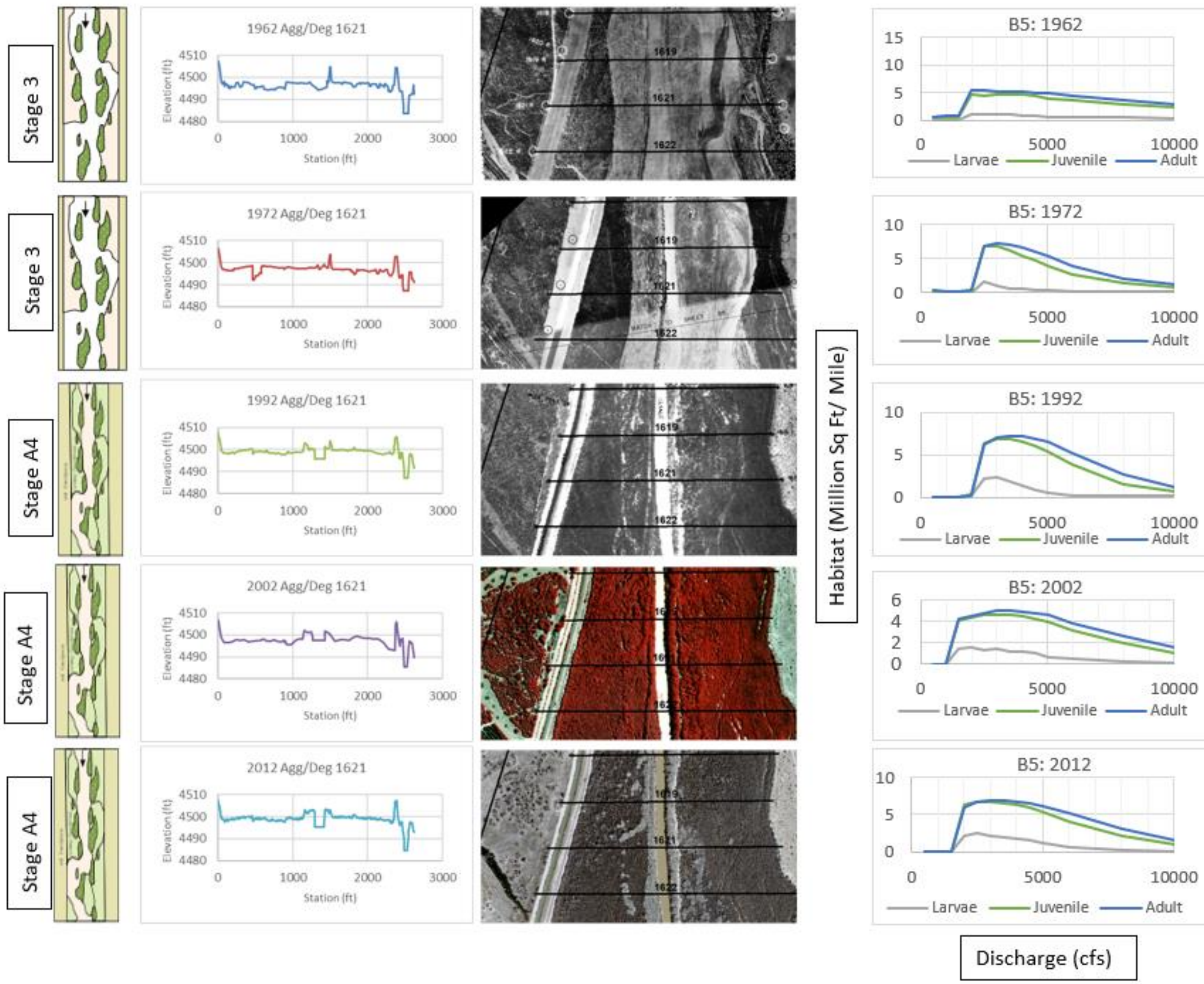

Figure F- 5 Geomorphology and habitat connections collage for subreach B5